The integrated stress response (ISR) is a focal point of tumorigenic pathways in KRAS-driven lung cancer

By

Nour Ghaddar

Experimental Medicine

McGill University, Montreal

September 2022

A thesis submitted to McGill University in partial fulfillment of the requirements of the degree of Doctoral of Philosophy

Abstract

Cancer cells are exposed to multiple forms of stress during their progression, such as genotoxic, metabolic, and proteotoxic stress. As a result, the integrated stress response (ISR) pathway is activated to accommodate to the various forms of stress. Phosphorylation of the eukaryotic initiation factor 2 at serine 52 of the alpha subunit (p-eIF2α) takes place in response to active ISR and reprograms the gene expression of stressed cells leading to induction of cell death or promotion of cell survival. We demonstrated the prognostic significance of the ISR in the development and treatment of lung adenocarcinoma (LUAD). Analysis of 928 primary lung adenocarcinomas of patients revealed that high p-eIF2α levels in tumors correlate with decreased survival of patients by~12 months. In a mouse model of KRAS-driven LUAD, we uncover a novel pro-tumorigenic function of the ISR by genetic and pharmacological means. We demonstrate for the first time that p-eIF2α stimulates the mitogen-activated protein kinase (MAPK) pathway by translational repression of the dual specificity phosphatase (DUSP6). This regulation is mediated by activation of the upstream p-eIF2α kinase PERK. In addition to uncovering a previously unidentified link in KRAS-driven lung cancer, our findings reveal that disrupting the ISR by pharmacological inhibitors is an effective treatment strategy for KRAS lung cancer. Indeed, the ISR inhibitor (ISRIB) and PERK inhibitor substantially decreased lung tumor growth in mouse and human KRAS-lung cancer models, regardless of the type of KRAS mutation. The strong anti-tumor effects of ISR disruption led us to explore other mechanisms downstream of the ISR. We found that the ISR activates YAP/TAZ signaling, which is an important player in KRAS lung cancer progression and acquisition of resistance to therapy. In addition, we delineate the role of the ISR in lineage diversity and tumor heterogeneity during KRAS LUAD progression by single-cell RNA sequencing (sc-RNA seq). As such, the ISR was found to drive high stemness and epithelial to mesenchymal transition (EMT) programs in KRAS LUAD cells. The ISR also employs a high-plasticity cell-state mechanism for successful lung tumor progression and evolution. The involvement of the ISR in the mentioned processes further emphasizes its role as master regulator of pro-tumorigenic pathways and highlights the therapeutic potential of ISR inhibitors as novel targets in KRAS lung cancer.

Résumé

Les cellules cancéreuses sont exposées à de multiples formes de stress au cours de leur progression, telles que le stress génotoxique, métabolique et protéotoxique. En conséquence, la voie de réponse intégrée au stress (ISR) est activée pour s'adapter aux différentes formes de stress. La phosphorylation du facteur d'initiation eucaryote 2 au niveau de la sérine 51 de la sous-unité alpha (p-eIF2α) a lieu en réponse à l'ISR actif et reprogramme l'expression génique des cellules stressées conduisant à l'induction de la mort cellulaire ou à la promotion de la survie cellulaire. Nous avons démontré l'importance pronostique de l'ISR dans le développement et le traitement de l'adénocarcinome pulmonaire (LUAD). L'analyse de 928 adénocarcinomes pulmonaires primaires de patients a révélé que des niveaux élevés de p-eIF2α dans les tumeurs étaient corrélés à une diminution de la survie des patients d'environ 12 mois. Dans un modèle murin de LUAD piloté par KRAS, nous découvrons une nouvelle fonction pro-tumorigène de l'ISR par des moyens génétiques et pharmacologiques. Nous démontrons pour la première fois que p-eIF2α stimule la voie de la protéine kinase activée par les mitogènes (MAPK) par la répression traductionnelle de la phosphatase à double spécificité (DUSP6). Cette régulation est médiée par l'activation de la p-eIF2α kinase PERK en amont. En plus de découvrir un lien jusque-là non identifié dans le cancer du poumon induit par le KRAS, nos découvertes révèlent que la perturbation de l'ISR par des inhibiteurs pharmacologiques est une stratégie de traitement efficace pour le cancer du poumon KRAS. En effet, l'inhibiteur de l'ISR (ISRIB) et l'inhibiteur de la PERK ont considérablement réduit la croissance des tumeurs pulmonaires dans les modèles de cancer du poumon KRAS chez la souris et chez l'homme, quel que soit le type de mutation de KRAS. Les forts effets anti-tumoraux de la perturbation de l'ISR nous ont amenés à explorer d'autres mécanismes en aval de l'ISR. Nous avons constaté que l'ISR active la signalisation YAP/TAZ, qui est un acteur important dans la progression du cancer du poumon KRAS et l'acquisition de la résistance au traitement. De plus, nous délimitons le rôle de l'ISR dans la diversité des lignées et l'hétérogénéité tumorale au cours de la progression de KRAS LUAD par séquençage d'ARN unicellulaire (sc-RNA seq). En tant que tel, il a été constaté que l'ISR entraînait des programmes de transition épithéliale à mésenchymateuse (EMT) élevés dans les cellules KRAS LUAD. L'ISR utilise également un mécanisme d'état cellulaire à haute plasticité pour la progression et l'évolution réussies des tumeurs pulmonaires. L'implication de l'ISR dans les processus mentionnés souligne davantage son rôle de régulateur principal des voies pro-

tumorigènes et met en évidence le potentiel thérapeutique des inhibiteurs de l'ISR en tant que nouvelles cibles dans le cancer du poumon KRAS.

Acknowledgements

I am forever grateful to my mentor Dr. Antonis Koromilas for his continuous guidance, passion, and wisdom throughout my PhD studies. I owe my scientific and personal development and growth to him. Thank you for your persistence and for showing me how to be the best version of myself.

I would like to thank my mother and role model, Dr. Fatina Siblini, for inspiring me with her strength and perseverance. I thank my loving father Ibrahim Ghaddar for support even when distance separates us. To my siblings Sahar, Karim and Nader, I cannot imagine doing this without your support and words of encouragement throughout my studies.

I would like to thank my colleagues in the laboratory of Dr. Koromilas. The best partner I could ever ask for, Jothi, for her immense help and support. It is our ability to work as one unit that helped me progress significantly during my studies. You always made my days at the lab brighter and never left me alone in dark times. I have the utmost respect and gratitude for Dr. Shuo Wang, I learned a lot from your talented hands. Thank you for being patient with me, teaching me almost everything you know and treating me as your own daughter. Dr. Cedric Darini for setting up the road for me and preparing me to face tough times. I had the best collaboration with you that led to a beautiful work. For the future scientists partaking this project, especially Jia Zou and Shiqi Diaou, I believe you will drive this project forward with your talent and passion for science. Thank you Hyungdong Kim for re-igniting the life in the eIF2B project with your hard work and perseverance and for being a great friend and colleague.

I would like to thank my committee members, Ivan Topisirovic, Josie Ursini-Siegel and Koren Mann and Gerardo Ferbeyre for having an open-door policy and being there for discussions about anything, anytime. Thank you for believing in me since my first committee meeting and providing me with reference letters even during the busiest times. Also, I would like to thank the LDI community, for being a wonderful and approachable community of scientists. I would not be able to achieve what I have achieved if it weren't for this thriving environment.

Finally, I would like to acknowledge the funding agencies the provided support during my PhD studies; the Fonds de recherche du Québec Santé (FRQS) doctoral funding and the McGill internal studentship awards.

Preface

This thesis is presented in the traditional format in accordance with the guidelines of the National Library of Canada. The data presented in this thesis is the original work of the candidate, and has been published, in part in the following peer-reviewed articles or manuscripts in preparation.

1. **Ghaddar N**, Wang S, Woodvine B, Krishnamoorthy J, van Hoef V, Darini C, Kazimierczak U, Ah-son N, Popper H, Johnson M, Officer L, Teodósio A, Broggini M, Mann KK, Hatzoglou M, Topisirovic I, Larsson O, Le Quesne J, and **Koromilas AE**. The Integrated Stress Response is tumorigenic and constitutes a therapeutic liability in KRAS-driven lung cancer. *Nature Communications*. 2021 July 30; 12(1):4651.

2. **Ghaddar N**, Wang S, Michaud V and **Koromilas AE**. Detection of Lung Tumor Progression in Mice by Ultrasound Imaging. *Journal of Visualized Experiments*. 2020 Feb 27; (156)**.**

3. **Ghaddar N**, Diao S, Wang S and **Koromilas AE**. The Integrated Stress Response activates YAP/TAZ to promote KRAS-driven lung cancer. *Manuscript in preparation*.

4. **Ghaddar N**, Diao S, Wang S and Koromilas AE. The Integrated Stress Response drives KRAS-driven lung cancer evolution and is essential for the emergence of a high-plasticity cell state. *Manuscript in preparation*.

The candidate was the lead investigator for the projects described in this thesis, but would like to acknowledge the contributions of colleagues in the described work.

1. Dr. Shuo Wang performed intratracheal injections of the lentiviruses in KRAS-G12D mouse model and generated data in figures 15, 27, 37.
2. Jothilatha Krishnamoorthy generated data in figures 22-24-32-33-34-35.
3. Bethany Woodvine generated data and performed analysis in figures 13, 14 and 21.
4. Cedric Darini generated data in figures 16, 19.
5. Nicolas Ah-son generated data in figure 20.
6. Vincent van Hoef performed analysis of figure 18.

7. Shiqi Diao performed analysis for figures 40-45, 60-68 and tables 5-7.
8. Myriam Johnson generated the KRAS G12C and WT KRAS H1703 cell lines.
9. Marios Lange generated IC50 and replicates of clonogenic assays of effect of MRTX1133 on eIF2αS/S and eIF2αA/A cells.
10. Christian Young performed FACS sorting of GFP positive eIF2αS/S and eIF2αA/A cells.

The Candidate has also contributed to several other projects whose research is discussed and referenced but not presented in this thesis. These studies have been published in the following articles.

1- Darini C, **Ghaddar N**, Chabot C, Assaker G, Sabri S, Wang S, Krishnamoorthy J, Buchanan M, Aguilar-Machecha A, Abdulkarim B, Deschenes J, Torres J, Ursini-Siegel J, Basik M and **Koromilas AE**. An Integrated Stress Response via PKR Suppresses HER2+ cancers and Increases the Efficacy of Trastuzumab Therapy. *Nature Communications*. 2019 May 13; 10(1):2139

2- Krishnamoorthy J, Tenkerian C, Gupta J, **Ghaddar N**, Wang S, Darini C, Taschke KA, Ghosh A, Gandin V, Topisirovic I, Kristof AS, Hatzoglou M, Simos G, **Koromilas AE.** Downregulation of PERK activity and eIF2α serine 51 phosphorylation by mTOR complex 1 elicits pro-oxidant and pro-death effects in tuberous sclerosis-deficient cells. *Cell death and disease*. 2018 Feb 15; 9(3):254

Table of contents

List of abbreviations

4E-BP: eIF4E binding protein

ATP: adenosine tri-phosphate

AKT/PKB: Protein kinase B

AMPK: AMP activated protein Kinase

ATF: Activating transcription factor

CHOP/GADD153: C/EBP homology protein/growth arrest and DNA damage dsRNA: double stranded RNA

CreP: constitutive repressor of eIF2α phosphorylation

CTGF: connective tissue growth factor

CYR61: cysteine-rich angiogenic inducer 61

DUSP: Dual specificity phosphtase

ECM: extracellular matrix

EGF: epidermal growth factor

ER: Endoplasmic reticulum

eIF: eurakyotic initiation factor

GADD34: growth and DNA-damage-inducible protein

GAP: Guanine activating protein

GCN2: General control non-derepressing kinase-2

GDP: guanosine diphosphate

GEF: Guanine exchange factor

GPCR: G-protein coupled receptor

GSK: Glycogen synthase kinase

GTP: guanosine triphosphate

HIF: Hypoxia induced factor

HRI: Heme regulated inhibitor

IFN: Interferon

IRE-1: Inositol-requiring enzyme -1

IκB: Inhibitor of κB

IRES: internal ribosomal entry site

ISR: Integrated stress response

LATS: Large tumor suppressor

m 7G: 7-methyl-guanosine

MAPK: Mitogen-activated protein kinase

mTOR: mammalian target of rapamycin

mTORC1: mTOR complex1

mTORC2: mTOR complex1

MST: mammalian STE20-like protein kinase

MEF: Mouse embryonic fibroblasts

NF-κB: Nuclear factor kappa-light-chain-enhancer of activated B cells

ORF: Open reading frame

PABP: poly-A binding protein

PDX: Patient-derived xenograft

PERK: PKR like endoplasmic reticulum (ER) kinase

PKR: Protein kinase activated by dsRNA

PIC: Pre-initiation complex

PP1: Protein phosphatase 1

PTEN: Phosphate and tensin homolog deleted of chromosome 10

UPR: Unfolded Protein Response

uORF: upstream open reading frame

UTR: Untranslated region

JNK: c-Jun-N-terminal kinase

STAT: Signal transducer and activator or transcription

TC: Ternary complex

ROS: Reactive oxygen species

RTK: Receptor tyrosine kinase

TAZ: PDZ-binding motif

YAP: Yes-associated protein

List of figures:

Introduction figures:

Result figures

List of tables:

Chapter 1
Introduction

1. mRNA translation initiation and translational control

1.1 Regulation of mRNA translation initiation.

Functional expression of genes requires the tight control of messenger RNA (mRNA) translation[1]. This regulation involves the well-timed incorporation of translation factors in association with adequate supply of energy levels along with the lowest mutation rates, to produce a fully functional protein that can fulfill its purpose[1]. Efficient and accurate protein synthesis is eventually facilitated by ribosomes, which identify open reading frames (ORFs) within the mRNA and assemble polypeptides with amino acid sequences corresponding to the codon sequence on the mRNA [2,3]. As such, the production of a fully functional protein by translation of an mRNA is divided into three highly controlled steps; initiation, elongation and termination[1]. It is inevitable that each step has its own essential factors and tight regulation for the successful production of proteins[1]. In eukaryotes, translation initiation is the most crucial step, composed of a highly organized network of biomolecules working in coherence[4-6]. Translation initiation starts with the scanning mechanism that leads to the recognition of the AUG start codon in the mRNA[7]. This involves an active 43S pre-initiation complex (PIC) which is composed of the methionyl initiator transfer RNA (Met-tRNA$_i$) bound to the small 40S ribosomal subunit[7]. After that, generation of the ternary complex The scanning process requires energy provided by guanosine triphosphate (GTP) that is carried by the eukaryotic initiation factor 2 (eIF2) and generates the ternary complex (TC).[8] As soon as the mRNA leaves the nucleus to begin a round of translation, the TC is loaded onto an activated mRNA near the 5'-cap[7]. This attachment is promoted by the eukaryotic initiation factors eIF1, -1A, -5 and the multi-subunit eIF3 (**Figure 1**)[7]. In addition, attachment to the m^{7}G 5'-cap is further facilitated by the eIF4F complex; composed of the cap-binding factor eIF4E, the scaffold protein eIF4G and the ATP-dependent RNA helicase eIF4A[7]. Since the 5'-untranslated region (UTR) might contain secondary structures, the RNA helicase activity of eIF4A can resolve them[9]. Translation of a mRNA is further enhanced by attachment of the poly-A binding protein (PABP) to the poly-A tail. At this point, the 5'-cap and the 3'-poly-A tail are joined together forming a closed loop, which is essential in translation initiation (Figure 1).[4,7] After attaching to the 5'-UTR, the PIC scans the mRNA, codon by codon, aided by GTP hydrolysis from the TC, until it encounters the

AUG codon which matches the complementary anticodon found on the Met-tRNA$_i$[4]. Binding of the initiator tRNA to mRNA codons in the P site of the 40S ribosomes triggers the disassembly of the PIC, highlighted by eIF1 dissociation, phosphate (P_i) release from eIF2 and conformational rearrangements of eIF5, 1A, -2β and -3c of the PIC[7]. GDP-eIF2 dissociates from the PIC and eIF5B-GTP mediates the

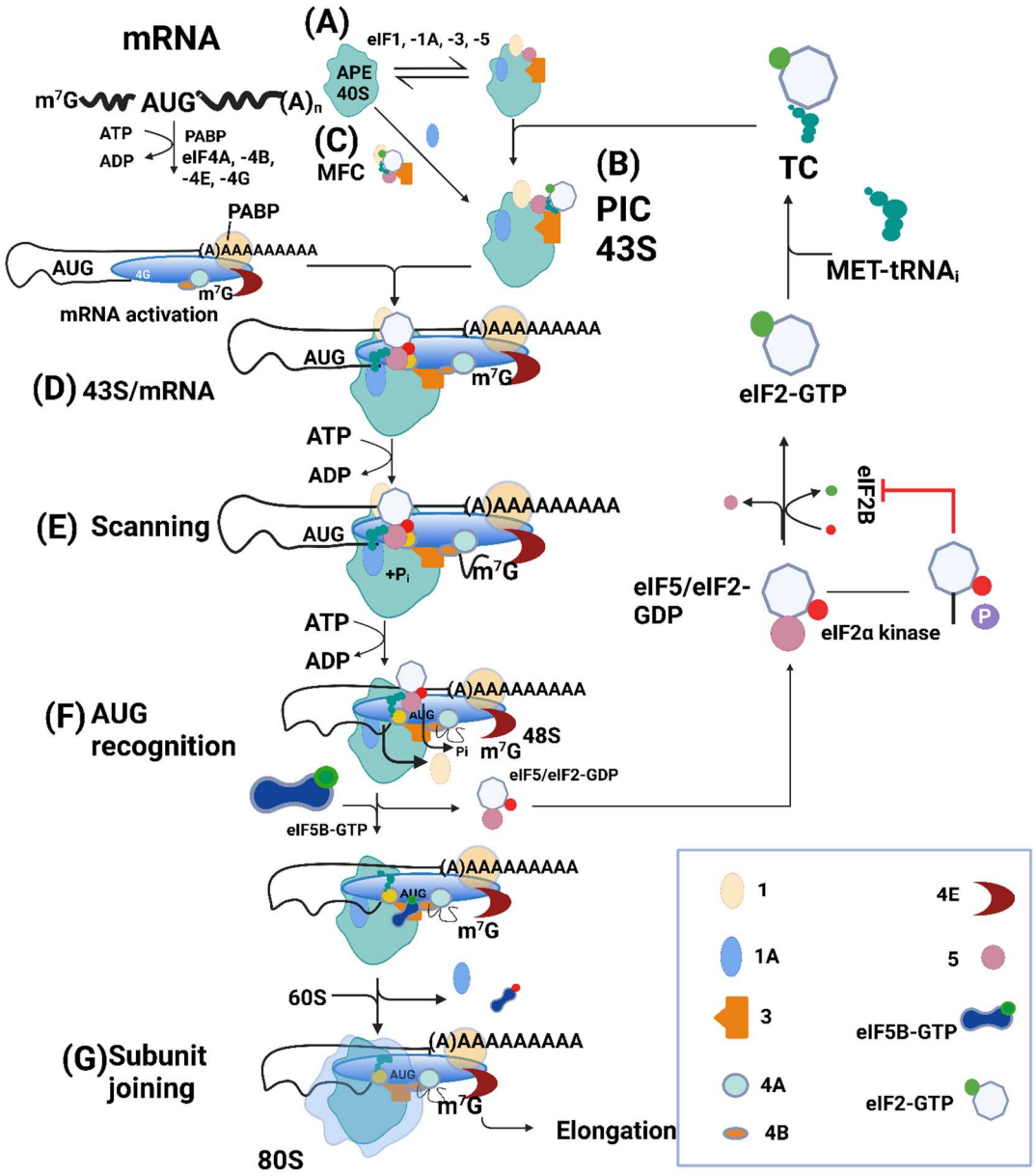

Figure 1 Overview of the canonical eukaryotic translation initiation pathway. (A) The eukaryotic initiation factors eIF1, -1A and 3 first bind to the 40S subunit with A, P and E

decoding sites. (B) Binding of the ternary complex (TC) and eIF5 forms the 43S pre-initiation complex (PIC). (C) The single-step assembly of the multi-factor complex (MFC) to the 40S to form the PIC is also depicted. (D) After loading of the PIC on the activated messenger RNA (mRNA), scanning of the mRNA is initiated with the help of GTP hydrolysis from TC. (E) Upon recognizing the AUG start codon, eIF1 and P_i from eIF2 are dissociated from the complex. (F) eIF5B-GTP is recruited to the complex followed by subsequent release of eIF5/eIF2-GDP for another round of initiation. (G) eIF5B-GTP joins the 60S subunit to PIC and is then released as eIF5B-GDP with eIF1A. (H)The 80S subunit is formed and ready for the elongation step. Adapted from[7].

joining of the large 60S subunit to produce the 80S initiation complex[7]. Subsequent steps then prepare the PIC for the elongation phase, while the released GDP-eIF2 is recycled to GTP-eIF2 by the guanine exchange factor (GEF) eIF2B for another round of initiation[7]. The importance of eIF2 in the initiation process is further highlighted by an additional step of regulation governed by the integrated stress response (ISR)[10-12].

During their lifecycle, cells encounter multiple forms of stress, such as metabolic, oxidative, hypoxic, proteotoxic and genotoxic stress, among others[12-14]. Under these conditions, the phosphorylation of the alpha subunit of eIF2 at serine 51 (serine 52 in *S. cerevisiae* and *Homo sapiens*[15]), herein referred to as p-eIF2α, impedes the GEF activity of eIF2B and thus hinders the recycling process and formation of the TC[11]. As a result, general translation initiation is blocked. However, translation of most mRNAs with uORFs occurs via cap-dependent translation via ribosome bypass of uORF or ribosome reinitiation [8]. This allows for delayed re-initiation, as part of a process essential to initiation called the Integrated Stress Response (ISR)[8,16].

1.2 The Integrated Stress Response (ISR) in translational control

Throughout their lifetime, healthy proliferating cells are often inevitably exposed to multiple forms of stress[11]. Fortunately, cells possess multiple processes that help them overcome

stressful conditions and resume homeostasis. One such process occurs at the level of mRNA translation initiation called the Integrated Stress Response (ISR). It is formed of four kinases that have conserved kinase domains but divergent regulatory domains that allows their activation in response to different forms of stress (Figure 2)[10,11,17,18].

1.2.1 HRI

The heme-regulated inhibitor (HRI, *EIF2AK1*) is mainly known to be activated by a heme shortage. HRI possesses heme-binding domains that serve as a sensor for heme deficiency[19]. Its activation due to heme shortage inhibits globin synthesis to balance heme/globin cellular levels[19]. An additional role of HRI involves the protection of erythroid precursors during iron deficiency, erythropoietic protoporphyria and β-thalassemia[19]. Due to its role, HRI was thought to be activated exclusively in erythroid cells[20]. However, it was later shown to be activated in multiple different cell types and in response to various cell stressors such as oxidative and mitochondrial stress, heat shock and cytosolic protein aggregation[21,22]. Recent studies have also tied activation of HRI to mitochondrial stress via cleaved DELE1[20].

1.2.2 PKR

The double-stranded RNA-dependent protein kinase (PKR, *EIF2AK2*) contains a double-stranded RNA (dsRNA) binding domain which permits its activation by viral dsRNAs[23]. As result, PKR activation restricts the translation of viral and cellular mRNA and promotes apoptosis via phosphorylation of eIF2α [17,24]. Indeed, the essential role of PKR lies in its activity as a viral sensor. PKR is autophosphorylated and activated upon its dimerization, where phosphorylation on Thr 446 in the activation loop of the kinase domain is required for its full activity[17]. It is also stimulated in response to pro-inflammatory stimuli, cytokines, growth factors, and oxidative stress[24]. Aside from eIF2α, PKR mediates the activation of p53, STAT transcription factors, MAPK and NF-κB signaling[17]. Although PKR generally promotes apoptosis, it can play a pro-survival role depending on specific stress stimuli and in certain cell types[17]. PKR can increase cell survival by activating NF-κB and PI3K signaling pathways.

1.2.3 PERK

The PKR-like ER kinase (PERK, *EIFAK3*) is activated by endoplasmic reticulum stress as part of the unfolded protein response (UPR), which is an important process in maintaining proteostasis in the endoplasmic reticulum (ER)[25-28]. Accumulation of misfolded proteins in the ER leads to ER stress which activates the UPR[17]. In its inactive state, PERK has its N-terminal domain inserted in the ER lumen where it is associated with the Hsp70 chaperone binding immunoglobulin protein (BiP)[29,30]. Accumulation of unfolded proteins slated for the secretory pathway leads to UPR activation and dissociates BiP from PERK, leading to its dimerization and activation[17,31]. PERK is activated by Thr980 phosphorylation which stabilizes the activation loop and the helix αG in the C-terminal lobe, which is in contact with eIF2α[17]. Phosphorylation of eIF2α then inhibits the synthesis of new polypeptides and restores ER homeostasis[17]. Another mechanism of activation can be directly through binding of unfolded or misfolded proteins to the PERK luminal domain[32,33]. Independently of eIF2, PERK activates the nuclear factor (erythroid-derived 2)-like two (NRF2) and, along with PKR, glycogen synthase kinase-3β (GSK-3β)[17].

1.2.4 GCN2

The general control non-derepressible 2 (GCN2, *EIF2AK4*) is mainly activated by deacetylated His-tRNA due to low amino acid content[34]. Specifically, uncharged transfer RNAs (tRNAs) bind to the histidyl-tRNA synthetase (HisRS)-related domain and activate GCN2[17].

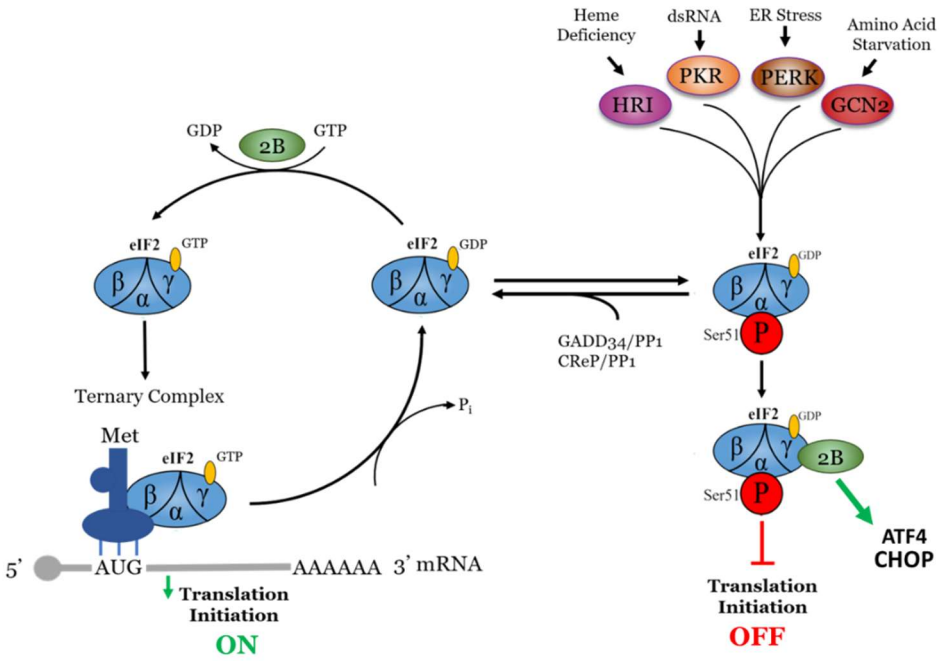

Figure 8. The Integrated Stress Response (ISR) as an important regulator of translation initiation. Activation of the four kinases, PKR, PERK, GCN2 and HRI in response to different forms of stress lead to phosphorylation of eukaryotic initiation factor 2 (eIF2) at Serine 51 of the α subunit. The unphosphorylated GTP-bound form of eIF2 is essential for forming the ternary complex to initiate mRNA translation. However, the phosphorylated form in response to stress causes a global inhibition of mRNA translation except mRNAs with open reading frames (ORFs) in their 5'-untranslated regions such as ATF4. Adapted from[10].

However, its activation expands beyond that to include stressors such as ultraviolet light, viral infection, serum starvation and oxidative stress[11]. Interestingly, it was recently found that GCN2 can be also activated by the ribosomal protein uL10, which is present in the P1/P2 stalk of the large ribosomal subunit[35-37]. In yeast, optimal GCN2 activation occurs by autophosphorylation of Thr 882 and Thr 887[17]. As opposed to the previous kinases, the only well-documented substrate of GCN2 is eIF2α[17].

1.2.5 Translation of select mRNAs with uORFs in their 5'-UTR

eIF2 is formed of 3 subunits (α, β and γ), however, activating any one of the mentioned kinases leads to the phosphorylation of the α subunit of eIF2 at Serine 52 (p-eIF2α)[10]. This event shifts eIF2 to a non-competitive inhibitor of the GEF eIF2B, which is formed of two copies of 5 subunits (α, β, γ, δ and ε)[11]. It is the ε subunit of eIF2B that carries its catalytic nucleotide exchange activity[10,11]. The γ subunit of eIF2 interacts with the ε subunits of eIF2B which leads to an open conformation of eIF2γ, facilitating the exchange of GDP and GTP[38]. However, phosphorylation of eIF2α due to an active ISR sterically hinders eIF2γ-eIF2Bε interactions and impedes the formation of an active TC[11] (Figure 2). Although this event causes a global inhibition of initiation of mRNAs, the translation of select mRNAs is paradoxically promoted. For example, the mRNAs encoding the Activating Transcription Factor 4 (*ATF4*) and *ATF5* have uORFs in their 5'-UTR that prevent their translation under normal conditions[8]. Specifically, the most well-characterized ISR effector ATF4 has multiple uORFs in its 5'-UTR which requires the TC to re-initiate for proper translation[5,8,39-41]. Under normal conditions, ribosomes scan the mRNA and encounter the first uORF. However, TC incorporates to the ribosome in time to translate the second inhibitory uORF instead, leading to decomposition of the complex and failed translation of ATF4[40]. In stressed conditions, due to limited available amounts of TC, the

ribosome to scan further until it reaches the main ORF and forms a proper translation machinery with TC, leading to elevated translation of the mRNA (Figure 3)[42].

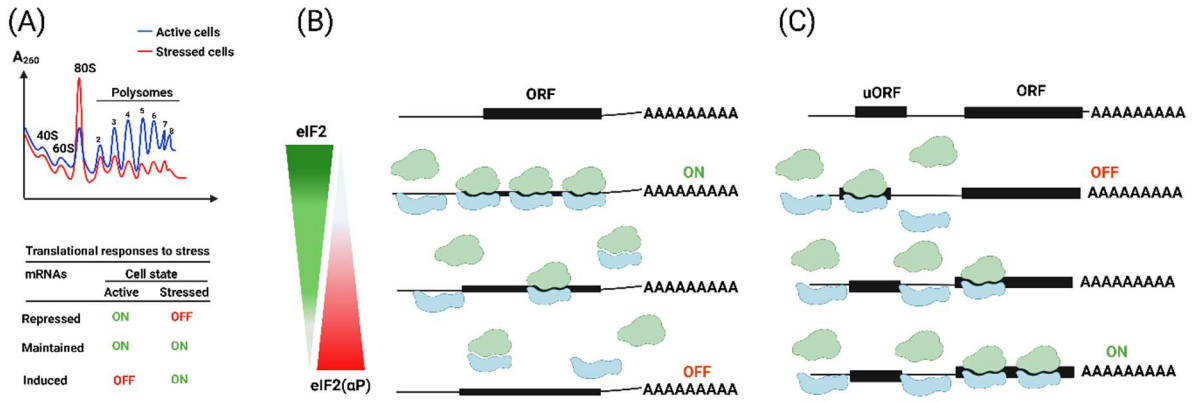

Figure 9. Effect of ISR on mRNAs with uORF. (A) Polysome profiles at A260 of active and stressed cell extracts sedimented on 15-50% sucrose gradients. (B) Ribosome interactions with mRNAs having normal ORFs or (C) uORFs depending on eIF2αP status during ISR. Taken from[43].

1.2.6 Termination of ISR

Termination of ISR is also required to determine cell fate decisions and restore homeostasis[44]. The protein phosphatase 1 complex (PP1) is formed of a catalytic subunit (PP1c) and one of two regulatory subunits[12]. The PP1 regulatory subunit 15A (PPP1R15A) also known as growth and DNA-damage-inducible protein (GADD34) and PP1R15B or the constitutive repressor of eIF2α phosphorylation (CreP) are both activated by ATF4[44-46]. While CreP is responsible for maintaining normal levels of eIF2αP even under unstressed conditions, GADD34 significantly dephosphorylates p-eIF2α under stressed conditions since it also contains uORFs in its 5'-UTR and is directly upregulated by p-eIF2α. As such, the two phosphatases are better translated, when eIF2α is phosphorylated, as part of a feedback mechanism to dephosphorylate p-eIF2α and restore homeostasis[10]. GADD34 and CreP are also involved in determining pro-death or pro-survival fates in cells with active ISR[10].

1.3 The importance of translation initiation in cancer

The multi-layered complexity of cancer can be shown by the hallmarks that define the disease [47-49]. It is now well-established that successful progression of tumors goes beyond hyperproliferation and evasion of cell death to include multiple components, especially those related to the tumor microenvironment[50]. In effect, cancer cells should master a proper regulation of mRNA translation oriented towards their successful proliferation by unlocking the expression of mRNAa with specific pro-tumorigenic functions and blocking the expression of those that hinder their progression. Since translation initiation is the rate-limiting step in protein synthesis, it is inevitable that cancer cells have developed mechanisms to master its control[51-57]. The selective translation of mRNAs at the level of initiation mostly takes place either via regulation of the eIF4F complex or through the ISR[55,57,58].

The eIF4F complex is frequently deregulated in cancer[9,59,60]. Specifically, eIF4E expression is upregulated in a wide range of cancers[9]. However, its overexpression does not increase the rate of translation[9]. eIF4E-sensitive mRNA either possess long, highly structured 5'-UTRs, special elements in their 5'-UTR or encode ribosomal proteins[9]. eIF4E expression as well as its phosphorylation stimulate the expression mRNAs with roles in survival (MCL) and invasion (e.g. Snail and MMP3)[9]. However, variation in mRNA responsiveness across tumor types may occur[9]. A tightly regulated process in cap-dependent translation initiation is blockage of eIF4F assembly by the 4E binding proteins (4EBP1, being the most well-studied among the three isoforms[9]) in nutrition and growth-factor restricted cells[58]. Specifically, 4EBP1 prevents the assembly of eIF4G to eIF4E[61]. eIF4E is mostly regulated by two important signaling pathways; (i) the PI3K (phosphoinositide 3-kinase)/AKT /mTOR (mammalian target of rapamycin) and (ii) Ras (Rat sarcoma)/MAPK (mitogen-activated protein kinase)/MNK (MAPK interacting kinases)[55]. These pathways often play a pro-tumorigenic function in cancer development. Mammalian target of Rapamycin complex 1 (mTORC1) activation by various stimuli phosphorylates 4EBP and releases eIF4E to resume its initiation function[61-64]. On the other hand, MNK stimulates eIF4E phosphorylation at Ser 209 to initiate translation[55]. eIF4E phosphorylation plays an important role in tumor progression and metastasis[55]. The importance of the oncogenic activity of eIF4F is highlighted by the development of inhibitors that target the components of eIF4F complex. These include targeting eIF4E function, eIF4E phosphorylation and eIF4A activity[9,59,60]. Additionally, eIF4F levels are elevated in cells resistant to chemotherapy or targeted therapy, making it an attractive target for combination therapies[59,65].

Uncontrolled proliferation exposes the cancer cell to multiple forms of stress, such as ER stress, hypoxia, amino acid depletion, DNA damage and reactive oxidative species (ROS)[13,14,66]. In effect, the ISR is more readily triggered in cancer cells compared to normal cells, leading to adaptation of the cells to the type of stress[67]. The adaptation process can either aid the cancer cell in survival and progression or trigger pro-death signaling pathways[28,68]. This dual nature of ISR is due to its core function in generally inhibiting the majority of mRNAs while selectively upregulating specific mRNAs that play a role in cell adaptation to stress[69]. Promotion of cell-survival or induction of cell death in response to ISR depends on the type of cancer, nature of stress and on the oncogenic driver[70,71]. The pro-survival role of the ISR is highlighted in medulloblastoma, pancreatic cancer, BRAF-mutated melanoma and aggressive prostate cancer[66,72-74]. On the other hand, the ISR can induce apoptosis in other types of cancer such as gliobastoma multiforme (GBM), breast cancer and Acute Myeloid Leukemia (AML)[75-77]. The pro-death or pro-survival function of the ISR is also activated in response to therapy to either confer resistance or contribute to cell death, respectively[71].

Depending on the nature of stress, different kinases of the ISR can be activated. PERK induction due to hypoxic stress or perturbations in the ER stress and the ensuing activation of the UPR generally aids in cell survival by inhibiting apoptosis[78,79] and increasing pro-survival mechanisms such as induction of micro-RNA miR-211, NFkB and autophagy[14,80,81]. PERK activity is also implicated in increased angiogenesis, epithelial to mesenchymal transition and resistance to oxidative stress[82-84]. PERK facilitates the induction of the pro-tumorigenic PI3K-Akt pathway[85]. Amino acid starvation leads to activation of GCN2 which can upregulate key autophagy genes due to increased ATF4 expression that results from induced phosphorylation of eIF2α[86]. The autophagic process confers a pro-survival mechanism in this case due to recycling of cytoplasmic components and replenishment of cellular ATP concentrations as well as amino acid levels[71]. Autophagy can assist with degradation of problematic proteins (e.g. ERphagy) [87]. GCN2 activation also induces asparagine synthase (ASNS), PCK2, amino acid synthesis and transport and modulates ROS levels to promote survival in tumor cells[86,88,89]. On the other hand, persistence of stress can drive ATF4 towards transcribing pro-apoptotic genes, particularly BCL2 family members[71]. Although activation of the PKR-p-eIF2α arm triggers pro-survival pathways such as NFkB signaling, it also activates pro-death pathways such as the Fas-associated death domain (FADD) protein and the phosphatase and tensin homolog (PTEN) tumor suppressor[90-92].

Ultimately the end-result would be the induction of cell-death by the activation of this arm. The HRI kinase activity was initially thought to be limited to erythroid cells, however, recent data implicate its role in non-erythroid cells[93]. Its activation is shown to be not only limited to heme-unavailability, but also to different stressors such as oxidative stress, osmotic stress and heat shock, among others[94]. The pro-survival role of HRI is exhibited in its activation of the NF-κB pathway and relieving the repression of the anti-apoptotic MCL-1[95,96]. Oncogenic drivers can also activate different kinases in the ISR. For example, Bcr.Abl expression in Chronic Myeloid Leukemia (CML), activated Ras or c-Myc all lead to the activation of the PERK-p-eIF2α arm in order to facilitate tumor growth[10].

2- Therapeutically targeting eIF2α phosphorylation in cancer

To this day, direct inhibitors of eIF2α phosphorylation do not exist. However, phosphorylation of eIF2α can be targeted indirectly either by upstream kinases, downstream phosphatases or indirectly antagonizing its function in translational control[10,11,38,97]. Targeting the ISR can not only act as an effective anti-cancer regimen, but also sensitize cancer cells to chemo- or targeted therapies[11]. In addition, targeting the ISR could provide insight into the importance of this process in cancer biology and progression.

2.1 Targeting the upstream kinases

The mentioned functions of the ISR kinases in cancer led to development of specific inhibitors either to further uncover their roles in cancer or to validate their implications as therapeutic targets[10,17,98-101]. Since the function of the four kinases converge to phosphorylation of eIF2α, it is possible that targeting one kinase would lead to intervention of other kinases to increase eIF2α phosphorylation as a compensatory pathway[10,11,17]. However, as mentioned above, different kinases are dominant in different types of cancer[17]. Therefore, determining which kinase is predominantly active in each cancer is important before deciding which kinase to target. GCN2 and PERK activation generally lead to pro-survival mechanisms in cancer, suggesting that inhibiting these kinases might be a plausible therapeutic target[86,102-104]. The most advanced kinase inhibitors are the PERK inhibitors, which are competitive ATP inhibitors [102,105,106]. These inhibitors are selective and effective in targeting tumor growth. However, more studies need to be done to determine whether the anti-tumor activity of PERK inhibitors is due to

downregulation of p-eIF2α or due to p-eIF2α-independent pathways such as phosphorylation of Nrf2 or fork-head transcription factor (FOXO1)[107,108]. Inhibiting GCN2 is of particular interest due to its activation by a broad range of stressors in the ISR[17]. GCN2 inhibition sensitized ALL to L-asparaginase *in vitro* and *in vivo*.[104] However, a plausible therapeutic strategy would be also to induce the activity of GCN2 and PERK, considering the dual nature of ISR in different cancers[71]. Activators of GCN2 and PERK have been studied in cancer therapy as single agents or in combination[71].

2.2 Targeting the eIF2α phosphatases

The phosphatases GADD34 and CreP dephosphorylate p-eIF2α through recruitment of PP1[109]. While Salubrinal inhibits the activity of both GADD34 and CreP, Guanabenz and Sephin1 are specific to GADD34 and Raphin1 is specific to CreP[110-113]. Among those, Salubrinal and Guanabenz have been implicated in studies in cancer. Recently, our group showed that Salubrinal sensitizes HER2 breast cancer tumors to Trastuzumab. Also, Guanabenz sensitizes glioblastoma cancer cells to sunitinib[76,114].

2.3 Antagonizing the translational effects of p-eIF2α by targeting eIF2B

The integrated stress response inhibitor (ISRIB) was recently identified to rescue the inhibition of mRNA translation by eIF2α phosphorylation by enhancing eIF2B GEF activity[11]. Mechanistically, ISRIB anneals together two tetrameric forms of eIF2B, which helps in further binding of the last monomeric pair[38,115]. The high rate of eIF2B decameric assembly aided by ISRIB increases the binding of eIF2 to eIF2B leading to close proximity of eIF2γ with the GEF eIF2Bε and more GDP-GTP exchange on eIF2, thus more translation[115]. As a result, the inhibitory effects of p-eIF2α on translation are dampened[115]. However, ISRIB's function in inducing translation is highly dependent on the presence of p-eIF2α[116,117]. In other words, ISRIB will function in cells only with an active ISR[117]. Therefore, ISRIB therapeutic function is dependent on cancer cells with a highly activated ISR[116,117]. The usage of ISRIB as a singular agent in targeting cancer has been used in the context of lung adenocarcinoma as well as aggressive prostate cancer[74,114]. Importantly, administration of ISRIB in mice had no toxic side-effects and prolonged the survival of mice due to cancer in both models[118]. In combination

therapies, ISRIB has been shown to sensitize pancreatic cancer cells to Gemcitabine treatment and breast cancer cells to bortezomib[73,119].

3 YAP/TAZ signaling in cancer

3.1 Overview of YAP/TAZ tumorigenic function

The activity of the transcriptional factor yes-associated protein (YAP) and its co-activator with PDZ-binding motif (TAZ) are essential for initiation, progression and metastasis of multiple cancer types[120]. The biology and regulation of YAP/TAZ were first discovered in *Drosophila* studies, where their overactivation by the HIPPO pathway components led to organ-overgrowth[120]. The components of the HIPPO pathway consist of serine-threonine kinases mammalian STE20-like protein kinase 1/2 (MST1/2) and the large tumour suppressor 1/2 (LATS1/2). The paralogues YAP and TAZ are transcriptional regulators that control cell proliferation, apoptosis, movement and fate[121]. Their regulation and localization are essential for early developmental events as well as for tissue homeostasis, repair and regeneration[121]. YAP/TAZ are key downstream effectors of the HIPPO pathway[121]. When the Hippo pathway is 'ON', LATS1/2 phosphorylate YAP/TAZ at 5 serine residues on YAP and 4 on TAZ[122]. After that, phosphorylated YAP and TAZ are subjected to one of two fates; either their retention in the cytoplasm by binding to 14-3-3 proteins or subjection to proteasomal degradation[123] When the HIPPO pathway is 'OFF', YAP/TAZ are free to translocate to the nucleus where they bind to the TEA domain family members (TEAD) and express gene targets by enhancer acetylation and recruitment of the transcriptional machinery[124] (Figure 4). Therefore, the components of the HIPPO pathway are considered tumor suppressors.

YAP/TAZ are hyperactivated and considered prognostic markers in various types of cancers[125]. Their tumor promoting activities includes initiation and progression of tumors, modulating the tumor microenvironment, activating stemness programs, mediating metastasis, acquiring resistance to therapy and controlling the immune response[120,123,126-128]. Among the cancer-associated activities of YAP/TAZ is promotion of cell proliferation in cancers by activating transcriptional programs that relate to cell cycle progression[124,129,130]. Genetic studies in KRAS-driven mouse models have shown the importance of YAP/TAZ in lung tumor

progression and promotion to aggressive tumors[131,132]. Furthermore, YAP/TAZ activate metastatic programs in cancer cells and is highly implicated in epithelial to mesenchymal transition (EMT)[125,127]. YAP/TAZ expression is often more elevated in metastatic tumors compared to non-metastatic ones[131-134]. Increased nuclear localization of YAP/TAZ correlate with malignancy (high historical grade, late TNM stage, lymph-node metastasis) in addition to poor patient outcome [135,136]. Moreover, recent studies have shown that YAP/TAZ is highly active in Cancer Stem Cells (CSCs) and activates stemness programs in these cells[137-139]. Moreover, YAP/TAZ drive cellular stemness and plasticity in glioblastoma[140]. YAP/TAZ activity is also linked to resistance to chemotherapy, radiotherapy as well as targeted therapy where active YAP/TAZ promotes survival and anti-apoptotic programs for resistance acquisition [120,125,141]. For example, YAP activity promotes resistance to RAF and MEK inhibitors in multiple tumor cells with *BRAF*, *NRAS* or *KRAS* activation [141]. The resistance acquisition is attributed to stiffness of the extracellular matrix or mechanotransduction[120]. YAP/TAZ activate genes that play a prominent role in cancer development, progression, and metastasis[142]. The YAP/TAZ transcriptional signature displays various oncogenic traits such as sustaining proliferation, inhibiting apoptosis, maintaining stemness, and developing resistance to therapies[142]. For example, bona fide target genes of YAP/TAZ include *AREG* (an EGF-like growth factor), *Cyr61* and *CTGF* which, in epithelial cells induce growth and angiogenesis[122]. The importance of YAP/TAZ is also inevitable in the tumor microenvironment where it mediates a cross-talk between cancer cells and normal cells[120]. In cancer associated fibroblasts (CAFs), YAP/TAZ induces the production of inflammatory interleukins and deposition of a rigid extracellular matrix[120]. Moreover, in epithelial cells, YAP/TAZ induces the secretion of chemo-attractants for T-cell suppressing myeloid cells favoring immune tolerance[120]. The Hippo pathway has also been implicated in tumor immunity, where LATS1/2 activates T cells through an interferon 1 (IFN1) program[126]. Another example is the upregulation of CXCL5 by YAP. CXCL5 attracts myeloid derived tumor suppressor cells (MDSCs) and binds to CXCR2 receptors. secrete chemo-attractants for T-cell suppressing myeloid cells[122,134].

Although the general role of YAP/TAZ in cancer is their pro-tumorigenicity as mentioned above, Pearson *et al.* have identified a novel tumor suppressor activity with YAP/TAZ activation[143]. Indeed, this binary role of YAP/TAZ activity is dependent on the type of cancer, where they act as tumor suppressors in neuroendocrine cancers such as retinoblastoma and small

cell lung cancer (SCLC). They further stratified the different cancer types to YAP^{ON} and YAP^{OFF} gene signatures, where YAP^{ON} signatures are associated to tumors in which YAP is pro-tumorigenic, and YAP^{OFF} signatures identify cancers where YAP is a tumor suppressor[143]. These signatures align with pharmaceutical, genetic, metabolic and adhesive profiles that can be core differentiators between YAP^{ON} and YAP^{OFF} cancers and can aid in identifying their characteristics to improve choices of therapy in the clinic[143,144].

3.2 Regulation of YAP/TAZ in cancer

It has been thought that YAP/TAZ activation and stabilization relies solely on HIPPO pathway inactivation. However, since the HIPPO pathway components are rarely mutated in tumors, the HIPPO tumor suppressor pathway curbs YAP/TAZ activation in normal tissues, but is not the sole regulator of the pro-tumorigenicity of YAP/TAZ activity[120,145]. In fact, more evidence have recently emerged that the upstream kinase LATS1/2, part of the HIPPO pathway, is only partly involved in YAP/TAZ oncogenic activities[146-152]. Also, inactivation of the HIPPO pathway components is insufficient for tumor induction in multiple organs such as breast, lung, kidney[120]. In most cancers, the regulation of YAP/TAZ is often linked with other cancer-related pathways such as G-protein coupled receptors (GPCRs), transforming growth factor beta (TGF-β) and WNT pathways[128]. Moreover, YAP activation is often linked to other pro-tumorigenic pathways such as phosphoinositide 3-kinase (PI3K) and 3-phosphoinositide-dependent protein kinase 1 (PDK1) that inhibit the HIPPO pathway[125]. However, studies have shown that in liver and intestine, HIPPO components are largely involved in tumor progression[120]. Due to this paradigm, Zanconato *et al.* suggest that the pro-tumorigenic activity of YAP/TAZ is due to HIPPO independent mechanisms or LATS1/2 activation depending on context[120].

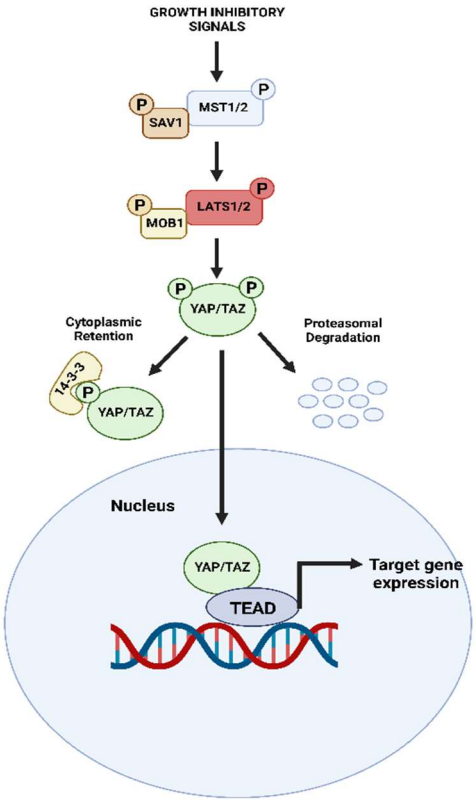

Figure 10 Regulation of YAP/TAZ. The core inhibitory kinases mammalian STE20-like protein kinase 1 (MST1) and MST2, and the large tumour suppressor 1 (LATS1) and LATS2, cooperate with salvador family WW domain-containing protein 1 (SAV1), MOB kinase activator 1A (MOB1A) and MOB1B to phosphorylate the transcriptional co-activators yes-associated protein (YAP) and its paralogue, transcriptional co-activator with PDZ-binding motif (TAZ), leading to inhibition of their transcriptional activity through 14-3-3-mediated cytoplasmic retention and priming them for ubiquitin-mediated proteasomal degradation. LATS1/2 may be phosphorylated by Neurofibromin 2 (NF2) as well as other yet unidentified kinases. Unphosphorylated YAP/TAZ are free to enter the nucleus and interact with the TEA domain family members (TEAD1–TEAD4) to activate genes implicated in cell survival and proliferation. Taken from[128].

YAP/TAZ are regulated by soluble extracellular factors, cell-cell adhesions and mechanotransduction[128]. Therefore, YAP/TAZ activity is highly dependent on cellular organization. In the highly proliferating tumor tissue, cells are often disorganized and require YAP/TAZ function to modulate cell-cell and cell-matrix interactions by producing secretory

proteins such as amphiregulin (AREG), cysteine-rich angiogenic inducer 61 (CYR61) and connective tissue growth factor (CTGF)[128]. Also, the importance of the extracellular matrix (ECM) for YAP/TAZ regulation have been shown in studies where cells grown on high ECM stiffness (mirroring tumor tissue microenvironment) have highly active YAP/TAZ as shown by their nuclear localization whereas those grown on low ECM stiffness have inactive YAP/TAZ localized in the cytoplasm[146,149]. GPCRs also regulate YAP/TAZ activity by activating RHO GTPase that inhibit LATS kinase activity. The leukemia inhibitory factor receptor (LIFR) and epidermal growth factor (EGF) also activate YAP/TAZ. Also, WNT, TGFβ and bone morphogenic protein (BMP) also activate YAP/TAZ[128]. Upon WNT activation, YAP/TAZ accumulate in the nucleus and β-catenin is stabilized[153]. TGFβ stimulates TAZ to bind to SMAD2/3-4 complexes and translocate to the nucleus to activate transcription programs[154].

3.3 YAP/TAZ as therapeutic targets

The intimate involvement of YAP/TAZ in various essential tumorigenic programs makes them an attractive target for therapy. Direct inhibition of YAP/TAZ is more plausible than targeting their multiple upstream regulators since they are regulated by various axes that increases their activation by feedback mechanisms. Verteporfin disrupts interactions between YAP/TAZ and TEAD thus inhibiting YAP/TAZ-induced transcription[155]. Its therapeutic potential has been shown on uveal melanoma cells and liver tumorigenesis[151,155]. A peptide-based mimic of vestigial-like family member 4 (VGLL4) which inhibits YAP-TEAD interaction has been developed and shown to inhibit tumor growth in models of gastric cancer[156]. However, this peptide requires further development[128,156]. Statins is a class of drugs that inhibit the mevalonate cholesterol biosynthetic pathway[157]. This pathway stimulates RHO-GTPase activity and YAP/TAZ nuclear localization[157,158]. Inhibition of RHO-mevalonate pathway had anti-proliferative effects in breast cancer cells[157]. In addition, clinical studies have found that statins negatively correlate with cancer occurrence and survival[159].

4 The ERK/MAPK signaling

4.1 Overview of the ERK/MAPK pathway

The mitogen-activated protein kinase (MAPK) cascades are essential signaling pathways that regulates diverse cellular and physiological processes such as cell proliferation, survival, growth, migration, immunity and stress responses[160-166]. These cascades can activate five main protein kinase axes, namely, the MAPK kinase kinase kinase (MAP4K), MAPK kinase kinase (MAP3K), MAPK kinase (MAPKK), MAPK and MAPK-activated protein kinases (MAPKAPK)[162]. Generally, MAPKs are kinases that are activated when phosphorylated at serine/threonine and tyrosine residues within the signature motif T—X—Y in the activation loop of the kinase[167,168]. Their effectors include transcription factors, MAPK-activated protein kinases (MAPKAP kinases), phosphatases, and other classes of proteins[161]. Important components of the

MAPK signaling pathway are the extracellular-regulated kinases ERK1/2 and ERK5, the p38 kinases and c-Jun N-terminal kinase (JNK) 1, 2, and 3[169]. Among those, the ERK signaling pathway plays a prominent role in cell division, growth and survival[170,171]. ERK1/2 is phosphorylated and activated downstream of several kinases in the MAP3K axis which constitutes Ras/Raf/ MAPK/ERK kinase (MEK) 1 and 2[161]. ERK1/2 can also be activated downstream of several MAPKAPKs (ribosomal s6 kinases, MAP kinase-interacting serine/threonine-protein kinases, mitogen- and stress-activated protein kinases and cytosolic phospholipase A2)[162]. The MAPK/ERK cascade plays an important role in cell growth, differentiation and proliferation. Thus, its disruption may lead to dire consequences in the cells

and ultimately in the body[162]. The ERK/MAPK signaling pathway is activated by growth factors, cytokines, viruses, G-protein-coupled receptor ligands and oncogenes[162]. Among the components of the ERK family, ERK 1 and 2 are the most important members in the MAPK/ERK cascade[162]. Upon their direct bispecific phosphorylation of Tyr and Thr residues in the 8 'TEY box' of the sub-functional region by MEK, activated ERK1/2 translocate to the nucleus[162]. Nuclear ERK1/2 activates a plethora of transcription factors that regulate essential cellular biological functions such as proliferation, survival and mobility[162]. Such target transcription factors include proto-oncogene c-Fos, proto-oncogene c-Jun, ETS domain-containing protein Elk-1, proto-oncogene c-Myc and cyclic AMP-dependent transcription factor ATF2 (Figure 8)[162]. However, cytoplasmic

ERK1/2 also has essential functions mainly implicated in negative feedback pathways, where it phosphorylates SOS, Raf1 and MEK[162].

Figure 8. The MAPK cascades. MAPKs are present in the cytoplasm and can be translocated to the nucleus. They phosphorylate and activate cytosolic proteins and nuclear transcription factors. MAPK, mitogen-activated protein kinase; MAP4K, MAPK kinase kinase

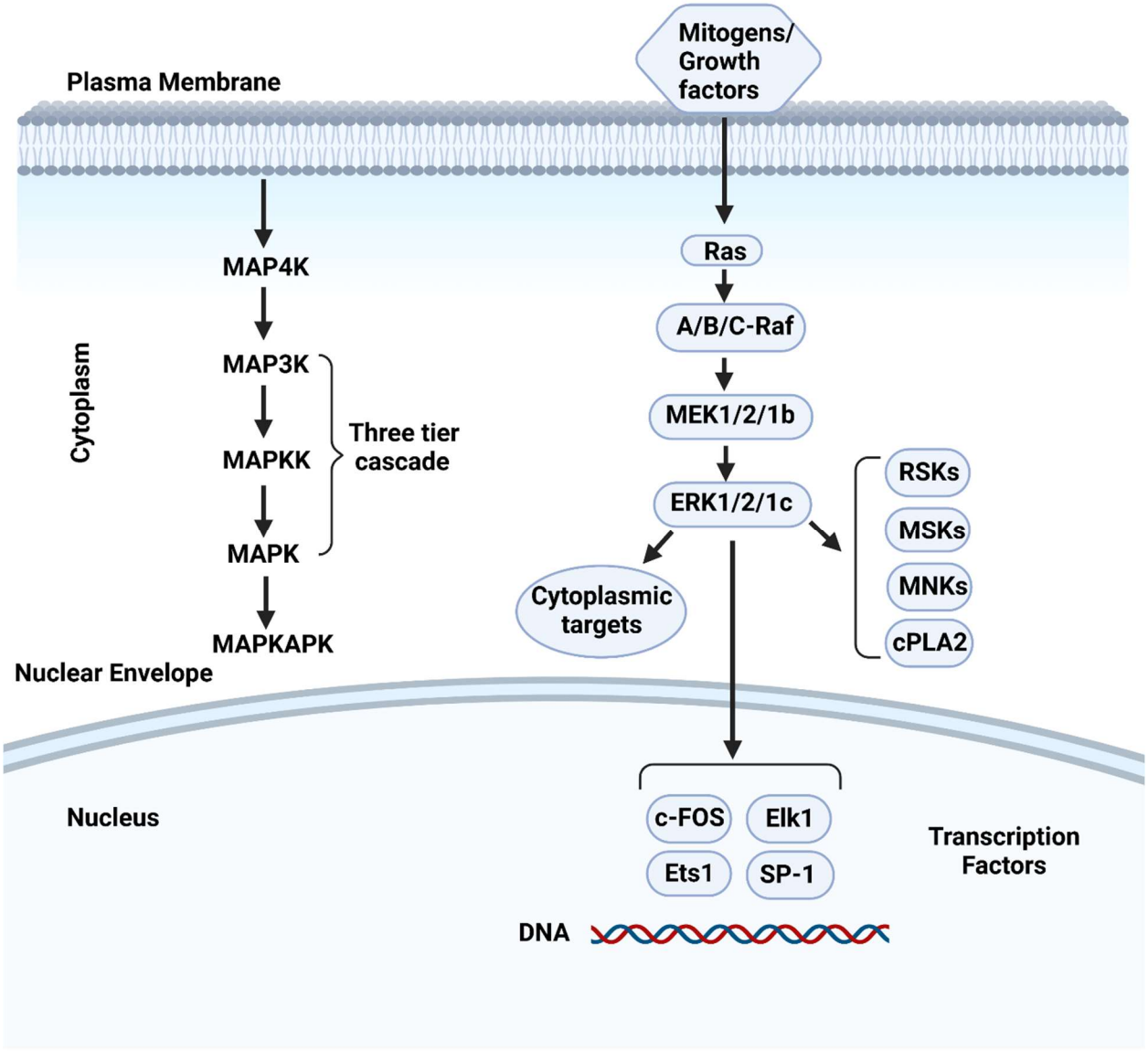

kinase; MAP3K, MAPK kinase kinase; MAPKK, MAPK kinase; MAPKAPK, mitogen-activated protein kinase-activated protein kinases; MEK, Ras/Raf/MAPK; RSK, ribosomal s6 kinase; MSK, mitogen- and stress-activated protein kinases; MNK, MAP kinase-interacting serine/threonine-protein kinases; cPLA2, cytosolic phospholipase A2; c-FOS, proto-oncogene c-

Fos; Elk1, ETS domain-containing protein Elk-1; Ets1, Protein C-ets-1; SP-1, transcription factor Sp1. Adapted from [162].

4.2 The ERK/MAPK pathway in cancer

In addition to neurological and developmental disorders, ERK/MAPK hyperactivation, specifically through Ras-ERK, triggers the development of most types of cancer[162]. Various human cancers, such as ovarian, colon, breast and lung cancer have high ERK expression[172-174]. Indeed, hyperactivation of ERK/MAPK activates transcription factors involved in cellular proliferation and differentiation, in addition to anti-apoptotic regulation, which are essential components of tumor development. ERK/MAPK regulates multiple pathways implicated in proliferation and anti-apoptosis such as regulating cell cycle proteins like G1/S specific cyclin D1[162]. Several studies have shown that MEK/ERK inhibition can inhibit proliferation and induce apoptosis in multiple cancer models[162].

Moreover, the ERK/MAPK pathway activates important factors that play a role in tumor invasion and metastasis[162]. Several studies have demonstrated the importance of having active ERK1/2 in successful metastasis and invasion of tumor cells[175]. For example, matrix metalloproteases (MMPs) are essential in invasion and metastasis due to their role in hydrolyzing the extracellular matrix[176]. MMP-2, MMP-7 and MMP-9 are activated downstream of ERK1/2 phosphorylation[177-180]. Therefore, therapeutically blocking the ERK/MAPK pathway would significantly reduce the invasion potential of migrating cancer cells. Another important hallmark of cancer that implicates ERK/MAPK pathway is angiogenesis[162]. ERK/MAPK can activate transcription factors that increase VEGF expression and promote vascularization[181-183]. ERK/MAPK can also inhibit thrombospondin-1 which promotes blood vessel formation[184]. Studies have shown that inhibiting ERK/MAPK signaling can inhibit tumor angiogenesis[182,183].

4.3 The dual specificity phosphatases (DUSPs) in the MAPK signaling pathway

The dual specificity phosphatases (DUSPs) and MAP kinase phosphatases (MKPs) negatively regulate MAPKs by de-phosphorylating either the threonine or the tyrosine or both

residues in the conserved signature T—Y—X motif in the activation loop of the kinase[185]. They share a common N-terminal domain but have a conserved C-terminal catalytic domain[167]. The family of DUSPs consists of ten subfamilies that are categorized into three groups depending on sequence homology, cellular localization and substrate specificity[185]. Group I composed of four inducible nuclear MKPs (DUSP1/MKP-1, DUSP2, DUSP4/MKP-2, and DUSP5). Group II composed of three ERK-specific MKPs (DUSP6/MKP-3, DUSP7/MKP-X, and DUSP9/MKP-4), and Group III composed of three MKPs that inactivate p38 and stress-activated JNK MAPKs (DUSP8, DUSP10/MKP-5, and DUSP16/MKP-7).

Among the DUSPs, DUSP6 is particularly interesting due to its dual role in oncogenesis, where it possesses tumor suppressive and pro-tumorigenic activities depending on context, although its phosphatase activity is exclusive to ERK[167]. DUSP6 has a tumor suppressive role in pancreatic cancer, non-small cell lung cancer, esophageal squamous cell and nasopharyngeal carcinoma, and ovarian cancer[167]. On the other hand, DUSP6 is oncogenic in human glioblastoma, thyroid carcinoma, breast cancer and acute myeloid carcinoma[167].

In the MAPK signaling pathway, DUSP6 is activated after interacting with ERK1/2 at dual threonine and tyrosine residues of the TEY motif[186]. The catalytic activity of DUSP6 requires the substrate binding of phosphothreonine and phosphotyrosine of ERK1/2 on its MAPK binding (MKB) domain. This binding causes a conformational change on the catalytic site of DUSP6 and enhances its phosphatase activity leading to ERK1/2 dephosphorylation[187]. When dephosphorylated, ERK1/2 disassembles from the MKB domain to its inactive state[187]. (Figure 9).

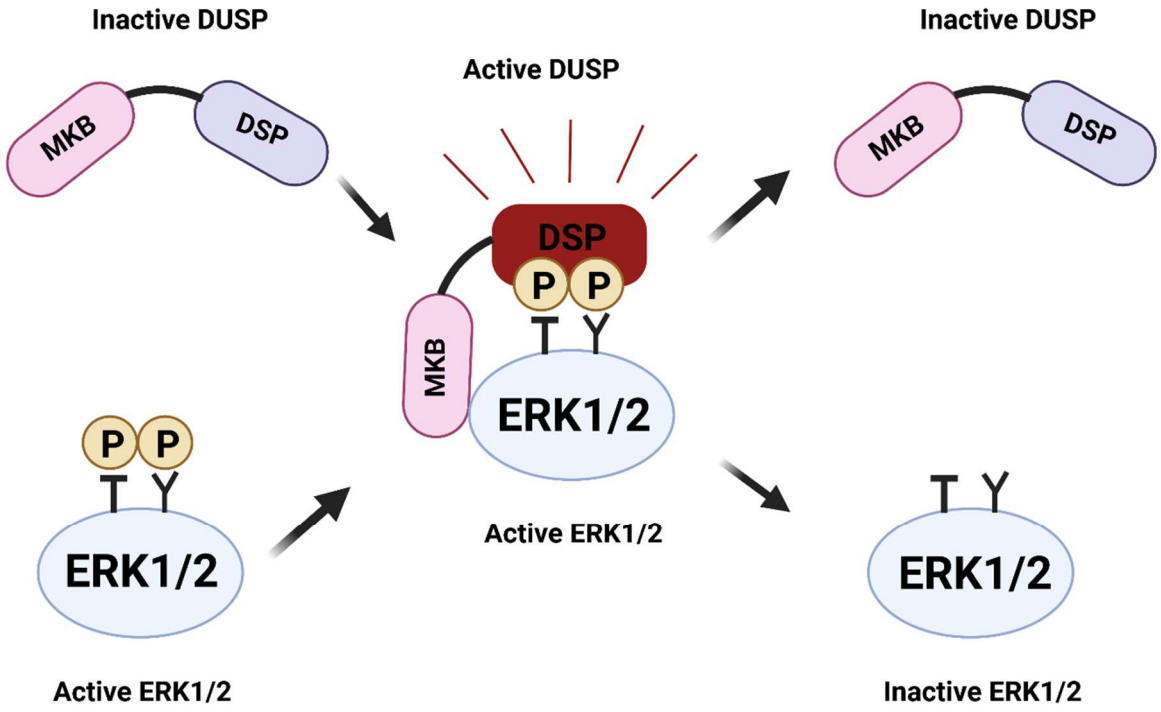

Figure 9. Inactivation of ERK1/2 by DUSPs. The MAPK binding domain (MKB) on DUSP interacts with active ERK1/2 to cause a conformational change on DUSP and activate its phosphatase activity. Binding of the dual specificity phosphatase catalytic domain (DSP) to its substrate ERK1/2 prompts its dephosphorylation and inactivation. Adapted from [187].

5 Overview of lung adenocarcinoma (LUAD)

The multi-layered complexity of cancer has not failed to reach almost every organ of the human body. The essence of this disease is conserved from one organ to the next, in its hyperproliferative capacity and uncontrolled evasion of cell death, but dramatic differences in each organ in terms of structure and function prevent the possibility of finding the "Magic Bullet" that can eradicate cancer, regardless of type and location. Advances in studying its capacity to strive revealed multiple hallmarks that define cancer's characteristic to utilize its

microenvironment to progress and metastasize[48]. Among all organs, the cancer of the lung is the deadliest and most frequent, with 2 million new cases and 1.76 million deaths per year[188]. Histologically, lung cancer is divided to Non-small cell lung cancer (NSCLC), which makes up 85% of the disease, and small-cell lung cancer (SCLC), which is 15% of the disease (Figure 5). SCLC usually arises near the bronchi and is caused by smoking. NSCLC is further sub-divided into three types based on where the cancer arises. Adenocarcinoma (LUAD) makes up 40% of lung cancer cases, arises in cells lining the alveoli and appears mostly in non-smokers. Squamous cell carcinoma makes up 30% of lung cancer cases and arises in flat cells lining the inside of the airways, near the bronchi and almost always appears in smokers. The fast-spreading large cell carcinoma makes up 15% of lung cancer cases and can appear anywhere in the lung[189,190]. We focus on LUAD in this study since it accounts for most lung cancer cases.

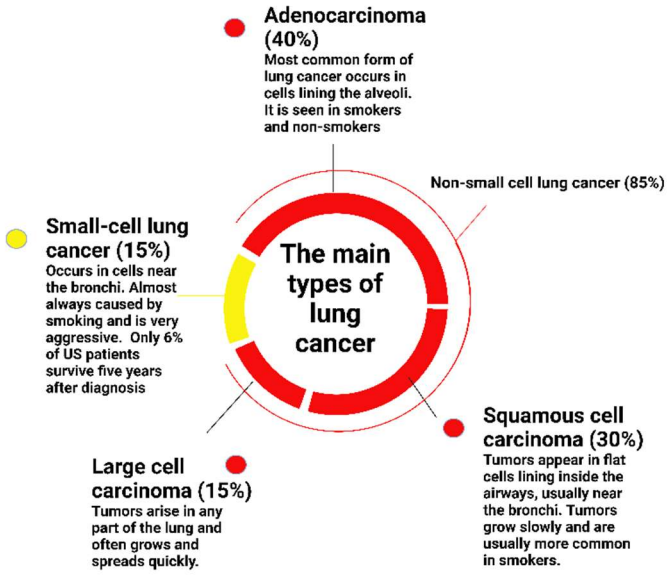

Figure 11 Types of Lung cancer. Depending on histological characteristics, lung cancer is divided to small cell lung cancer (SCLC, 15%) or non-small cell lung cancer (NSCLC, 85%). NSCLC is further subdivided based on location of neoplastic growth into large cell carcinoma, squamous cell carcinoma and adenocarcinoma. Adapted from[189].

5.1 Types (histological patterns/ classifications) and driver mutations of LUAD

Lung adenocarcinoma (LUAD) should be characterized and differentiated from other types of lung cancer since targetable genetic mutations in LUAD can be identified and drugs from their treatment can cause side effects in other types of cancer[191]. LUAD can be identified under the microscope by being poorly differentiated carcinoma, lacking glandular differentiation, and by expression of specific markers by immunohistochemistry (IHC) such as TTF-1 and/or Napsin A[191]. Adenocarcinoma is further classified depending on extent of invasiveness by the World Health Organization (WHO) into adenocarcinoma in situ (AIS, preinvasive lesion), minimally invasive adenocarcinoma (MIA) or (overt) invasive adenocarcinoma[191]. Of these, the disease-free survival of AIS and MIA after resurrection is 100%[192]. Invasive adenocarcinoma is further subdivided according to pattern into lepidic, papillary, acinar, micropapillary and solid adenocarcinoma[191,193]. Determining genetic alterations in LUAD is essential to improve targeted therapy[193]. Molecular profiling of LUAD revealed that somatic mutations mostly occur in the following genes; *TP53* (46%), *KRAS* (33%), *KEAP1* (17%), *STK11* (17%), *EGFR* (14%), *NF1* (11%), *BRAF* (10%), *SETD2* (9%), *RBM10* (8%), *MGA* (8%), *MET* (7%), *ARID1A* (7%), *PIK3CA* (7%), *SMARCA4* (6%), *RB1* (4%), *CDKN2A* (4%), *U2AF1* (3%), and *RIT1* (2%)[194]. Fusion events were also found in ROS1, RET, PRKCB, NTRK, MET and ALK genes[190]. However, 75% of lung adenocarcinoma genetic alterations promote the RTK/RAS/RAF signaling pathway, highlighting the importance of targeting this pathway[194].

5.2 KRAS mutations in LUAD

Among the 3 Rat sarcoma (RAS) genes (N-, K- and H-RAS), mutations in KRAS are the most frequent in cancer, especially in lung cancer[190,195]. RAS genes encode GTPases that cycle between a GTP-active and a GDP-inactive form and are activated in response to extracellular cues to induce intracellular transduction pathways[196]. Activation usually takes place via receptor tyrosine kinases (RTKs) such as EGFR, ALK or MET that promote the GEF activity of SOS1 and SOS2 to replace GDP with the more abundant GTP[196]. As a result, the RAF family of kinase is recruited and downstream intracellular pathways are activated such as the mitogen-activated

protein kinase (MAPK) pathway and PtdIns 3-kinase (PI3K)-Akt pathway, which are essential for proliferation and survival of cells[196]. In contrast, GTPase activating proteins (GAPs) increase hydrolysis of GTP, switching KRAS to a GDP-bound off state (Figure 6)[197]. In lung adenocarcinoma (LUAD), missense mutations of KRAS are found in codons 12 and 13 of exon 2 (G12C > G12V > G12D > G13C > G13D) and codon 61 (Q61H > Q61L > Q61R)[190,196,198] (Figure 7). Mutated KRAS has more affinity to bind GTP, thus causing an amplification of its effector pro-oncogenic pathways such as PI3K-Akt and MAPK pathway[190]. In LUAD patients, KRAS mutations are often co-occurrent with the following mutations; P53 (41%), STK11 (28%), KEAP1 (24%), RBM10 (16%), and PTPRD (15%)[199,200]. Mutant KRAS has been considered undruggable for decades, however, recent advances have developed specific inhibitors for KRAS, specifically for KRAS G12C, which is the most mutated form in LUAD.

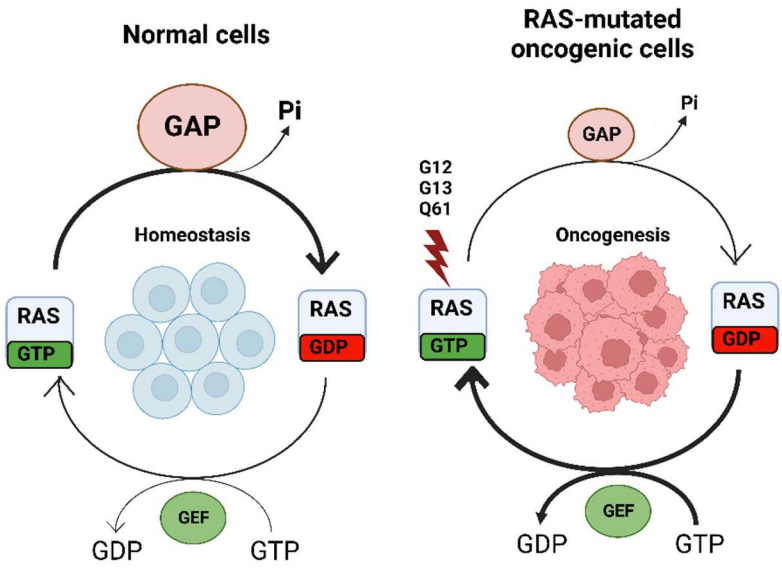

Figure 12. RAS mutations disrupt homeostasis and drive oncogenesis. RAS proteins are essential for achieving homeostasis and normally cycle between a GTP-bound active and a GDP-bound inactive state. GTPase Activating Proteins (GAPs) increase intrinsic GTP hydrolysis activity of RAS, while Guanine Exchange Factors (GEFs) facilitate binding of GTP. Mutations

in RAS prevents van der Waals interactions between RAS and GAP, hence favoring RAS in a GTP-bound active form. Adapted from[201] .

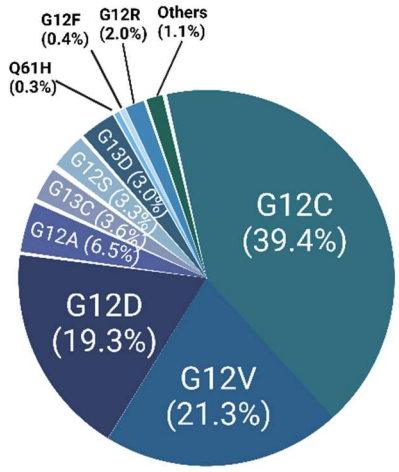

Figure 13 KRAS mutations and their frequency in human LUAD. Adapted from [196].

5.3 Genetically engineered mouse model to study KRAS LUAD

Recapitulating KRAS LUAD in mice has been feasible using the Lox-Stop-Lox conditional LSL-KRAS mutations genetically engineered mouse model[202,203]. Upon targeting alveolar type 2 (AT2) cells using Lenti- or Adenoviruses expressing Cre-recombinase, mutant KRAS is activated leading to tumor progression to adenoma. Lung tumor progression to adenocarcinoma requires the concomitant mutation of TP53 tumor suppressor[204]. Indeed, p53 deficiency adds an additional layer of genomic instability that drives malignant progression and metastasis. This can be achieved either by breeding LSL-KRAS mutant mice with lox/loxp53 mice or by delivering shRNA p53 along with the Cre-expressing lenti- or adenoviruses[205]. LSL-KRAS mutation mouse models can also be combined with LKB1/STK11 mutant or deficient mouse models[206]. These models mirror human LUAD progression at the histopathological level[202,207]. Therefore, they have contributed immensely to understanding the biological

implications of KRAS LUAD progression, in addition to therapeutic potentials in this disease. However, mutation burden of the mouse KRAS-driven LUADs differ from the human counterparts, where simpler mutations take place in the mouse model[208].

5.4 Targeting the MAPK pathway in KRAS mutated LUAD

The MAPK signaling cascade involves the activation of the first KRAS effector RAF, followed by stimulation of the dual kinases MEK1/2, leading to phosphorylation and activation of ERK1/2 kinases. Activated ERK1/2 translocate to the nucleus to activate transcription factors that function in proliferation, differentiation and survival of cells in a highly context-dependent manner (Figure 10)[170,209]. It is then certain that hyperactivation of the MAPK pathway by KRAS mutations would lead to continuous amplification of effector processes that lead to tumor progression, making it an attractive therapeutic target[162]. Before the advent of KRAS G12C inhibitors, the pharmaceutical industry has focused immensely on the production of inhibitors of the MAPK pathway. This is due to the high proliferative capacity that this effector pathway provides in KRAS tumors. These included inhibitors against Raf, MEK and ERK kinases [210,211]. However, these inhibitors were unsuccessful for the treatment of KRAS tumors, with the main reason being the intolerable toxicities generated by these inhibitors [196]. The high toxicities are mainly due to the importance of the activity of these kinases in regulating homeostasis in normal cells [212].

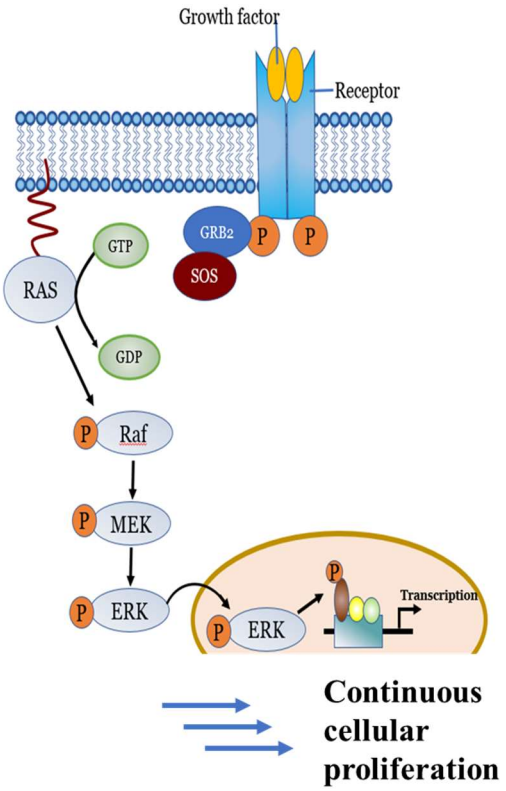

Figure 10 KRAS mutations amplify the MAPK pathway. The constant presence of KRAS in its GTP-bound form hyperactivates the MAPK pathway, leading to continuous cellular proliferation.

5.5 Current therapies implemented in LUAD

Therapies in LUAD are applied based on the stage of the cancer, type of expressed biomarkers and type of mutations driving the cancer. Historical or conventional therapy is defined by chemotherapy and platinum-based therapies. Targeted therapies have appeared after molecular profiling and identifying somatic mutations that confer sensitivity to tyrosine kinase inhibitors (TKIs) such as EGFR and ALK targeted therapies, as well as angiogenesis inhibitors (bevacizumab). These are also used as biomarkers to predict the response to TKIs. Despite the success of targeted therapies, resistance to TKIs eventually develops in three ways; (i) the targeted gene amplifies or mutates to disrupt specific binding of the drug, (ii) off-targeted resistance by overamplification of the effector pathways through alternative activators, (iii) phenotypic transformation from NSCLC to SCLC. To overcome resistance and increase durability of TKIs, combination with chemotherapy or immune checkpoint inhibitors is often

implemented and has shown to increase survival in clinical trials. The recent development of KRAS G12C inhibitors have brought promise to targeting the undruggable KRAS in LUAD. The presence of a unique pocket in KRAS G12C led to the development of inhibitors that can bind to that pocket and lock KRAS in its inactive GDP-bound form[213]. Clinical trials have shown that patients with KRAS G12C-driven LUAD are 30-50% responsive to KRAS inhibitors. Trials combining KRAS G12C inhibitors with other therapies such as immune checkpoint inhibitors and SHP2 inhibitors are underway[214].

Immunotherapy has been a promising therapeutic strategy in cancer. The ability of cancer cells to hijack the immune system can be overcome by the recent advent of immune checkpoint inhibitors (ICIs). The programmed cell death 1 receptor (PD-1)/programmed cell death ligand 1 (PD-L1) pathway and the cytotoxic T-lymphocyte-associated protein 4 (CTLA-4) pathway constitute the well-known brake system of the immune system[215]. The clinical success of immune checkpoint inhibitors (ICIs) that target CTLA4 and the PD1 axis allowed them to enter the realm of standard of care for lung cancer patients and has advanced the treatment of patients with NSCLC. CTLA4 is expressed on CD4+ and CD8+ T lymphocytes and inhibits T cell activation. PD-1, expressed on T-, B- and NK cells, and PD-L1 expressed on tumor cells negatively modulate the immune response. Anti-CTLA4, anti-PD1 and anti-PDL-1 antibodies are implemented based on histological classifications of the tumor as well as expression of the biomarkers[188]. As single-agents, anti-PD1 and anti-PD-L1 have greatly improved patient-survival compared to second-line chemotherapy and platinum-doublet chemotherapy[188]. In NSCLC, the expression of PD-L1 on the tumors is used as a predictive biomarker for anti-PD-1 and anti-PDL-1 therapies, where they can be used as a first-line of treatment in patients whose tumors express greater than or equal to 50% of PD-L1 (for pembrolizumab and atezolizumab) or for tumors expressing greater than or equal to 1% PD-L1 (for ipilimumab and nivolumab)[188]. ICIs have also had superior results in combination with chemotherapy, where median overall survival was improved in combination treatments compared in chemotherapy alone, regardless of PD-L1 expression level[190,216]. Although single-agent anti-PD-1 and anti-PD-L1 therapies are ineffective in oncogene-driven NSCLC, combination strategies with targeted therapy are currently under clinical studies and depend on the type of oncogenic driver[190,216]. Immune-mediated toxicities are inevitable but lower in incidence than chemotherapy, with 3-6% of patients with NSCLC experiencing adverse effects with PD-1 and PD-L1 inhibitors[190,216].

The first step is identifying the stage of the cancer[190]. Since stage I and stage II LUAD is considered resectable, surgery would be the best option for these cancers[190]. Otherwise, stereotactic body radiotherapy (SBRT) would be implemented for unresectable tumors[190]. Ongoing studies on unresectable stage I and II LUAD are investigating neoadjuvant therapy with or without chemotherapy followed by surgery[190]. Patients with unresectable stage III LUAD are mostly treated with chemoradiotherapy and adjuvant PD-L1 inhibitors[190,216].

5.6 The role of YAP/TAZ activation in KRAS lung cancer

Several studies have shown the importance of YAP/TAZ activation not only in tumor progression but also in tumor malignancy and metastasis in lung adenocarcinoma[131,217,218]. In a mouse model of $KRAS^{G12D}$ and p53 loss-driven LUAD, KRAS mutations did not cause YAP activation, but YAP was required for tumor progression[217]. KRAS-driven tumors can even develop a dependency on YAP activation that can bypass KRAS addiction[129]. Furthermore, studies in LUAD mouse models revealed that YAP inhibition suppresses brain metastasis[219,220]. Indeed, YAP1 even cooperates with KRAS to drive a mesenchymal state and lead to poor patient survival[221]. The mentioned YAP-induced pro-tumorigenic programs give rise to resilient LUAD cells that can resist therapy and thus rescue the cells from RAS suppression[221]. YAP activation confers resistance in KRAS and EGFR-driven cancer cells against MEK/RAF inhibitors[141].

5.7 Lineage plasticity in KRAS LUAD

Intra-tumoral heterogeneity is an essential component in the complexity of cancer. The cancer cell of origin propagates and differentiates to give rise to multiple clusters in the tumor tissue, each acquiring different transcriptional programs that may attribute to proliferation, stemness and malignancy[222]. Accordingly, the reliance of each cluster on different tumorigenic programs provides an escape for tumors from therapeutic targets. Cancer cells are constantly under physiological and oncogenic stress[222,223]. As a result, cells activate differentiation programs that can alter their fate or identity; a phenomenon known as cell plasticity that has been recently added as a hallmark of cancer. Delineating the multiple clusters that generate intra-tumor heterogeneity might provide further knowledge in tumor biology, leading to improvements in current therapy. The advent of single-cell RNA sequencing (scRNA-seq) permitted the dissection of such plasticity. Specifically, scRNA-seq studies on the LUAD mouse model driven

by active KRAS G12D and loss of TP53 (KP model) revealed that cancer cells can acquire highly plastic transcriptional programs that can drive tumor progression and malignancy[204,224,225]. Importantly, such plasticity is also seen in human LUAD with critical clinical correlations. Specifically, cancer cells diverge from their initial AT2-like subtype by acquiring a set of differentiation transcriptional programs leading to diverse lineages, including an EMT-specific lineage[204,222,225]. In an effort to uncover the drivers of lineage heterogeneity, LaFave *et al.* found that NKX2.1, a driver of lung differentiation, is lost as cancer cells progresses from AT2-like to EMT phenotype[224]. In addition, mediators of EMT such as the SOX2 and RUNX family proteins are more activated as the tumor differentiates and RUNX2 can be an active marker for highly plastic cells[224]. Marjanovic *et al*. identified a highly mixed program termed the high plasticity cell state (HPCS) that gives rise to different cell states[204]. They pinpoint the expression of TIGIT as a marker of this state. The highly plastic signature in both studies has a higher potential for proliferation, metastasis, and drug resistance. In a more recent finding, Yang *et al*. added an extra layer of understanding to the biological nature of lineage plasticity in KRAS-driven LUAD by continuous lineage tracing of tumors developed in the KP model to track tumor evolution from the cancer cell of origin to metastasis[225]. They identified specific evolutionary trajectories based on a transcriptional "Fitness Score", with the lowest score being the AT2-like subtype, then Gastric-like, Lung mixed and finally the mesenchymal states with the highest score[225]. Furthermore, they reveal that tumor evolution from the primary AT2-like cell types proceeds in two fates; either through a Gastric-like transcriptional program or through the lung mixed state, to eventually reach a third fate cluster which is the aggressive EMT cluster[225] (Figure 11) The importance of identifying and studying the mechanisms of cancer cell plasticity lies in providing further understanding of tumor biology coupled with potential therapeutic targeting of potential drivers of plasticity.

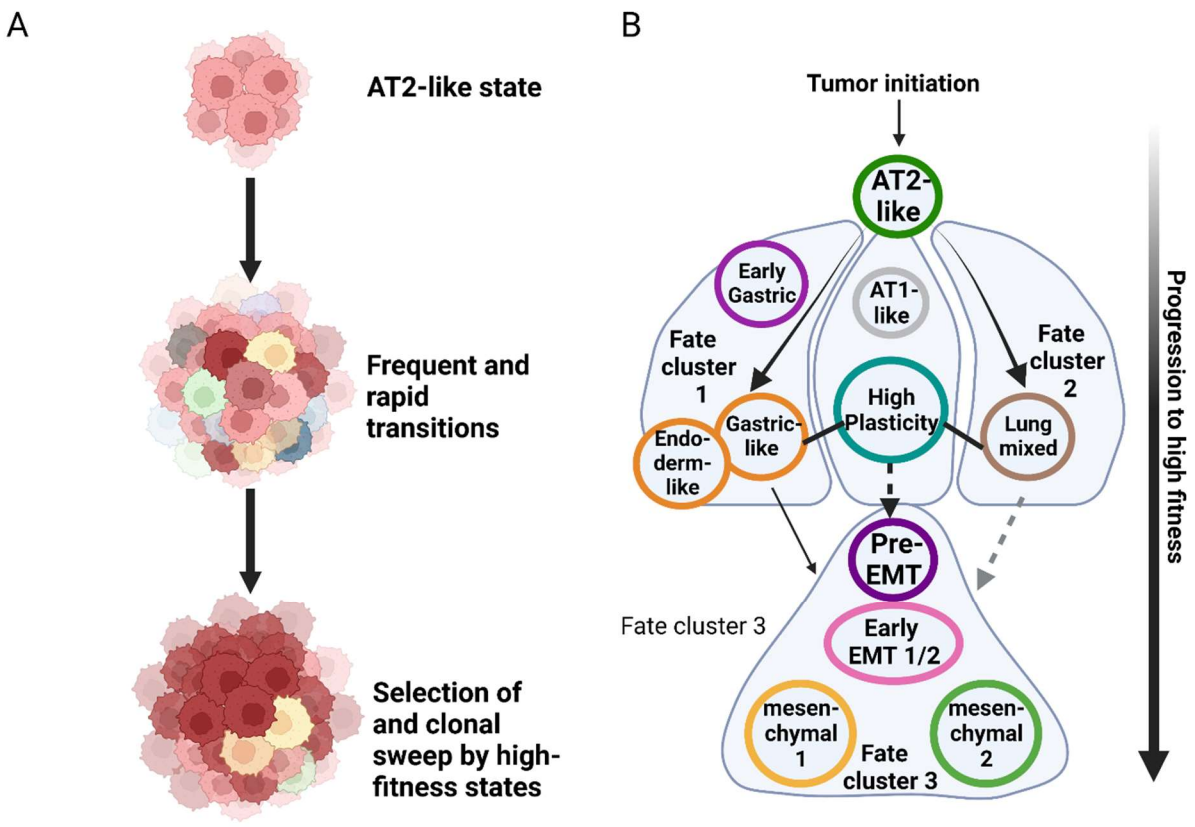

Figure 11 Tumor evolution during KRAS-driven LUAD progression. (A) Description of evolution of intra-tumoral transcriptional heterogeneity and plasticity during tumor progression. (B) Summary of the three major Fate Clusters partaken during tumor evolution. Taken from [225].

6. Rationale, study design and hypothesis

6.1 Rationale

Herein, we aimed to characterize the role of the ISR in KRAS-driven LUAD progression to validate its potential as a therapeutic target of the disease. RAS mutations induce PERK-eIF2αP arm in mouse embryonic fibroblast-transformed cells[226]. Therefore, we reasoned that RAS mutations employ this adaptive arm to accommodate to constant insults of stress imposed on tumor cells during cancer development.

6.2 Study design

We employed transgenic mice to recapitulate KRAS-mutated LUAD with a conditional mutation of p-eIF2α. Specifically we crossed KRAS$^{+/LSL\text{-}KRAS\ G12D}$ mice bearing a loxP-STOP-LoxP (LSL)-*KRAS G12D* allele, which is conditionally activated in the lungs by viral vectors expressing CRE recombinase with mice containing either a conditional homozygous S51A mutation of *eIF2S1* allele (fTg/0;eIF2α$^{A/A}$) or wild type *eIF2S1* (fTg/0;eIF2α$^{S/S}$)[202,227]. We induced lung tumor formation by infection with lentiviruses expressing CRE under the control of carbonic anhydrase 2 promoter[205], which is active in type I and II alveolar epithelial lung cells[228]. The CRE lentiviruses also produced TP53 shRNA from an U6/H1 promoter to accelerate lung tumor formation (Figure 12) [205,229].

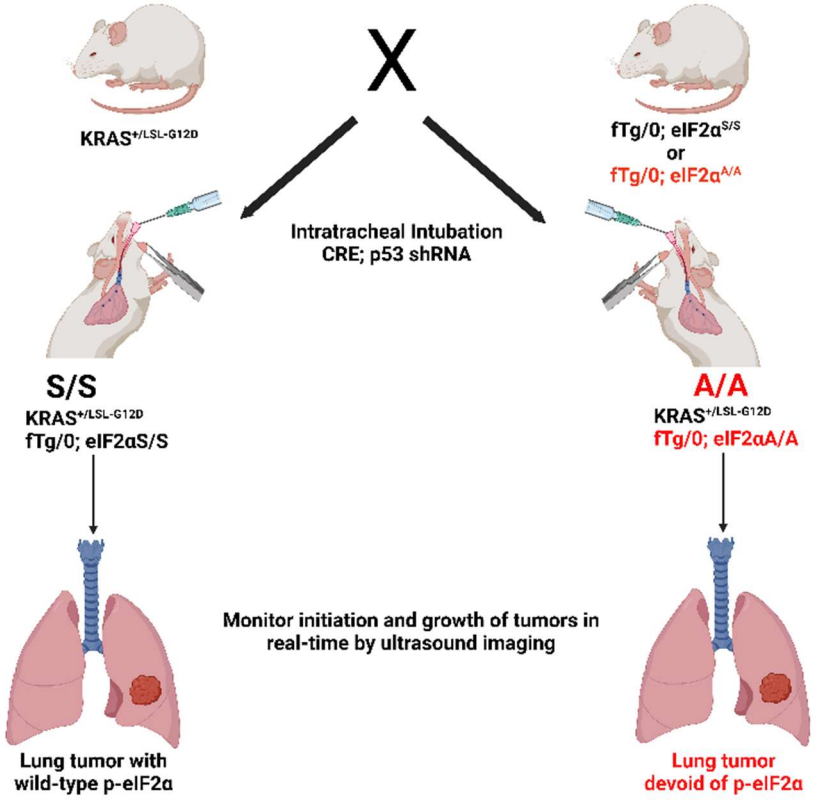

Figure 12. Mouse mating scheme. KRAS+/LSL-G12D mice containing a latent CRE-loxP KRAS G12D allele were crossed with either fTg/0;eIF2α$^{S/S}$ or fTg/0;eIF2α$^{A/A}$ mice. The

offspring mice were subjected to intra-tracheal intubation of CRE-expressing lentiviruses and TP53 shRNA. Adapted from[229] .

6.3 Hypothesis

6.3.1 The role of eIF2α phosphorylation in KRAS-lung cancer

Induction of the ISR in response to oncogenic stress can either lead to increased cell survival and continuous cellular proliferation, or to increased cell death. How the ISR determines cell fate decisions in KRAS lung cancer remains unclear. Studies have shown that ISR activation is required for the proliferative capacity of lung tumors and has a cytoprotective property in drug-treated lung cancer[230-236]. For example, oncogenic KRAS employs ATF4 to regulate amino acid homeostasis as a response to nutrient stress[236]. Furthermore, Albert *et al.* show that ATF4 is activated across multiple stages and molecular subtypes of human lung adenocarcinoma[235]. Further evidence for the role of p-eIF2α in KRAS lung cancer progression can be answered using a genetically engineered mouse model of KRAS-induced lung cancer, as explained above. We suggest that p-eIF2α is required for successful progression of KRAS lung cancer.

6.3.1.1 Objectives

1- Delineate the role of p-eIF2α in the mouse KRAS-LUAD model by monitoring lung cancer progression in mice in the presence ($eIF2\alpha^{S/S}$) or absence ($eIF2\alpha^{A/A}$) of eIF2α phosphorylation using ultrasound imaging.

2- Generate primary cell lines of the mouse model.

3- Determine the main molecular mechanism in the observed phenotype.

4- Verify the role of p-eIF2α in human KRAS LUAD.

5- Ensure the clinical relevance of the observed results by assessing possible drug targets.

6.3.2 Regulation of YAP/TAZ by eIF2α phosphorylation in KRAS lung cancer

Wu *et al.* show that YAP is activated downstream of the PERK-eIF2α axis in hepatocellular carcinoma[237]. Due to the importance of YAP/TAZ activity in non-small cell lung cancer progression, prognosis and therapy[238], it would be reasonable to identify a possible connection between eIF2α-P and YAP/TAZ activity in KRAS lung cancer. The importance of this study is highlighted by the absence of a promising therapeutic target of YAP/TAZ.

6.3.2.1 Objectives

1- Examine the subcellular localization of YAP/TAZ in lung sections of mouse KRAS LUAD in the presence ($eIF2\alpha^{S/S}$) or absence ($eIF2\alpha^{A/A}$) of eIF2α phosphorylation by IHC staining.

2- Determine the importance of YAP/TAZ activity in the phenotype observed.

3- Explore the possibility of therapeutically targeting YAP/TAZ using p-eIF2α drug targets.

6.3.3 The importance of eIF2α phosphorylation in KRAS lung cancer evolution

Recently, several studies have provided insight into subclonal diversity that arises during lung cancer progression in the genetically engineered KRAS lung adenocarcinoma mouse model by the advent of scRNA sequencing[204,223-225]. Particularly, Marjanovic *et al.* highlight the emergence of a high plasticity cell state (HPCS) cluster during lung cancer evolution that is essential to generate aggressive clusters that lead to EMT and resistance to therapy[204]. The ISR has been found to drive breast cancer plasticity leading to retention of a stem-cell-like phenotype[239]. Thus, we hypothesize that eIF2α phosphorylation drives the emergence of HPCS in KRAS lung cancer.

6.3.3.1 Objectives

1- Isolate eIF2α$^{S/S}$ and eIF2α$^{A/A}$ tumor cells and subject them to scRNA seq

2- Dissect the transcriptional signatures of the various clusters that arise during lung cancer progression.

3- Identify potential biomarkers of HPCS and verify their regulation by eIF2α phosphorylation by comparing eIF2α$^{S/S}$ and eIF2α$^{A/A}$ lung tumor sections.

4- Verify the observed results in human lung cancer background.

5- Determine the effect of therapeutically targeting p-eIF2α on clonal diversity.

Chapter 2

Materials and Methods

1. Mouse models

1.1 Transgenic mice

To elucidate the role of p-eIF2α in lung cancer progression, tumor growth has to be compared between cells having a wild-type p-eIF2α and those lacking it. This can be done by using mouse models having a point mutation on the eIF2α allele that can hinder the phosphorylation on this site. Specifically, mice have been engineered where Serine is switched to Alanine on Serine 51 of eIF2α, which is the site of phosphorylation that leads to functional ISR activation[227]. However, the importance of phosphorylation of eIF2α at Serine 51 was unveiled when mice bearing a homozygous mutation of eIF2αS51A died shortly after birth[227]. The cause of the early onset of death was correlated to hypoglycemia associated with defective gluconeogenesis, in addition to deficiency in pancreatic β-cells[227]. The observations revealed the importance of p-eIF2α in metabolic homeostasis[227]. However, the advent of LoxP-flanked genes can overcome this hurdle. For our model, we used homozygous eIF2α Serine 51 to Alanine (ftg/0;eIF2α$^{A/A}$) mice whose lethality was rescued by the LoxP-flanked eIF2α transgene. The transgene also expressed green fluorescent protein (EGFP) upon Cre recombinase-mediated deletion of eIF2α. An adequate ftg/0;eIF2α$^{S/S}$ wild-type control was also used in our studies. To study the role of p-eIF2α in KRAS-driven lung cancer, we crossed the ftg/0;eIF2α$^{A/A}$ and the ftg/0;eIF2α$^{S/S}$ mice with mice bearing a LoxP-STOP-LoxP (LSL)-KRAS G12D allele which is conditionally activated by viral vectors having CRE recombinase, under the control of carbonic anhydrase 2 promoter. By intratracheally injecting the CRE-bearing viruses in the lungs of mice, alveolar type 1 and type 2 lung cells are infected since they exclusively express carbonic anhydrase 2. As a result, only the infected alveolar cells in ftg/0;eIF2α$^{A/A}$ mice would lack the phosphorylation of eIF2α and thus KRAS lung tumor progression would proceed in the absence of the phosphorylation. In addition, the CRE lentiviruses also had an shRNA for TP53 to accelerate lung tumor progression. Indeed, lung cancer mouse models with KRAS mutations and loss of p53 were the most reminiscent of advanced human lung adenocarcinoma.

1.2 KRAS LUAD PDX in nude mice.

A KRAS G12C lung adenocarcinoma patient derived xenograft (PDX) donor mouse was purchased from Jackson Laboratories (Tumor ID: TM00186 - LG0481F Lung). When tumor volume of the initial PDX reached 1000 mm^3, the PDX was initially passed to 5 mice to achieve enough PDX material for the experimental design. The plan was to see whether the small molecule inhibitor ISRIB had effects on KRAS LUAD PDXs. For passing the PDX, the tumor was carefully excised from the mouse and incubated with ice-cold FBS. The tumor was then cut into small pieces, around 3-5 mm per cubed side, for preparation cryo-preserved samples which were prepared by incorporation into cell freezing solution (90% FBS, 10% DMSO). The rest of the tumor was passaged subcutaneously into mice with two tumors on each flank. For the surgery, the mice were put to deep sleep by isoflurane. A small excision was carefully performed at the flank side of the mouse. The tumor was chopped into small pieces and diluted with FBS. Around 0.5 mL of the tumor+FBS mixture was injected into the excised flank using a Trochar needle. For the preclinical PDX study, mice were injected daily with either vehicle or 10 mg/kg ISRIB by oral gavage. Tumors were measured twice per week until they reached ~ 2 cm in diameter.

1.3 Intratracheal orthotopic transplantation of LLC cells in lungs of mice.

Healthy Lewis Lung Carcinoma (LLC) cells were at 80% confluency. 2 x 10^5 cells were diluted in ice-cold PBS at a 1:1 ratio. Cells were then intratracheally injected into C57/BL6 mice. Tumors should start forming within 10 days of injection. Mice were randomized to 6 per group of the following treatments: Vehicle, ISRIB alone, PERK inhibitor (GSK 2606414) alone, ISRIB + AMG510 (KRAS G12C covalent inhibitor), and PERK inhibitor + AMG510. Injections were done daily by oral gavage and tumors were monitored and quantified weekly.

1.4 Monitoring lung tumor progression in real time via ultrasound imaging.

Lung tumor initiation in mice can be detected by ultrasound imaging via the formation of B-lines, reflected by white lines traversing the screen on the ultrasonograph[240]. These can be counted and quantified per mouse. Tumor progression can be also quantified by measurement of the volume of tumors in the ultrasonograph[240].

1.5 Isolation of tumor cells from lungs of mice for sc-RNA seq.

When tumors have reached an appropriate volume and after sacrificing the mice, perfuse the lungs with SMEM (or RPMI) and immediately place the lungs on a petri-dish on ice with 500 uL of digestion solution (DS) (0.6 U/mL of Dispase ll [Gibco, catalog #17105-041; stock=50 U/mL], 0.166 U/mL of Collagenase lV [Thermofisher Scientific, catalog #17104019; stock= 50U/mL], 10 U/mL of DNase I [Sigma-Aldrich, catalog # 69182-3; stock=1U/uL]). The lung was chopped into very small pieces using autoclaved blade, 1 mL extra of DS was used for the process. Transfer the chopped lung into a 15 mL conical tube containing 5 mL of DS after precoating the tube with 0.05% BSA in PBS. The tube was incubated with rotation in 37ºC rotating oven for 30 minutes – one hour. The mixture was strained through 100um cell strainer into 50 mL conical tube and wash with ~ 15 mL of ice-cold 2% FBS in SMEM (or RPMI). The cells were pushed through the strainer mesh using a plunger. The cells were spun down for 5 minutes at 1500 rpm. Supernatant was removed and cells resuspended with 1 mL of ice-cold SMEM (or RPMI) +2% FBS. 10 mL of ACK (Amonium-Chloride-Potassium) lysing buffer [ThermoFisher Scientific, catalog # A1049201] was added for the lysing of red blood cells and incubate for 1 minute. The reaction was stopped by adding 15 mL of ice-cold SMEM (or RPMI) + 2% FBS. The mixture was strained through 40 um strainer (use plunger) and spun down for 5 minutes at 300G at 4ºC. The pellet was washed 2 times with ice-cold PBS + 2% FBS. The appropriate number of cells was aliquoted in 100 µL FACS buffer (PBS + 2% FBS + 2 mM EDTA) for staining and incubated with the appropriate stains for 20 minutes in the fridge. The pellet was washed 2 times with 1000 uL of PBS + 2% FBS, resuspended with 250 uL of FACS buffer and passed through 70 µm strainer. For staining, the cells were stained with 1:250 EpCAM stain, 1:400 CD45, 1:250 anti-mouse Lineage cocktail stain (anti-mouse CD3ε, clone 145-2C11; anti-mouse Ly-6G/Ly-6C, clone RB6-8C5; anti-mouse CD11b, clone M1/70; anti-mouse CD45R/B220, clone RA3-6B2; anti-mouse TER-110/ Erythroid cells, clone Ter-119) and 1:10000 DAPI (2 mM stock).

1.6 Drug treatments in mice by oral gavage.

ISRIB and PERK inhibitor (GSK2606414) were suspended in a solution of Hydroxymethyl propyl cellulose (0.5% in water) and 0.1% Tween 80, pH= 4, at indicated concentrations.

1.7 Urethane and KRAS G12D induced lung tumorigenesis

Four-week-old male and female C57BL/6 mice, which were either proficient (eIF2α$^{S/S}$; n=10) or haplo-insufficient for p-eIF2 (eIF2α$^{S/A}$; n=12)[241] were subjected to a single intraperitoneal injection of urethane (Sigma) at 1 g/kg in pups between 21 and 28 days old[242]. After 40 weeks of urethane induction, mice were sacrificed and macroscopic tumors were visualized.

2. Cell culture and treatments

2.1 Generation of primary cell culture from mouse lung cancer cells.

Lung lobes were chopped into ~1 mm^3 pieces after lung perfusion, incubated in DMEM media + 1 mg/mL collagenase in digestion solution at 37ºC in rotating oven for 2 hours. Cells were centrifuged at 200*xg* for 3 minutes, washed 3 times with ice-cold PBS, and incubated with 2 mL of Trypsin EDTA solution [Life Technologies] for 5 minutes at 37ºC. The pellet was resuspended in appropriate media: RPMI with 10% FBS, 1% penicillin/streptomycin, 1X essential amino acids (50X stock, Life Technologies), 1X non-essential amino acids (100X stock, Life Technologies) and 0.075% of sodium bicarbonate. After proper development of tumor cells, eIF2α$^{S/S}$ and eIF2α$^{A/A}$ GFP positive cells were sorted by FACS.

2.2 Cell lines and treatments

"H358, H23, H1299, H1703, and LLC were maintained in RPMI 1640 medium (Wisent) supplemented with 10% fetal bovine serum (FBS, Wisent) and 1% antibiotics (penicillin/streptomycin, 100 units/mL; Life Technologies). H1299 cells were engineered to overexpress WT KRAS 4B, KRAS 4B G12C, KRAS 4B G12V, and KRAS 4B G12D by the transfection of PCDNA3.1 plasmids bearing the *KRAS* 4B cDNAs and selection in 500 ug/ml G418 (Gibco)[243-245]. The inserted cDNAs were verified by Sanger sequencing. The functionality of mutated *KRAS* cDNAs was determined by analyzing downstream signaling pathways (i.e., ERK phosphorylation) as well as by determining the interaction of KRAS proteins with BRAF using NanoBRET KRAS/BRAF Interaction Assay (Promega) or by using the KRAS Activation Assay Kit (Cell Biolabs, San Diego, CA). H1703 cells overexpressing either green fluorescence protein (GFP)-WT KRAS or GFP- KRAS G12C were established by infection with retroviruses expressing the GFP tagged *KRAS* 4B cDNAs[246]. Primary KRAS G12D eIF2α$^{S/S}$ and

eIF2α$^{A/A}$ lung tumor cells were isolated from mice at 20 weeks of lung tumor formation. Mouse lung lobes were washed with ice-cold sterile phosphate-buffered saline (PBS), chopped into ~1 mm^3 pieces, and incubated with 1 mg/mL collagenase in serum-free DMEM media 2 h at 37 °C under continuous rotation. The homogenate was centrifuged at 200 × *g* for 3 min, the pellet was washed three times with ice-cold PBS and suspended in 2 mL of trypsin-EDTA solution (Life Technologies) for 5 min at 37 °C under rotation. After three washes in ice-cold PBS and centrifugation at 200xg for 3 min, the pellet (~1 × 10^7 cells) was suspended in RPMI 1640, 10% FBS, antibiotics (100 units penicillin/streptomycin), 0.075% Sodium Bicarbonate $NaHCO_3$ (Life Technologies), 1X essential amino acids (Life Technologies), 1X non-essential amino acids (Life Technologies). GFP-positive KRAS G12D eIF2α$^{S/S}$ and eIF2α$^{A/A}$ cells were sorted by flow cytometry and maintained in the same RPMI 1640 media. Downregulation of mouse DUSP6 or PERK was performed by treatments with a mix of 4 siRNAs (Dharmacon) containing the sequences listed in Supplementary Table 1. Colony formation assays were performed with 10^3 cells subjected to anti-tumor treatments for 14 days as indicated in figure legends. Cells were fixed in 4% v/v paraformaldehyde and stained with 0.2% w/v crystal violet. Colonies were scored using an automated cell colony counter (GelCount; Oxford Optronix). (E)-2-benzylidene-3-(cyclohexylamino)-2,3-dihydro-1H-inden-1-one (BCI) inhibitor was obtained from Millipore Sigma, GSK2606414 from MedKoo, ISRIB from Selleck Chemicals."[229]

2.3 shRNA targeting ATF4

Generation of stable eIF2α$^{S/S}$ pools expressing ATF4 shRNAs (listed in Table 1) by infection with pLKO.1 lentiviruses and selection at 5 µg/mL puromycin.

2.4 Knockdown of genes by siRNAs

Mix of 4 siRNAs for each of the following genes; DUSP6, PERK, YAP/TAZ, LATS1/2 and MST1/2 was used and listed in Table 1. 2x10^5 of eIF2α$^{S/S}$ and eIF2α$^{A/A}$ cells were seeded. Next day, lipid-based transfection was performed on cells using Lipofectamine 2000. 24 hours after transfection, targeted cells were seeded for either protein extraction or colony formation assays.

Table 1. Sequences of siRNA, shRNA and qPCR of the corresponding target genes.

Application	Target gene	Sequence
shRNA	ATF4	#1: 5'- CCGGCCAGAGCATTCCTTTAGTTTACTCGAGTAAACTAAAGGAAT GCTCTGGTTTTTG-3' #2: 5'- CCGGCGGACAAAGATACCTTCGAGTCTCGAGACTCGAAGGTATCT TTGTCCGTTTTTG-3'
RT PCR	DUSP6	F 5'-ATA GAT ACG CTC AGA CCC GTG-3' R 5'-ATC AGC AGA AGC CGT TCG TT-3'
	ACTIN	F 5'-CAGCAGATGTGGATCAGCAAG-3' R 5'-GCATTTGCGGTGGACGAT-3'
	GAPDH	F 5'-GAGAGTGTTTCCTCGTCCCG-3' R 5'-CAATCTCCACTTTGCCACTGC-3'
siRNA	PERK (EIF2AK3)	#1 GGUUGGGUCUGAUGAAUUU #2 GUUACUAUCUGCCAUACUA #3 GAACGAGUCCGGAUUUUAA #4 GGAAGGUCAUGGCGUUUAG
	DUSP6	#1 GAACGAUGCUUACGACAUU #2 CAUCGAAUCUGCCAUUAAU #3 CCUCGGACAUUGAGUCUGA #4 GAAAUGGCGAUCUGCAAGA
	YAP	#1 GGAGAAGUUUACUACAUAA #2 CCACCAAGCUAGAUAAAGA #3 GAGAUGCAAUGAACAUAGA #4 CAAUAGUUCCGAUCCCUUU
	TAZ	#1 GGCCAGAGAUACUUCCUUA #2 CCACAGGGCUCAUGAGUGU #3 GGAUUAGGAUGCGUCAAGA #4 CGAGAUGGAUACAGGUGAA
	LATS1	#1 GCAGAGUACUAGCAAAUUU #2 GCAGCUGCCAGGCCUAUUA #3 GGAACAGUCAUAACAUGGA #4 GAAACGUUCCUCAGUCGAU
	LATS2	#1 GCGGCAAUAUUUAGACUUU #2 GAAAUAGCCGGCAGCGAUU #3 GGGCCAAGAUGGACAAGUC #4 UCAGGGAAAUCCGAUAUUC
	MST1	#1 UGACAGCCCUCACGUAGUC #2 GCAAUAUUCAUGAUUCCUA #3 GUCAAUAUUGCGAGACUUA #4 CUACGGAACAAGACGUUAA
	MST2	#1 GCAGAGUACUAGCAAAUUU #2 GCAGCUGCCAGGCCUAUUA #3 GGAACAGUCAUAACAUGGA #4 GAAACGUUCCUCAGUCGAU

2.5 Colony formation assays

1500 cells were seeded in 6 well plates. The next day, the media was changed to media containing the treatment of interest. The media was changed every 4 days to ensure proper growth of cells for a period of 14-21 days or until 80% colonies are formed in the vehicle control well. Quantification of colonies was done using the automated cell colony counter (GelCount, Oxford Optronix).

2.6 IC50 determination assay by Sulforhodamine staining

Plating efficiency was first verified by determining the linear range of the curve between cell density and absorbance at 570 nm. This will be determined by the length of the experiment and rate of cell division. The efficient cell number (according to cell line) was inoculated in 96-well plates to a final of 100 µL of media in each well. The next day, serial dilution of the drug was added in a 2:1 ratio to a final of 200 µL of media. After 4-5 days of incubation, cells were fixed using 10% (wt/vol) Trichloroacetic acid for 1h at 4C. The solution was then discarded and the wells rinsed 4 times with a gentle flow of tap water. The residual water was removed (shaking vigorously) and air-dried. 150 µL of Sulforhodamine B (SRB) (Sigma, S1402-25G) stain (0.2% SRB powder in 1% acetic acid) was added and incubated for 30 minutes at room temperature. The wells were then washed 4 times with 1% acetic acid using a squirt bottle. Acetic acid was removed as much as possible by shaking vigorously and the plate was left to air-dry in a chemical fume hood. The SRB stain was then dissolved in 100 µL of Tris-base, 10mM and pH 8.4 added to the wells of the plate placed on a rocker. Absorbance of the plate was read at 570 nm using a plate reader. To calculate the IC50 value, determine the % survival values at each concentration [(Average of triplicate readings-blank)/(Average of NT wells-blank)] * 100. The % survival (y-axis) was plotted against the drug concentration and a logarithmic regression line was fitted. The equation for IC50 determination was then applied: IC50= EXP ((50-b)/m)). Equation can also be determined using the GraphPAD IC50 determination tool in regression analysis of the curve.

2.7 Polysome profiling, RNA isolation and Real time PCR

"For polysome profiling analysis cells were lysed in 10 mM Tris HCl, pH 7.4, 150 mM NaCl, 0.5 % NP40, 10 mM $MgCl_2$, 100 µg/ml cycloheximide, 2 mM dithiothreitol, 100 U/ml RNA Guard and fractionated on 10–55% sucrose gradients by ultracentrifugation (SW41 rotor; Beckman 30,000 rpm, 3 h at 4 °C)[98]. The gradients were prepared with the ISCO model 160 Gradient Former and fractionated into 500 µl fractions using the ISCO density gradient fractionation system Foxy Jr. Fraction Collector while measuring the absorbance at 254 nm. Total RNA and polyribosomal RNA (1 µg) isolated by Trizol (Thermo Fisher Scientific) was subjected to reverse transcription (RT) with 100 µM oligo (dT) primer using the SuperScript III Reverse Transcriptase kit (Invitrogen) according to the manufacturer's instruction. Real-time (quantitative) PCR was performed using the SensiFast SYBR Lo-ROX kit (Bioline) with primers listed in Table 1. The qPCR assays included primers for mouse GAPDH and actin mRNAs as internal controls according to the Minimum Information for Publication of Quantitative Real-Time PCR Experiments (MIQE) guidelines[247]."[229]

2.8 Flow Cytometry analysis

"For the cell death assay with propidium iodine staining: cells were plated the day before at ~20% confluency to achieve 80–90% confluency in six-well plates at 72 h of treatment. PERK inhibitor was added the next day and media was refreshed with the inhibitor every 24 h. After treatment, the cells were lifted by incubating with phosphate buffer saline (PBS) plus 0.5 mM EDTA for 5 min at 37 ºC and an equal volume of media with 10% FBS. Cells were centrifuged at 500 × *g* for 5 min and washed two times with ice-cold PBS. Cells were resuspended with ice-cold 70% ethanol in PBS and stored at −20 ºC for at least 30 min. For propidium iodide (PI) staining, cells were spun down at 1000 × g for 5 min and washed twice with ice-cold PBS. Cells were resuspended in PI buffer (4 µL Triton X-100, 40 µg PI, 0.5 mg RNAse A, up to 1 mL with PBS), incubated at 37 ºC for 30 min followed by FACS analysis using BD LSRFortessa flow cytometer. FACS data were collected using FACSDiva software and analyzed using FlowJo software."[229]

For sorting of cells for scRNA-seq: FACS buffer (PBS + 2% FBS + 2 mM EDTA) for staining and incubate with the appropriate stains for 20 minutes in the fridge. Wash 2 times with 1000 uL of PBS + 2% FBS, resuspend with 250 uL of FACS buffer and pass through 70 µm strainer. For staining, the cells were stained with 1:250 EpCAM stain, 1:400 CD45, 1:250

Lineage cocktail stain, and 1:10000 DAPI (2 mg/mL stock). Cells were sorted by BD FACSAria. In brief, single GFP-positive cells were first selected against EpCAM-APC-positive staining. Cells sorted were negative for lineage cocktail stain (PE-positive). CD45+ cells were also shown on gating strategy and were also sorted.

2.9 RNA-seq data analysis

"Total RNA of KRAS G12D eIF2α$^{S/S}$ and eIF2α$^{A/A}$ cells (four replicates each) was isolated with Trizol (Thermo Fisher Scientific) and RNA-Seq libraries were prepared following the TruSeq Stranded Total RNA protocol (Illumina) according to the manufacturer's instructions and 50 base single-end reads were obtained using a HiSeq2500 system in Rapid Mode (Illumina). The resulting reads were mapped to the mm10 genome assembly using HISAT and quantified using default settings[248,249]. Differential expression was performed using the random variance model as implemented in the anota2seq package (1.8.0)[250]. Genes with absolute log(FC) > 1 and False Discovery rates (FDRs) < 0.05 were considered differentially expressed. Upstream Regulator analysis was performed as implemented in IPA. Briefly, this analysis is based on the prior knowledge of expected effects between transcriptional regulators and their target genes (Ingenuity® Knowledge Base). The analysis examines how many known targets of each transcription regulator are present in the dataset and compares their direction of change to what is expected from the literature to predict likely transcriptional regulators. If the observed direction of change is mostly consistent with an activation state of the transcriptional regulator, a prediction is made about that activation state. Gene set enrichment analysis (GSEA v4.0.3, Broad Institute) was performed on all genes ranked according to fold change, using the Gene Ontology geneset v5.2 (MSigDB)[251]. The number of permutations was 1000 and only sets containing between 15 and 500 genes were retained."[229]

2.10 Analysis of YAP^{ON} and YAP^{OFF} signatures in eIF2α$^{S/S}$ and eIF2α$^{A/A}$ cells

Construction of the PPI network

PPI networks were traced an predicted using an online database; The Search Tool for the Retrieval of Interacting Genes (STRING; http://string-db.org). Common DEGs in YAP ON and

YAP OFF signatures were imported from Pearson *et al.* Cancer Cell 2021. Cytoscape (version 2.8; https://cytoscape.org/) was used to visualize the PPI network.

Functional annotation of DEGs by KEGG and GO analysis

Analyses of DEGs were done by the following programs: DAVID (version 6.8; https://david.ncifcrf.gov/home.jsp). We used Gene Ontology (GO) since it is based on three aspects of biology: biological processes (BP), cellular components (CC), and molecular functions (MF). Kyoto Encyclopedia of Genes and Genomes (KEGG; https://www.kegg.jp/) was used as a biological information database. Significance was defined at $P < 0.05$.

Function and pathway enrichment analysis by Metascape

We used Metascape (http://metascape.org/gp/index.html#/main/step1)17 to perform functional and pathway enrichment analysis, and construct PPI networks.

Identification of significant modules and hub genes

The Cytoscape plug-in Molecular Complex Detection (MCODE, version 1.5.1; http://apps.cytoscape.org/apps/mcode) was used to identify important modules of the network map. The criteria of MCODE analysis were degree cut-off = 2, MCODE score > 4.5, Max depth = 100, node score cut-off = 0.2, and k-score = 2. The hub genes were identified in the PPI network by using the Cytoscape app cytoHubba (https://apps.cytoscape.org/apps/cytohubba).

2.11 scRNA-seq analysis

GSEA analysis

GSEA analysis was done by GSVA package in R and subsequently scaled values as *z*-scores. The gene set used was c2 gene set from Molecular Signatures Database (MSigDB).

Single-cell RNA sequencing

Single cell RNA-seq data analysis was generated using R Studio V4.2.1 and R package Seurat version 4. Data were initially filtered to only include all cells with at least 350 genes and all genes in greater than 3 cells. Data were initially normalized using the NormalizeData function with a scale factor of 10,000 and the LogNormalize normalization method. Variable genes were identified using the FindVariableFeatures function. Data were scaled and centered using linear regression on the counts and the cell cycle score difference. PCA was run with the RunPCA function using the previously defined variable genes. Isolated cells were batch corrected through the R package Harmony V1.0 (https://github.com/immunogenomics/harmony). Harmony is a flexible multi-dataset integration algorithm for scRNA-seq by correcting the low-dimensional embedding of cells from principal component analysis (PCA). It first uses soft clustering to find potential clusters, and then uses a soft k-means clustering algorithm to find clusters that favors the cells from multiple datasets and penalizes for any specified unwanted technical or biological factors. It then learns a simple linear adjustment function by computing cluster-specific linear correction factors, such as individual cell-types and cell state, from the cluster-specific centroids from each dataset. Each cell is weighted and corrected by its cell-specific linear factor. It then iterates the clustering and correction until the cell cluster assignments are stable. We used Harmony V1.0 to integrate our scRNA-seq patient data, correcting for individual scRNA-seq Run IDs (as each individual patient was each their own Run ID). Cell clusters were identified via the FindNeighbors and FindClusters function using a resolution of 1.0 for eIF2$\alpha^{S/S}$ sample and 0.8 for eIF2$\alpha^{A/A}$ sample and Uniform Manifold Approximation and Projection (UMAP) clustering algorithms were performed. FindAllMarkers table was created and clusters were defined by user-defined criteria.

3. Protein analysis assays

3.1 Immunoblotting

"Cells were washed twice with ice-cold PBS and proteins were extracted in ice-cold lysis buffer containing 10 mM Tris-HCl, pH 7.5, 50 mM KCl, 2 mM $MgCl_2$, 1% Triton X-100, 3 µg/ml aprotinin, 1 µg/ml pepstatin, 1 µg/ml leupeptin, 1 mM dithiothreitol, 0.1 mM Na_3VO_4, and 1 mM phenylmethylsulfonyl fluoride. Extracts were kept on ice for 15 min, centrifuged at 10,000 × *g* for 15 min (4 °C), and supernatants were stored at −80 °C. Proteins were quantified by

Bradford assay (Bio-Rad). The expression of different proteins was tested in parallel by loading 50 µg of protein extracts from the same set of samples on two identical sodium dodecyl sulfate (SDS)-polyacrylamide gels. After protein transfer to Immobilon-P membrane (Millipore), the two identical blots were cut into smaller pieces based on the size of proteins to be tested. One piece was probed for the phosphorylated protein of interest whereas the other identical piece for the corresponding total protein. The antibodies used for immunoblotting are listed in Table 2. Proteins were visualized by enhanced chemiluminescence (ECL) according to the manufacturer's specification (Amersham Biosciences). Quantification of bands in the linear range of exposure was performed by the ImageJ 1.51e software (NIH, Maryland, USA)."[229]

Table 2. List of antibodies used in the study.

Antibody	Species	Company	Cat #	WB	IHC
eIF2α-P	Rabbit monoclonal	Abcam	Ab32157	1:1000	1:150
eIF2α	Mouse monoclonal	Cell signaling technology	L57A5	1:1000	
PERK-P T982	Rabbit	Lilly Research Laboratories	PMID: 26130148		
PERK (for human cell lines)	Rabbit monoclonal	Cell signaling technology	3192S	1:1000	
PERK (for mouse cell lines)	Mouse		PMID: 21954288		
ATF4	Rabbit monoclonal	Cell signaling technology	11815S	1:1000	
DUSP6	Rabbit monoclonal	Abcam	Ab76310	1:1000	1:100
ERK-P	Rabbit polyclonal	Cell signaling technology	9101S	1:1000	1:100
Actin	Mouse monoclonal	Santa Cruz Biotechnology	Sc-8432	1:1000	
α-Tubulin	Mouse monoclonal	Sigma-aldrich, Roch	T5168	1:1000	
ERK total	Rabbit polyclonal	Cell Signaling Technology	9102S	1:1000	
Ki67	Rabbit polyclonal	Abcam	15580		1:500
YAP S127	Rabbit monoclonal	Cell Signaling Technology	13008	1:1000	
YAP	Rabbit monoclonal	Cell Signaling Technology	14074	1:1000	1:200
TAZ S89	Rabbit monoclonal	Cell Signaling Technology	59971	1:1000	
TAZ	Rabbit polyclonal	Cell Signaling Technology	4883	1:1000	
LATS1	Rabbit Polyclonal	Cell Signaling Technology	9153	1:1000	
LATS2	Rabbit monoclonal	Cell Signaling Technology	5888	1:1000	
Mouse IgG-horseradish peroxidase-conjugated	Goat	KPL	474-1806	1:2000	
Rabbit IgG-horseradish peroxidase-conjugated	Goat	Jackson immunoResearch	111-035-144	1:2000	
Biotinylated anti-rabbit IgG	Horse	Vector	BA-1100		1:150

3.2 Preparations of TMAs

"TMAs were constructed from a continuous series of archival primary resected LUADs obtained by University Hospital Leicester NHS Trust between 1998 and 2015. Samples were excluded if the patient had any previous lung cancer diagnosis. Whole diagnostic H&E sections were reviewed, and 3× representative tumor cores (1 mm) were taken in triplicate from FFPE blocks and embedded in a total of 23 acceptor blocks. Outcome and pathological data of patients were collected from local and national databases. TMAs were sectioned at 4.5 μM. All TMAs were H&E stained, and patterns ascribed to individual cores according to WHO guidelines; where necessary, whole sections images from donor blocks were examined to confirm growth pattern. This study was approved by the Northampton Research Ethics Committee (reference 14/EM/1159) and University Hospitals Leicester NHS Trust Research and Innovation Department (reference UHL 11363)."[229]

3.3 Histology and immunohistochemistry

"Mouse tissues were fixed in 10% buffered formalin phosphate, paraffin embedded, and sectioned. Paraffin was removed from the sections after treatment with xylene, rehydrated in graded alcohol, and used for H&E staining and immunostaining. Antigen retrieval was performed in sodium citrate buffer. Primary antibodies were incubated at 4 °C overnight and secondary antibodies were incubated at room temperature for 90 min (antibodies are listed in Table 2). Sections were counterstained with 20% Harris modified hematoxylin (Thermo Fisher Scientific), mounted in Permount solution (Thermo Fisher Scientific), and scanned using an Aperio Scanscope AT Turbo scanner (Leica biosystems). Quantification of stained sections was performed using Aperio Imagescope software (Leica Biosystems) according to the manufacturer's specifications.

For human specimens, IHC was used to examine p-eIF2 and cytokeratin expression in a duplex chromogenic assay and to examine p-eIF2, p-ERK, and cytokeratin expression in a multiplex fluorescent assay. IHC was performed on the Roche DISCOVERY Ventana® platform using Roche DISCOVERY reagents. Sections were de-paraffinized and antigen retrieval (64 min, 95 °C, pH 9.0) was performed. Endogenous peroxidase was inhibited, and non-specific Ig binding was blocked using Goat Ig, for 20 min each.

For the duplex assay, p-eIF2α primary antibody was incubated on slides and detected using a secondary antibody. The Roche AMP HQ kit was used to amplify p-eIF2 DAB staining. Antibody denaturation (8 min, 100 °C, pH 6.0) and neutralization steps (20 min, DISC inhibitor) was performed prior to further blocking (12 min, Goat Ig) and cytokeratin antibody incubation. A purple detection kit was used to detect cytokeratin AE1/AE3. The slides were counterstained with haematoxylin and sections were dehydrated and mounted. Primary and secondary antibodies are listed in Table 3.

Target Protein	**Primary Antibody**	**Secondary Antibody**	**Detection**
Cytokeratin	Novocastra TM Liquid Mouse Monoclonal Antibody Multi-Cytokeratin Leica, NCL-L-AE1/AE3 1:250 28 mins, 37°C	DISCOVERY OmniMap Anti-Mouse HRP Roche, 760-4310 16 mins, 37°C	Opal 650 Akoya, FP1496001KT 1:300 8 mins, 37°C
p-eIF2α	Phospho-eIF2α (Ser51)(D9G8)XP® Rabbit mAb. Cell Signalling Technology,	DISCOVERY OmniMap Anti-Rabbit HRP Roche, 760-	Opal 570 Akoya, FP1488001KT

	3398 1:25 6 hours, room temperature	4311 32 mins, 37°C	1:400 8 mins, 37°C
ERK-P	Phosphor-p44/42 MAPK (Erk1/2) (Thr202/Tyr204) (D13.14.4E)XP® Rabbit mAB Cell Signalling Technology, 4370 1:100 44 mins, 37°C	DISCOVERY Roche UltraMap Anti-Rabbit HRP Roche, 760-4315 12 mins, 37°C	Opal 520 Akoya, FP1487001KT 1:75 8 mins, 37°C

Table 3. Primary and secondary antibodies used for duplex assay of human specimens.

Duplex stained slides were scanned at x40 on the Hamamatsu NanoZoomer-XR C12000. Slide images were imported, de-arrayed, and analyzed using the Visiopharm® digital pathology platform. An app was developed to detect and outline tumor areas using the purple cytokeratin stain. A further app identified individual cells and generated a H-score based on DAB/purple intensity within the tumor area (H-score = 3 × % strong staining + 2 × % moderate staining + % weak staining). Quantitative H-scores were generated from digital TMA images using Visiopharm® software, based on the intensity and proportion of cytoplasmic p-eIF2 staining within tumor cells as identified by cytokeratin staining. Visiopharm® H-scores were validated against a manually scored TMA. For p-eIF2 analysis, patients were divided into two groups based on a positive/negative cut-off value determined through correlation of IHC images and H-scores; cores with an H-score of <6 were deemed to be immunohistochemically negative. This automated method was validated against manual H-scoring of a representative TMA (120 donor cores), giving a Spearman's Rho of 0.939, $p < 0.001$. For each patient, the median of p-eIF2 H-scores from up to 3 cores/tumor was used.

For the fluorescent multiplex assay, antibodies were applied in the sequential order in Table 3 with an antibody denaturation (8 min, 100 °C, pH 6.0) and neutralization (20 min. DISC inhibitor) steps in between. The slides were scanned at ×20 in the Akoya Vectra® and tumor regions were analyzed using Akoya inform Advanced Image Analysis software. Tissue and cells were segmented based on the fluorescent channels and mean pixel intensity data were collected for each marker at the single-cell level."[229]

4. Statistical analysis of patient data

"For patient data, statistical analysis was performed using RStudio (1.0.153). Spearman's rank correlation was used to validate Visiopharm® H-scores and assess the relationship between p-eIF2 and Ki67. P-eIF2 was directly measured and quantified by IHC in 928 human LUADs, providing a broad range of staining intensities. H-scores were generated using Visiopharm® software based on the intensity and proportion of cytoplasmic p-eIF2 staining. The automated scores were validated against manual H-scoring of a representative TMA (120 donor cores), giving a Spearman's Rho of 0.939, $p < 0.001$. Patient survival was visualized by Kaplan–Meier plots and significance assessed by a log-rank test and Cox Proportional regression for univariate

survival models. The associations between patient survival and p-eIF2 were examined using overall, cancer-specific, and recurrence-free survival endpoints. For each patient, the median of the 3-core p-eIF2 H-scores was used. Associations between p-eIF2 and histological pattern/WHO type were assessed using non-parametric Mann–Whitney–Wilcoxon and the Kruskal–Wallis tests."[229]

Chapter 3: Results

1. P-eIF2α as an important biomarker for survival and aggressiveness in LUAD patients

Phosphorylation of the eukaryotic initiation factor 2 at the α subunit has been implicated in different types of cancers[10]. However, its level of expression can be correlated to either cell death, due to activation of anti-tumorigenic pathways, or cell survival, due to activation of pro-proliferative pathways. This dual role of p-eIF2α depends on multiple variables, the most important of which is cell-context. It has been shown that p-eIF2α is a poor prognostic marker in many cancers[10,74]. On the other hand, p-eIF2α expression induces anti-tumorigenic pathways leading to prolonged patients' lives, such as the case with HER2 breast cancers[76]. In this study of LUAD patient tumor microarrays (TMAs), p-eIF2α is a poor prognostic marker[229].

1.1 Role of p-eIF2α in survival of patients with LUAD

Dr. John LeQuesne's lab comprises a tumor microarray (TMA) of 928 patients with LUAD. The patients' survival was monitored over the span of 5 years. Staining the TMA with p-eIF2α revealed that patients having high levels of p-eIF2α in their tumors had significantly worse survival outcome than patients with low staining of p-eIF2α (Figure 13). Specifically, tumors displaying negative staining of p-eIF2α led to prolonged survival of patients, around 12 months longer, compared to patients with tumors positive for p-eIF2α. This suggests that p-eIF2α can be a prognostic marker in patients with LUAD.

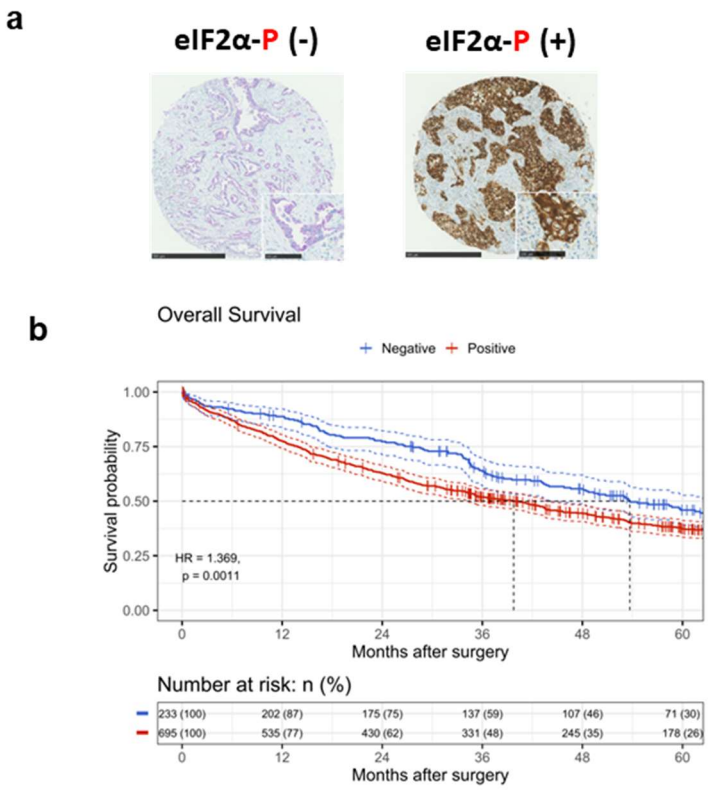

Figure 13. p-eIF2α prognosticates LUAD patient survival. (a) Negative (-) or positive (+) staining for p-eIF2α in human LUAD representative TMAs. Scale bars correspond to 500 and 100 μm on the core image and enlarged image, respectively. (b) Kaplan-Meier curve for LUAD patient overall survival; Blue line indicates patients with negative p-eIF2α TMA stains and the red line indicates positive p-eIF2α TMA stains. Significance was determined using log-rank test (two-sided). Confidence intervals are represented by the dashed lines around the survival curves. HR=hazard ratio.

1.2 eIF2α-P determines the degree of invasiveness of LUAD in patients

Not only is p-eIF2α a prognostic marker of LUAD patient survival, but it may also be used as a marker of aggressiveness. When plotted against histological core/regional histological growth patterns, p-eIF2α H-score was highest in the highly aggressive solid growth pattern and lowest in the minimally aggressive Leipidic pattern (Figure 14A). Similarly, according to the

WHO tumor type classification, p-eIF2α H-score was lowest in early in situ/ minimally invasive lesions (AIS/MIA), followed by Leipidic predominant adenocarcinoma (LPA) and was highest in the invasive-predominant groups (Figure 14B). An interesting exception was with mucinous adenocarcinoma (MUCA) which is a highly invasive lesion that displayed low levels of p-eIF2α. Concordantly, p-eIF2α staining correlated with increased tumor cell proliferation in the LUAD TMA's as indicated with staining of Ki-67 (Figure 14C). Results from this stratification ae further detailed in Table 4. Collectively, the data implicate p-eIF2α as a prognostic marker in human LUAD as well as a marker of invasiveness and tumor cell proliferation in this type of cancer.

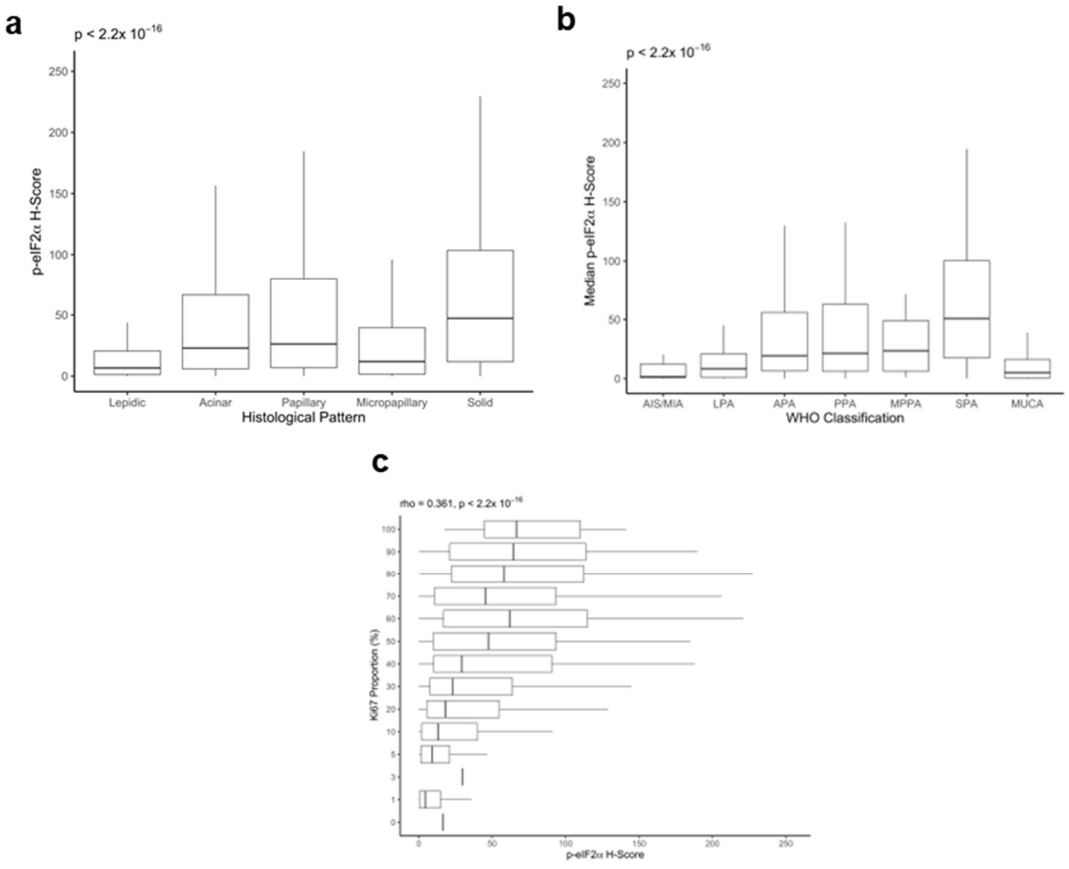

Figure 14 P-eIF2α expression correlates with invasive growth patterns and cell proliferation in human LUAD. (a) p-eIF2α H-scores plotted against core/regional growth pattern (lepidic n=286, acinar n = 917, papillary n=266, micropapillary n=85, solid n=636). (Kruskal-Wallis chi-squared (two-sided)= 197.21, $p<2.2 \times 10^{-16}$, excludes outlying values). (b) Median p-eIF2α H-scores plotted against WHO tumor type (adenocarcinoma in situ/minimally invasive adenocarcinoma

(AIS/MIA) n=22, lepidic-predominant adenocarcinoma (LPA) n=87, acinar-predominant adenocarcinoma (MPPA) n=20, solid-predominant adenocarcinoma (SPA) n=254, mucinous adenocarcinoma (MUCA) n=65) (Kruskal-Wallis cho-squared (two-sided)=144.81, $p < 2.2 \times 10^{-16}$, excludes outlying values). (c) p-eIF2α H-score plotted against core/regional Ki67 proportion within tumor tissue (Spearman's Rho = 0.361, $p<2.2 \times 10^{-16,}$ excludes outlying values). For box plots, the three solid lines represent the 75% percentile, the median, and the 25% percentile in turn. The whisker boundaries represent ±1.5*IQR, (IQR = 75% percentile – 25% percentile).

Table 4. Stratification of human LUAD TMAs according to the univariate and multivariate Cox Model based on p-eIF2α staining, stage, sex, performance status and WHO classification.

		Univariate Cox Model			Multivariate Cox Model		
		HR	**95% CI**	**p-value**	**HR**	**95% CI**	**p-value**
P-eIF2α (Negative vs Positive)	Positive	1.427	1.162 – 1.752	< 0.001	1.091	0.882 – 1.349	0.422
Stage (1 vs 2 vs 3+)	2	1.128	0.786 – 1.619	0.510	1.086	0.756 – 1.561	0.655
	3	2.059	1.579 – 2.686	< 0.001	1.828	1.395 – 2.395	< 0.001
Sex (Male vs Female)	Female	0.676	0.574 – 0.795	< 0.001	0.719	0.609 – 0.849	< 0.001
Performance Status (0 vs 1 vs 2+)	1	1.269	1.047 – 1.537	0.0156	1.284	1.059 – 1.556	0.0110
	2	2.012	1.638 – 2.470	< 0.001	1.986	1.616 – 2.441	< 0.001
WHO (AIS/MIA/LPA vs APA/PPA vs SPA/MPPA)	APA/ PPA	1.932	1.418 – 2.631	< 0.001	1.682	1.229 – 2.301	0.0011
	SPA/ MPPA	2.348	1.705 – 3.234	< 0.001	1.786	1.283 – 2.486	< 0.001

2. Deciphering the role of ISR in LUAD using a mouse model of KRAS lung cancer

The results strongly suggest an indispensable role of the ISR in LUAD progression, invasion and proliferation. To further investigate this notion, we employed a mouse model of KRAS lung cancer based on LoxP-STOP-LoxP LSL-KRAS G12D allele that is conditionally activated in the lungs by CRE recombinase[202]. Activating somatic mutations of KRAS G12D by itself rarely advances beyond adenomas. However, an additional deletion of p53 drives the formation of LUAD within 12 weeks[202]. Since 31-46% of LUAD cases are due to co-mutations of *KRAS/TP53*, we reasoned that the model representative of LUAD. This mouse model was then crossed with either mice having the wild-type form of *eIF2S1* allele (fTg/0;eIF2α$^{S/S}$), where phosphorylation can take place at serine 51 on eIF2α in response to activated forms of stress, or mice with a conditional homozygous S51A mutation of *eIF2S1* allele (fTg/0;eIF2α$^{A/A}$), where Serine 52 is switched to Alanine only upon cre-recombinase activity, rendering an inactive ISR upon stress stimulation[227] (Figure 12) . Intratracheal intubation of CRE-expressing lentiviruses under the control of carbonic anhydrase 2 promoter, which is expressed in type 1 and 2 alveolar cells, induces the formation of KRAS-driven lung tumors via removal of the STOP element within the LSL-KRAS G12D cassette[202]. In addition to activating endogenous KRAS G12D, the CRE-expressing lentiviruses harbor TP53 shRNA from a U6/H1 promoter to accelerate lung tumor formation. Tumor initiation and progression in the lungs of mice can be monitored by ultrasound imaging (Figure 12).

2.1 p-eIF2α is an essential driver of KRAS-lung tumorigenesis in mice

After 7 weeks of intubation of CRE-lentiviruses, various types of KRAS/TP53 precursor lesions have been formed, ranging from hyperplasia to adenoma[202]. At this timepoint, the initiating lesions can be visualized by ultrasound imaging as white vertical B-lines traversing the ultrasound screen (Figure 15A). These are a result of a strong reflection of ultrasound wave due to encountering a small mass at the pleural surface of the lung[252]. As a result, the reflected white B-lines can be quantified at the 7-week timepoint to represent the number of precursor lesions at the surface of the lungs. The number of precursor lesions formed on the lungs of eIF2α$^{S/S}$ mice

was significantly higher than that of eIF2α$^{A/A}$ mice (Figure 15A). After 18 weeks of lentiviral intubation, the tumors formed on the lungs are large enough for volume measurements on ultrasound. These appear as deep clefts interrupting the pleural surface and in constant mobility in-sink with breathing/ heartbeats of the animal[240]. The 18-week formed lung tumors include advanced lesions of adenoma and adenocarcinoma, which are of interest in KRAS lung cancer[202]. The volume of 18-week lung tumors in eIF2α$^{S/S}$ mice was significantly larger than that of eIF2α$^{A/A}$ mice (Figure 15A). The differences in tumor growth persisted even after 24 weeks of intubation (Figure 15A). Together, these data imply that the phosphorylation of eIF2α in response to stress is essential for initiation and progression of KRAS/TP53 LUAD. Furthermore, upon monitoring the survival of mice after initiation of tumors, the lives of mice with tumors devoid of p-eIF2α were prolonged ~18 weeks longer than that of mice possessing wild-type p-eIF2α (Figure 15B). This further confirms the prognostic ability of p-eIF2α to determine survival in KRAS LUAD.

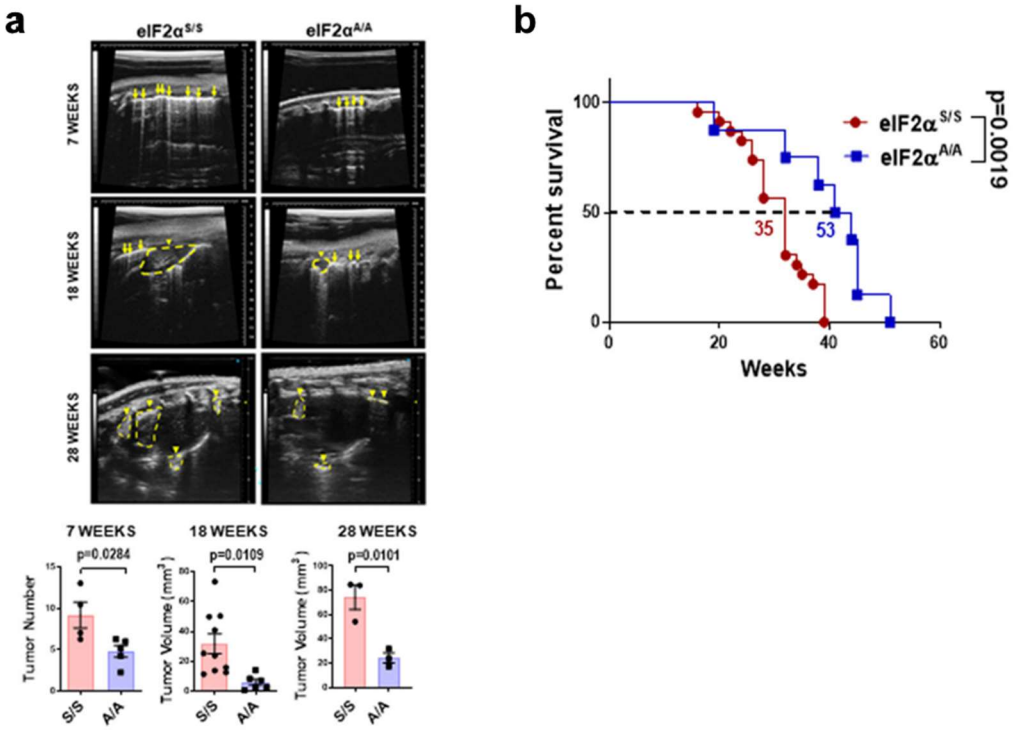

Figure 15 p-eIF2α promotes tumor progression in mouse KRAS-driven LUAD. (A) Ultrasound images representing initiating tumors at 7 weeks ($eIF2\alpha^{S/S}$ n = 4, $eIF2\alpha^{A/A}$ n = 5, P value = 0.028) and progressing tumors at 18 weeks ($eIF2\alpha^{S/S}$ n = 10, $eIF2\alpha^{A/A}$ n = 6, P value = 0.0109) and 28 weeks of KRAS G12D expression ($eIF2\alpha^{S/S}$ n = 3, $eIF2\alpha^{A/A}$ n = 3, P value = 0.0101) with 6 x 10^5 functional lentiviral particles per unit. Tumor location is indicated by an The arrow indicates tumor location and intermittent yellow lines indicate tumor size. Data represent Mean ± SEM (B) Survival of $eIF2\alpha^{S/S}$ mice depicted by blue curve (n=23) whereas that of $eIF2\alpha^{A/A}$ mice by red curve (n=9). Data represent Mean ± SEM with two-sided Log-rank, Mantel-Cox Test, P value = 0.0019.

2.2 The ISR and invasiveness in mouse KRAS-LUAD

The major histological types of LUAD can be divided, from least to most invasive, to adenocarcinoma in situ, carcinoma and invasive adenocarcinoma. After subjecting the $eIF2\alpha^{S/S}$ and $eIF2\alpha^{A/A}$ lungs to H&E staining, the tumor histological patterns were stratified to the different invasive patterns (Figure 16). The correlation between p-eIF2α H-scores and patient LUADs led to the speculation that $eIF2\alpha^{S/S}$ tumors will have more invasive patterns compared to $eIF2\alpha^{A/A}$ tumors. However, this was not the case, as growth patterns were similar in both cohorts. This might indicate that the correlation of p-eIF2α with invasiveness is not restricted to KRAS/TP53 mutations in LUAD but might be the case in other LUAD mutations which are included in the LUAD patient cohort.

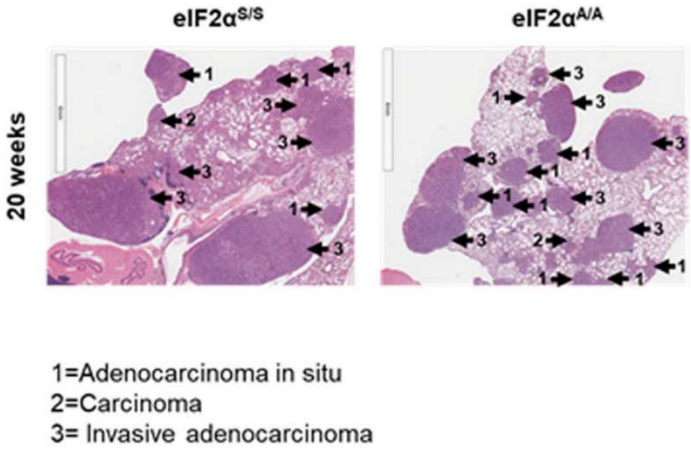

Figure 16 Representative H&E staining of KRAS G12D eIF2α$^{S/S}$ (n = 5) and eIF2α$^{A/A}$ (n = 5) lung sections at 20 weeks post-induction of KRAS G12D. Arrows indicate types of tumors. 1 = adenocarcinoma in situ. 2 = Carcinoma. 3 = invasive adenocarcinoma. Scale bars correspond to 4 mm of core images.

3. The ISR is upstream of essential pro-tumorigenic pathways in KRAS lung cancer

The induction of LUAD tumors in the KRAS G12D mouse model is in an immunocompetent background. To identify the cell-autonomous capacity of p-eIF2α to drive the progression of KRAS LUAD, we isolated cells from the lungs of the eIF2α$^{S/S}$ and eIF2α$^{A/A}$ mice and injected them subcutaneously into nude mice (Figure 17). eIF2α$^{S/S}$ tumors progressed at a much faster pace compared to eIF2α$^{A/A}$. This confirms the ability of p-eIF2α to drive proliferation of KRAS lung tumor cells, independently of the tumor microenvironment. Therefore, during the progression of KRAS-mutated LUAD, p-eIF2α employs pro-tumorigenic signaling pathways to sustain the proliferative capacity of KRAS LUAD. To identify the pathways under the control of p-eIF2α in KRAS LUAD, we subjected the eIF2α$^{S/S}$ and eIF2α$^{A/A}$ cells to RNA sequencing. Data analysis revealed that 2249 genes were deregulated in eIF2α$^{S/S}$ vs eIF2α$^{A/A}$ tumor cells. Ingenuity pathway analysis (IPA) revealed the upregulation of bona fide ISR constituents and UPR regulators such as the activating transcription factor 4 *(ATF4*), *DDIT3* (CHOP), CREB-binding protein (*CREBBP*), in addition to the upstream eIF2α kinase PERK (*EIF2AK3*) (Figure 18B). Interestingly, UR analysis indicated the upregulation of the ERK signaling pathway in S/S vs A/A tumor cells. Due to the tight dependence of KRAS LUAD to the MAPK pathway, we further investigated its regulation by p-eIF2α.

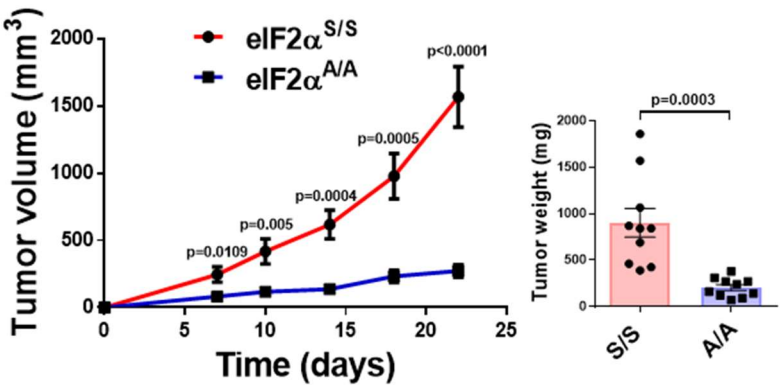

Figure 17 P-eIF2α promotes tumor progression in a cell-autonomous manner. Subcutaneous growth of primary KRAS G12D eIF2α$^{S/S}$ and eIF2α$^{A/A}$ in nude mice (n=10, P value = 0.0003). Tumor mass (mg) at the endpoint of the experiment is shown in the histogram graph. Data represent Mean ± SEM. Significance in differences between two datasets was determined using two-tailed unpaired *t*-tests. *P* values are indicated on the graphs.

A

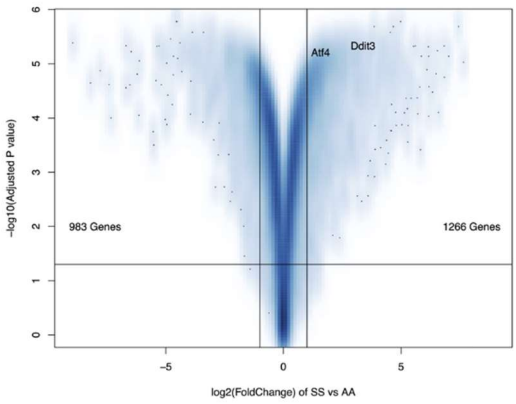

B

Regulator	log2(FC)	Description	Regulation State	Z score	P Value
CTNNB1	0.722	transcription regulator	Activated	2.013	1.02E-11
ATF4	1.577	transcription regulator	Activated	4.092	6.15E-08
LHX1		transcription regulator	Activated	2.144	9.23E-08
IL6	1.502	cytokine	Activated	2.641	4.22E-07
CREBBP	0.076	transcription regulator	Activated	2.985	0.00000173
HIF1A	1.358	transcription regulator	Activated	2.238	0.00000204
ERK1/2		group	Activated	2.271	0.0000164
EIF2AK3	0.31	kinase	Activated	2.408	0.0000081
DDIT3	3.384	transcription regulator	Activated	2.909	0.000215
HOXA10	-1.285	transcription regulator	Inhibited	-2.164	2.05E-07
Esrra	-0.585	transcription regulator	Inhibited	-3.431	0.00003
ASXL1	0.391	transcription regulator	Inhibited	-2.111	0.000216
MFN2	-0.553	enzyme	Inhibited	-2	0.00106
Hbb-b1		transporter	Inhibited	-2.121	0.00129

Figure 18 P-eIF2α regulates important tumorigenic pathways in KRAS G12D lung tumors as revealed by RNA-seq analysis of eIF2α$^{S/S}$ and eIF2α$^{A/A}$ genes. (A) Volcano plot showing the differences in mRNA expression between eIF2αS/S and eIF2αA/A mouse KRAS G12D tumors. (B) Top activated or inhibited upstream regulators based on Upstream Regulator (UR) analysis used in IPA to compare eIF2α$^{S/S}$ and eIF2α$^{A/A}$ genes.

3.1 p-eIF2α upregulates the MAPK signaling pathway by translationally inhibiting DUSP6

Immunohistochemical staining of p-ERK of the S/S and A/A lung tumors indicated that p-ERK staining was significantly higher in tumors proficient for p-eIF2α compared to those devoid of the phosphorylation (Figure 19A). This observation was regardless of histological pattern (Figure 19B). We also employed another mouse model of KRAS lung tumorigenesis based on urethane (ethyl carbamate) treatment. Upon inducing lung tumorigenesis in wild-type eIF2α$^{S/S}$ mice and mice with the heterozygous S51A mutation of *EIF2S1* (eIF2αS/A), we noticed that fewer and smaller tumors were formed in S/A mice than in S/S mice. Immunohistochemical staining of p-ERK was much lower in the eIF2α$^{S/A}$ lung tumors compared to those of eIF2α$^{S/S}$ (Figure 20). This provides further evidence that p-ERK is indeed regulated by p-eIF2α. The

correlation between p-eIF2α and p-ERK was also evident in human LUADs, where multiplex fluorescent IHC analysis of the TMAs revealed a positive correlation at a single-epithelial cell level between cytoplasmic p-eIF2α and p-ERK (Figure 21).

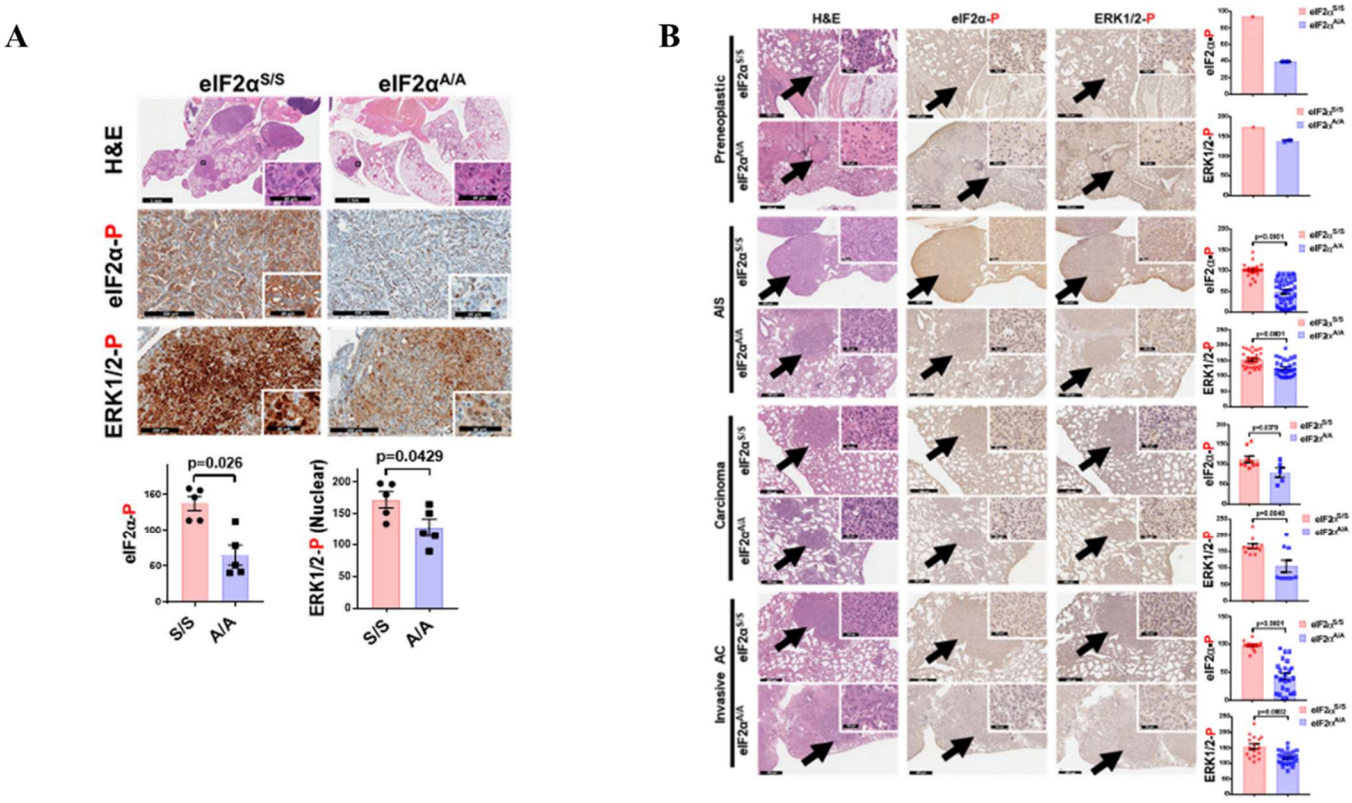

Figure 19 p-eIF2α activates p-ERK signaling in mouse KRAS LUAD. (A) H&E staining of mouse lungs and IHC staining of tumors for phosphoeIF2 (eIF2α-P) and phospho-ERK (ERK-P) at 20 weeks after CRE-lentivirus intubation (eIF2α$^{S/S}$ n = 5, eIF2α$^{A/A}$ n = 5 P value = 0.0026). Graphs represent the average H-score of tumors per lung section of eIF2α$^{S/S}$ and eIF2α$^{A/A}$ mice. Scale bars for H&E staining correspond to 3 and 2 mm of the core images of eIF2α$^{S/S}$ and eIF2α$^{A/A}$ tumors, respectively, and 60 μm of enlarged images. For IHC staining images, scale bars correspond to 200 and 60 μm of core and enlarged tumor images, respectively. (B) . H&E staining and IHC analyses for p-eIF2 (eIF2α-P) and p-ERK (ERK-P) in mouse KRAS G12D eIF2α$^{S/S}$ (n=5) and eIF2α$^{A/A}$ (n=5) lung sections with tumors of different histology. The graphs indicate the H-scores of p-eIF2 (eIF2α-P) and p-ERK (ERK-P) for each type of lung tumor at 20 weeks after KRAS G12D induction in eIF2α$^{S/S}$ and eIF2α$^{A/A}$ mice. Scale bars correspond to 400

μm and 60 μm of core and enlarged tumor images, respectively. Statistical significance was determined using two-tailed unpaired t-test. Data represent mean ± SEM.

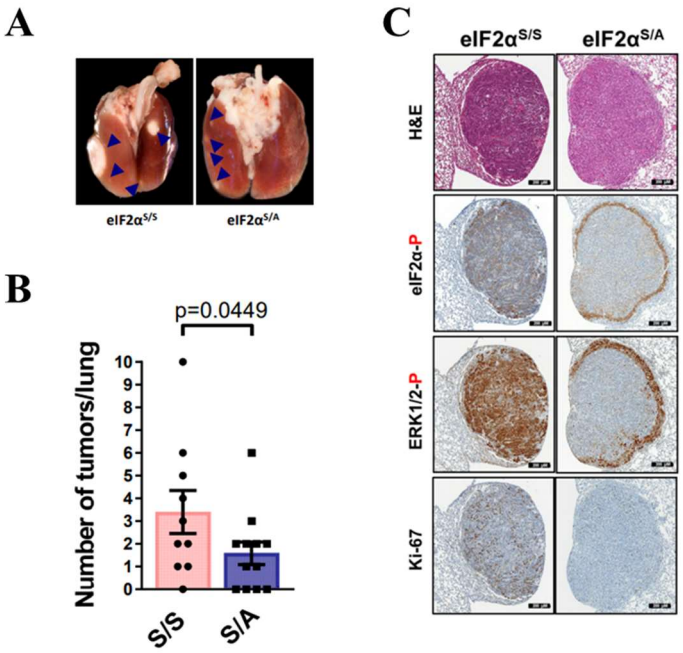

Figure 20 p-eIF2 promotes urethane-induced lung carcinogenesis. (A) Representative images of KRAS lung tumors in WT eIF2α mice (eIF2α$^{S/S}$) as well as mice with a heterozygous germline S51A mutation of eIF2S51 (eIF2α$^{S/A}$) after 40 weeks of urethane treatment. (B) Number of macroscopic tumors formed in mouse eIF2α$^{S/S}$ (n=10) and eIF2α$^{S/A}$ (n=12) lungs. Data represent mean ± SEM. Statistical significance was determined using one-tailed unpaired t-test with p= 0.0449. (C) Reduced p-eIF2 (eIF2α-P) in urethane-treated mouse lung tumors correlates with decreased p-ERK (ERK-P) and decreased proliferation (Ki-67). Scale bars correspond to 200 μm on core images in C

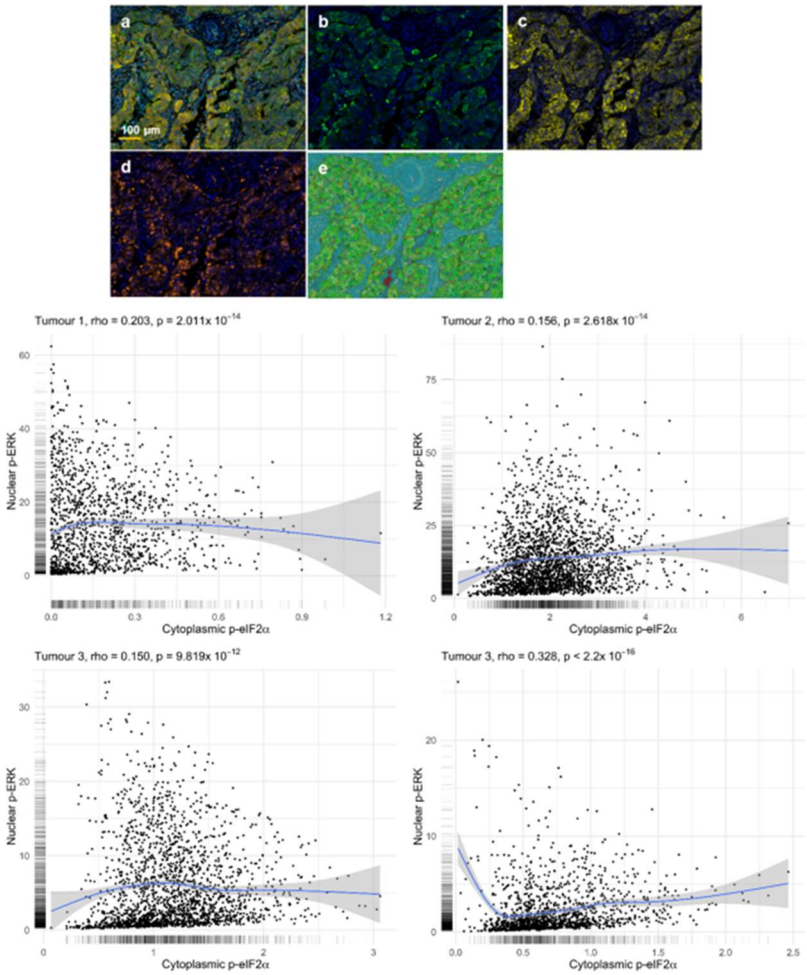

Figure 21 Positive correlation between cytoplasmic p-eIF2α and nuclear p-ERK in human LUAD samples. Representative fluorescent multiplex IHC images indicating the following: (a) Composite image; (b) Cytokeratin (green) with DAPI counterstain; (c) p-eIF2α (yellow) with DAPI counterstain; (d) p-ERK with DAPI counterstain; (e) InForm segmentation of the tissue and subcellular compartments. Tissue is segmented into epithelium (green), stroma (blue) and background (red). Individual cells are segmented into nuclei (green) and surrounded by cytoplasm. Scatterplots show the relationship between single-cell measures of cytoplasmic p-eIF2α and nuclear p-ERK within 4 different epithelial tumor cells. Each plot also has a smoothed GAM (generalized additive model) and a measure of linear trend (Spearman's Rho and associated P value). Exact p values: Tumor 1 (p = 2.011x10-14), Tumor 2 (p = 2.618x10-14), Tumor 3 (p = 9.819x10-12) and Tumor 4 (p < 2.2x10-16).

To further investigate the mechanistic link between p-eIF2α and p-ERK, we cultured the primary lung tumor cells of eIF2α$^{S/S}$ and eIF2α$^{A/A}$ mice. By western blotting, p-ERK was indeed more upregulated in cells with wild-type p-eIF2α (Figure 22A). Interestingly, this was not the case with the upstream kinase p-MEK, as levels did not differ between cells proficient and deficient of p-eIF2α. This led to the speculation that perhaps the deregulation of p-ERK by p-eIF2α was due to a phosphatase. The Dual specificity phosphatase DUSP6 exclusively de-phosphorylates ERK through the TxY motif and is a tumor suppressor in LUAD[167]. DUSP6 levels were significantly upregulated in the absence of p-eIF2α, as shown by western blots and immunohistochemical staining (Figure 22, 23). Together, the data suggests that the presence of p-eIF2α suppresses the expression of DUSP6, which leads to the upregulation of p-ERK. To further verify this notion, downregulation of DUSP6 by a mix of 4 different siRNAs in both eIF2α$^{S/S}$ and eIF2α$^{A/A}$ tumor cells restored p-ERK levels in wild-type p-eIF2α tumor cells similar to those in wild-type cells with scrambled siRNAs (Figure 22). In addition, downregulation of DUSP6 rescued the survival of eIF2α$^{A/A}$ cells in clonogenic assays (Figure 23). Also, treatment with BCI, an inhibitor of both DUSP1 and DUSP6, led to a larger activation of p-ERK in eIF2α$^{A/A}$ compared to eIF2α$^{S/S}$ cells, suggesting that p-ERK dephosphorylation is released more in a background lacking p-eIF2α (Figure 24). Collectively, these results indicate that p-eIF2α activates p-ERK1/2 by suppressing DUSP6.

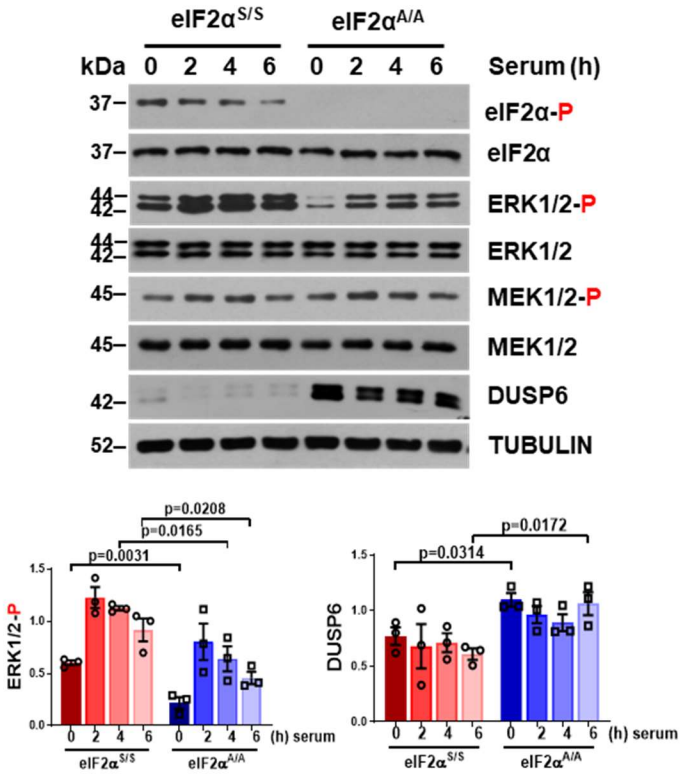

Figure 22 Absence of p-eIF2α reduces p-ERK levels and increases DUSP6 expression. KRAS G12D eIF2α$^{S/S}$ and eIF2α$^{A/A}$ tumor cells were deprived from serum for 18 h followed by serum stimulation (10% FBS) for the indicated time. Protein extracts (50 µg) were subjected to immunoblotting for the indicated proteins. The graphs represent quantitative analyses from three biological replicates. Phosphorylated ERK (ERK-P) was normalized to total ERK and DUSP6 to either ACTIN or TUBULIN. Data represent mean ± SEM. Significance in differences between two datasets was determined using two-tailed unpaired t-test. P values are indicated in the bar graphs (ns non-significant).

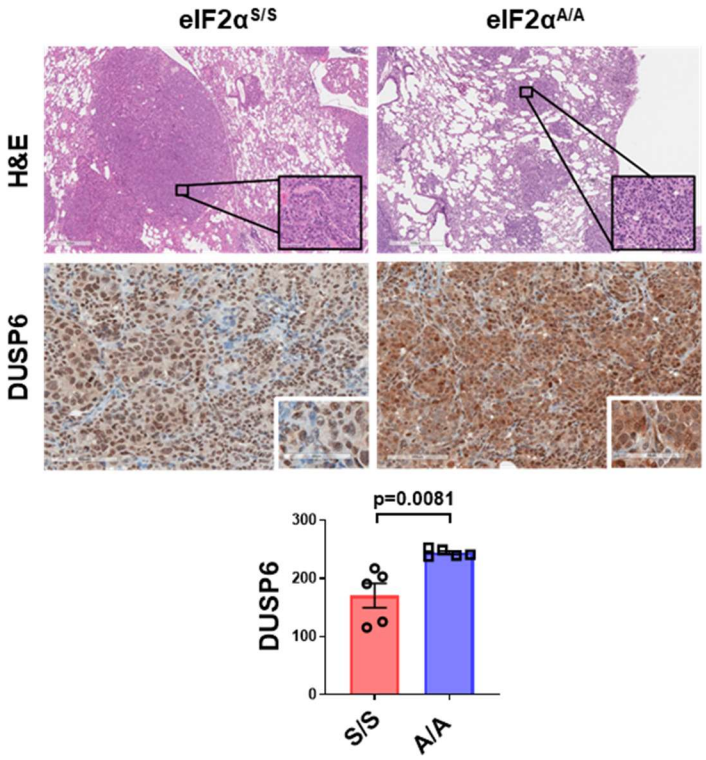

Figure 23 p-eIF2α inhibits DUSP6 expression in mouse KRAS-LUAD tumors. H&E staining of mouse lungs and IHC staining of tumors for DUSP6 at 20 weeks after KRAS G12D induction. Graphs represent the average H-score of tumors per lung section of $eIF2\alpha^{S/S}$ (n = 5) and $eIF2\alpha^{A/A}$ (n = 5) mice with P value = 0.0081. Scale bars for H&E staining correspond to 600 µm and 60 µm of core and enlarged tumor images, respectively. For IHC staining of DUSP6, scale bars correspond to 100 and 60 µm of` core and enlarged tumor images, respectively. Data represent mean ± SEM. Significance in differences between two datasets was determined using two-tailed unpaired t-test. P values are indicated in the bar graphs (ns non-significant).

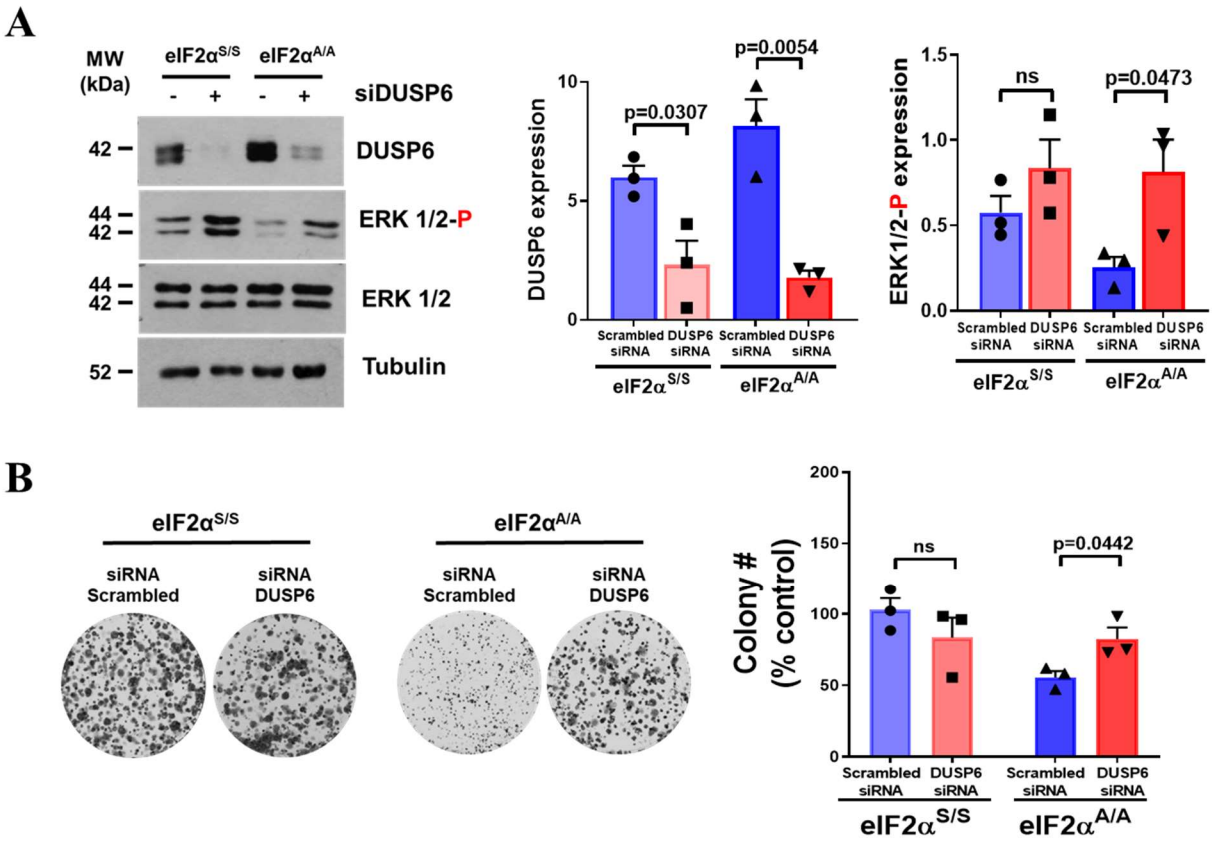

Figure 24 p-eIF2α employs DUSP6 to inhibit p-ERK expression and increase proliferation. (A) Immunoblotting and (B) clonogenic assays of KRAS G12D eIF2α$^{S/S}$ and eIF2α$^{A/A}$ mouse lung tumor cells treated with either scrambled siRNAs or a mix of four different DUSP6 siRNAs. Graphs represent quantitative analyses from three biological replicates. Data represent mean ± SEM. Significance in differences between two datasets was determined using two-tailed unpaired t-test. P values are indicated in the bar graphs (ns non-significant).

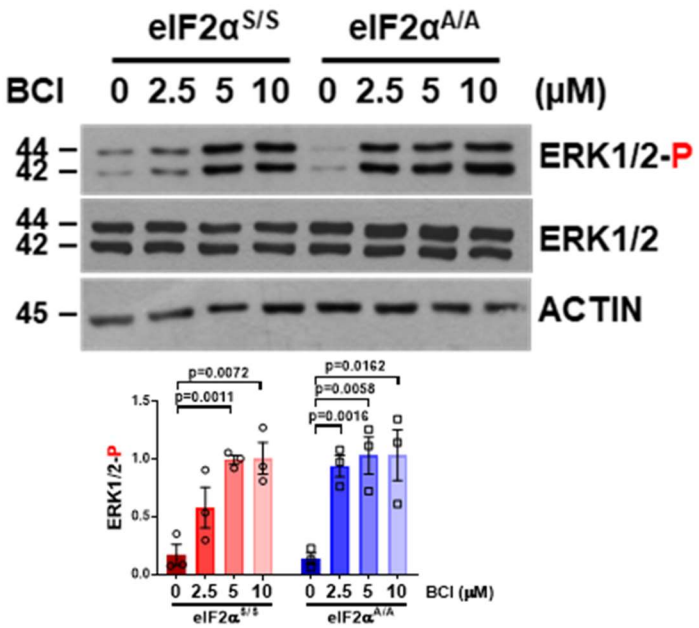

Figure 25. The DUSP inhibitor BCI restores p-ERK levels in eIF2α$^{A/A}$ cells. Immunoblotting of mouse KRAS G12D eIF2α$^{S/S}$ and eIF2α$^{A/A}$ lung tumor cells prior to and after treatment with the indicated concentrations of BCI (μM) for 1h. Data represent mean ± SEM. Statistical significance was determined using two-tailed unpaired t-test. P values are indicated within the bar graphs. The quantifications of blots are from 3 biological replicates.

Downstream of p-eIF2α, ATF4 is often activated to regulate genes that can overcome a stressed microenvironment. Therefore, we speculated that ATF4 might be transcriptionally suppressing DUSP6. However, knockdown of ATF4 using two different shRNAs did not affect p-ERK levels, nor did it affect DUSP6 levels (Figure 26). In addition, RT-PCR of total RNA of eIF2α$^{S/S}$ and eIF2α$^{A/A}$ cells revealed that DUSP6 mRNA was significantly downregulated in in the eIF2α$^{A/A}$ cells, suggesting that the regulation of DUSP6 by p-eIF2α might occur at the translational level (Figure 27). Following this observation, we subjected both cell types to polysome profiling. This revealed that DUSP6 mRNA was more associated with the heavy polysomes of eIF2α$^{A/A}$ cells compared to eIF2α$^{S/S}$ cells, after normalization to glyceraldehyde 3-phosphate dehydrogenase (GAPDH) and ACTIN mRNAs in corresponding total and poly-ribosomal mRNA fractions, indicating a better translation of DUSP6 mRNA in the absence of p-eIF2α (Figure 27). Therefore, p-eIF2α translationally represses DUSP6. This translational

discrimination of DUSP6 by p-eIF2α might be due to long 5'-and 3'-UTRs (700-2000nt) on the DUSP6 mRNA.

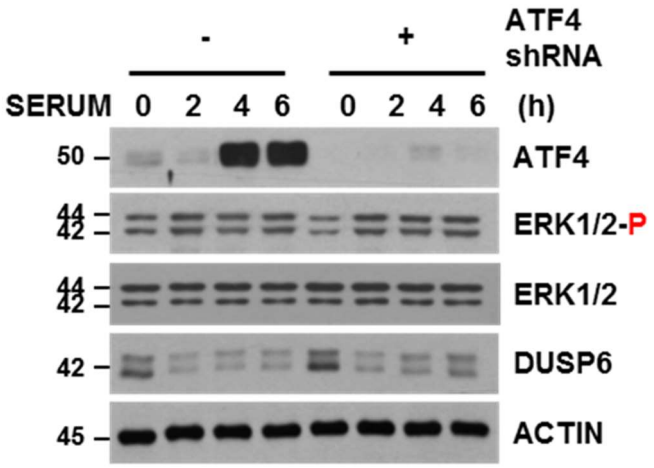

Figure 26 Regulation of p-ERK and DUSP6 through p-eIF2α does not occur via ATF4. KRAS G12D eIF2α$^{S/S}$ tumor cells infected with either pLKO or shRNA to ATF4 were deprived from serum for 18 h followed by serum stimulation (10% FBS) for the indicated time. Protein extracts (50 µg) were subjected to immunoblotting for the indicated proteins. The graphs are representatives from two biological replicates of two different shRNAs to ATF4.

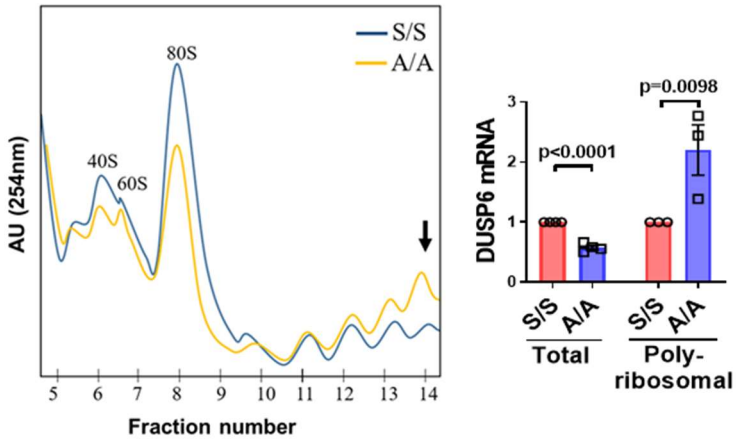

Figure 27. p-eIF2α translationally inhibits DUSP6 mRNA. Polysome profiling of KRAS G12D eIF2α$^{S/S}$ and eIF2α$^{A/A}$ cells. Arrowhead indicates the poly-ribosomal fraction used for mRNAs detection. DUSP6 mRNA was normalized to glyceraldehyde 3-phosphate

dehydrogenase (GAPDH) and ACTIN mRNAs in total (n = 4, P value < 0.0001) and poly-ribosomal fractions (n = 4, P value = 0.0098). Data represent mean ± SEM. Significance in differences between two datasets was determined using two-tailed unpaired t-test. P values are indicated in the bar graphs (ns non-significant).

3.2 Mutant KRAS upregulates the PERK-p-eIF2α arm in human and mouse LUAD cancer cells

Analysis of RNA-seq data implicated the involvement of PERK (*EIF2AK3*) in mouse KRAS G12D tumorigenesis (Figure 18). To uncover the role of PERK in mutant KRAS LUAD, we compared the levels of PERK activation between mutant and wild-type KRAS human LUAD (Figure 28). Indeed, p-PERK and p-eIF2α were more upregulated in cells having mutant KRAS G12C (H23 and H3558) compared to a lung cancer cell line with wild-type KRAS (H1703). This upregulation also correlated with increased p-ERK in the KRAS G12C cells compared to the KRAS wild-type H1703, and was further enhanced with thapsigargin (TG) treatment, which activates the UPR. In addition, in H1299 cells that had an ectopic expression of KRAS G12D, KRAS G12C or KRAS G12V had a higher expression of p-PERK and p-eIF2α compared to H1299 cells ectopically expressing wild-type KRAS. However, H1299 cells harbor the NRAS Q61K allele, which might interfere with activities of the KRAS mutation. Therefore, we used another system of cells, H1703, which endogenously contain wild-type KRAS, and we ectopically expressed either wild-type KRAS or KRAS G12C. Similarly to H1299 cells, KRAS G12C H1703 cells had a higher expression of p-PERK and p-eIF2α, associated with a higher p-ERK expression, compared to wild-type KRAS H1703 cells. Taken together, these results suggest that LUAD cells with mutant KRAS upregulates the PERK-p-eIF2α arm.

In terms of effect on survival, treatment with the PERK inhibitor, GSK2606414, had a stronger reduction in the colony-forming efficacy of mutant KRAS cells than wild-type KRAS cells (Figure 29). This was also the case with cells that overexpress mutant KRAS G12C compared to their isogenic wild-type KRAS counterparts. Therefore, upregulation of the PERK-p-eIF2α arm by mutant KRAS renders them more susceptible to PERK inhibition. To further ascertain the implication of PERK in KRAS LUAD, knockdown of PERK using a mix of 4 siRNAs reduced greatly the clonogenicity of eIF2α$^{S/S}$ cells, to levels similar to that of eIF2α$^{A/A}$ cells, whereas it

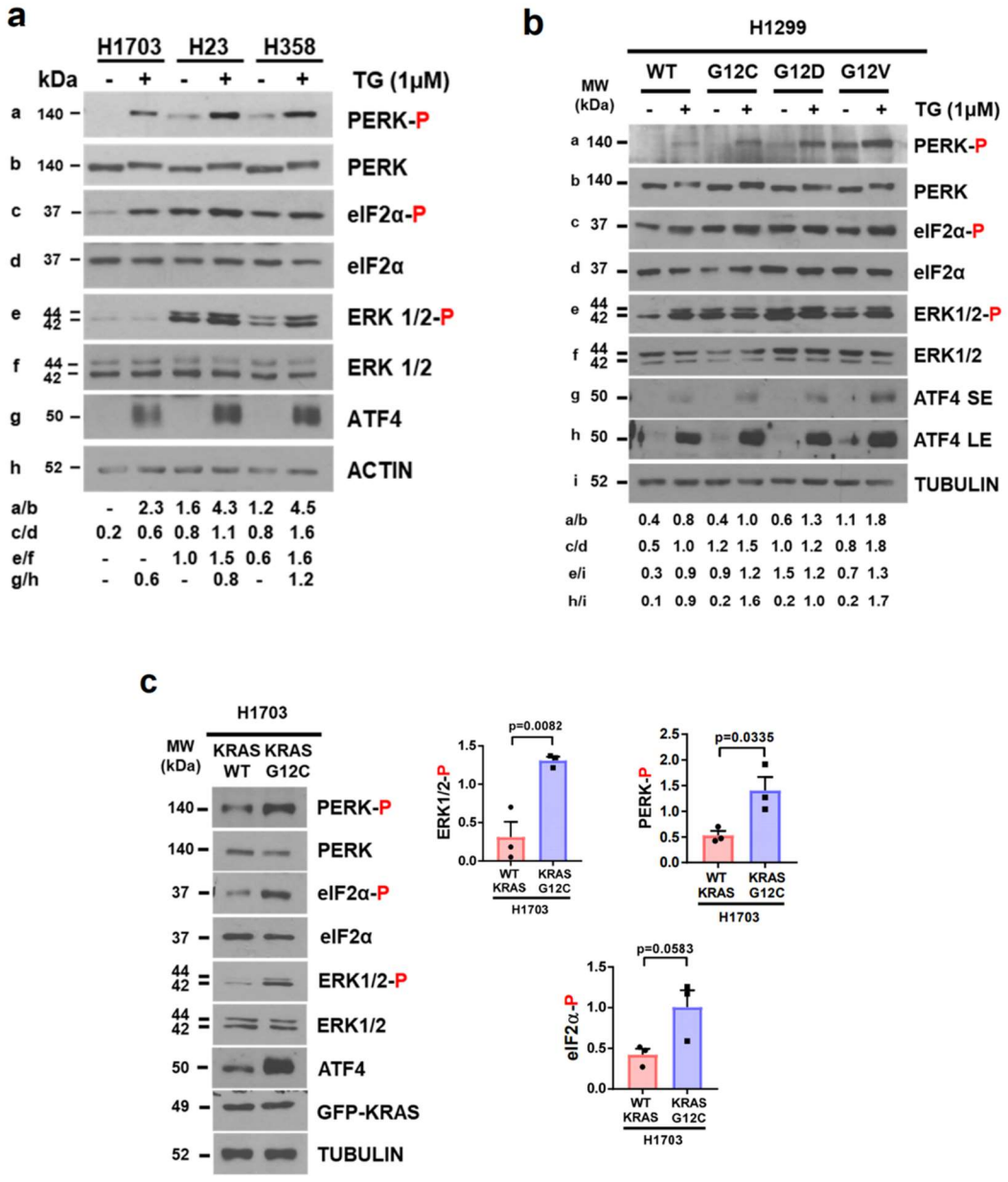

Figure 28. Mutant KRAS upregulates the PERK/p-eIF2α arm in human LUAD cells. (a) Immunoblot analysis of either WT KRAS (H1703) or mutant KRAS G12C (H23, H358) LUAD cells prior to or after treatment with 1μM thapsigargin (TG) for 1.5 h. (b) Immunoblot analysis of H1299 cells overexpressing either WT KRAS or mutant KRAS (G12C, G12D or G12V) prior to and after treatment with 1μM TG for 1.5 h. (a-b) Blots are from 1 experiment. (c) Immunoblotting of H1703 cells overexpressing a GFP-tagged form of either WT KRAS or KRAS G12C. p-ERK, p-PERK and p-eIF2α were normalized to corresponding total proteins whereas DUSP6 expression was normalized to ACTIN or TUBULIN. N=3 independent experiments. Data represent mean ± SEM. Statistical significance was determined using two-tailed unpaired t-test. SE: Short Exposure. LE: Long Exposure.

had no effect on eIF2α$^{A/A}$ cells (Figure 30). However, there was a slight significant increase in the colony-forming efficacy of eIF2α$^{A/A}$ cells. This may be attributed to p-eIF2α independent PERK functions. Indeed, the PERK inhibitor promoted death in eIF2α$^{S/S}$ cells, as shown by flowcytometry analysis (Figure 31). Therefore, mutant KRAS LUAD is highly reliant on PERK-p-eIF2α arm for proliferation and survival.

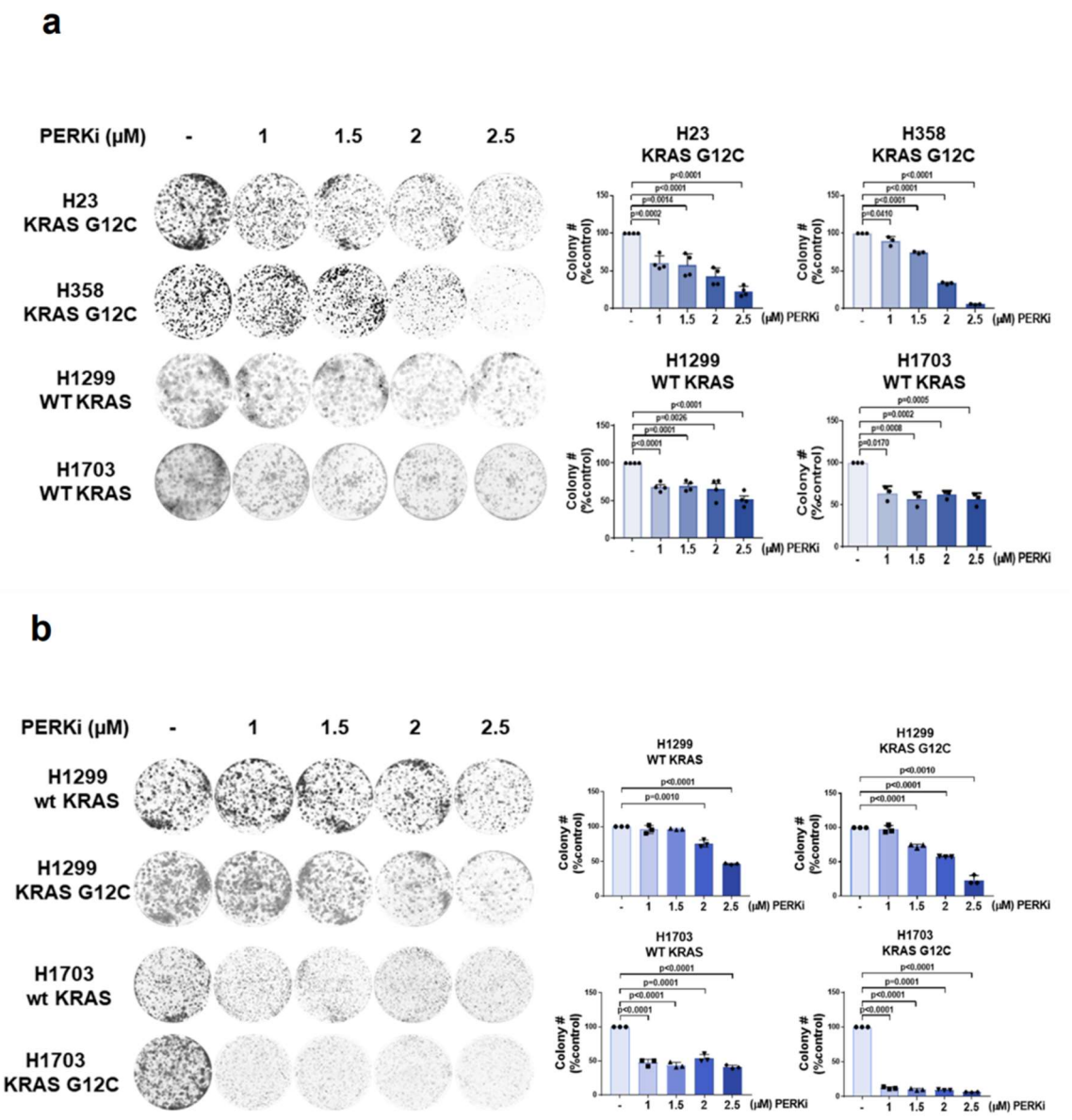

Figure 29 Mutant KRAS sensitizes human LUAD cells to anti-proliferative effects of PERK inhibition (a) Colony formation assays of human LUAD cells with endogenous WT KRAS (H1299, H1703) or KRAS G12C (H358, H23) prior to and after treatment with increasing concentrations of PERK inhibitor GSK2606414 (PERKi). (b) Colony formation assays of H1299 and H1703 overexpressing either WT KRAS or KRAS G12C before and after treatment with increasing concentrations of PERKi. (a, b) Graphs represent data from 3 biological replicates.

Data represent mean ± SEM. Statistical significance was determined using two-tailed unpaired t-test.

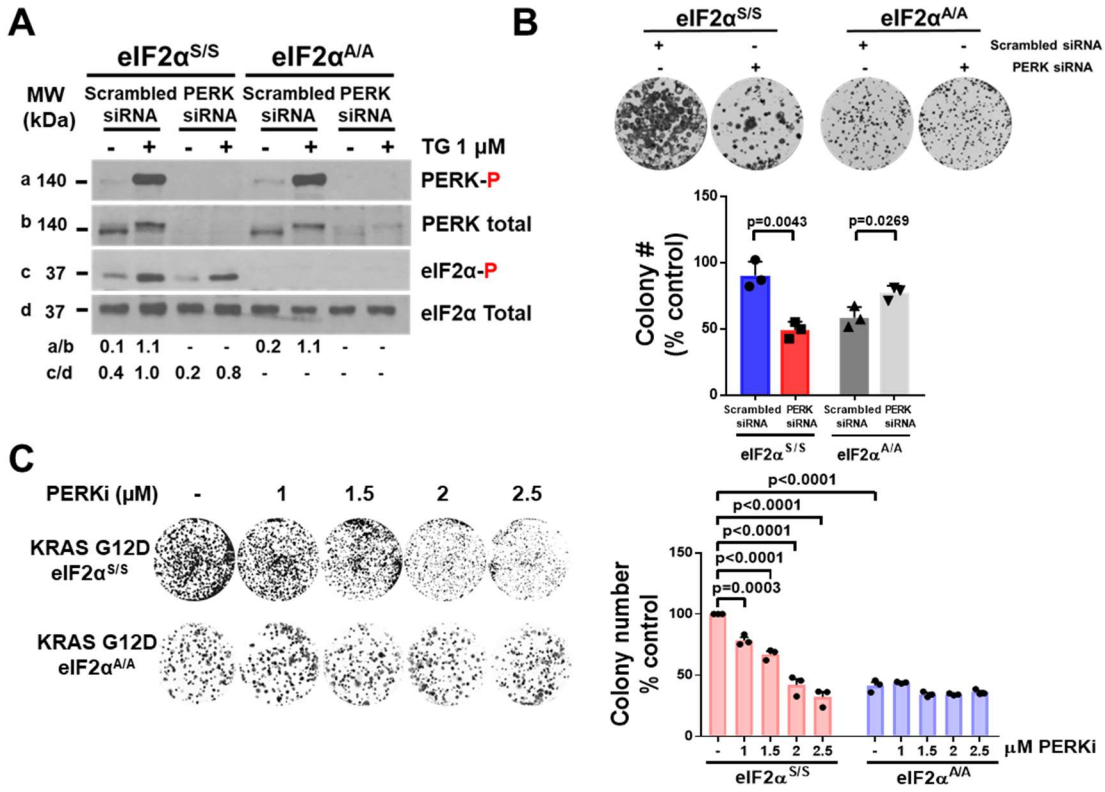

Figure 30. PERK dictates the pro-survival and translational effects of p-eIF2α in KRAS G12D tumor cells. (A) Immunoblotting of mouse KRAS G12D eIF2α$^{S/S}$ and eIF2α$^{A/A}$ lung tumor cells subjected to treatments with either scrambled siRNAs or a mix of four different PERK siRNAs followed by 1 μM thapsigargin (TG) treatment for 1.5 h, (n = 1). (B) Clonogenic assays of KRAS G12D eIF2α$^{S/S}$ and eIF2α$^{A/A}$ cells subjected to either scrambled siRNAs or PERK siRNAs treatments. The graph represents data from three biological replicates. c Colony-forming efficacy of mouse KRAS G12D eIF2α$^{S/S}$ and eIF2α$^{A/A}$ cells after treatment with the indicated concentrations of the PERK inhibitor (PERKi) GSK2606414. Graphs represent data from three biological replicates. Data represent mean ± SEM. Significance in differences between datasets was determined using two-sided one-way Anova, Tukey's multiple comparison test. P values are indicated on the bar graph.

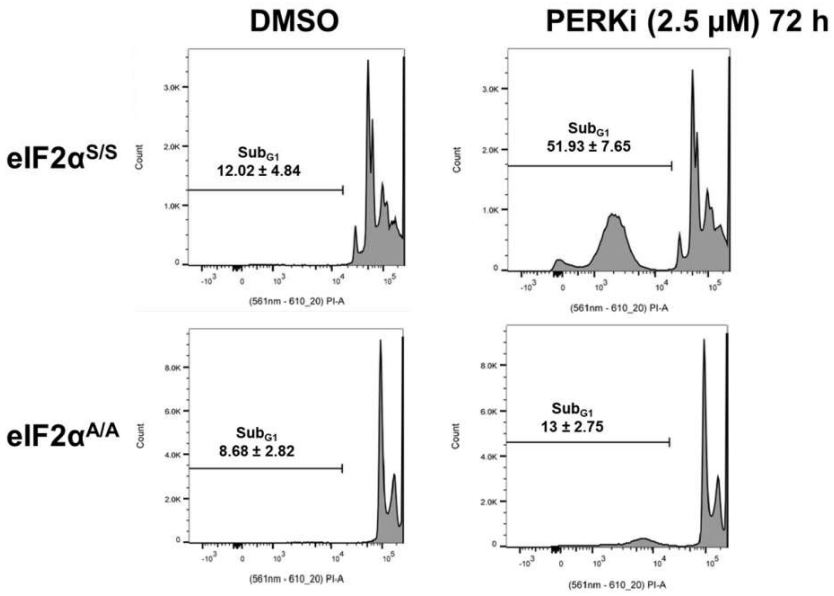

Figure 31. PERK is pro-survival in KRAS G12D lung cancer cells. Mouse KRAS G12D eIF2α$^{S/S}$ and eIF2α$^{A/A}$ lung tumor cells were treated with PERK inhibitor GSK2606414 (PERKi) for 72 h and subjected to propidium iodide staining and flow cytometry analysis. Cell death was assessed by the analysis of cells in sub-G1. The data represent the average of 3 biological replicates. The mean value of subG1 ± SEM is shown in each graph.

Based on the above observations, we reasoned that the regulation of p-ERK by p-eIF2α is through the kinase PERK. To verify this notion, we treated the eIF2α$^{S/S}$ and eIF2α$^{A/A}$ cells with the GSK2606414 PERK inhibitor, after inducing ER stress with thapsigargin (TG) (Figure 32). Indeed, increasing concentrations of the PERK inhibitor led to decreased p-eIF2α, followed by a significant increase in DUSP6 levels which associate with decreasing p-ERK. This pattern was exclusive to eIF2α$^{S/S}$ cells, as eIF2α$^{A/A}$ DUSP6 and p-ERK levels were unchanged with PERK inhibitor treatment.

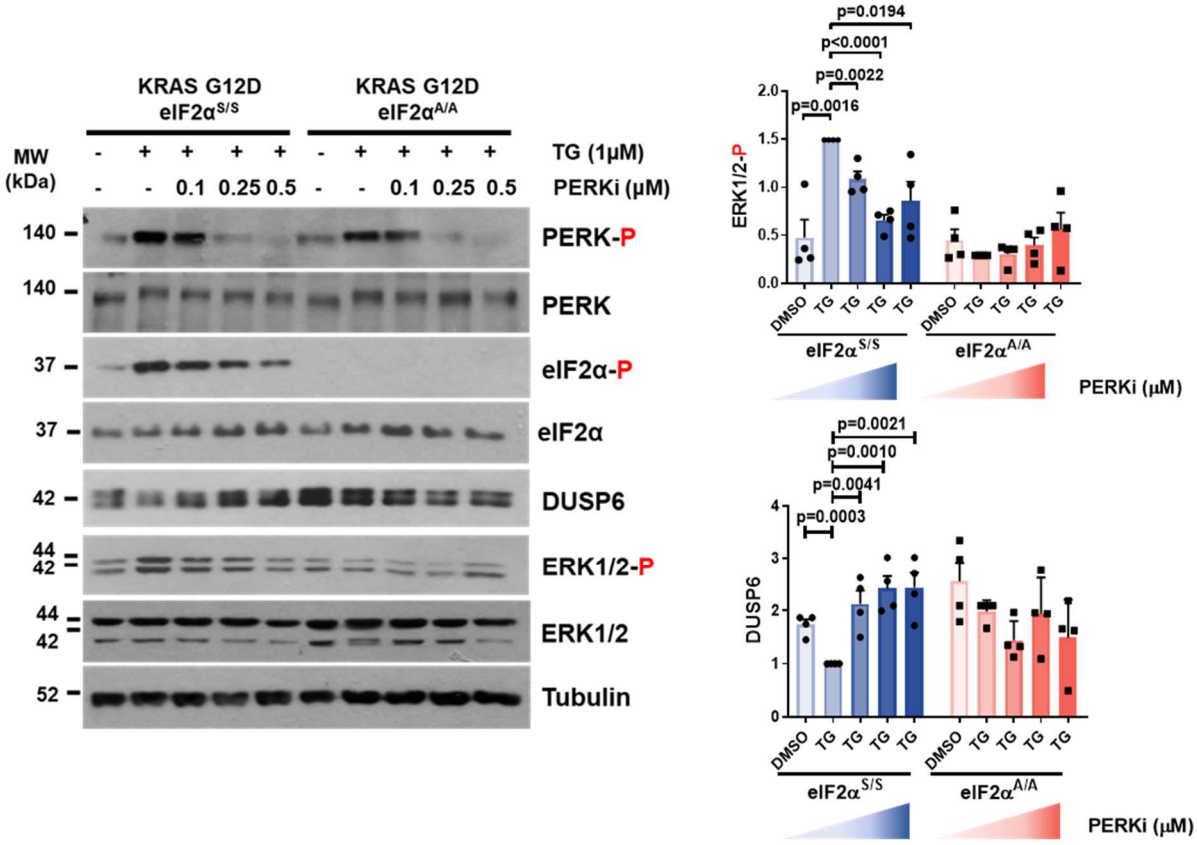

Figure 32. PERK/p-eIF2 arm suppresses DUSP6 and increases p-ERK in mutant KRAS lung tumors. KRAS G12D eIF2α$^{S/S}$ and eIF2α$^{A/A}$ cells were untreated or pre-treated with 1 μM thapsigargin (TG) for 30 min followed by treatments with increasing concentrations of PERKi for 1 h. Protein extracts (50 μg) were subjected to immunoblotting for the indicated proteins. Quantifications of blots were performed from four biological replicates (n=4). Phosphorylated ERK (ERK-P), PERK (PERK-P), and phospho-eIF2 (eIF2α-P) were normalized to corresponding total protein whereas DUSP6 expression was normalized to ACTIN or TUBULIN. Data represent mean ± SEM. Significance in differences between two datasets was determined using two-tailed unpaired t-test. P values are indicated on the bar graph.

3.3 Assessing the therapeutic potential of targeting the ISR in KRAS LUAD

We sought to explore possible therapeutic regiments in targeting p-eIF2α in KRAS LUAD. In addition to the PERK inhibitor, we investigated the effects of the integrated stress response inhibitor (ISRIB), which antagonizes the translational effects of p-eIF2α by de-activating eIF2B, on KRAS LUAD progression. Firstly, we tested the implications of ISRIB on the MAPK pathway in eIF2α$^{S/S}$ and eIF2α$^{A/A}$ cells. As with the effects of PERK inhibitor, after induction of the UPR with TG, ISRIB upregulated DUSP6, followed by p-ERK downregulation, exclusively in eIF2α$^{S/S}$ cells, whereas it had no effects on the MAPK pathway in eIF2α$^{A/A}$ cells (Figure 33). The effects of both ISRIB and PERK inhibitor on the MAPK pathway in human LUAD cells H23 and H358 were similar to those in eIF2α$^{S/S}$ cells (Figure 34, 35). However, there was no effect on the MAPK pathway when wild-type cells H1703 were treated with both drugs (Figure 33). These data support the notion that inhibiting the translational function of p-eIF2α can efficiently impair p-ERK in mouse and human KRAS-mutant LUADs.

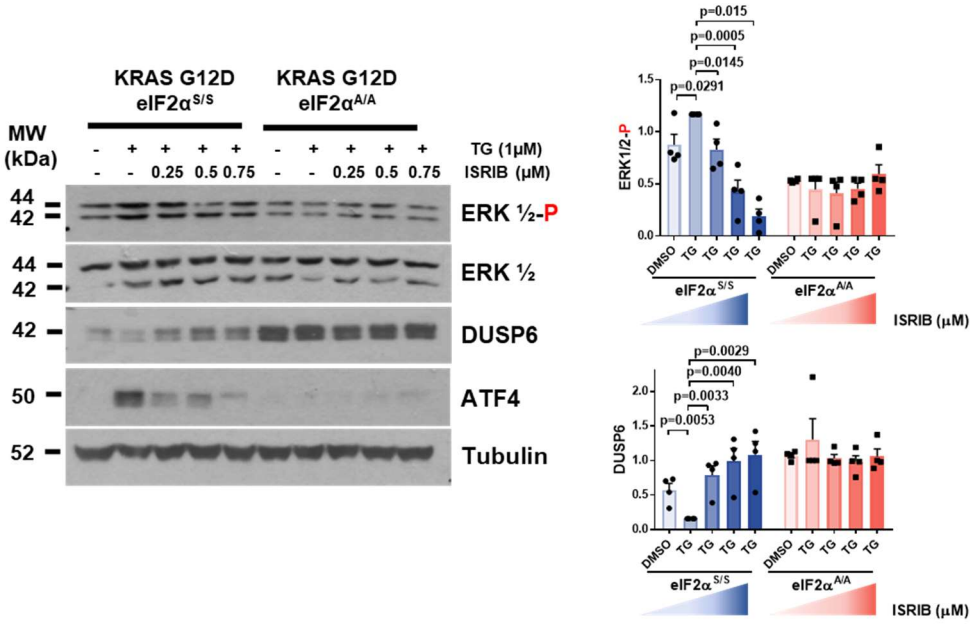

Figure 33. ISR inhibition antagonizes p-eIF2α function in mutant KRAS lung tumor cells. Mouse KRAS G12D eIF2α$^{S/S}$ and eIF2α$^{A/A}$ cells were left untreated or pre-treated with 1 μM

thapsigargin (TG) for 30 min followed by treatments with increasing ISRIB concentrations for 1 h. Protein extracts (50 µg) were subjected to immunoblotting for the indicated proteins. Quantifications of blots for phosphorylated ERK (ERK-P) and DUSP6 in eIF2α$^{S/S}$ and eIF2α$^{A/A}$ cells were obtained from four biological replicates. ERK-P was normalized to total ERK whereas DUSP6 expression to Tubulin. ATF4 was used as a marker of the antagonistic effects of ISRIB on p-eIF2-mediated mRNA translation in the tumor cells. Data represent mean ± SEM. Significance in differences between two datasets was determined using two-tailed unpaired t-test.

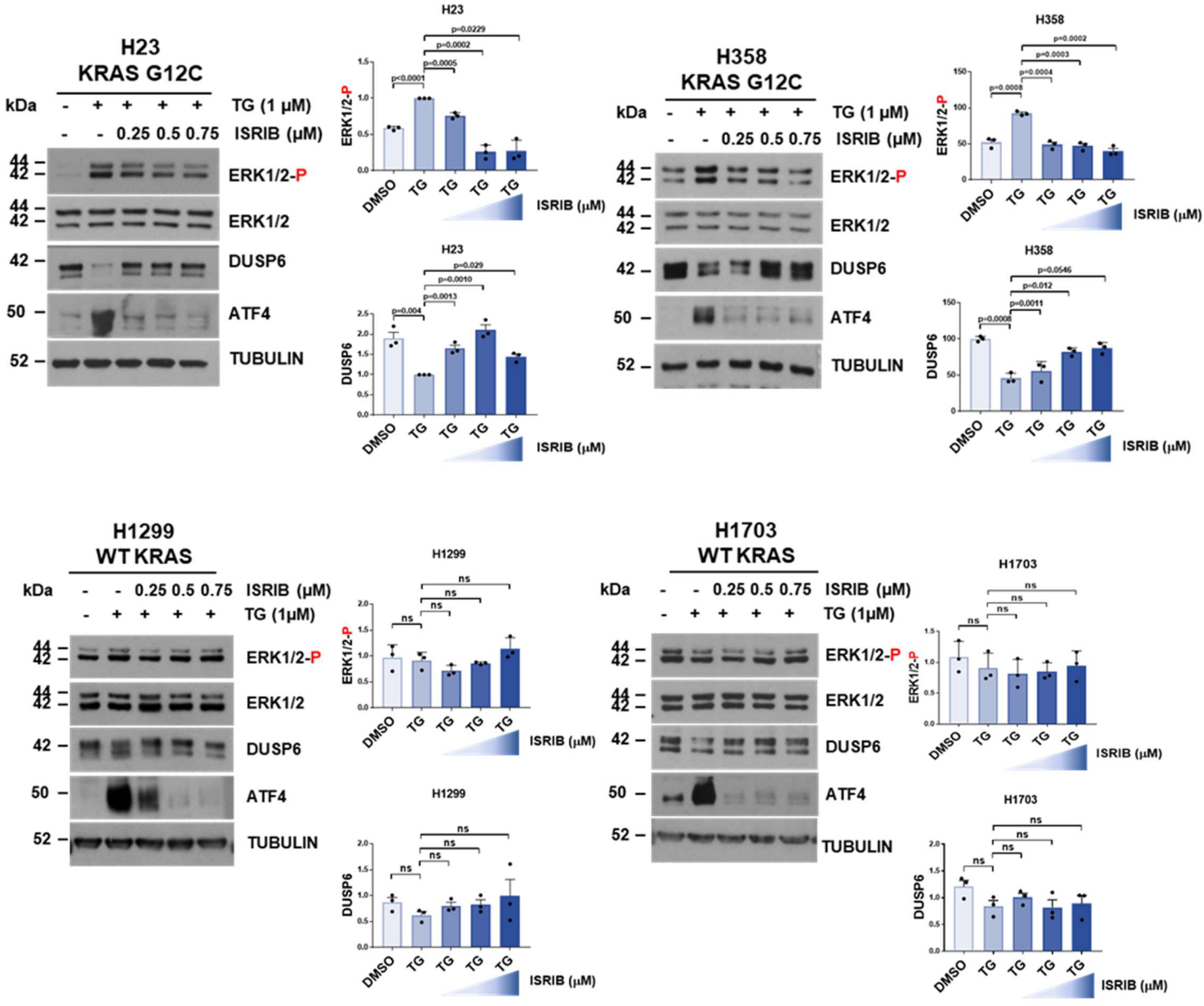

Figure 34. The ISR decreases DUSP6 and stimulates p-ERK in human LUAD cells under stress. Human LUAD cells with either WT KRAS (H1299, H1703) or KRAS G12C (H23, H358) were treated with 1μM thapsigargin (TG) for 30 min followed by treatments with increasing concentration of ISRIB for 1 h at the indicated concentrations. Protein extracts (50 μg) were immunoblotted for the indicated proteins. Quantification of proteins was performed from 3 biological replicates. p-ERK was normalized to total ERK whereas DUSP6 expression to ACTIN or TUBULIN. Data represent mean ± SEM. Statistical significance was determined using two-tailed unpaired t-test.

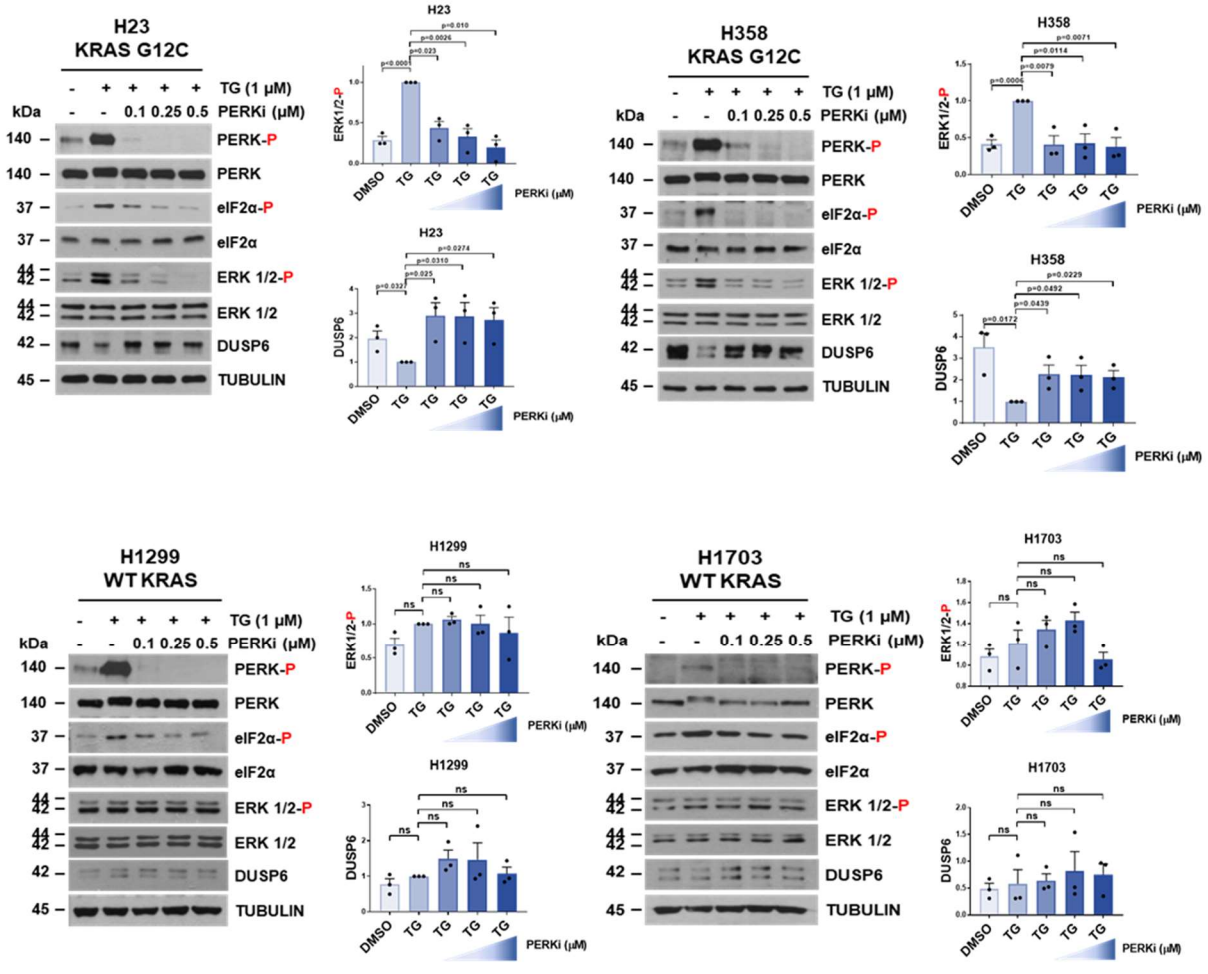

Figure 35. Activation of PERK-p-eIF2α decreases DUSP6 and stimulates p-ERK in human LUAD cells under stress. Human LUAD cells with either WT KRAS (H1299, H1703) or KRAS G12C (H23, H358) were treated with 1μM thapsigargin (TG) for 30 min followed by treatments with increasing concentration of PERK inhibitor (PERKi) for 1 h at the indicated concentrations. Protein extracts (50 μg) were immunoblotted for the indicated proteins. Quantification of proteins was performed from 3 biological replicates. p-ERK was normalized to total ERK whereas DUSP6 expression to ACTIN or TUBULIN. Data represent mean ± SEM. Statistical significance was determined using two-tailed unpaired t-test.

Next, we used multiple *in vivo* models to verify the therapeutic potential of ISRIB and PERK inhibitor. We subcutaneously injected H1299 cells, ectopically expressing either wild-type or mutant KRAS G12C, in nude mice (Figure 36). Treatment with PERK inhibitor led to a stronger reduction of growth of KRAS G12C H1299 tumors compared to wild-type KRAS H1299 tumors. Interestingly, ISRIB had no effect on tumor growth of wild-type KRAS H1299 tumors, but significantly reduced the growth of KRAS G12C H1299 tumors (Figure 36). This might be due to the more direct effect of ISRIB on the translational functions of p-eIF2α, as opposed to the PERK inhibitor which targets the upstream kinase and might lead to effects independent of p-eIF2α. However, this confirms a specific anti-tumor effect of ISRIB on KRAS-mutated tumors.

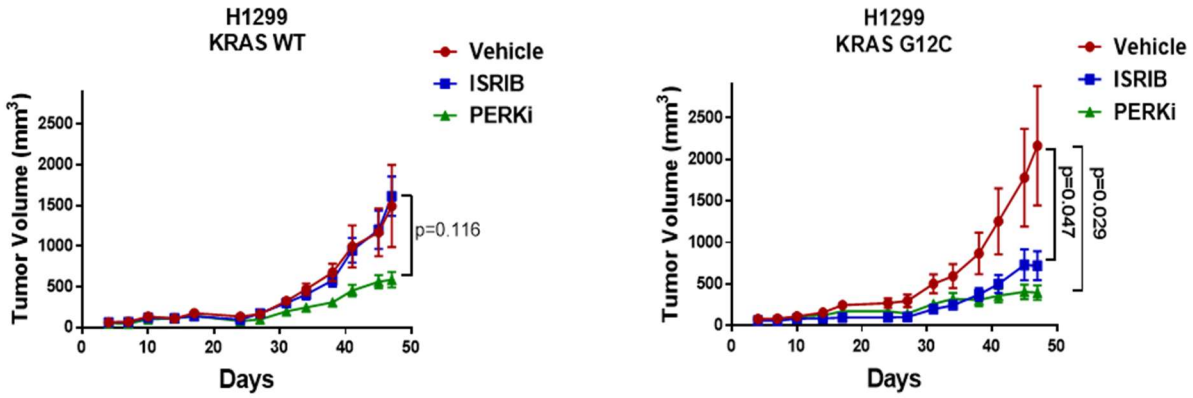

Figure 36 Pharmacological inhibition of ISR impairs mutant KRAS lung tumor growth and not wild-type KRAS lung tumor growth in human lung cancer cells. H1299 cells overexpressing

either wild type KRAS or KRAS G12C were transplanted subcutaneously in nu/nu mice followed by treatments with vehicle control (n = 8 for wild type KRAS; n = 6 for KRAS G12C), 10 mg/kg ISRIB (n = 10 for wild type KRAS; n = 8 for KRAS G12C) or 150 mg/kg PERK inhibitor GSK2606414 (PERKi) (n = 10 for wild type KRAS; n = 6 KRAS G12C). Data represent mean ± SEM, two-sided one-way ANOVA, Dunnett's multiple comparison test, P values are indicated on the graph.

As a second model, we orthotopically injected mouse Lewis Lung Carcinoma (LLC) cells that have a mutation of KRAS G12C in the lungs of B6 mice. We used this model to determine the effects of PERK inhibitor and ISRIB on lung tumorigenesis *in vivo* in an immunocompetent model. Therefore, the experimental design involved B6 mice orthotopically transplanted with LLC cells treated with either vehicle, ISRIB or PERK inhibitor. After 12 days of transplantation, and after viewing B-lines on ultrasound, implying the initiation of tumors, we started the treatments daily for 6 weeks (Figure 37). Tumor volume measurements were taken weekly by ultrasound and denoted in Figure 37. We observed that treatment of each inhibitor alone significantly reduced the growth of tumor in this model. Also, IHC staining showed that ISRIB significantly increased DUSP6 levels in tumors of lung sections in this model, followed by significant reductions in p-ERK levels in this model.

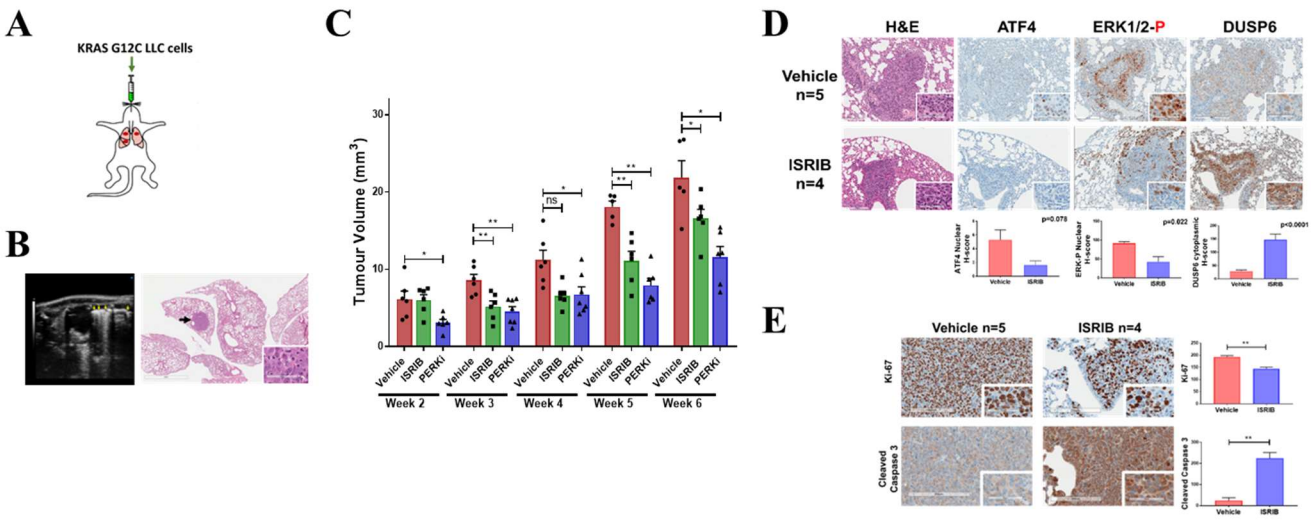

Figure 37. Therapeutically targeting the ISR decreases lung tumor formation in orthotopically injected LLC cells. (A) Illustration describing the method of orthotopic injection of $2x10^5$ LLC cells by intratracheal intubation. (B) Ultrasound imaging (left) and H&E staining (right) of mouse lungs 10 days after orthotopic transplantation depicting tumor development before initiation of treatment. (C) Graph indicates lung tumor volume at the indicated weeks of tumor growth as analyzed by ultrasound imaging of mice treated with vehicle (n = 6), 10 mg/kg ISRIB (n = 6), and 150 mg/kg PERKi (n = 7). Data represent mean ± SEM, two-sided one-way ANOVA, Dunnett's multiple comparison test, P values are indicated on the graph. (D) H&E staining along with the expression of nuclear ATF4, nuclear p-ERK and cytoplasmic DUSP6 in vehicle-control or ISRIB-treated LLC tumors at the sixth week of treatment. Scale bars correspond to 200 and 60 µm of core and enlarged tumor images, respectively. (E) IHC analysis of Ki-67 and Cleaved Caspase 3 in vehicle-control treated (n=5) and ISRIB-treated LLC tumors (n=4) in mice after 6 weeks of treatment. Data represent mean ± SEM. Statistical significance was determined using two-tailed unpaired t-test.

Furthermore, in a third model of LUAD, tumors were autochthonously induced by lentiviral intubation in the KRAS G12D immunocompetent model. Treatment of either Vehicle or ISRIB was administered daily after 10 weeks of tumor induction. In this model, we purposefully avoided the treatment of PERK inhibitor, due to adverse side-effects caused by this inhibitor on mice, ranging from loss of appetite and weight to death of the animal due to increased pancreatic toxicity caused by this drug. After 24 weeks of treatment, we noticed that tumor volume was significantly reduced in ISRIB-treated mice compared to vehicle-treated mice (Figure 38). A similar trend had followed after 38 weeks of treatment, during which 50% of vehicle-treated mice had died, whereas only 2 out of 6 ISRIB-treated mice had succumbed. Concordantly, the survival of mice treated with ISRIB was significantly prolonged compared to vehicle-treated mice. Similarly, ISRIB reduced the growth around 30% of a KRAS G12C PDX that was transplanted subcutaneously in nude mice (Figure 39). Therefore, ISR inhibitors indeed demonstrate anti-tumor effects and therapeutic potential in the treatment of KRAS LUAD.

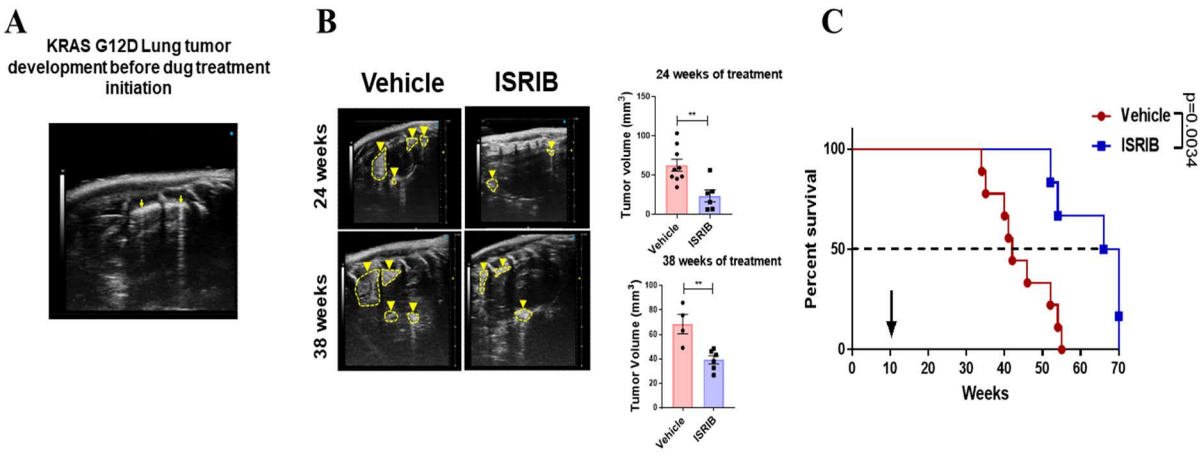

Figure 38 Effect of ISRIB on KRAS G12D lung tumor growth and survival of mice. Immune-competent mice bearing KRAS G12D lung tumors were subjected to treatments with either vehicle (n = 9) or 10 mg/kg ISRIB (n = 6). Ultrasound imaging in panel e indicates lung tumor formation in live mice at 24 or 38 weeks after treatment initiation. Graphs indicate tumor volume assessed by ultrasound imaging. The survival curve in (f) refers to immune-competent mice bearing KRAS G12D tumors treated with either vehicle control (n = 9) or 10 mg/kg ISRIB (n = 6). Arrowhead indicates initiation of drug treatment 10 weeks after KRAS G12D induction in the

lungs by the intratracheal intubation of CRE-expressing lentiviruses, at which point detectable lung tumors were formed (Supplementary Fig. 11b). d, f Data represent mean ± SEM. Significance in differences between two datasets was determined using two-tailed unpaired t-test.

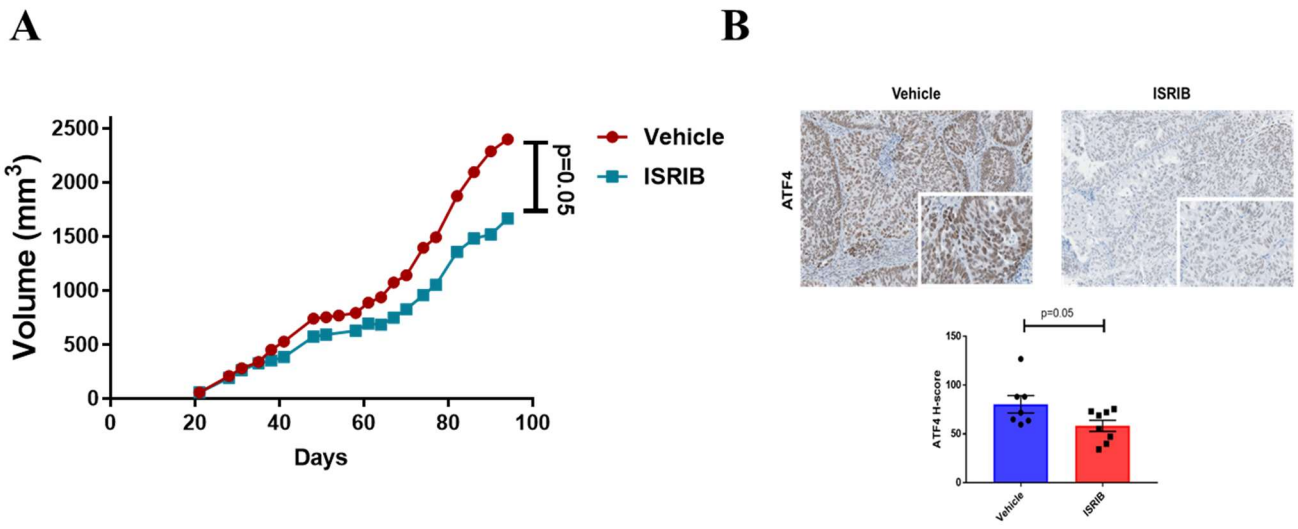

Figure 39 ISRIB reduces KRAS G12C LUAD progression in a PDX model. (A) Subcutaneous growth of KRAS G12D PDX in nude mice (Vehicle; n=5, ISRIB; n=5). (B) IHC staining of ATF4 in cross sections of the PDX.

4. YAP/TAZ activation is required for the pro-tumorigenic effects of p-eIF2α in KRAS mutated LUAD

The HIPPO tumor suppressor pathway is highly implicated in KRAS-mutated LUAD, specifically in resistance to therapy and increased survival[129,132,221]. Since there is a functional connection between p-eIF2α and the HIPPO transcriptional activators YAP/TAZ in liver cancer and under oxidative stress[237,253], we sought to further investigate if this connection is evident in KRAS LUAD.

4.1 Analysis of p-eIF2α gene transcriptional signature reveals top hits overlapping with YAP/TAZ activation

Pearson *et al.* were able to stratify different types of cancers into YAP/TAZ positive (YAP^{ON}) and YAP/TAZ deficient (YAP^{OFF}) tumors[143]. YAP^{ON} cancers exhibit a dependency on YAP activity for proliferation and growth, whereas YAP acts as a tumor-suppressor in YAP^{OFF} cancers[143]. They defined YAP^{ON} tumors as adenocarcinoma, squamous cell carcinoma and sarcoma and YAP^{OFF} tumors to be blood, neural and neuro-endocrine cancers[144]. Using transcriptomic data from thousands of cell lines and multiple primary tumors, they generated YAP/TAZ negative (YAP^{OFF}) and YAP/TAZ positive (YAP^{ON}) gene expression patterns via principle component analysis[144]. Upon aligning $eIF2\alpha^{S/S}$ vs. $eIF2\alpha^{A/A}$ transcriptional signatures with YAP^{ON} vs YAP^{OFF} gene expression signatures, we found that multiple genes overlap between the two expression signatures, which highlights a regulation of YAP activity by p-eIF2α (Figure 40). Particularly, 212 genes upregulated by p-eIF2α (SS_AA_UP) and 132 genes downregulated by p-eIF2α (SS_AA_DOWN) were also regulated in the YAP^{ON} expression signature, and 59 genes upregulated by p-eIF2α (SS_AA_UP) and 44 genes downregulated in p-eIF2α (SS_AA_DOWN) were also regulated in the YAP^{OFF} gene expression signature. Enrichment analysis revealed important processes regulated by the 212 common genes found in p-eIF2α and YAP^{ON} mediated signatures (Table 5). Analysis of KEGG pathways indicated that the top pathways are PI3K-Akt, Rap1 and MAPK signaling pathways, which are important pro-tumorigenic pathways. DAVID analysis identified top scores in biological processes to be positive regulation of cell proliferation, the MAPK cascade, EMT transition, canonical WNT signaling pathway, regulation of angiogenesis, cell-cell junction organization and immune response to tumor cells (Figure 41). CC enrichment analysis found that genes related to cell-cell junction, adherens junction and collagen-containing extracellular matrix were enriched (Figure 42, Table 6). Analysis of MF pathways indicated that top regulated pathways are growth factor binding, extracellular matrix structural constituent, and fibronectin binding. For the 132 genes downregulated by p-eIF2α and upregulated in YAP^{ON} expression signature, KEGG and MF analyses were not possible due to low number of genes. However, BP and CC analyses revealed the top pathways regulated such as focal adhesion, cell-substrate junction and collagen-containing extracellular matrix (Figure 43, Table 6). Analyses of the 59 genes upregulated by p-eIF2α in YAP^{OFF} background revealed BP, CC and MF pathways related with tumor-cell interactions with the immune response, such as leukocyte cell-cell adhesion, antigen receptor-

mediated signaling pathway and regulation of T cell activation. Since genes upregulated by p-eIF2α overlap the most with YAP^{ON} gene expression signature, we built a PPI network for all identified 212 genes, and selected top 10 scores of the network interaction (Figure 44). These hits function positively in regulating cell proliferation, epithelial-mesenchymal transition, and are associated with pathways in cancer: *EGFR, EGR1, FGFR1, IL6, JAG1, SNAI2, SOX9, TGFBR1, VEGFA, WNT5A.* Using an MCC algorithm revealed 2 important modules from the PPI network. Module A, concerned with epithelial to mesenchymal transition and positive regulation of endothelial cell proliferation (*FGFR1, WNT5A, TGFBR1, JAG1, SNAI2, VEGFC, IGFBP3, MCAM*). Module B, concerned with JAK-STAT signaling pathway and Cytokine-cytokine receptor interaction (*LIFR, IL11, CTF1, OSMR*) (Figure 45). However, the core genes in the network contain 6 genes in module A, indicating that module A is very important in all DEGs. This data reveal that p-eIF2α integrates YAP^{ON} genes for successful proliferation and survival of LUAD cancer cells, and employs YAP-related genes to implement an epithelial-to-mesenchymal (EMT) program, angiogenesis and cell proliferation for LUAD progression.

Figure 40. p-eIF2α-regulated genes overlap with genes upregulated in YAP^{ON} cancer types. Comparison of transcriptional signature of p-eIF2α regulated genes to those regulated by YAP^{ON}

(PC1+) and YAP^{OFF} (PC1-) genes. Red circle highlights the top 212 genes upregulated by p-eIF2α and overlapping with genes regulated in YAP^{ON} cancers.

Table 5. List of p-eIF2α upregulated genes overlapping with YAP^{ON} transcriptional signature identified in BP, CC and MF analyses. The identified genes represent top hits from the 212 overlapping genes.

ONTOLOGY	Description	GeneRatio	pvalue	geneID
BP	epithelial to mesenchymal transition	12/192	1.08E-07	SOX9/JAG1/SNAI2/WNT5A/EFNA1/FGFR1/SPRY2/TGFBR1/IL17RD/TGFBR3/HAS2/IL6
	canonical Wnt signaling pathway	15/192	8.21E-07	SOX9/BICC1/KLF4/DKK3/SNAI2/WNT5A/FZD6/EGFR/EXT1/NPHP3/EGR1/TRPM4/LYPD6/PLEKHA4/IGFBP6
	epithelial cell migration	16/192	8.81E-07	FSTL1/SOX9/KLF4/VEGFA/WNT5A/GADD45A/VEGFC/DCN/EFNA1/FGFR1/TGFBR1/PTPRG/HAS2/CARD10/PRKD1/KRT16
	cell-cell junction organization	11/192	8.68E-06	IRX3/VEGFA/CDH6/SNAI2/DSG2/VCL/EXT1/TGFBR1/LSR/GJC1/GJB2
	epithelial cell proliferation	15/192	5.24E-05	SOX9/VEGFA/SNAI2/WNT5A/CEBPB/EGFR/VEGFC/FGFR1/B4GALT1/TGFBR1/HES1/TGFBR3/HAS2/IL6/PRKD1
	cell growth	15/192	0.00014	SOX9/VEGFA/FLRT3/NGF/WNT5A/EGFR/VCL/SERPINE2/EXT1/SGK1/PLXNA3/TGFBR1/ENPP1/TNC/RGS4
	regulation of epithelial cell proliferation	13/192	0.000159	SOX9/VEGFA/SNAI2/WNT5A/EGFR/VEGFC/FGFR1/B4GALT1/TGFBR1/HES1/TGFBR3/HAS2/PRKD1
	positive regulation of MAPK cascade	15/192	0.000164	VEGFA/ADORA1/WNT5A/GADD45A/EGFR/EFNA1/GHR/FGFR1/SPRY2/TGFBR1/PDGFC/IL6/CSPG4/IL11/IGFBP6
	regulation of angiogenesis	10/192	0.002964	KLF4/VEGFA/WNT5A/GADD45A/VEGFC/DCN/EFNA1/SPRY2/IL6/PRKD1
CC	cell-cell junction	22/197	6.42E-09	VEGFA/JAG1/FLRT3/CDH6/NDRG1/DSG2/VCL/PODXL/B4GALT1/STEAP1/TGFBR1/WTIP/LSR/CDC42EP1/GJC1/PMP22 SHROOM1/GJB2/PVR/GJB5/FLOT1/PRKD1
	adherens junction	10/197	9.81E-06	VEGFA/JAG1/CDH6/NDRG1/VCL/WTIP/CDC42EP1/SHROOM1/PVR/FLOT1
	collagen-containing extracellular matrix	14/197	0.000118	EDIL3/WNT5A/COL12A1/DCN/COL15A1/SERPINE2/ANGPTL2/FBLN1/SDC3/TNC/ACAN/COL6A1/CSPG4/TGFBI
	endoplasmic reticulum lumen	11/197	0.000323	FSTL1/FKBP10/WNT5A/COL12A1/RCN3/COL15A1/IGFBP3/TNC/PDGFC/IL6/COL6A1
	Golgi lumen	6/197	0.000642	NGF/WNT5A/DCN/SDC3/ACAN/CSPG4
	focal adhesion	12/197	0.001135	MCAM/FLRT3/LRP1/EGFR/VCL/FLNC/CDC42EP1/TNC/CSRP2/PVR/FLOT1/CSPG4
	connexin complex	3/197	0.001165	GJC1/GJB2/GJB5
	cell-substrate junction	12/197	0.001359	MCAM/FLRT3/LRP1/EGFR/VCL/FLNC/CDC42EP1/TNC/CSRP2/PVR/FLOT1/CSPG4
MF	growth factor binding	11/195	2.73E-07	OSMR/LIFR/EGFR/GHR/FGFR1/SORT1/TGFBR1/IGFBP3/TGFBR3/COL6A1/IGFBP6
	extracellular matrix structural constituent	9/195	9.28E-05	EDIL3/COL12A1/DCN/COL15A1/FBLN1/TNC/ACAN/COL6A1/TGFBI
	fibronectin binding	4/195	0.000307	VEGFA/FBLN1/IGFBP3/IGFBP6
	growth factor activity	8/195	0.000338	VEGFA/JAG1/NGF/VEGFC/BTC/PDGFC/IL6/IL11

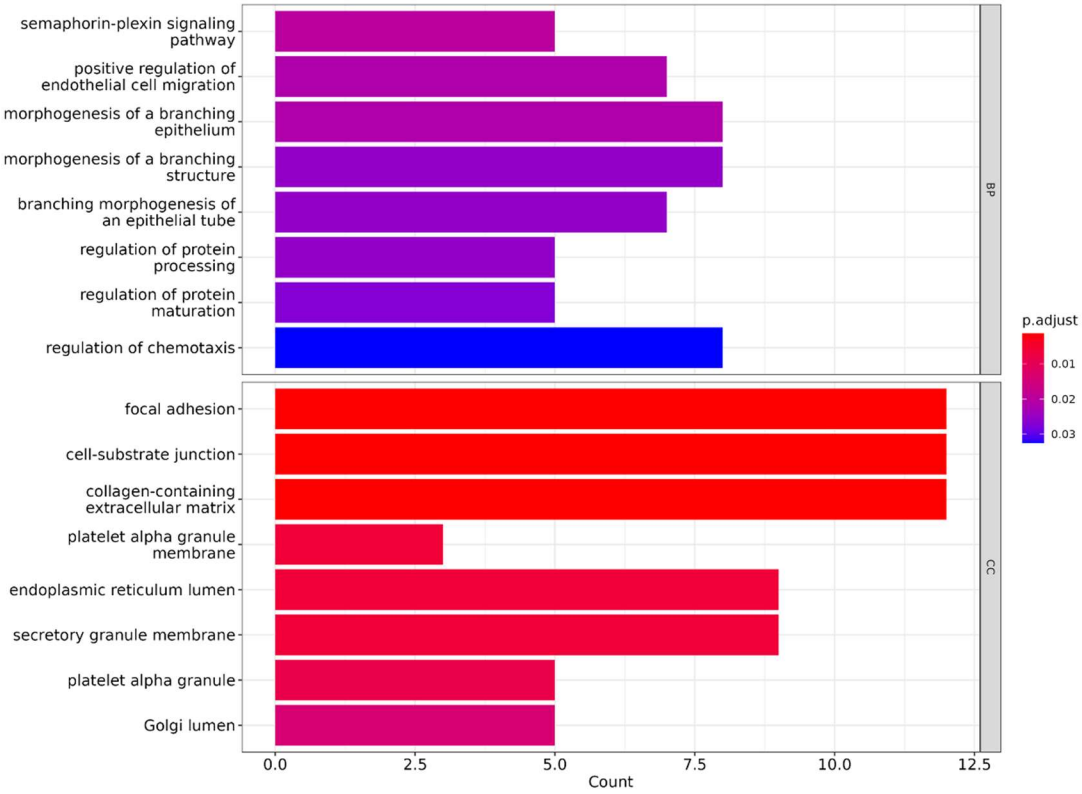

Figure 41 DAVID analysis of p-eIF2α upregulated regulated genes overlapped with YAP^{ON} transcriptional signatures. X-axis: Gene count. Enrichment analysis for BP: Biological Process; CC: Cellular Component, KEGG: Kyoto Encyclopedia for Genes and Genomes; MF: Molecular Function.

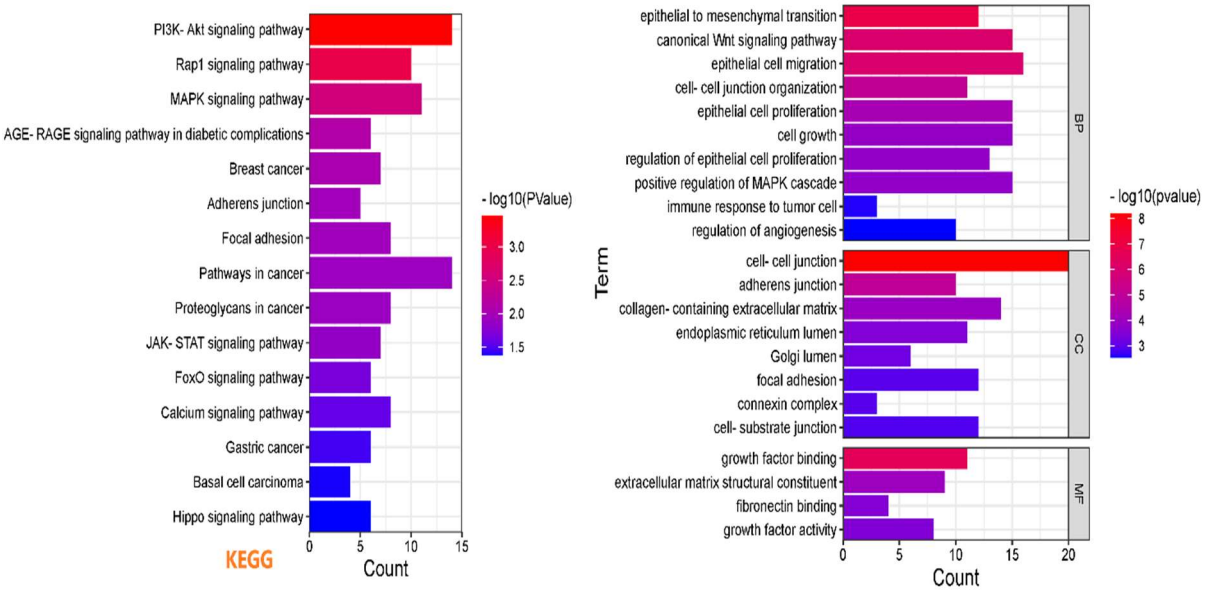

Figure 42. DAVID analysis of p-eIF2α downregulated genes overlapped with YAP^{ON} transcriptional signatures. X-axis: gene count. Enrichment analysis for BP: Biological Process; CC: Cellular Component.

Table 6. List of p-eIF2α downregulated genes overlapping with YAP^{ON} transcriptional signature identified in BP, CC and MF analyses. The identified genes represent top hits from the 132 overlapping genes.

ONTOLOGY	Description	GeneRatio	pvalue	geneID
BP	semaphorin-plexin signaling pathway	5/121	8.05E-06	SEMA5A/EDN1/SEMA7A/RAC1/PLXNA2
	positive regulation of endothelial cell migration	7/121	2.22E-05	SEMA5A/CCBE1/EDN1/SPARC/RAC1/FGF1/EGF
	morphogenesis of a branching epithelium	8/121	2.64E-05	CSF1/EDN1/MMP14/COL4A1/FGF1/ADM/EGF/FOXD1
	morphogenesis of a branching structure	8/121	4.44E-05	CSF1/EDN1/MMP14/COL4A1/FGF1/ADM/EGF/FOXD1
	branching morphogenesis of an epithelial tube	7/121	5.99E-05	CSF1/EDN1/MMP14/COL4A1/FGF1/EGF/FOXD1
	regulation of protein processing	5/121	6.17E-05	CCBE1/MMP14/SERPINE1/CAST/NOL3
	regulation of protein maturation	5/121	7.66E-05	CCBE1/MMP14/SERPINE1/CAST/NOL3
	regulation of chemotaxis	8/121	0.0001	BST1/SEMA5A/CSF1/EDN1/SEMA7A/RAC1/SERPINE1/FGF1
	positive regulation of epithelial cell migration	7/121	0.00013	SEMA5A/CCBE1/EDN1/SPARC/RAC1/FGF1/EGF
CC	focal adhesion	12/126	1.69E-05	TLN2/PROCR/FHL1/HSPA1B/PDLIM1/MMP14/ARHGAP24/ARHGAP31/REXO2/RAC1/HSPA1A/TGFB1I1
	cell-substrate junction	12/126	2.09E-05	TLN2/PROCR/FHL1/HSPA1B/PDLIM1/MMP14/ARHGAP24/ARHGAP31/REXO2/RAC1/HSPA1A/TGFB1I1
	collagen-containing extracellular matrix	12/126	2.13E-05	BGN/CTSF/SPARC/MXRA7/SEMA7A/SERPINE1/COL4A1/COL4A2/WNT5B/ADAM19/TGFB1I1/NID2
	platelet alpha granule membrane	3/126	0.00017	PCDH7/PHACTR2/SPARC
	endoplasmic reticulum lumen	9/126	0.00018	CSF1/EDN1/CRTAP/CKAP4/COL4A1/SUMF1/COL4A2/WNT5B/UGGT2
	secretory granule membrane	9/126	0.00019	BST1/PCDH7/PHACTR2/SPARC/LAMP1/CKAP4/PTPRB/RAC1/CD14
	platelet alpha granule	5/126	0.0003	PCDH7/PHACTR2/SPARC/SERPINE1/EGF
	Golgi lumen	5/126	0.00056	BGN/MMP14/GOLIM4/WNT5B/HS3ST1
	endocytic vesicle	8/126	0.00167	DYSF/CLTB/SPARC/LAMP1/ABCA1/GOLIM4/WNT5B/EGF

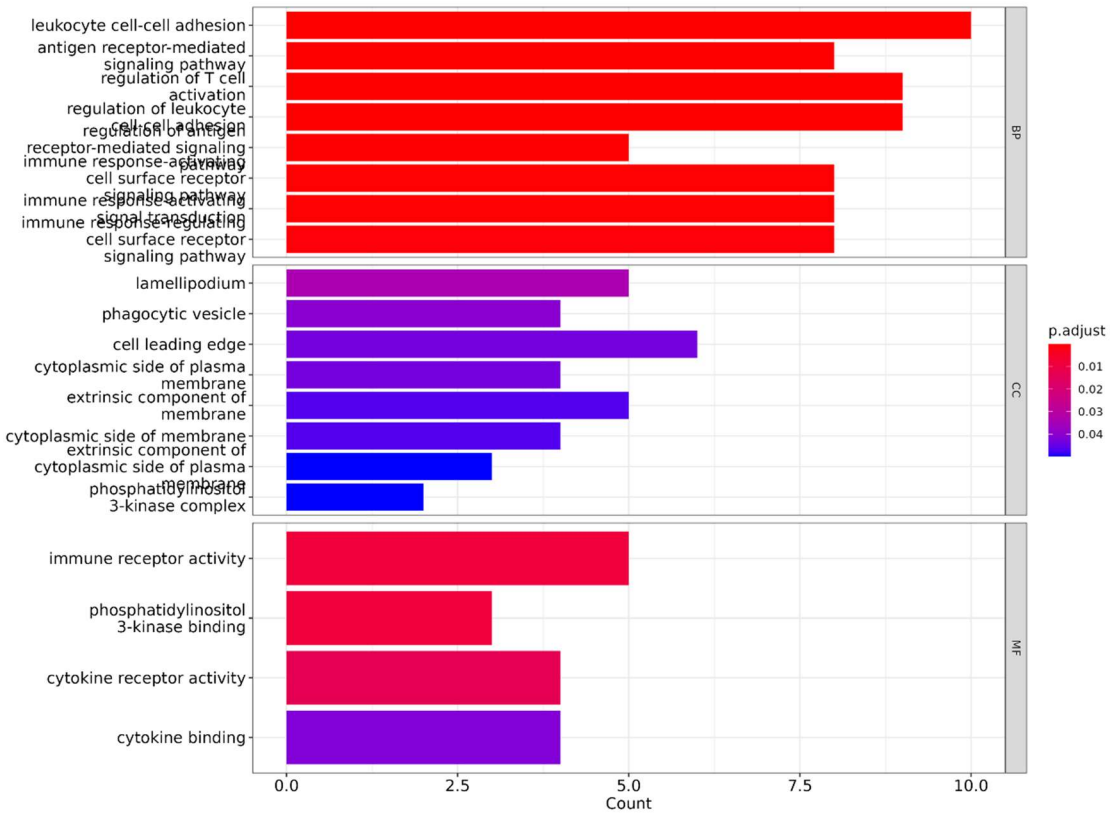

Figure 43. DAVID analysis of p-eIF2α upregulated genes overlapped with YAP^{OFF} transcriptional signatures. X-axis: Gene count. Enrichment analysis for BP: Biological Process; CC: Cellular Component, MF: Molecular Function

ONTOLOGY	Description	GeneRatio	pvalue	geneID
BP	leukocyte cell-cell adhesion	10/54	1.12E-07	ITGB7/ADORA2A/FCGR2B/LCK/IL12RB1/FCHO1/NFKBID/CCR7/CD300A/CORO1A
	antigen receptor-mediated signaling pathway	8/54	4.46E-07	PLCL2/FCGR2B/BLNK/LCK/FCHO1/NFKBID/CCR7/CD300A
	regulation of T cell activation	9/54	5.08E-07	ADORA2A/FCGR2B/LCK/IL12RB1/FCHO1/NFKBID/CCR7/CD300A/CORO1A
	regulation of leukocyte cell-cell adhesion	9/54	5.33E-07	ADORA2A/FCGR2B/LCK/IL12RB1/FCHO1/NFKBID/CCR7/CD300A/CORO1A
	regulation of antigen receptor-mediated signaling pathway	5/54	1.27E-06	PLCL2/FCGR2B/LCK/CCR7/CD300A
	immune response-activating cell surface receptor signaling pathway	8/54	2.11E-06	PLCL2/FCGR2B/BLNK/LCK/FCHO1/NFKBID/CCR7/CD300A
	immune response-activating signal transduction	8/54	2.11E-06	PLCL2/FCGR2B/BLNK/LCK/FCHO1/NFKBID/CCR7/CD300A
	immune response-regulating cell surface receptor signaling pathway	8/54	4.08E-06	PLCL2/FCGR2B/BLNK/LCK/FCHO1/NFKBID/CCR7/CD300A
CC	lamellipodium	5/55	0.00025	IQGAP2/PDXP/ABI3/CORO1A/TESC
	phagocytic vesicle	4/55	0.00061	FMNL1/NCF4/PLD4/CORO1A
	cell leading edge	6/55	0.00106	IQGAP2/ADORA2A/PDXP/ABI3/CORO1A/TESC
	cytoplasmic side of plasma membrane	4/55	0.00129	FES/LCK/PTPN7/GNGT2
	extrinsic component of membrane	5/55	0.00185	FES/PIK3C2B/LCK/PIK3R5/GNGT2
	cytoplasmic side of membrane	4/55	0.0021	FES/LCK/PTPN7/GNGT2
	extrinsic component of cytoplasmic side of plasma membrane	3/55	0.00271	FES/LCK/GNGT2
	phosphatidylinositol 3-kinase complex	2/55	0.00299	PIK3C2B/PIK3R5
MF	immune receptor activity	5/55	7.90E-05	IL5RA/FCGR2B/IL2RG/IL12RB1/CCR7
	phosphatidylinositol 3-kinase binding	3/55	8.73E-05	LCK/PIK3AP1/CORO1A
	cytokine receptor activity	4/55	0.0002	IL5RA/IL2RG/IL12RB1/CCR7
	cytokine binding	4/55	0.00083	IL5RA/IL2RG/IL12RB1/CCR7

Table 7. List of p-eIF2α upregulated genes overlapping with YAP^{OFF} transcriptional signature identified in BP, CC and MF analyses. The identified genes represent top hits from the 59 overlapping genes.

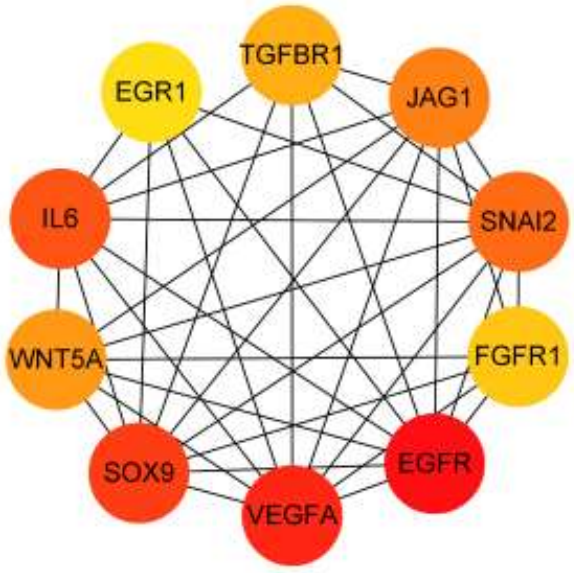

Figure 44. PPI network interaction of core genes underlying p-eIF2α-regulated YAP^{ON} genes.

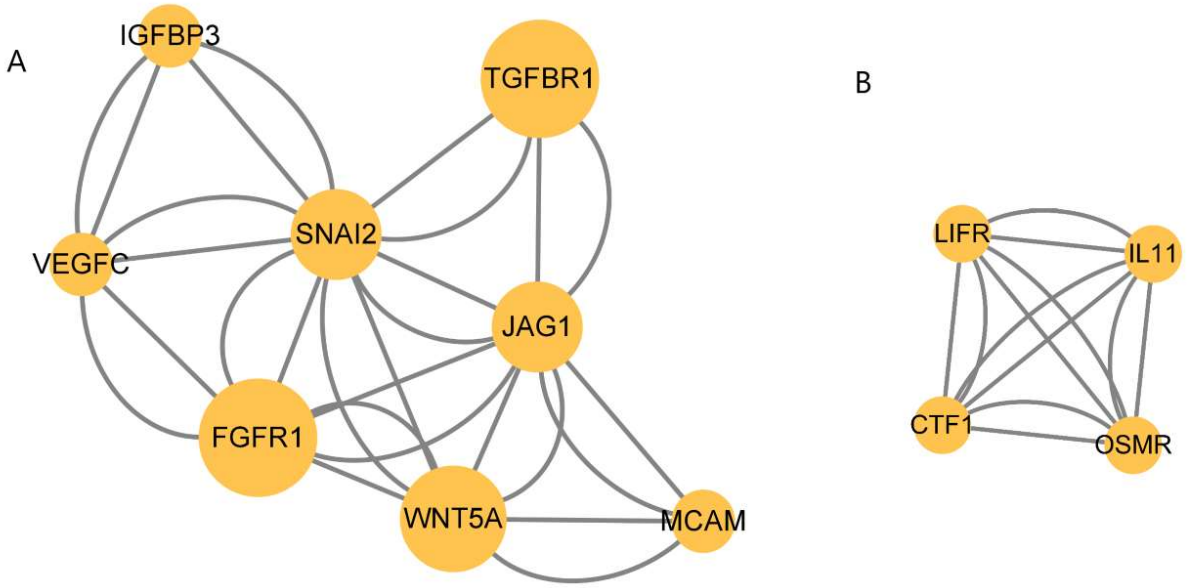

Figure 45. MCC algorithm reveals 2 modules from PPI network of p-eIF2α-regulated YAP^{ON} genes. Module (A) concerned with epithelial to mesenchymal transition and positive regulation of endothelial cell proliferation (FGFR1, WNT5A, TGFBR1, JAG1, SNAI2, VEGFC, IGFBP3, MCAM). Module (B) concerned with JAK-STAT signaling pathway and Cytokine-cytokine receptor interaction (LIFR, IL11, CTF1, OSMR).

4.2 Regulation of HIPPO pathway components by p-eIF2α in KRAS LUAD

Upon immunoblotting for HIPPO pathway components in eIF2α$^{S/S}$ and eIF2α$^{A/A}$ cells, phosphorylation of YAP1 at serine 127 (YAP-P) and TAZ at serine 89 (TAZ-P) were upregulated in cells lacking p-eIF2α compared to cells wild-type for p-eIF2α (Figure 46). This was concordant with upregulation of total protein levels of the core kinases LATS1 and LATS2 in cells deficient for p-eIF2α compared to p-eIF2α-proficient cells. In addition, TEAD2 expression levels were upregulated in p-eIF2α-wild-type compared p-eIF2α mutant cells. This regulation was ATF4-dependent since knocking down ATF4 with two different shRNAs led to

increased phosphorylation of YAP and TAZ (Figure 47). However, the knockdown only increased levels of LATS2 but not of LATS1 protein. Upon quantifying polyribosomal mRNA levels of LATS1 and LATS2, only LATS1 mRNA was better associated with the polyribosomal fraction of eIF2α$^{A/A}$ cells compared to eIF2α$^{S/S}$ cells, while total LATS1 mRNA levels were the same between the two cells (Figure 48). This implies that p-eIF2α inhibits the translation of LATS1. On the other hand, total LATS2 mRNA was significantly upregulated in the eIF2αA/A cells compared to wild-type cells. Therefore, p-eIF2α inhibits LATS2 mRNA expression but not translation. Furthermore, YAP nuclear localization was increased in eIF2α$^{S/S}$ lung tumor sections at 20 weeks post-tumor induction compared to those of eIF2α$^{A/A}$ (figure 49).

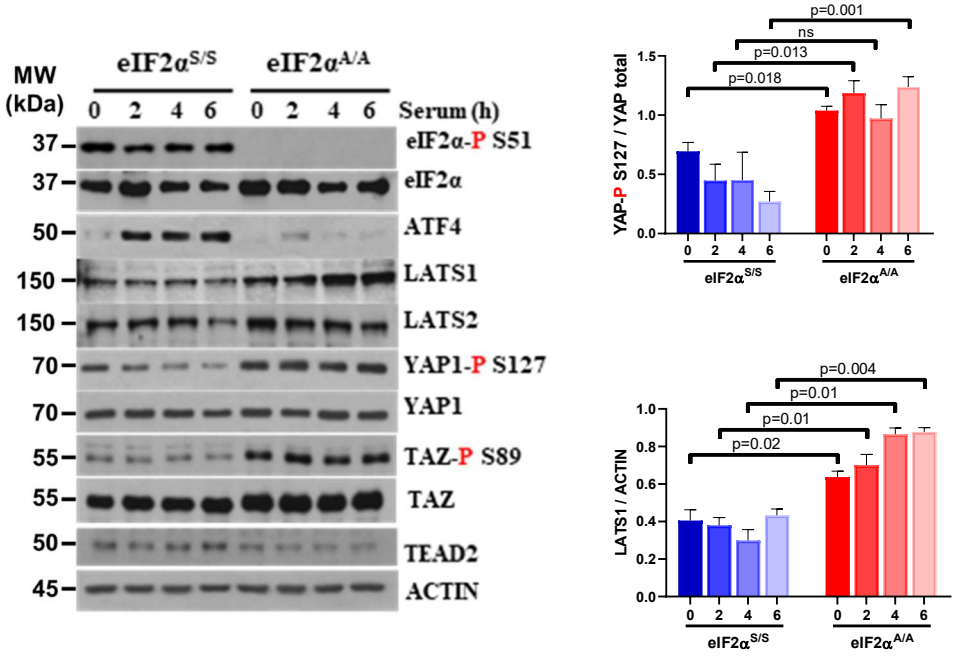

Figure 46. p-eIF2α inhibits the HIPPO signaling to activate YAP/TAZ. eIF2α$^{S/S}$ and eIF2α$^{A/A}$ KRAS G12D LUAD cells were deprived from serum for 18 hours prior to treatment with 10% FBS at the indicated timepoints. Protein extracts (50 µg) were subjected to immunoblotting for the indicated proteins. Data represent mean ± SEM of 3 independent experiments.

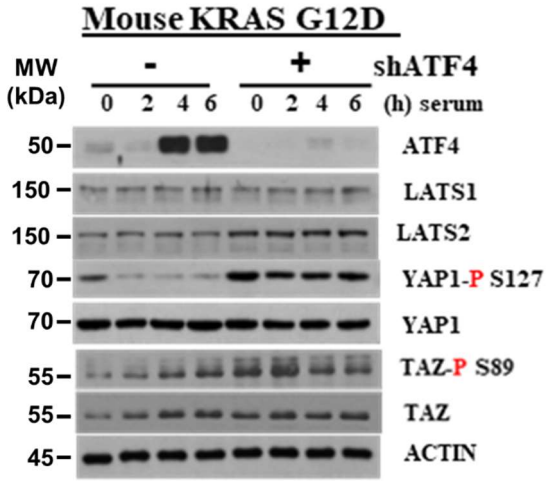

Figure 47. ATF4 regulates YAP/TAZ signaling in KRAS-G12D LUAD. Immunoblot analysis of ATF4-proficient and ATF4-deficient (shRNA) KRAS-G12D LUAD cells. Cells were treated with 10% FBS after serum-deprivation for 18 hours. The immunoblots are representative of two independent experiments with two different shRNAs for ATF4.

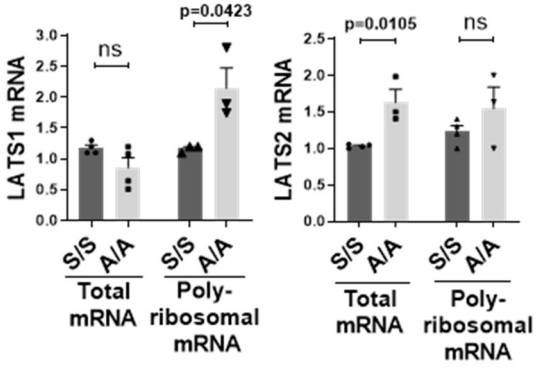

Figure 48. p-eIF2α regulates LATS1/2 poly-ribosomal mRNA. Quantification of total and poly-ribosomal-bound LATS1,2 mRNAs by qPCR after normalization to GAPDH and ACTIN

mRNAs. Data represent mean ± SEM. Significance in differences between two datasets was determined using two-tailed unpaired t-test. P values are indicated in the bar graphs (ns non-significant).

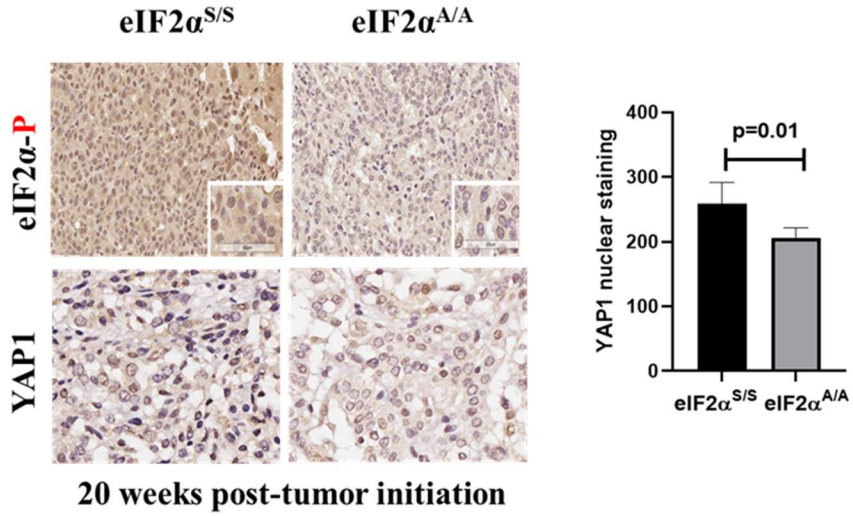

Figure 49. p-eIF2α induces YAP1 nuclear localization in mouse KRAS-G12D LUAD. IHC staining of YAP1 in eIF2α$^{S/S}$ and eIF2α$^{A/A}$ tumors. Graphs represent the average H-score of tumors per lung section of eIF2αS/S (n = 5) and eIF2α$^{A/A}$ (n = 5) mice with P value = 0.01. Data represent mean ± SEM. Significance in differences between two datasets was determined using two-tailed unpaired t-test. P values are indicated in the bar graphs.

4.3 The pro-tumorigenic effect of eIF2αP relies on YAP/TAZ activation.

To characterize the role of YAP/TAZ activation in the po-tumorigenic effects of p-eIF2α, we performed knockdown studies of YAP and TAZ by siRNAs in S/S and A/A cells. Inactivation of YAP alone or TAZ alone by siRNA in eIF2α$^{S/S}$ cells strongly inhibits their proliferation in colony formation assays, whereas no effects are observed in eIF2α$^{A/A}$ cells with YAP knockdown and around 30% of inhibition of colony efficacy was observed with TAZ knockdown (Figure 50). However, knockdown of both genes in significantly obliterated the

colony forming efficacy in both cell types, highlighting the importance of both genes in proliferation of LUAD cells. This suggests a strong dependency of the proliferative effects of p-eIF2α on YAP/TAZ activity.

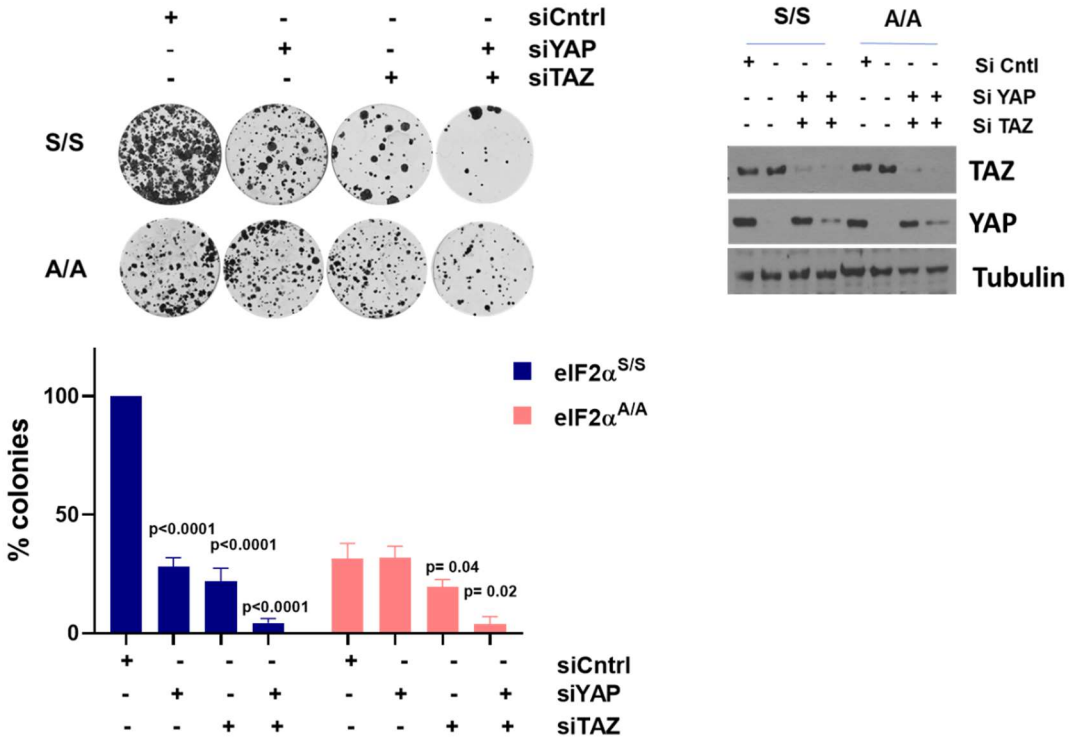

Figure 50. YAP/TAZ activation is essential for pro-tumorigenic effects of p-eIF2α. (A) Clonogenic assays of eIF2α$^{S/S}$ and eIF2α$^{A/A}$ cells treated with either scrambled, YAP alone, TAZ alone, or YAP/TAZ siRNAs. (B) Graphs representing the average % colony number formed after each siRNA. Data represent mean ± SEM from 3 biological replicates. Significance in differences between two datasets was determined using two-tailed unpaired t-test. P values are indicated in the bar graphs. (C) Immunoblot analysis of eIF2α$^{S/S}$ and eIF2α$^{A/A}$ KRAS-G12D cells showing efficient knockdown of YAP and TAZ proteins after siRNA knockdown.

4.4 Mechanism of YAP/TAZ activation might not be through canonical HIPPO pathway

Inactivation of MST1/2, the core kinases of the HIPPO pathway, in eIF2α$^{S/S}$ vs. eIF2α$^{A/A}$ cells reduced the phosphorylation of YAP at S127 in eIF2α$^{S/S}$ but not in eIF2α$^{A/A}$ cells (Figure 51A). This might indicate that the phosphorylation of YAP at S127 in the absence of but the decrease was not dramatic. Surprisingly, LATS1/2 downregulation caused a significant decrease in colony forming efficacy of both eIF2α$^{S/S}$ and eIF2α$^{A/A}$ cells (Figure 52). However, these data indicate that the pro-tumorigenic dependency of p-eIF2α on YAP/TAZ might be irrespective of the core kinases of the HIPPO pathway.

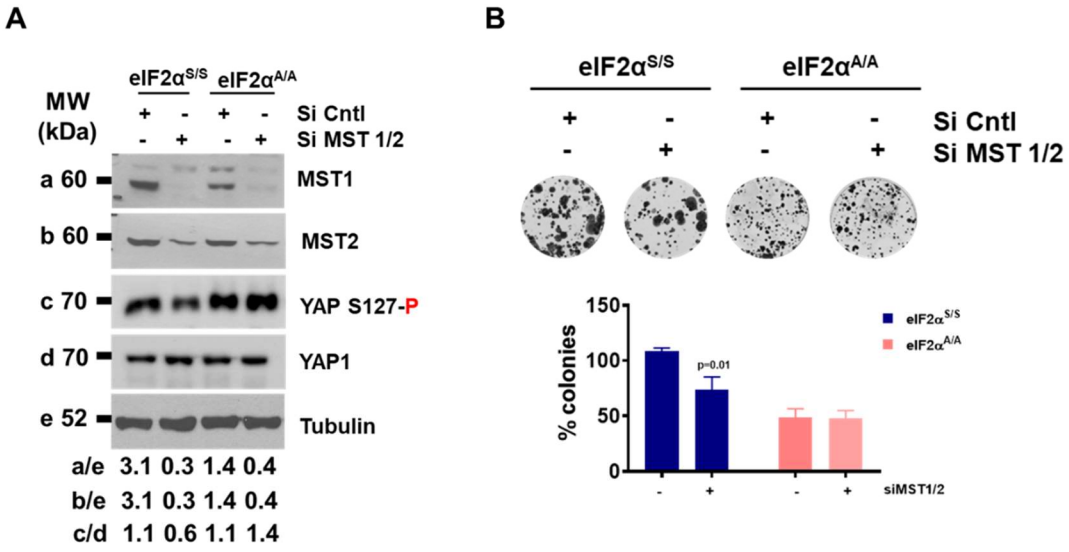

Figure 51. p-eIF2α is dependent on MST1/2 for YAP activation but not for proliferation. (A) immunoblotting for the indicated proteins and (B) clonogenic assays in eIF2α$^{S/S}$ and eIF2α$^{A/A}$ cells subjected to siRNA Control (Cntl) or MST1/2.

The eIF2αP-ATF4 arm upregulates the GADD34-PP1 phosphatase complex. Recent studies have implicated GADD34-PP1 as an inhibitor of YAP activity[254]. Treatment with eIF2αP-inducing drugs (Salubrinal & Guanabenz) increased YAP1-P in eIF2α$^{S/S}$ cells to levels similar to basal levels of YAP-P in eIF2α$^{A/A}$, meanwhile no induction of YAP-P was observed in eIF2α$^{A/A}$ cells. Salubrinal and Guanabenz inhibit the GADD34-PP1 phosphatase complex (Figure 53). Therefore, p-eIF2α might recruit GADD34-PP1 to inactivate YAP by dephosphorylation. GADD34 knockdown studies would give further indication of its implications in YAP activity.

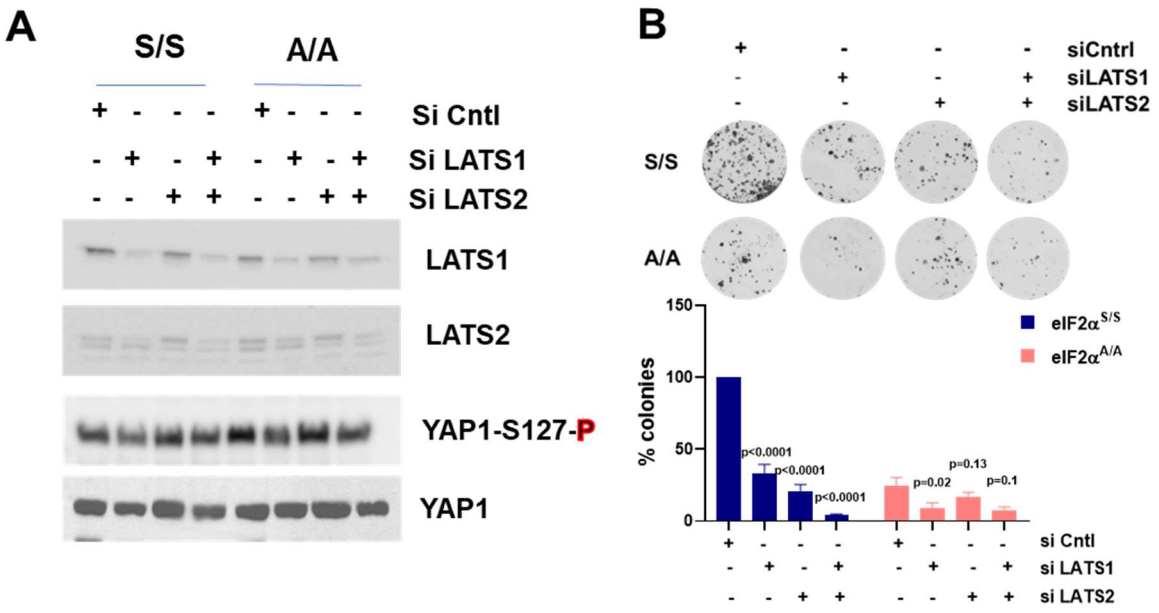

Figure 52. p-eIF2α is independent on LATS1/2 for YAP activation nor for proliferation. (A) immunoblotting for the indicated proteins and (B) clonogenic assays in eIF2α$^{S/S}$ and eIF2α$^{A/A}$ cells subjected to siRNA Control (Cntl) or LATS1/2. Immunoblot is representative of one experiment and clonogenic assays are from one biological replicate done in three technical replicates. Data represent Mean ± SEM of the three technical replicates.

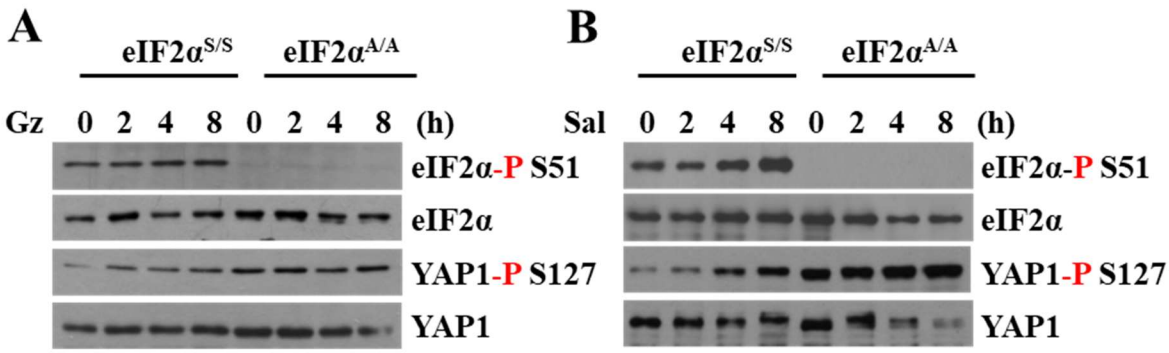

Figure 53. GADD34-PP1 might inactivate YAP. Immunoblotting of eIF2α$^{S/S}$ and eIF2α$^{A/A}$ cell extracts (50µg) treated with either (A) Guanabenz (Gz) or (B) Salubrinal (Sal) at the indicated timepoints. Immunoblots represent one experiment.

5. P-eIF2α as a driver of lineage diversity and high plasticity in KRAS LUAD

Recent studies investigating the ability of lung cancer cells to differentiate and lead to tumor heterogeneity reveal the importance of a high plasticity cell state (HPCS) clusters in lineage plasticity and progression to an EMT phenotype[204,224,225]. These studies were done in genetically engineered mouse models (GEMM) that mimic lung tumor progression driven by the *KRAS* oncogene and loss of *TP53*. The possibility of a specific cluster giving rise to lineage diversity prompted us to isolate the lung tumor cells of the eIF2α$^{S/S}$ and eIF2α$^{A/A}$ mice and perform scRNA sequencing analysis to obtain a better understanding of the role of p-eIF2α in tumor evolution.

5.1 Evidence of p-eIF2α driving high-plasticity in KRAS LUAD cells *in vitro*

The high-plasticity cell state during *KRAS* lung cancer progression has been identified by scRNA seq studies in Tuomas Tammela's group and verified in other studies[224,225,255]. Their studies highlight that in KRAS lung cancer, tumor evolution and intra-tumoral heterogeneity is not only dependent on loss of expression of tumor cells of origin properties, but also on additional gain of lineage diversity[224,255]. Among the various identified clusters, Marjanovic *et al.* detected an essential "highly mixed" cluster that gives rise to heterogeneity during tumor evolution[255]. They named that cluster the "high plasticity cell state" (HPCS) and associated multiple genes that are highly enriched in this transcriptional program[255]. As a preliminary investigation, we tried to align the different cluster signatures identified by Marjanovic *et al.* to bulk RNA-seq analysis of cultured primary eIF2α$^{S/S}$ and eIF2α$^{A/A}$ cells. HPCS as well as EMT cluster genes were strongly expressed in the eIF2α$^{S/S}$ transcriptome compared to that of eIF2α$^{A/A}$ (Figure 54). According to this preliminary analysis and upon awaiting results from scRNA seq of eIF2α$^{S/S}$ and eIF2α$^{A/A}$ tumor cells, I investigated the expression of the HPCS marker TIGIT that was highly enriched in this cluster and identified by Marjanovic et al. in cultured primary eIF2α$^{S/S}$ and eIF2α$^{A/A}$ cells.

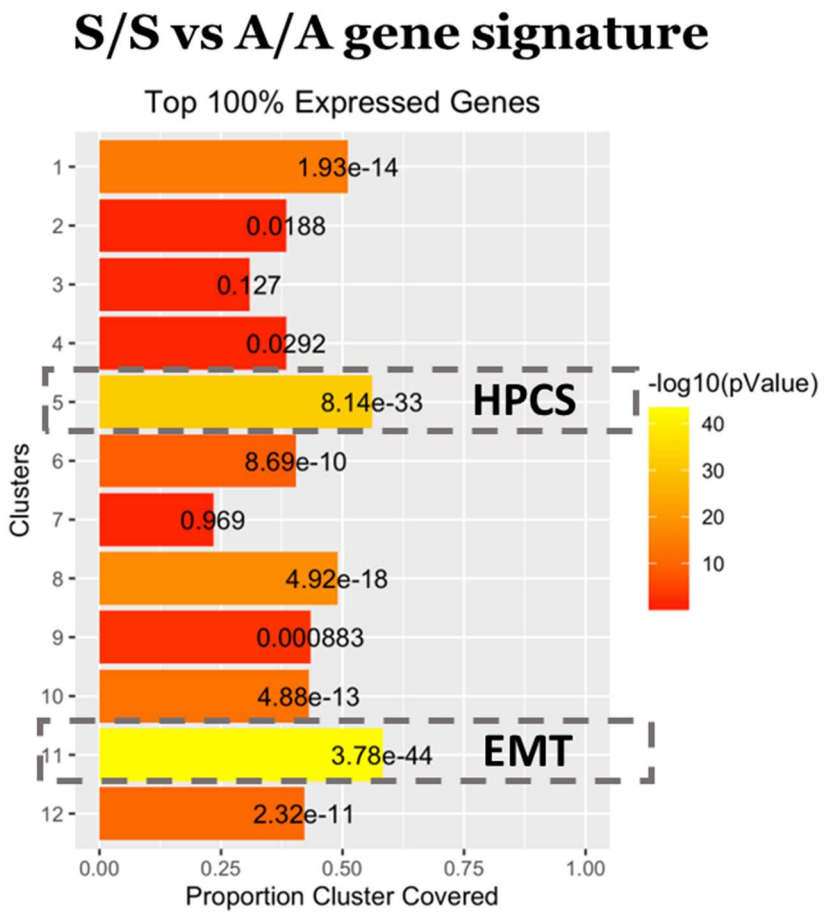

Figure 54. HPCS and EMT cluster genes are strongly enriched in gene expression signatures of eIF2α$^{S/S}$ vs eIF2α$^{A/A}$ tumor cells. Alignment of bulk RNA seq transcriptional profiles of primary eIF2α$^{S/S}$ and eIF2α$^{A/A}$ cells to gene expression of clusters (12 clusters) identified in scRNA seq data by Marjanovic et al. Dashed box highlights cluster 5 (HPCS) and 11 (EMT).

Marjanovic et al. identified a biomarker that is enriched in the HPCS transcriptional signature called TIGIT (T cell immunoreceptor with IgG and ITIM domains). This marker was unprecedented since it is uniquely expressed in T-cells and very few researchers reported its expression in epithelial cells. In an attempt to further study the possibility of p-eIF2α driving a HPCS signature, we compared TIGIT expression in cultured primary eIF2α$^{S/S}$ and eIF2α$^{A/A}$ cells. We saw that indeed eIF2α$^{S/S}$ cells exhibited significantly higher expression of TIGIT (Figure 55). We sorted eIF2α$^{S/S}$ and eIF2α$^{A/A}$ cells that displayed high TIGIT expression (TIGIT+) and no TIGIT expression (TIGIT-). We noticed that the absence of TIGIT decreased the colony

formation efficacy of both eIF2α$^{S/S}$ and eIF2α$^{A/A}$ cells, which confirms the ability of HPCS signature to drive proliferation (Figure 56). Interestingly, eIF2α$^{A/A}$ cells had the capacity to lose TIGIT expression with increased time in culture, while eIF2α$^{S/S}$ cells preserved the expression of TIGIT (Figure 57). This indicates the p-eIF2α has the ability to sustain TIGIT expression *in vitro.*

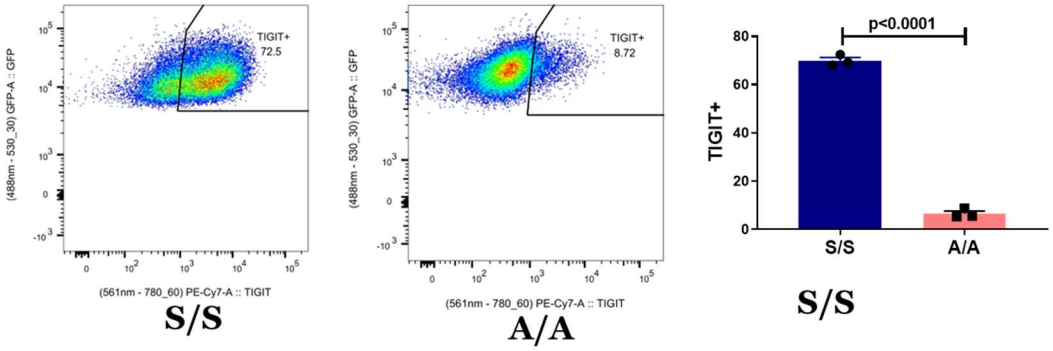

Figure 55. TIGIT expression in eIF2α$^{S/S}$ and eIF2α$^{A/A}$ culture cells. FACS analysis of TIGIT expression in eIF2α$^{S/S}$ and eIF2α$^{A/A}$ cultured cells. Representative of 3 independent experiments.

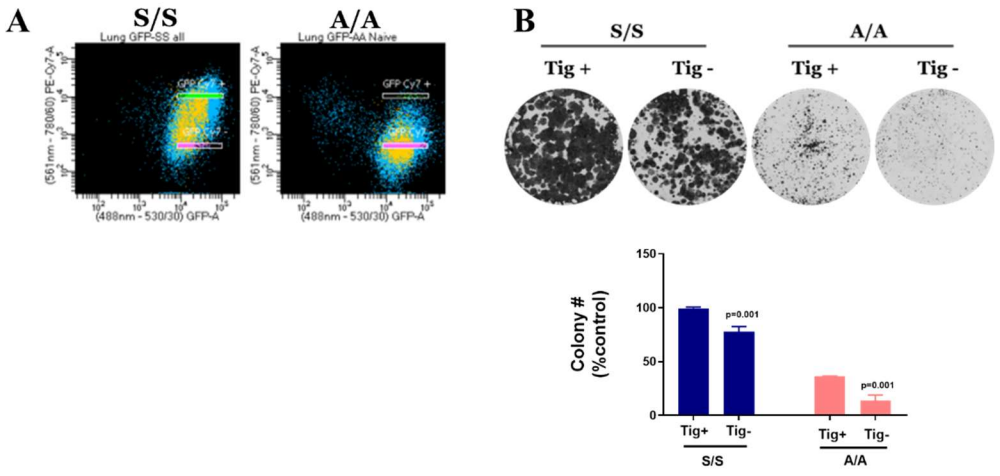

Figure 56. TIGIT is required for p-eIF2α-dependent proliferation in KRAS LUAD cells. (A) Sorting strategy to isolate TIGIT+ and TIGIT- cells from eIF2α$^{S/S}$ and eIF2α$^{A/A}$ cells. (B) Clonogenic assays of TIGIT+ and TIGIT- eIF2α$^{S/S}$ and eIF2α$^{A/A}$ cells with the corresponding representative graph. Representative of 3 technical replicates.

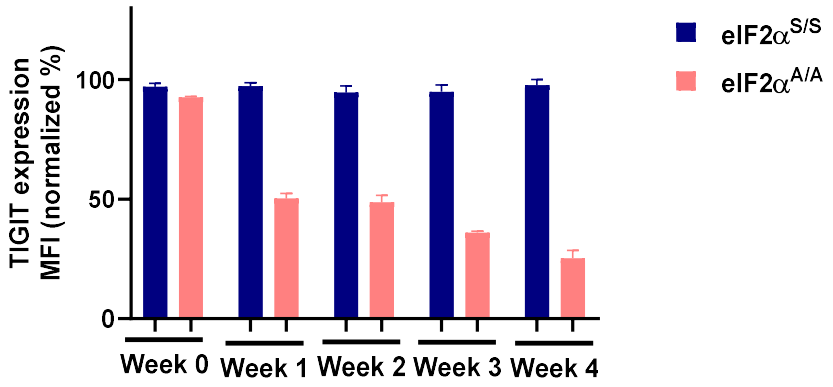

Figure 57. p-eIF2α retains TIGIT expression in KRAS G12D lung cancer cells. Bar graphs represent progression of Mean Fluorescence Intensity (MFI) of TIGIT in eIF2α$^{S/S}$ and eIF2α$^{A/A}$ cells. Data represents Mean ± SEM of three technical replicates.

Another prominent feature of the HPCS-expressing cells is their ability to confer resistance to chemotherapy[204]. This notion prompted us to test the effects of a novel KRAS G12D inhibitor (MRTX1133) on eIF2α$^{S/S}$ and eIF2α$^{A/A}$ cultured cells. Clonogenic assays and IC50 analyses revealed that eIF2α$^{S/S}$ cells had more resistant to KRAS inhibitors compared to eIF2α$^{A/A}$ cells.

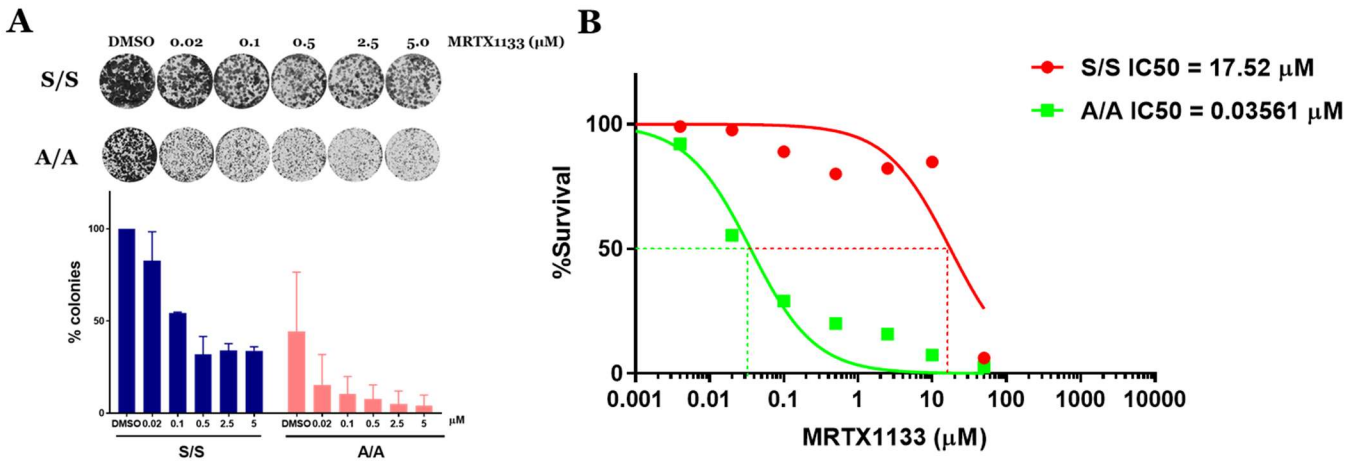

Figure 58. Effect of KRAS G12D inhibitor (MRTX1133) on proliferation of eIF2α$^{S/S}$ and eIF2α$^{A/A}$ cells. (A) Clonogenic assays of eIF2α$^{S/S}$ and eIF2α$^{A/A}$ cells subjected to MRTX1133 treatment at the indicated concentrations. Figure and graph represent one biological experiment

with three technical replicates. Data represents Mean ± SEM. (B) IC50 assay reveals a lower IC50 for MRTX1133 in eIF2α$^{A/A}$ cells (0.03561 μM) compared to eIF2α$^{S/S}$ cells (17.52 μM). Experiment was done in three biological replicates. Data represents mean ± SEM.

5.2 scRNA seq of S/S and A/A tumor cells reveals striking differences in tumor evolution

At 27 weeks post-tumor induction, upon verifying that the tumors have reached an appropriate size by ultrasound imaging (Figure 59), we isolated the GFP positive eIF2α$^{S/S}$ and eIF2α$^{A/A}$ tumor cells from mice by sorting.

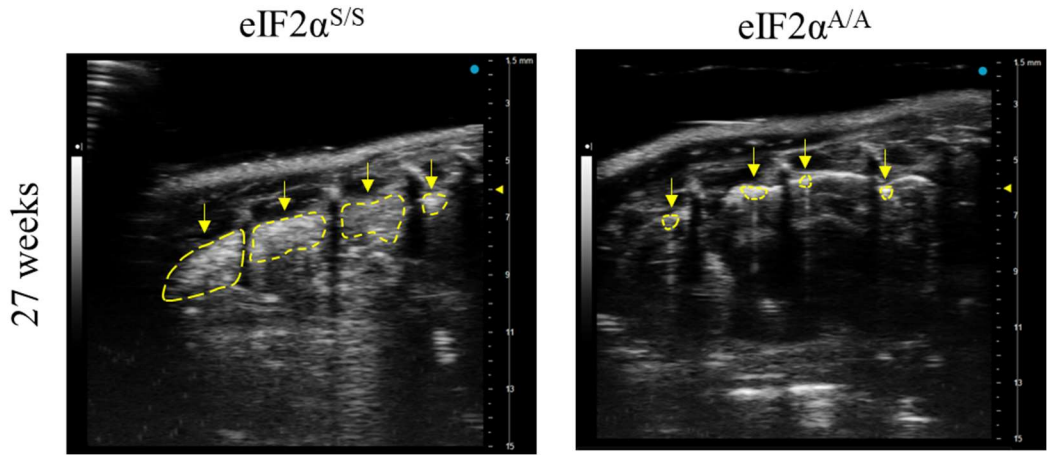

Figure 59. Representative ultrasound images of KRAS G12D eIF2α$^{S/S}$ and eIF2α$^{A/A}$ tumors prior to isolation of cells for scRNA-seq analysis.

Analysis of the different clusters formed by eIF2αS/S and eIF2αA/A tumor cells revealed 10 clusters in eIF2α$^{S/S}$ cells (SS0, SS1, SS1D, SS2, SS3, SS4, SS5A, SS5, and SSR) and 8 clusters in eIF2α$^{A/A}$ cells (AA0, AA0D, AA1, AA2, AA3, AA4, and AA5) (Figure 60). The clusters were numbered respectively according to their evolution based on pseudo-time analysis (Figure 61). Upon delineating the characteristics of the clusters, we noticed that eIF2α$^{A/A}$ cells harbored more initiating tumor AT2 (Alveolar type II)-like signatures compared to eIF2α$^{S/S}$ cells (Figure 62). Specifically, eIF2α$^{S/S}$ cells lost the AT2-gene *SFTPC* more dramatically as the tumor evolved

compared to that in eIF2α$^{A/A}$ cells (Figure 63). In addition, analysis of phenotypic scores obtained from analysis of tumor progression in a KP model identified by Yang *et al.* [225] confirmed a more AT2-like signature in eIF2α$^{A/A}$ compared to eIF2αS/S clusters and also revealed more EMT-like and aggressive signatures in eIF2α$^{S/S}$ cells compared to eIF2α$^{A/A}$ cells (Figure 63). Furthermore, eIF2α$^{S/S}$ tumor clusters had more stemness signature compared to clusters in eIF2α$^{A/A}$, especially in the later-evolving clusters (SS5 and SS5A) (Figure 64). This means that p-eIF2α cells might have the ability to drive stemness and EMT in KRAS-driven LUAD, especially that the high stemness and EMT-like clusters SS5A, SS5 and SSR are not present in the eIF2αA/A clusters, indicating that the absence of p-eIF2α in LUAD forms a block on tumor progression to more aggressive subtypes. Analysis of the cluster signatures also revealed high expression of YAP-HIPPO signature pathway in the eIF2α$^{S/S}$ clusters, particularly in the latter SS5A, SS5 and SS5R clusters (Figure 65). In all, the data indicate that p-eIF2α might drive the emergence of subclones with EMT, stemness and aggressive characteristics that increase tumor progression and lineage plasticity.

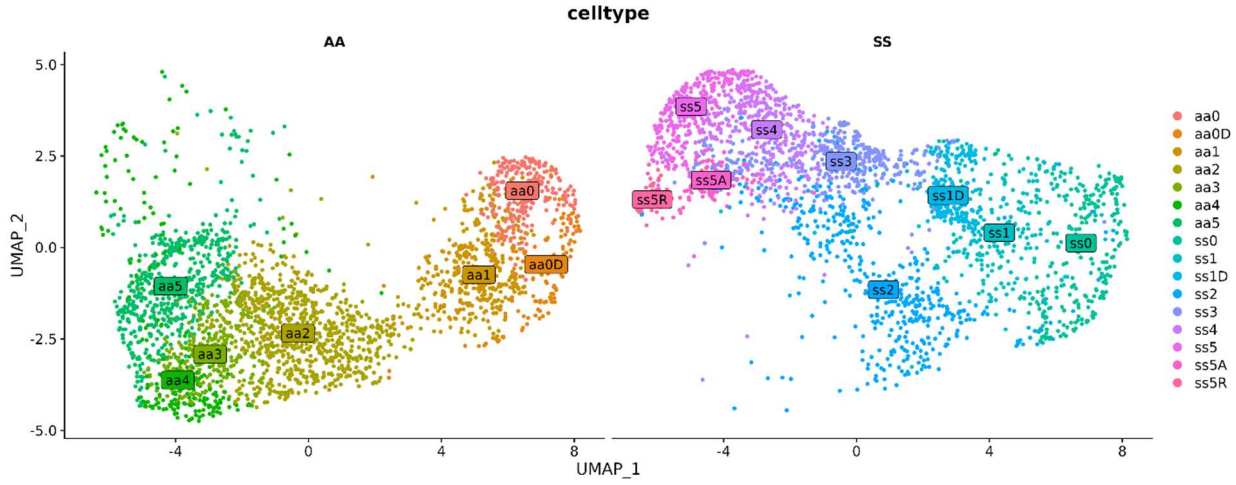

Figure 60. UMAP analysis reveals different clusters in eIF2α$^{S/S}$ and eIF2α$^{A/A}$ KRAS G12D lung cancer cells

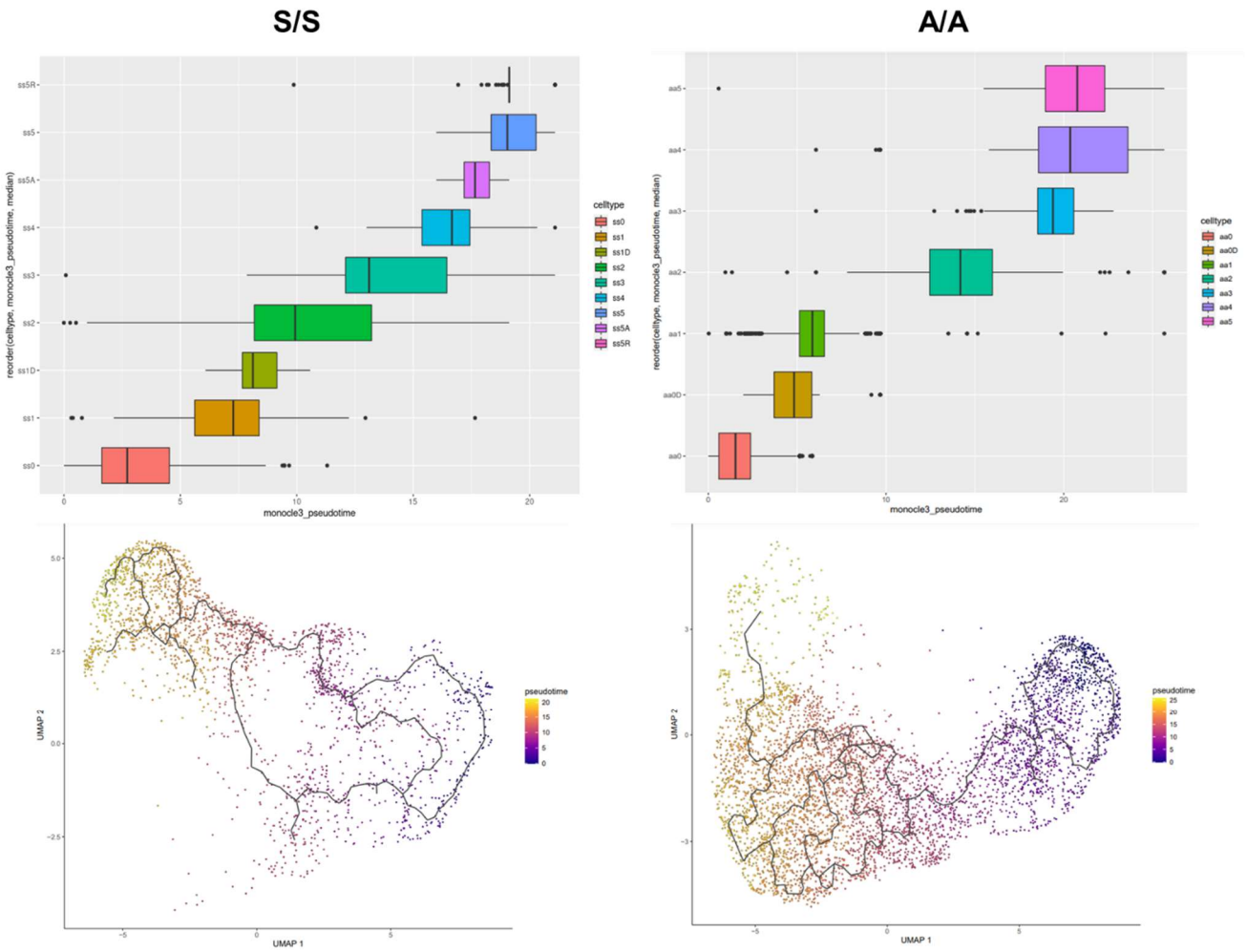

Figure 61. Pseudo-time analysis of the different clusters identified in eIF2α$^{S/S}$ and eIF2α$^{A/A}$ KRAS G12D LUAD cells reveals possible trajectories of tumor evolution in both cell types.

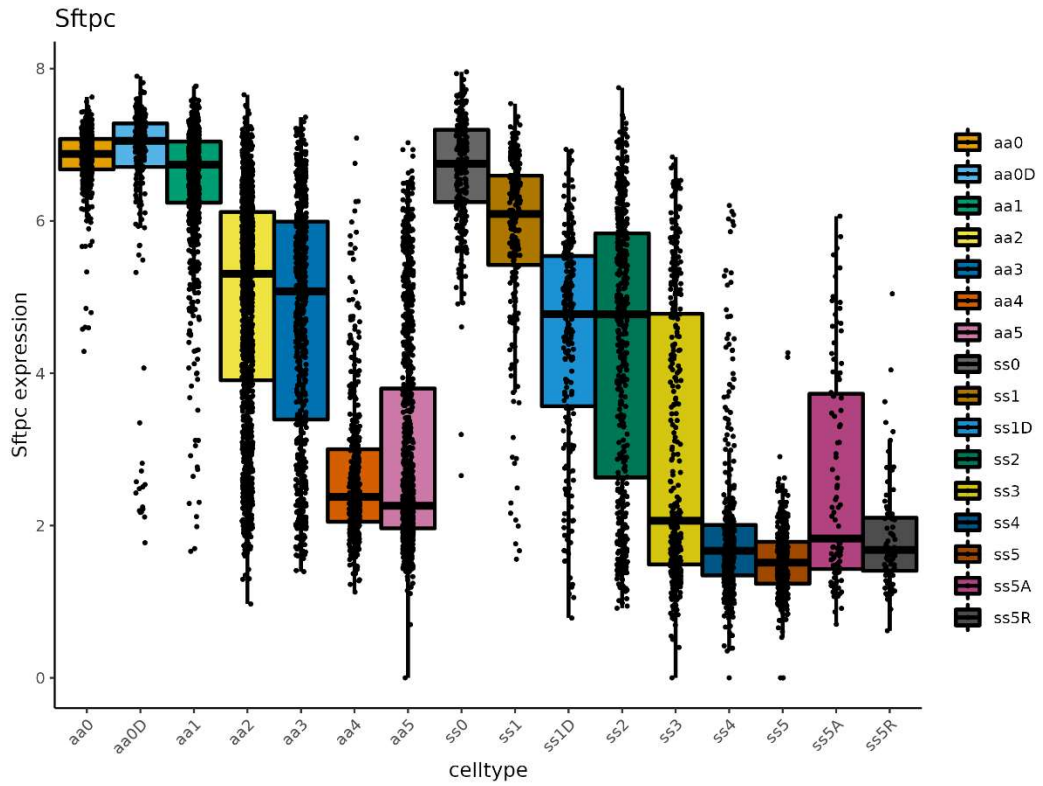

Figure 62. SFTPC gene expression in the eIF2α$^{S/S}$ and eIF2α$^{A/A}$ KRAS G12D LUAD cells.

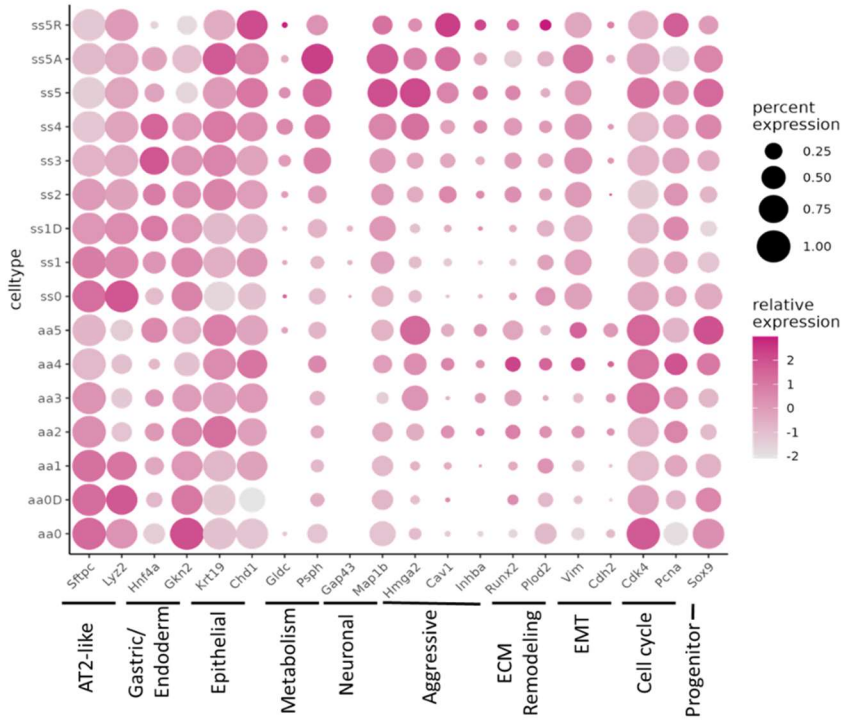

Figure 63. Distribution of mean of phenotypic scores across eIF2α$^{S/S}$ and eIF2α$^{A/A}$ KRAS G12D tumors. Each dot represents the cluster's mean for the indicated genes.

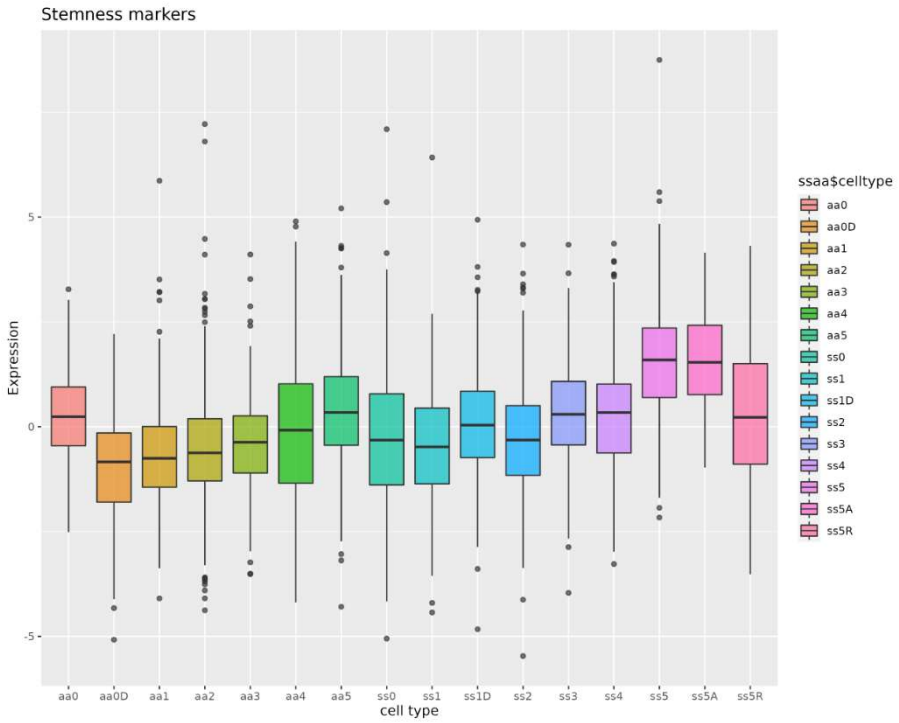

Figure 64. Analysis of stemness signature in the eIF2α$^{S/S}$ and eIF2α$^{A/A}$ identified clusters.

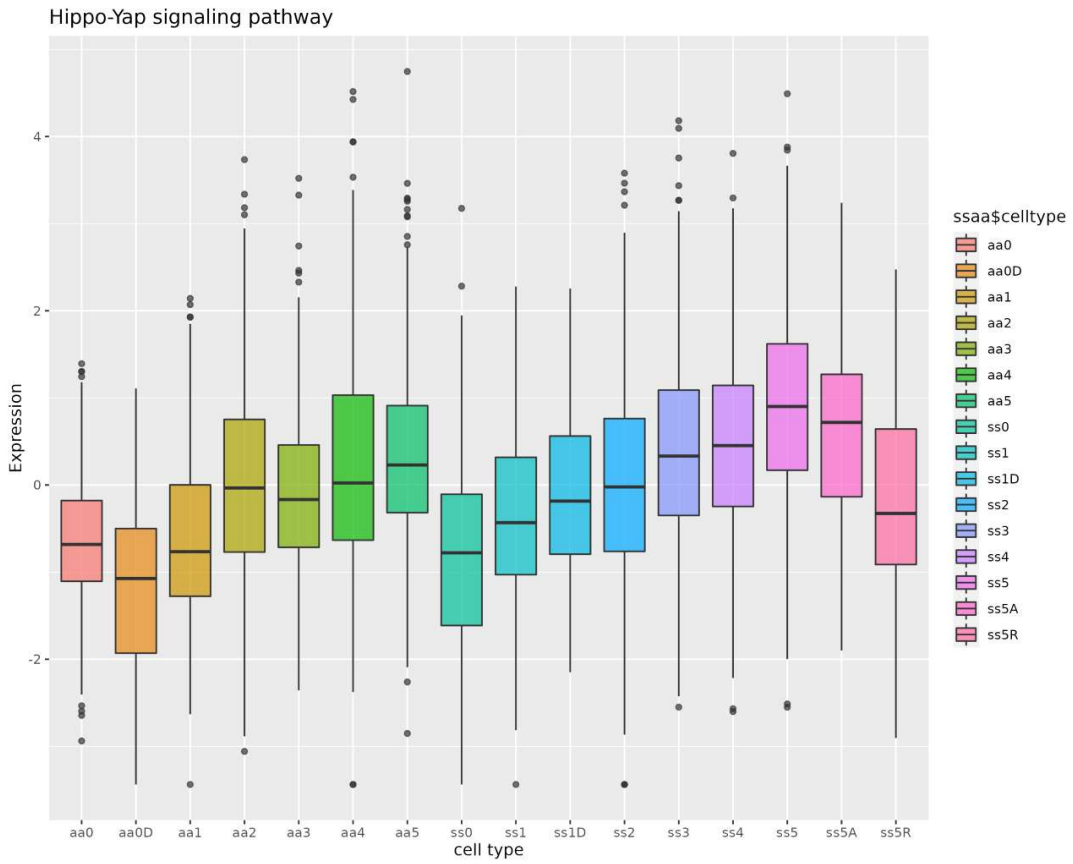

Figure 65. Analysis of HIPPO-YAP signaling pathway in eIF2α$^{S/S}$ and eIF2α$^{A/A}$ identified clusters.

5.3 p-eIF2α might drive a high-plasticity cell state (HPCS) signature in KRAS LUAD

We compared the characterized clusters of the GEMM KP model, a LUAD mouse model driven by KRAS and absence of p53, by Marjanovic *et al*. to the clusters developed in the eIF2α$^{S/S}$ and eIF2α$^{A/A}$ model. Interestingly, the eIF2α$^{S/S}$ clusters were enriched for a high-plasticity cell state (HPCS) program which forms a key transition state in LUAD development and gives rise to increased heterogeneity and EMT states (Figure 66). Violin plots of the different S/S and A/A clusters against the HPCS signature revealed that clusters SS4, SS5 and SS5A are the most enriched for HPCS. Furthermore, eIF2α$^{S/S}$ clusters displayed higher expression of the solute carrier protein Slc4a11 (Figure 67) and Integrin α2 (Itga2) (Figure 68),

which are bona fide markers of HPCS. This data further supports the notion of p-eIF2α driving plasticity in LUAD tumors.

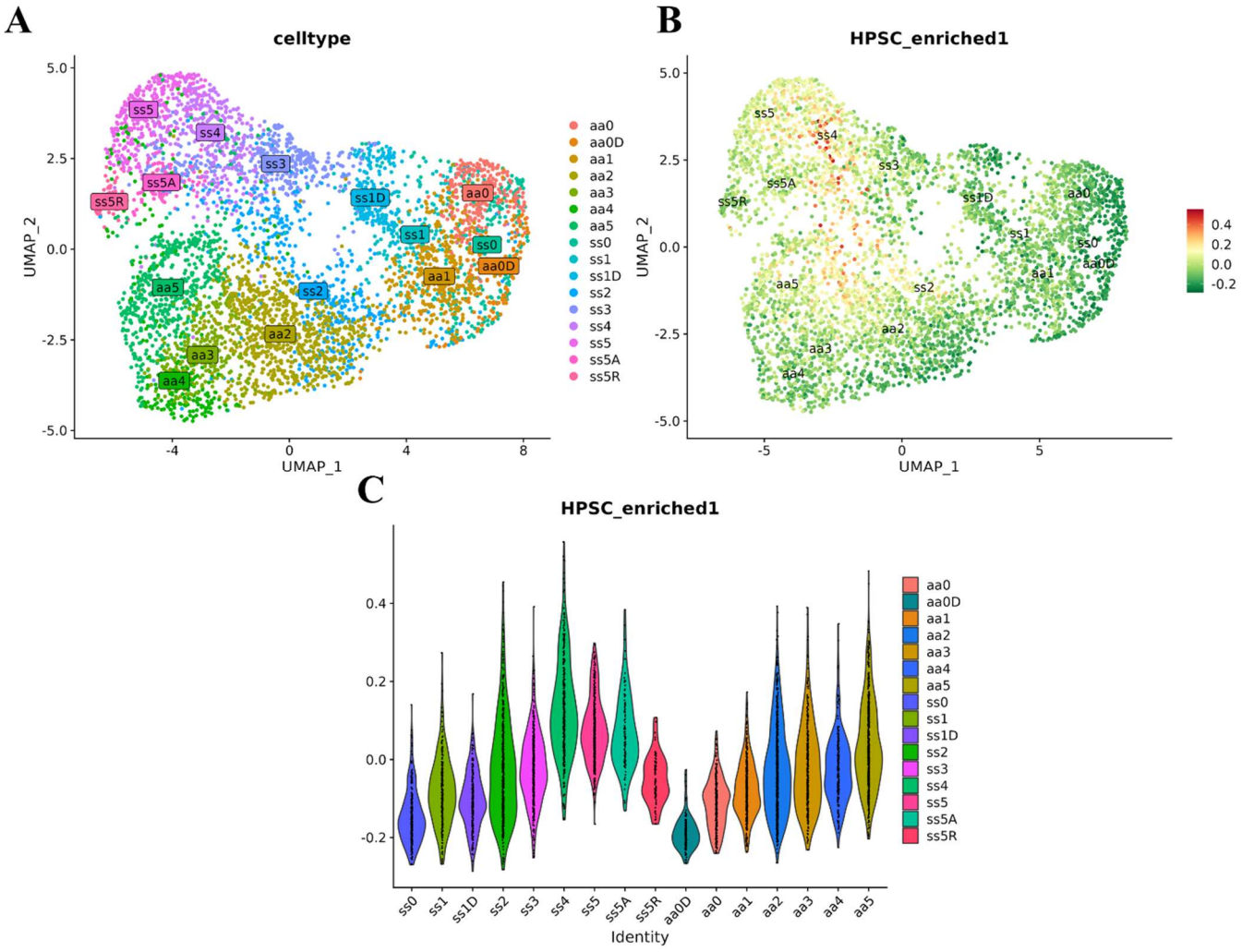

Figure 66. A high-plasticity cell-state gene expression signature emerges in wild-type p-eIF2α clusters. (A) Combined UMAP of eIF2α$^{S/S}$ and eIF2α$^{A/A}$ clusters. (B) UMAP showing HPCS enrichment in the different eIF2α$^{S/S}$ and eIF2α$^{A/A}$ clusters. (C) Violin plot of HPCS signature in eIF2α$^{S/S}$ and eIF2α$^{A/A}$ clusters.

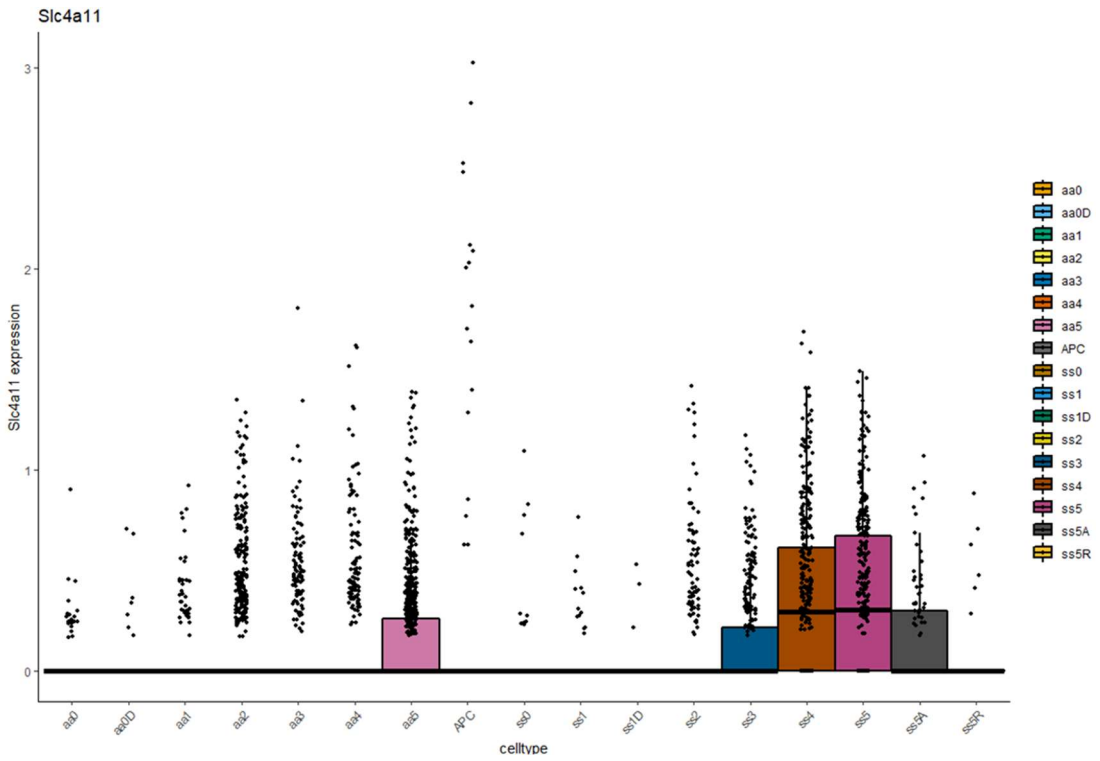

Figure 67. *Slc4a11* gene expression in eIF2α$^{S/S}$ and eIF2α$^{A/A}$ KRAS G12D tumor clusters.

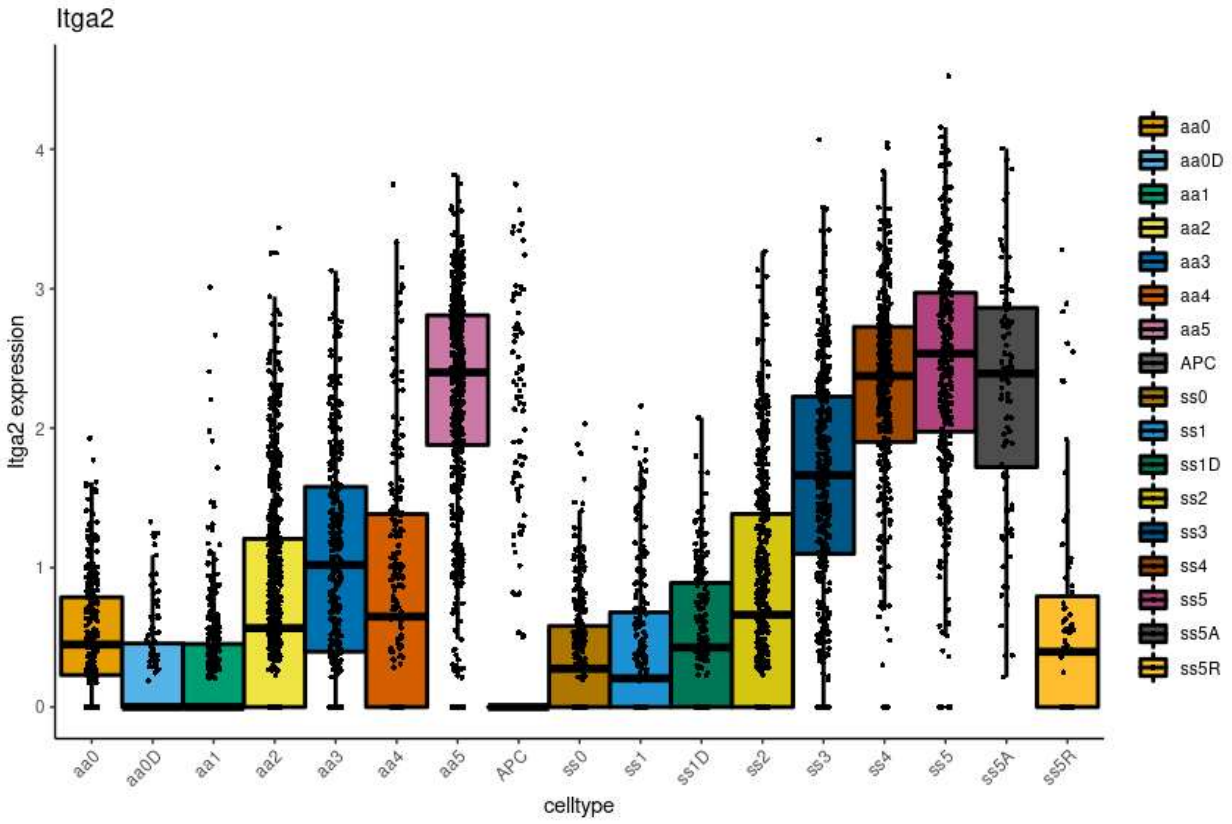

Figure 68. *Itga2* gene expression in eIF2α$^{S/S}$ and eIF2α$^{A/A}$ KRAS G12D tumor clusters.

Chapter 4: DISCUSSION

1. Clinical relevance of ISR in LUAD

With 1.76 million deaths per year, there is an ongoing urgent need to identify novel biomarkers in lung cancer that can delineate histopathological characteristics in the emerging tumors and act as prognostic markers to improve clinical decisions of therapy. We show that p-eIF2α can be a prognostic marker for survival and can also be a marker for tumor aggressiveness in LUAD patients.

1.1 Effect of ISR on different stages on malignant progression of LUAD

The clinical strength of this study lies in the close examination of 928 LUAD TMAs and investigating p-eIF2α as a biomarker in those TMAs. Correlative studies between p-eIF2α and aggressive histological types of LUAD patient tumors revealed a positive association between p-eIF2α level and aggressiveness, where the score was highest in invasive-predominant groups and lowest in minimally invasive lesions (Figure 14). However, mucinous adenocarcinoma (MUCA), which is the highest level of invasiveness in LUAD, had strikingly low levels of p-eIF2α (Figure 14). MUCA is a unique histologic subtype in that it has a low mutation burden and is often driven by a single oncogenic driver, most often KRAS[256,257]. Molecular profiling of the LUAD tumors would indicate further relationships between p-eIF2α and LUAD oncogenic drivers or tumor suppressors and can be further connected to histopathological differences.

1.2 Clinical outcomes and possible therapeutics

Upon stratifying the 928 LUAD TMAs into p-eIF2α positive and p-eIF2α negative tumors, the survival of patients with negative p-eIF2α was prolonged around 12 months longer

compared to those with positive p-eIF2α (Figure 13). In addition to invasiveness, p-eIF2α correlates with increased cellular proliferation in primary tumors of LUAD patients (Figure 14A). Therefore, the increase in survival is most probably attributed to the increase in aggressiveness of tumors and tumor proliferation with more p-eIF2α, which validates the assumption that p-eIF2α can indeed act as a prognostic marker in LUAD patients. A recent study has also shown the importance of ISR activation in patient LUAD progression[235]. Particularly, ATF4 is activated in different molecular subtypes and stages of LUAD[235]. ATF4 also controls the survival and migration of LUAD in conditions of nutritional stress[236,258]. High expression of other eukaryotic initiation factors such as eIF4E and eIF6 have also been implicated in survival of NSCLC patients[259-262]. Increased eIF4E expression correlates with poorer survival and higher invasion and metastasis in patient LUAD[259,261]. eIF6 expression also predicts poorer overall survival in LUAD[262].

P-eIF2α strongly correlates with ERK-P in primary patient tumors at the single-cell level which is consistent with the role of p-eIF2α in activating p-ERK in the mouse lung tumor models (Figure 21). P-eIF2α can be combined as a marker with other tumor markers such as p-ERK, mTOR and PDL-1 to examine tumor response to targeted therapies and to provide stronger predictive outcomes in LUAD patients[101]. However, more studies to support our findings need to be investigated. In that respect, treatment of patients displaying high p-eIF2 scores with ISR inhibitors can be a mode of personalized therapy.

1.3 Summary

P-eIF2α acts as a biomarker in predicting LUAD patient survival. P-eIF2α also drives an aggressive growth pattern in LUAD tumors in addition to higher proliferation of tumor cells. In conclusion, p-eIF2α can be a prognostic marker in patients with LUAD.

2. Role of p-eIF2α in mouse KRAS LUAD development

The clinically striking role of p-eIF2 in LUAD patient survival and tumor progression prompted the investigation of the possible biological and mechanistic effects of this factor in LUAD progression and development. The genetically engineered mouse model of KRAS-driven LUAD is widely studied and often used to investigate molecules implicated in lung tumorigenesis.

2.1 P-eIF2α is a driver of KRAS LUAD tumor progression

The number of initiated tumors in mice devoid of p-eIF2α was significantly less than those having p-eIF2α (Figure 15). Moreover, p-eIF2α was implicated in driving larger tumors (Figure 15). This means that p-eIF2α is essential not only in tumor progression, but can also drive initiation of tumors that are dependent on KRAS mutations. The prognostic role of p-eIF2α was recapitulated in the KRAS mouse model, where mice with p-eIF2α died faster than those devoid of p-eIF2α. However, upon investigating the growth patterns of these tumors, no differences were noticed in aggressiveness between the two models. A possible explanation would be the simplicity of the mouse LUAD model compared to human LUAD in terms of molecular and histopathological characteristics. It is expected that human LUAD would have a higher mutation burden than the mouse LUAD model, at least in later and more advanced stages of the disease.

2.2 P-eIF2α regulates the MAPK pathway in KRAS-driven LUAD

P-eIF2α translationally represses DUSP6 mRNA to upregulate p-ERK which is downstream of the pro-tumorigenic MAPK pathway. DUSP6 expression is antitumorigenic and is a marker of poor prognosis in LUAD[167,263]. Downregulation of DUSP6 by genetic (siRNA) and pharmacological means in cells lacking p-eIF2α restored p-ERK levels and increased survival in these cells, suggesting that DUSP6 translational repression is responsible for upregulation of the MAPK pathway by p-eIF2α. Recent studies have shown that hyperactivation of p-ERK by DUSP inhibitors exhibit anti-proliferative effects[264]. However, eIF2α-dependent activation of p-ERK by DUSP6 is below the anti-proliferative threshold in mouse KRAS G12D mouse lung tumors. Moreover, it was further shown that this hyperactivation is controlled by activation of both DUSP6 and DUSP4[265]. Gene expression profiles show an upregulation of DUSP4 in $eIF2\alpha^{S/S}$ cells compared to $eIF2\alpha^{A/A}$ cells, which means that the translational dampening of DUSP6 followed by upregulation of DUSP4 might keep p-ERK levels at optimum levels for its pro-tumorigenic function. If this is the case, genetic knockdown or knockout of DUSP4 in $eIF2\alpha^{S/S}$ cells might lead to hyperactivation of p-ERK to display its anti-proliferative function, which remains a matter of future investigation. Moreover, we observe a positive correlation between p-eIF2α and p-ERK at the single-cell level in LUAD patients, which further supports p-ERK as a downstream player of p-eIF2α. The distinctive translational repression of DUSP6 by p-eIF2α is a matter of interest, which might be explained by the long 3'- and 5'-UTRs (700-2000 nt) harbored by DUSP6. The mechanism of translational control of DUSP6 can be investigated by genetically altering 5'- and 3'-UTRs of DUSP6 and see if it affects its translation.

2.3 p-eIF2α employs transcriptional programs to aid its tumorigenic function in KRAS-LUAD

Aside from regulating the MAPK pathway, p-eIF2α controls other pro-tumorigenic pathways. UR analysis from RNA seq data revealed that p-eIF2α upregulates pathways under the control of *CTNNB1, LHX1*, *HIF1A,* and the pro-inflammatory IL6 pathway (Figure 18). On the other hand, p-eIF2α inhibits tumor suppressors like the homeobox protein *HOXA10*, estrogen-related receptor alpha (*ESRRA*), polycomb group protein *ASXL1,* and mitofusin 2 (*MFN2*) function. Also, p-eIF2α is involved in stimulation of growth factor receptor signaling, epithelial cell proliferation and mesenchymal cell differentiation. Moreover, Gene set enrichment analysis (GSEA) suggests a metabolic role of p-eIF2α where it negatively regulates mitochondrial respiration and oxidative phosphorylation. This may be due to upregulation of p-ERK which favors aerobic glycolysis[266].

2.4 Summary

P-eIF2α enables high proliferative capacity in KRAS G12D mouse lung tumor cells due to induction of the MAPK pathway. Nevertheless, RNA seq analysis reveals the importance of other tumorigenic programs employed by p-eIF2α that are essential for lung tumor growth, survival and differentiation.

3. The pro-tumorigenic effects of p-eIF2α involve the activation of YAP/TAZ signaling that might drive a stemness program in KRAS-driven LUAD

Recent studies have implied a functional connection between PERK-p-eIF2α and YAP/TAZ activation[237,253]. Stimulation of UPR through PERK-p-eIF2α axis can activate YAP/TAZ in liver cancer. YAP/TAZ also sustains ATF4 expression to confer resistance to chemotherapy in hepatocellular carcinoma[267]. Since YAP plays an oncogenic role in mutant KRAS cancers[268], we explored whether the pro-tumorigenic effects of PERK-p-eIF2α rely on activation of YAP/TAZ.

3.1 RNA seq analysis reveals that p-eIF2α activates a YAP ON gene expression signature

Comparison of $eIF2\alpha^{S/S}$ vs $eIF2\alpha^{A/A}$ transcriptional signatures with YAP ON and YAP OFF transcriptional signatures revealed 212 genes dependent on YAP and p-eIF2α (Figure 40). Top biological processes are those implicated in the positive regulation of cell proliferation such as the MAPK cascade, which means that there is a YAP/TAZ-dependent connection to the MAPK pathway in KRAS G12D lung tumor cells. Indeed, it has been shown that YAP functions downstream of ERK to activate genes implicated in neoplastic proliferation in pancreatic ductal adenocarcinoma in mice[268]. Therefore, examining YAP/TAZ activation in DUSP6 downregulated $eIF2\alpha^{S/S}$ and $eIF2\alpha^{A/A}$ cells will determine whether YAP/TAZ functions downstream of eIF2α-dependent ERK activation.

The analysis revealed that eIF2α-dependent regulation of epithelial to mesenchymal transition and positive regulation of cell proliferation are through YAP/TAZ signaling, which highlight the importance of dissecting the eIF2α-dependent YAP/TAZ signaling pathways in KRAS lung cancer. Therefore, a direct validation of the obtained results would be to acquire

RNA-seq signatures of p-eIF2α proficient and deficient cells that are impaired for YAP/TAZ by si/shRNAs or CRISPR.

3.2 The pro-tumorigenic function of p-eIF2α is dependent on YAP/TAZ activation

Western blot and IHC analyses confirm more YAP activation in the eIF2α$^{S/S}$ tumor cells. Single knockdown of YAP1 decreased the colony formation efficacy of eIF2α$^{S/S}$ cells by around 70%, whereas that in eIF2α$^{A/A}$ cells remained unchanged, suggesting that the pro-tumorigenic potential of p-eIF2α is highly dependent on YAP. Similarly, downregulation of TAZ caused a significant decrease of colonies in eIF2α$^{S/S}$ cells by around 70% when only 30% of eIF2α$^{A/A}$ cell proliferation was inhibited. However, YAP/TAZ double knockdown significantly disrupted the colony formation efficacy of both cell types, highlighting that dual YAP/TAZ knockdown is indispensable for general tumor growth, survival and proliferation. In addition, in the PDX model of KRAS G12C-driven LUAD, treatment of ISRIB inhibited tumor progression by 30%. Whether the 30% reduction of tumor growth is fully attributed to HIPPO activation in ISRIB-treated tumors remains to be a matter of investigation. Indeed, tumor heterogeneity often comes into interplay regarding PDX studies.

These results validate the function of YAP/TAZ in cell proliferation downstream of p-eIF2α. However, the functional implication of YAP/TAZ in EMT via p-eIF2α remains to be a matter of future investigation. A potential experiment would be to impair YAP/TAZ by genetic means (si/shRNA, CRISPR) in p-eIF2α-proficient and deficient cells and to subcutaneously transplant the cells in immunodeficient mice. This might reveal a biologically-relevant

implication of the proliferative effects of YAP/TAZ and potentially provide insight into whether EMT is taking place in the presence or absence of YAP/TAZ activation.

3.3 p-eIF2α might employ YAP/TAZ to drive stemness and EMT signatures

scRNA seq analyses confirm more activation of Hippo/YAP signaling in eIF2α$^{S/S}$ clusters compared to those in eIF2α$^{A/A}$ tumors (Figure 65). This provides further evidence that YAP/TAZ activation occurs downstream of p-eIF2α *in vivo*. Interestingly, the eIF2α$^{S/S}$ clusters evolve into a stemness cluster, that is characterized by high EMT potential and this cluster is not present in eIF2α$^{A/A}$ tumors (Figure 64). Further analyses might reveal a positive correlation between YAP-expressed genes and the stemness signature, which might indicate that YAP drives this stemness signature in cells wild-type for eIF2α-P.

YAP/TAZ signaling has been shown to maintain stemness properties in lung cancer cells[269]. A role of p-eIF2α-YAP/TAZ in maintaining stemness in KRAS lung cancer can be further investigated by first analyzing different stemness markers by IHC and immunoblot analyses in the eIF2α proficient and deficient tumors, to verify a functional implication of p-eIF2α in maintaining stemness of KRAS lung tumors. Second, the role of YAP/TAZ signaling downstream of p-eIF2α in stemness can be delineated by examining stemness markers in p-eIF2α-proficient and deficient cells impaired for YAP/TAZ and grown subcutaneously in nude mice. Bona fide stemness markers for IHC analysis in cancer include CD15, CD24, CD44, CD166, and ALDH1A1 and can be used for the purposes of this experiment[270].

3.4 Possible mechanisms mediated by p-eIF2α to activate YAP/TAZ

YAP/TAZ activation through p-eIF2α might be either through the HIPPO canonical pathway (through MST1/2 and LATS1/2) or through non-canonical pathways. The increase of LATS1/2 in S/S and A/A cells might indicate the involvement of the canonical HIPPO pathway in YAP/TAZ activation. Also, LATS2 was specifically upregulated in ATF4 knockdown cells as well as in mRNA expression levels in eIF2α$^{A/A}$ cells. However, knockdown studies of MST1/2 and LATS1/2 led to decreased clonogenicity of p-eIF2α proficient cells, although YAP S127 phosphorylation was downregulated. This might indicate that the regulation of YAP/TAZ might be through non-canonical pathways. One mechanism that might regulate YAP/TAZ activation is the β catenin-WNT pathway, where analysis of gene expression signature revealed the involvement of WNT signaling in eIF2α-dependent YAP ON genes and GSEA of p-eIF2α proficient versus deficient cells revealed that a top regulated pathway is β-catenin signaling (Figure 17 & 43). WNT signaling is an essential driver of LUAD initiation and progression[271]. Specifically, WNT signaling is activated in KRAS-mutated LUAD mouse models to maintain stem-cell features in lung cancer cells[272]. When WNT is inactive, β-catenin is sequestered in the cytoplasm within a destruction complex that also involves YAP/TAZ for stabilization[153]. Active WNT signaling releases YAP/TAZ from this complex, leading to their accumulation in the nucleus along with β-catenin and activation of WNT/YAP/TAZ-dependent biological effects[153]. Therefore, the hypothesis is that p-eIF2α drives a WNT activation leading to YAP/TAZ activation. β-catenin nuclear localization would be more evident in eIF2α$^{S/S}$ tumors compared to those of eIF2α$^{A/A}$. Also, the transcriptional signature of WNT/YAP/TAZ-dependent genes can be aligned with p-eIF2α/YAP genes to verify common activated genes. Functional analysis of WNT

signaling activation can be verified by treatment of eIF2α$^{S/S}$ and eIF2α$^{A/A}$ cells with recombinant WNT3a, where more activation/nuclear localization of YAP/TAZ would take place in eIF2α$^{A/A}$ cells compared to eIF2α$^{S/S}$ cells. Also, localization of β-catenin in the absence of YAP/TAZ (si/shRNA, CRISPR) should be monitored in eIF2α$^{S/S}$ and eIF2α$^{A/A}$ cells, where more nuclear accumulation of β-catenin would take place in cells lacking eIF2α phosphorylation.

As another mechanism to be investigated, Claudin 18 is a tight junction protein that regulates YAP activity by sequestering it in the cytoplasm in its phosphorylated form, thus preventing its activation[273]. This mechanism was also shown to limit stemness in lung adenocarcinoma[273]. According to gene expression profile analysis between eIF2α$^{S/S}$ and eIF2α$^{A/A}$ cells, Claudin 18 is significantly upregulated in the eIF2αA/A cells, suggesting a plausible mechanism of YAP/TAZ inhibition through Claudin 18 activation. Therefore, genetic knockdown of Claudin 18 would lead to more nuclear accumulation of YAP in eIF2α$^{A/A}$ cells compared to eIF2α$^{S/S}$ cells.

Furthermore, in liver cancer, it was shown that GADD34 inhibits YAP activity through UPR activation[254]. The GADD34 inducers Guanabenz and Sephin1 increased YAP phosphorylation p-eIF2α wild-type cells, but not in cells devoid of p-eIF2α, which suggests that YAP activation through GADD34 can also be a plausible mechanism. Genetic knockdown of GADD34 would give further insight regarding this matter.

3.5 Summary

The results show that p-eIF2α is highly dependent on YAP/TAZ activation for the pro-tumorigenic effects in KRAS LUAD mouse cancer cells. This is verified by the biological effects seen in genetic knockdown studies of YAP/TAZ as well as bioinformatic analyses of p-eIF2α-

proficient and deficient LUAD cells. However, the mechanism of this activation remains a matter of investigation. The importance of this study lies in lack of therapeutic venues that can target YAP/TAZ in cancer which urges further revealing of pathways or targets that can regulate YAP/TAZ activity. YAP/TAZ signaling might be employed by p-eIF2α to drive progression, stemness and EMT in KRAS-driven LUAD.

4 Targeting the ISR as a potential novel therapeutic venue in KRAS LUAD

KRAS mutations subject cancer cells to continuous forms of stress, such as genotoxic, proteotoxic and metabolic stress. This is due to hyperactivation of proliferative and anti-apoptotic programs which causes a huge expenditure of cellular resources and energy. To accommodate to this expenditure, cells trigger adaptive responses that activate transcriptional programs to sustain continuous growth and survival. We show that activation of the PERK-p-eIF2α arm is triggered as a cyto-protective response to KRAS mutations to activate pro-tumorigenic and pro-survival programs that can endure continuous exposure to stress.

4.1 PERK-eIF2αP arm is activated in KRAS mutated LUAD

Using mutant and wild-type KRAS cell lines, we show that KRAS mutations upregulate the PERK-eIF2αP arm. These results echo previous studies that show the adaptive role of the ISR in KRAS-transformed embryonic fibroblasts and human LUAD cells[226,235]. We reason that this upregulation renders the cells sensitive to inhibitors of the ISR such as ISRIB and PERK inhibitors. Since PERK might also regulate other pathways, we verified the specificity of PERK-p-eIF2α in the proliferation of cells by knockdown studies of PERK (Figures 28-32). These

studies revealed the reliance of the pro-tumorigenic capacity of PERK on p-eIF2α, since no effect was seen in knockdown of PERK in cells devoid of p-eIF2α.

Whether PERK is the kinase responsible for regulation of other p-eIF2α-dependent pathways mentioned in this study is a matter of future investigation. PERK can be downregulated in eIF2α$^{S/S}$ and eIF2α$^{A/A}$ cells and subjected to RNA sequencing to identify all potential pathways dependent on PERK in an p-eIF2α manner. The downregulation of PERK in eIF2α$^{A/A}$ cells would give indication of pathways that are p-eIF2α-independent. PERK has also been shown to be a driver of metastasis and invasion in cancer[118,274]. Similarly, YAP/TAZ activation was found to be downstream of the PERK-p-eIF2α arm in liver cancer[237]. Genetic knockdown of PERK can verify that YAP/TAZ activation occurs through PERK in KRAS-driven LUAD. Also, HPCS signature markers such as integrin-α and TIGIT can be explored in cells impaired for PERK to verify it as an upstream driver of the pro-tumorigenic pathways regulated by p-eIF2α.

4.2 PERK inhibitor and ISRIB as modes of therapy in KRAS LUAD

ISR inhibitors have shown anti-tumorigenic potential in multiple cancer models[71]. We verified the therapeutic potential of targeting p-eIF2α in KRAS LUAD using *in vivo* and *in vitro* models. Specifically, we show that the increase of p-eIF2α by KRAS mutations augments the sensitivity of KRAS cells to ISR inhibitors. ISRIB inhibits ISR activation by increasing eIF2B activity and rendering it insensitive to p-eIF2α inhibition[235,275]. In effect, ISRIB requires high levels of p-eIF2α to exhibit stronger effects of ISR inactivation[235]. This is the case when ISRIB is administered to wild-type KRAS cells that exhibit lower levels of p-eIF2α than mutant KRAS

cells. Indeed, mutant KRAS tumors are much more sensitive to ISRIB compared to wild-type KRAS tumors. However, the PERK inhibitor GSK2606414 reduced the growth of WT KRAS tumors, which have low ISR activity, but not as much as KRAS mutant tumors. This might be due to involvement of PERK in p-eIF2 independent pathways like nuclear factor erythroid 2-related factor 2 (NRF2)-HIF pathway in pancreatic and lung cancers[276]. ISR inhibitors reduced the growth of tumors and prolonged survival of mice in multiple *in vivo* models comprising orthotopic, autochtonous and subcutaneous models.

Although we attribute the anti-tumorigenic capacity of ISR inhibitors to MAPK inhibition, the ISR ability to regulate multiple pro-tumorigenic pathways makes it an attractive target in treatment of KRAS lung cancer. A striking characteristic of ISRIB is the lack of observed toxicity in mice even after prolonged treatments with ISRIB. Another important characteristic is ISRIB's ability to function as a tumor suppressor of KRAS cancers regardless of KRAS mutations, where we saw anti-tumor effects of ISRIB in both KRAS G12C and KRAS G12D tumors.

The ability of ISRIB and PERK inhibitor to regulate YAP/TAZ signaling and HPCS signature can be further explored to provide evidence of their therapeutic strength in targeting KRAS-driven LUAD. Specifically, the effect of ISRIB and PERK inhibitor on YAP/TAZ signaling can be examined mechanistically *in vitro* by monitoring YAP/TAZ localization after treatment with the small molecule inhibitors. Treatment of $eIF2\alpha^{S/S}$ mice with ISRIB and monitoring tumor evolution at the single-cell level would provide more clinical significance of the reliance of tumor cell evolution on p-eIF2α, where ISRIB can mirror biological effects seen in $eIF2\alpha^{A/A}$ in preventing or delaying the emergence of HPCS, EMT and stemness clusters.

4.3 Possibility of combination therapy

The KRAS G12D inhibitor (MRTX1133) significantly decreased clonogenic efficacy and yielded a significantly lower IC50 in eIF2α$^{A/A}$ cells compared to eIF2α$^{S/S}$ cells, indicating that p-eIF2α employs mechanisms to confer resistance against KRAS inhibitors. Therefore, ISR inhibitors might sensitize tumors to KRAS inhibitors[277]. It would be interesting to identify the mechanism of resistance to KRAS inhibitors employed by p-eIF2α. One possibility might be due to YAP/TAZ activation by p-eIF2α since YAP signaling is intimately involved in resistance to therapy in KRAS mutated cancers[129]. This can be investigated in eIF2α$^{S/S}$ cells impaired for YAP/TAZ by checking if they can be re-sensitized to KRAS inhibitors. Additionally, RNA sequencing of eIF2α$^{S/S}$ and eIF2α$^{A/A}$ cells treated with KRAS inhibitors might provide insights into potential pathways involved in resistance to KRAS inhibitors.

4.4 Summary

We provide evidence that ISR inhibitors are promising therapeutic targets for the treatment of KRAS lung cancer in multiple mouse models. ISR inhibitors halt tumor proliferation in vivo and prolong survival of mice with KRAS LUAD. These inhibitors impair the MAPK pathway exclusively in KRAS mutated LUAD. ISRIB might compensate for MAPK pathway inhibitors like MEK inhibitors which are toxic. In addition, a venue for further investigation would be the possibility of combination treatments with KRAS inhibitors with ISRIB, which may sensitize tumors to KRAS inhibitors.

5. P-eIF2α in tumor heterogeneity and plasticity

We harness the power of sc-RNA seq analysis to elucidate the role of p-eIF2α in sub-clonal diversity during KRAS LUAD progression. The different subclones that arise during KRAS-driven LUAD progression have been already characterized in previous studies[204,224,225], which gives the opportunity to compare sub-clonal diversity in the presence or absence of p-eIF2α.

5.1 Presence of p-eIF2α provides lineage diversity in KRAS LUAD and drives tumor evolution to high plasticity, EMT and aggressive subclones

Previous studies have shown the importance of the ISR in muscle stem cell regeneration[278]. In addition, breast cancer cells subjected to hypoxia implement the ISR to drive plasticity[239]. Our data show that presence of p-eIF2α aids in loss of fidelity towards normal lung tissue lineage as shown by the striking loss of AT2 lineage as clusters evolve to diverse subclones (Figure 62). p-eIF2α is required for adoption of different transcriptional states that drive tumor progression and differentiation, passing through HPCS and stemness signatures, and enabling metastatic signature as tumors advance to later stages. The ability of p-eIF2α to drive a metastatic and aggressive signature might explain its association with a more invasive histopathological characteristic in human LUAD. p-eIF2α alters the stages of development in KRAS lung cancer to make it more favorable towards tumor progression and aggressiveness. Particularly, p-eIF2α drives tumor development towards the distinctive cluster SS4, which is uniquely present in p-eIF2α wild-type cells and has high expression of HPCS signature. After passage through that cluster, p-eIF2α promotes stem-like signatures as seen in clusters 5A, 5R and 5. Another main difference between the $eIF2\alpha^{S/S}$ and $eIF2\alpha^{A/A}$ clusters is the presence of the

AA0D cluster, which we reasoned is the counterpart of SS1D cluster. The difference in both is that the AA0D cluster is associated with MHC class II protein complex assembly, which can be explained by increased translation in these cells due to absence of p-eIF2α. The SS1D cluster is associated with increased drug metabolism which might explain the increase in drug resistance that is seen in S/S cells. Lastly, the high stemness clusters present in S/S tumors SS5R, SS5 and SS5A while not in A/A tumors justifies the potential of EMT in p-eIF2α wild-type tumors. The HPCS cluster present in S/S and not in A/A is S/S4. However, further analyses need to be done to investigate EMT markers in $eIF2\alpha^{S/S}$ vs $eIF2\alpha^{A/A}$ tumors as well as analyses of metastasized organs such as liver and brain.

5.2 p-eIF2α might employ YAP/TAZ to increase plasticity, stemness and EMT in KRAS LUAD

YAP/TAZ activation has been found to drive glioblastoma differentiation by driving plasticity and stemness in glioblastoma subtypes[140]. We therefore reasoned that this activation may drive the stemness and EMT signatures that we see in S/S clusters. Box plot of HIPPO/YAP gene signature reveals increased expression of S/S compared to A/A clusters, particularly in high stemness clusters.

5.3 Summary

The ability to characterize the role of p-eIF2α in transitions between transcriptomic states during KRAS LUAD progression highlights the biological importance of the ISR in tumor heterogeneity and evolution. The intimate involvement of p-eIF2α with the HPCS during tumor evolution sheds light on the importance of targeting this factor in order to block sub-clonal

diversity. Indeed, the transition to stemness and EMT is highly dependent on p-eIF2α which regulates multiple pathways that drive stemness such as WNT signaling and YAP/Taz. Delineating the mechanisms underlying such connections is essential in the field of KRAS-driven LUAD to provide further biological understanding and support on the importance of targeting the ISR in this disease.

6. The role of eIF2α phosphorylation in KRAS lung cancer

We reveal a novel pro-tumorigenic role of the ISR in KRAS-driven lung cancer. The findings in this thesis implicate the activation of the ISR in KRAS lung cancer as a response to oncogenic-induced stress insults. In human LUAD tissue microarrays (TMAs), we found that eIF2α phosphorylation can be a prognostic marker in determining survival of patients. This was also the case in genetically modified mouse models of KRAS lung cancer, where survival of mice was significantly prolonged in the absence of eIF2α phosphorylation due to lower tumor burden in these mice. We found that activation of PERK and phosphorylation of eIF2α translationally inhibits DUSP6, which is an important tumor suppressor phosphatase that dephosphorylates and inactivates ERK1/2. We further demonstrate that the pro-tumorigenic role of the ISR is exclusive to KRAS-mutated tumors and not tumors with wild-type KRAS. Importantly, pharmacological inhibition of the ISR via either the PERK inhibitor or the integrated stress response inhibitor (ISRIB) significantly reduces tumor growth *in vitro* and multiple *in vivo* models.

We further demonstrate by RNA sequencing analysis that eIF2α phosphorylation regulates multiple pro-tumorigenic pathways essential for KRAS-driven tumor progression.

An important oncogenic pathway highly implicated in KRAS lung cancer is the YAP/TAZ pathway. We show that eIF2α phosphorylation regulates several YAP-associated genes in KRAS lung cancer. Moreover, we show by genetic ablation of YAP/TAZ the dependence of eIF2α phosphorylation on this pathway for tumor progression.

Lastly, we uncover the importance of eIF2α phosphorylation in subclonal diversity and emergence of a high plasticity cluster in KRAS lung cancer by scRNA seq. The absence of eIF2α phosphorylation in the mouse KRAS-driven lung cancer model significantly delays the ability of tumor cells to acquire plasticity programs that eventually lead to EMT. Specifically, eIF2α phosphorylation-deficient tumor cell clusters display an AT2-like primitive signature whereas the presence of eIF2α phosphorylation induces a rapid loss of this signature, concomitant with acquisition of multiple differentiation programs that lead to a high plasticity cell state signature as well as a stemness signature that are not present in eIF2α phosphorylation-deficient tumors. These data demonstrate a novel role of eIF2α phosphorylation in driving plasticity and stemness in KRAS lung cancer context.

7. Limitations in the study

One limitation in this study would be the time required for lung tumor initiation and progression to take place in the genetically engineered LUAD mouse model used. After administration of lentiviruses, the allotted time for lung tumors to properly develop to execute experiments is 24-30 weeks.

Also, although we show that ultrasound imaging is a valid technique for comparing lung tumor growth between two groups, it is not an accurate method for

detection of quantity or size of tumors in a single experiment. For that purpose, a more accurate method would be detection of tumors using CT scans.

Having GFP as a fluorescence marker of the lung tumors would not be the best marker due to the amount of autofluorescence present in the lung. This limited the possible use of Bioluminescence imaging for detection and quantification of tumors in live mice. Another valid fluorescence marker would be mCherry that is widely used in the KRAS mutate p53 knockout (KP) mouse model.

Finally, the last two years of this study, along with submission of the associated paper for revisions in the journal Nature Communications, took place during the COVID pandemic. Even with the two-month lockdown, allotted curfews by the Quebec government at 8 PM, and up to 6 months of delays in receiving reagents, Dr. Shuo Wang and I still came to the lab to execute experiments and provide evidence for the importance of p-eIF2α in lung cancer.

Chapter 5

Contribution to original knowledge

The major novel findings made by the candidate over the course of this research are outlined below.

1. The candidate was the first to demonstrate that eIF2α phosphorylation drives the progression of KRAS-driven lung cancer in a mouse model of the disease.

2. The candidate was the first to show that eIF2α phosphorylation activates the MAPK pathway by translationally inhibiting the phosphatase DUSP6.

3. The candidate was the first to report that pharmacological inhibitors of the PERK-eIF2α-P arm can be novel therapeutic targets in the treatment of KRAS-induced lung cancer. Particularly, the candidate shows that ISRIB is a non-toxic small molecule that can reduce tumor progression and increase survival of mice with KRAS lung cancer.

4. The candidate was the first to show that eIF2α phosphorylation employs YAP/TAZ signaling to drive KRAS lung cancer progression.

5. The candidate was the first to reveal the importance of eIF2α phosphorylation in driving sub-clonal diversity and emergence of plasticity and stemness in KRAS-driven lung cancer.

Chapter 6

REFERENCES

1 Hershey, J. W., Sonenberg, N. & Mathews, M. B. Principles of translational control: an overview. *Cold Spring Harb Perspect Biol* **4**, doi:10.1101/cshperspect.a011528 (2012).
2 Sloan, K. E. *et al.* Tuning the ribosome: The influence of rRNA modification on eukaryotic ribosome biogenesis and function. *Rna Biology* **14**, 1138-1152, doi:10.1080/15476286.2016.1259781 (2017).
3 McGlincy, N. J. & Ingolia, N. T. Transcriptome-wide measurement of translation by ribosome profiling. *Methods* **126**, 112-129, doi:10.1016/j.ymeth.2017.05.028 (2017).
4 Sonenberg, N. & Hinnebusch, A. G. Regulation of Translation Initiation in Eukaryotes: Mechanisms and Biological Targets. *Cell* **136**, 731-745, doi:10.1016/j.cell.2009.01.042 (2009).
5 Jackson, R. J., Hellen, C. U. T. & Pestova, T. V. The mechanism of eukaryotic translation initiation and principles of its regulation. *Nature Reviews Molecular Cell Biology* **11**, 113-127, doi:10.1038/nrm2838 (2010).
6 Hershey, J. W. B., Sonenberg, N. & Mathews, M. B. Principles of Translational Control: An Overview. *Cold Spring Harbor Perspectives in Biology* **4**, doi:10.1101/cshperspect.a011528 (2012).
7 Hinnebusch, A. G. in *Annual Review of Biochemistry, Vol 83* Vol. 83 *Annual Review of Biochemistry* (ed R. D. Kornberg) 779-812 (2014).
8 Hinnebusch, A. G., Ivanov, I. P. & Sonenberg, N. Translational control by 5 '-untranslated regions of eukaryotic mRNAs. *Science (New York, N.Y.)* **352**, 1413-1416, doi:10.1126/science.aad9868 (2016).
9 Pelletier, J., Graff, J., Ruggero, D. & Sonenberg, N. Targeting the eIF4F Translation Initiation Complex: A Critical Nexus for Cancer Development. *Cancer Res.* **75**, 250-263, doi:10.1158/0008-5472.can-14-2789 (2015).
10 Koromilas, A. E. Roles of the translation initiation factor eIF2 alpha serine 51 phosphorylation in cancer formation and treatment. *Biochimica Et Biophysica Acta-Gene Regulatory Mechanisms* **1849**, 871-880, doi:10.1016/j.bbagrm.2014.12.007 (2015).
11 Costa-Mattioli, M. & Walter, P. The integrated stress response: From mechanism to disease. *Science (New York, N.Y.)* **368**, 384-+, doi:10.1126/science.aat5314 (2020).
12 Pakos-Zebrucka, K. *et al.* The integrated stress response. *EMBO reports* **17**, 1374-1395, doi:10.15252/embr.201642195 (2016).
13 Clementi, E. *et al.* Persistent DNA damage triggers activation of the integrated stress response to promote cell survival under nutrient restriction. *Bmc Biology* **18**, doi:10.1186/s12915-020-00771-x (2020).
14 Akman, M. *et al.* Hypoxia, endoplasmic reticulum stress and chemoresistance: dangerous liaisons. *Journal of Experimental & Clinical Cancer Research* **40**, doi:10.1186/s13046-020-01824-3 (2021).
15 Adomavicius, T. *et al.* The structural basis of translational control by eIF2 phosphorylation. *Nat. Commun.* **10**, 2136, doi:10.1038/s41467-019-10167-3 (2019).
16 Leppek, K., Das, R. & Barna, M. Functional 5 ' UTR mRNA structures in eukaryotic translation regulation and how to find them. *Nature Reviews Molecular Cell Biology* **19**, 158-174, doi:10.1038/nrm.2017.103 (2018).
17 Donnelly, N., Gorman, A. M., Gupta, S. & Samali, A. The eIF2 alpha kinases: their structures and functions. *Cellular and Molecular Life Sciences* **70**, 3493-3511, doi:10.1007/s00018-012-1252-6 (2013).
18 Wek, R. C. Role of eIF2α Kinases in Translational Control and Adaptation to Cellular Stress. *Cold Spring Harb Perspect Biol* **10**, doi:10.1101/cshperspect.a032870 (2018).
19 Chen, J. J. Regulation of protein synthesis by the heme-regulated eIF2alpha kinase: relevance to anemias. *Blood* **109**, 2693-2699, doi:10.1182/blood-2006-08-041830 (2007).

20 Guo, X. Y. *et al.* Mitochondrial stress is relayed to the cytosol by an OMA1-DELE1-HRI pathway. *Nature* **579**, 427-+, doi:10.1038/s41586-020-2078-2 (2020).
21 Chen, J. J. Translational control by heme-regulated eIF2α kinase during erythropoiesis. *Current opinion in hematology* **21**, 172-178, doi:10.1097/moh.0000000000000030 (2014).
22 Burwick, N. & Aktas, B. H. The eIF2-alpha kinase HRI: a potential target beyond the red blood cell. *Expert Opin Ther Targets* **21**, 1171-1177, doi:10.1080/14728222.2017.1397133 (2017).
23 Lemaire, P. A., Lary, J. & Cole, J. L. Mechanism of PKR activation: Dimerization and kinase activation in the absence of double-stranded RNA. *Journal of Molecular Biology* **345**, 81-90, doi:10.1016/j.jmb.2004.10.031 (2005).
24 Garcia, M. A., Meurs, E. F. & Esteban, M. The dsRNA protein kinase PKR: Virus and cell control. *Biochimie* **89**, 799-811, doi:10.1016/j.biochi.2007.03.001 (2007).
25 Hetz, C., Chevet, E. & Oakes, S. A. Proteostasis control by the unfolded protein response. *Nat. Cell Biol.* **17**, 829-838, doi:10.1038/ncb3184 (2015).
26 Harding, H. P., Zhang, Y. H. & Ron, D. Protein translation and folding are coupled by an endoplasmic-reticulum-resident kinase. *Nature* **397**, 271-274, doi:10.1038/16729 (1999).
27 Han, J. *et al.* ER-stress-induced transcriptional regulation increases protein synthesis leading to cell death. *Nat. Cell Biol.* **15**, 481-+, doi:10.1038/ncb2738 (2013).
28 Hetz, C. & Papa, F. R. The Unfolded Protein Response and Cell Fate Control. *Mol Cell* **69**, 169-181, doi:10.1016/j.molcel.2017.06.017 (2018).
29 Carrara, M., Prischi, F., Nowak, P. R., Kopp, M. C. & Ali, M. M. U. Noncanonical binding of BiP ATPase domain to Ire1 and Perk is dissociated by unfolded protein C(H)1 to initiate ER stress signaling. *eLife* **4**, doi:10.7554/eLife.03522 (2015).
30 Kopp, M. C., Larburu, N., Durairaj, V., Adams, C. J. & Ali, M. M. U. UPR proteins IRE1 and PERK switch BiP from chaperone to ER stress sensor. *Nature Structural & Molecular Biology* **26**, 1053-+, doi:10.1038/s41594-019-0324-9 (2019).
31 Cui, W. J., Li, J. Z., Ron, D. & Sha, B. D. The structure of the PERK kinase domain suggests the mechanism for its activation. *Acta Crystallographica Section D-Biological Crystallography* **67**, 423-428, doi:10.1107/s0907444911006445 (2011).
32 Korennykh, A. & Walter, P. in *Annual Review of Cell and Developmental Biology, Vol 28* Vol. 28 *Annual Review of Cell and Developmental Biology* (ed R. Schekman) 251-277 (2012).
33 Wang, M. & Kaufman, R. J. Protein misfolding in the endoplasmic reticulum as a conduit to human disease. *Nature* **529**, 326-335, doi:10.1038/nature17041 (2016).
34 Hinnebusch, A. G. Translational regulation of GCN4 and the general amino acid control of yeast. *Annual Review of Microbiology* **59**, 407-450, doi:10.1146/annurev.micro.59.031805.133833 (2005).
35 Inglis, A. J. *et al.* Activation of GCN2 by the ribosomal P-stalk. *Proc. Natl. Acad. Sci. U. S. A.* **116**, 4946-4954, doi:10.1073/pnas.1813352116 (2019).
36 Harding, H. P. *et al.* The ribosomal P-stalk couples amino acid starvation to GCN2 activation in mammalian cells. *eLife* **8**, doi:10.7554/eLife.50149 (2019).
37 Ishimura, R., Nagy, G., Dotu, I., Chuang, J. H. & Ackerman, S. L. Activation of GCN2 kinase by ribosome stalling links translation elongation with translation initiation. *eLife* **5**, doi:10.7554/eLife.14295 (2016).
38 Sidrauski, C., McGeachy, A. M., Ingolia, N. T. & Walter, P. The small molecule ISRIB reverses the effects of eIF2alpha phosphorylation on translation and stress granule assembly. *eLife* **4**, doi:10.7554/eLife.05033 (2015).
39 Dalton, L. E., Healey, E., Irving, J. & Marciniak, S. J. in *Protein Phosphorylation in Health and Disease* Vol. 106 *Progress in Molecular Biology and Translational Science* (ed S. Shenolikar) 189-221 (2012).

40 Wortel, I. M. N., van der Meer, L. T., Kilberg, M. S. & van Leeuwen, F. N. Surviving Stress: Modulation of ATF4-Mediated Stress Responses in Normal and Malignant Cells. *Trends in Endocrinology and Metabolism* **28**, 794-806, doi:10.1016/j.tem.2017.07.003 (2017).
41 B'Chir, W. *et al.* The eIF2 alpha/ATF4 pathway is essential for stress-induced autophagy gene expression. *Nucleic acids research* **41**, 7683-7699, doi:10.1093/nar/gkt563 (2013).
42 Pavitt, G. D. Regulation of translation initiation factor eIF2B at the hub of the integrated stress response. *Wiley Interdiscip. Rev.-RNA* **9**, doi:10.1002/wrna.1491 (2018).
43 Pavitt, G. D. Regulation of translation initiation factor eIF2B at the hub of the integrated stress response. *Wiley Interdiscip. Rev.-RNA* **9**, 22, doi:10.1002/wrna.1491 (2018).
44 Novoa, I., Zeng, H. Q., Harding, H. P. & Ron, D. Feedback inhibition of the unfolded protein response by GADD34-mediated dephosphorylation of eIF2 alpha. *Journal of Cell Biology* **153**, 1011-1021, doi:10.1083/jcb.153.5.1011 (2001).
45 Jousse, C. *et al.* Inhibition of a constitutive translation initiation factor 2 alpha phosphatase CReP, promotes survival of stressed cells. *Journal of Cell Biology* **163**, 767-775, doi:10.1083/jcb.200308075 (2003).
46 Kojima, E. *et al.* The function of GADD34 is a recovery from a shutoff of protein synthesis induced by ER stress - elucidation by GADD34-deficient mice. *Faseb Journal* **17**, 1573-+, doi:10.1096/fj.02-1184fje (2003).
47 Fouad, Y. A. & Aanei, C. Revisiting the hallmarks of cancer. *American Journal of Cancer Research* **7**, 1016-1036 (2017).
48 Hanahan, D. Hallmarks of Cancer: New Dimensions. *Cancer Discovery* **12**, 31-46, doi:10.1158/2159-8290.cd-21-1059 (2022).
49 Senga, S. S. & Grose, R. P. Hallmarks of cancer-the new testament. *Open Biology* **11**, doi:10.1098/rsob.200358 (2021).
50 Erin, N., Grahovac, J., Brozovic, A. & Efferth, T. Tumor microenvironment and epithelial mesenchymal transition as targets to overcome tumor multidrug resistance. *Drug Resistance Updates* **53**, doi:10.1016/j.drup.2020.100715 (2020).
51 Bhat, M. *et al.* Targeting the translation machinery in cancer. *Nature reviews. Drug discovery* **14**, 261-278, doi:10.1038/nrd4505 (2015).
52 Leibovitch, M. & Topisirovic, I. Dysregulation of mRNA translation and energy metabolism in cancer. *Advances in biological regulation* **67**, 30-39, doi:10.1016/j.jbior.2017.11.001 (2018).
53 Robichaud, N., Sonenberg, N., Ruggero, D. & Schneider, R. J. Translational Control in Cancer. *Cold Spring Harb Perspect Biol* **11**, doi:10.1101/cshperspect.a032896 (2019).
54 Hershey, J. W. B., Sonenberg, N. & Mathews, M. B. Principles of Translational Control. *Cold Spring Harb Perspect Biol* **11**, doi:10.1101/cshperspect.a032607 (2019).
55 Siddiqui, N. & Sonenberg, N. Signalling to eIF4E in cancer. *Biochemical Society transactions* **43**, 763-772, doi:10.1042/bst20150126 (2015).
56 Tahmasebi, S., Sonenberg, N., Hershey, J. W. B. & Mathews, M. B. Protein Synthesis and Translational Control: A Historical Perspective. *Cold Spring Harb Perspect Biol* **11**, doi:10.1101/cshperspect.a035584 (2019).
57 Robichaud, N. & Sonenberg, N. Translational control and the cancer cell response to stress. *Current opinion in cell biology* **45**, 102-109, doi:10.1016/j.ceb.2017.05.007 (2017).
58 Bitterman, P. B. & Polunovsky, V. A. eIF4E-mediated translational control of cancer incidence. *Biochimica et Biophysica Acta (BBA) - Gene Regulatory Mechanisms* **1849**, 774-780, doi:https://doi.org/10.1016/j.bbagrm.2014.09.007 (2015).
59 Boussemart, L. *et al.* eIF4F is a nexus of resistance to anti-BRAF and anti-MEK cancer therapies. *Nature* **513**, 105-+, doi:10.1038/nature13572 (2014).

60 Dai, L. *et al.* Targeting EIF4F complex in non-small cell lung cancer cells. *Oncotarget* **8**, 55731-55735, doi:10.18632/oncotarget.18469 (2017).
61 Ma, X. M. & Blenis, J. Molecular mechanisms of mTOR-mediated translational control. *Nature Reviews Molecular Cell Biology* **10**, 307-318, doi:10.1038/nrm2672 (2009).
62 Populo, H., Lopes, J. M. & Soares, P. The mTOR Signalling Pathway in Human Cancer. *International Journal of Molecular Sciences* **13**, 1886-1918, doi:10.3390/ijms13021886 (2012).
63 Koromilas, A. E. M(en)TORship lessons on life and death by the integrated stress response. *Biochimica et biophysica acta. General subjects* **1863**, 644-649, doi:10.1016/j.bbagen.2018.12.009 (2019).
64 Hay, N. & Sonenberg, N. Upstream and downstream of mTOR. *Genes & development* **18**, 1926-1945 (2004).
65 Bhat, M. *et al.* Targeting the translation machinery in cancer. *Nature Reviews Drug Discovery* **14**, 261-278, doi:10.1038/nrd4505 (2015).
66 Corazzari, M. *et al.* Oncogenic BRAF induces chronic ER stress condition resulting in increased basal autophagy and apoptotic resistance of cutaneous melanoma. *Cell death and differentiation* **22**, 946-958, doi:10.1038/cdd.2014.183 (2015).
67 McConkey, D. J. The integrated stress response and proteotoxicity in cancer therapy. *Biochemical and Biophysical Research Communications* **482**, 450-453, doi:10.1016/j.bbrc.2016.11.047 (2017).
68 Holcik, M. & Sonenberg, N. Translational control in stress and apoptosis. *Nature reviews. Molecular cell biology* **6**, 318-327, doi:10.1038/nrm1618 (2005).
69 Ye, J. B. & Koumenis, C. ATF4, an ER Stress and Hypoxia-Inducible Transcription Factor and its Potential Role in Hypoxia Tolerance and Tumorigenesis. *Current Molecular Medicine* **9**, 411-416, doi:10.2174/156652409788167096 (2009).
70 Tameire, F. *et al.* ATF4 couples MYC-dependent translational activity to bioenergetic demands during tumour progression. *Nat. Cell Biol.* **21**, 889-+, doi:10.1038/s41556-019-0347-9 (2019).
71 Tian, X. B. *et al.* Targeting the Integrated Stress Response in Cancer Therapy. *Frontiers in Pharmacology* **12**, doi:10.3389/fphar.2021.747837 (2021).
72 Stone, S. *et al.* Dual role of the integrated stress response in medulloblastoma tumorigenesis. *Oncotarget* **7**, 64124-64135, doi:10.18632/oncotarget.11873 (2016).
73 Palam, L. R., Gore, J., Craven, K. E., Wilson, J. L. & Korc, M. Integrated stress response is critical for gemcitabine resistance in pancreatic ductal adenocarcinoma. *Cell Death Dis.* **6**, doi:10.1038/cddis.2015.264 (2015).
74 Nguyen, H. G. *et al.* Development of a stress response therapy targeting aggressive prostate cancer. *Sci. Transl. Med.* **10**, doi:10.1126/scitranslmed.aar2036 (2018).
75 Zhang, Y. Q. *et al.* EZH2i EPZ-6438 and HDACi vorinostat synergize with ONC201/TIC10 to activate integrated stress response, DR5, reduce H3K27 methylation, CIpX and promote apoptosis of multiple tumor types including DIPG. *Neoplasia* **23**, 792-810, doi:10.1016/j.neo.2021.06.007 (2021).
76 Darini, C. *et al.* An integrated stress response via PKR suppresses HER2+cancers and improves trastuzumab therapy. *Nat. Commun.* **10**, doi:10.1038/s41467-019-10138-8 (2019).
77 Ishizawa, J. *et al.* ATF4 induction through an atypical integrated stress response to ONC201 triggers p53-independent apoptosis in hematological malignancies. *Science Signaling* **9**, doi:10.1126/scisignal.aac4380 (2016).
78 Hamanaka, R. B., Bobrovnikova-Marjon, E., Ji, X., Liebhaber, S. A. & Diehl, J. A. PERK-dependent regulation of IAP translation during ER stress. *Oncogene* **28**, 910-920, doi:10.1038/onc.2008.428 (2009).

79 Hu, J. S. *et al.* Activation of ATF4 mediates unwanted Mcl-1 accumulation by proteasome inhibition. *Blood* **119**, 826-837, doi:10.1182/blood-2011-07-366492 (2012).
80 Chitnis, N. S. *et al.* miR-211 Is a Prosurvival MicroRNA that Regulates chop Expression in a PERK-Dependent Manner. *Mol. Cell* **48**, 353-364, doi:10.1016/j.molcel.2012.08.025 (2012).
81 Deng, J. *et al.* Translational repression mediates activation of nuclear factor kappa B by phosphorylated translation initiation factor 2. *Molecular and cellular biology* **24**, 10161-10168, doi:10.1128/mcb.24.23.10161-10168.2004 (2004).
82 Karali, E. *et al.* VEGF Signals through ATF6 and PERK to Promote Endothelial Cell Survival and Angiogenesis in the Absence of ER Stress. *Mol. Cell* **54**, 559-572, doi:10.1016/j.molcel.2014.03.022 (2014).
83 Feng, Y. X. *et al.* Epithelial-to-Mesenchymal Transition Activates PERK-eIF2 alpha and Sensitizes Cells to Endoplasmic Reticulum Stress. *Cancer Discovery* **4**, 702-715, doi:10.1158/2159-8290.cd-13-0945 (2014).
84 Harding, H. P. *et al.* An integrated stress response regulates amino acid metabolism and resistance to oxidative stress. *Mol. Cell* **11**, 619-633, doi:10.1016/s1097-2765(03)00105-9 (2003).
85 Mounir, Z. *et al.* Akt Determines Cell Fate Through Inhibition of the PERK-eIF2 alpha Phosphorylation Pathway. *Science Signaling* **4**, doi:10.1126/scisignal.2001630 (2011).
86 Ye, J. B. *et al.* The GCN2-ATF4 pathway is critical for tumour cell survival and proliferation in response to nutrient deprivation. *Embo Journal* **29**, 2082-2096, doi:10.1038/emboj.2010.81 (2010).
87 Daskalaki, I., Gkikas, I. & Tavernarakis, N. Hypoxia and Selective Autophagy in Cancer Development and Therapy. *Frontiers in Cell and Developmental Biology* **6**, doi:10.3389/fcell.2018.00104 (2018).
88 Mendez-Lucas, A., Hyrossova, P., Novellasdemunt, L., Vinals, F. & Perales, J. C. Mitochondrial Phosphoenolpyruvate Carboxykinase (PEPCK-M) Is a Pro-survival, Endoplasmic Reticulum (ER) Stress Response Gene Involved in Tumor Cell Adaptation to Nutrient Availability. *J. Biol. Chem.* **289**, 22090-22102, doi:10.1074/jbc.M114.566927 (2014).
89 Chaveroux, C. *et al.* Identification of GCN2 as new redox regulator for oxidative stress prevention in vivo. *Biochemical and Biophysical Research Communications* **415**, 120-124, doi:10.1016/j.bbrc.2011.10.027 (2011).
90 Bonnet, M. C., Weil, R., Dam, E., Hovanessian, A. G. & Meurs, E. F. PKR stimulates NF-kappa B irrespective of its kinase function by interacting with the I kappa B kinase complex. *Molecular and cellular biology* **20**, 4532-4542, doi:10.1128/mcb.20.13.4532-4542.2000 (2000).
91 Donze, O., Dostie, J. & Sonenberg, N. Regulatable expression of the interferon-induced double-stranded RNA dependent protein kinase PKR induces apoptosis and Fas receptor expression. *Virology* **256**, 322-329, doi:10.1006/viro.1999.9618 (1999).
92 Mounir, Z. *et al.* Tumor Suppression by PTEN Requires the Activation of the PKR-eIF2 alpha Phosphorylation Pathway. *Science Signaling* **2**, doi:10.1126/scisignal.2000389 (2009).
93 Burwick, N. & Aktas, B. H. The eIF2-alpha kinase HRI: a potential target beyond the red blood cell. *Expert Opinion on Therapeutic Targets* **21**, 1171-1177, doi:10.1080/14728222.2017.1397133 (2017).
94 Yerlikaya, A. Heme-regulated inhibitor: an overlooked eIF2 alpha kinase in cancer investigations. *Medical Oncology* **39**, doi:10.1007/s12032-022-01668-1 (2022).
95 Abdel-Nour, M. *et al.* The heme-regulated inhibitor is a cytosolic sensor of protein misfolding that controls innate immune signaling. *Science (New York, N.Y.)* **365**, 47-+, doi:10.1126/science.aaw4144 (2019).

96 Smith, K. H. *et al.* The Heme-Regulated Inhibitor Pathway Modulates Susceptibility of Poor Prognosis B-Lineage Acute Leukemia to BH3-Mimetics. *Molecular Cancer Research* **19**, 636-650, doi:10.1158/1541-7786.mcr-20-0586 (2021).
97 Nguyen, H. G. *et al.* Development of a stress response therapy targeting aggressive prostate cancer. *Sci. Transl. Med.* **10**, 11, doi:10.1126/scitranslmed.aar2036 (2018).
98 Baltzis, D. *et al.* The eIF2alpha kinases PERK and PKR activate glycogen synthase kinase 3 to promote the proteasomal degradation of p53. *The Journal of biological chemistry* **282**, 31675-31687, doi:10.1074/jbc.M704491200 (2007).
99 Kline, C. L. B. *et al.* ONC201 kills solid tumor cells by triggering an integrated stress response dependent on ATF4 activation by specific eIF2 alpha kinases. *Science Signaling* **9**, doi:10.1126/scisignal.aac4374 (2016).
100 Mounir, Z. & Koromilas, A. E. Uncovering the PKR pathway's potential for treatment of tumors. *Future oncology (London, England)* **6**, 643-645, doi:10.2217/fon.10.45 (2010).
101 Koromilas, A. E. The integrated stress response in the induction of mutant KRAS lung carcinogenesis: Mechanistic insights and therapeutic implications. *BioEssays : news and reviews in molecular, cellular and developmental biology* **44**, e2200026, doi:10.1002/bies.202200026 (2022).
102 Atkins, C. *et al.* Characterization of a Novel PERK Kinase Inhibitor with Antitumor and Antiangiogenic Activity. *Cancer Res.* **73**, 1993-2002, doi:10.1158/0008-5472.can-12-3109 (2013).
103 Rozpedek, W. *et al.* The Role of the PERK/eIF2 alpha/ATF4/CHOP Signaling Pathway in Tumor Progression During Endoplasmic Reticulum Stress. *Current Molecular Medicine* **16**, 533-544, doi:10.2174/1566524016666160523143937 (2016).
104 Nakamura, A. *et al.* Inhibition of GCN2 sensitizes ASNS-low cancer cells to asparaginase by disrupting the amino acid response. *Proc. Natl. Acad. Sci. U. S. A.* **115**, E7776-E7785, doi:10.1073/pnas.1805523115 (2018).
105 Axten, J. M. *et al.* Discovery of GSK2656157: An Optimized PERK Inhibitor Selected for Preclinical Development. *Acs Medicinal Chemistry Letters* **4**, 964-968, doi:10.1021/ml400228e (2013).
106 Axten, J. M. *et al.* Discovery of 7-Methyl-5-(1-{ 3-(trifluoromethyl)phenyl acetyl}-2,3-dihydro-1H-indol-5 -yl)-7H-pyrrolo 2,3-d pyrimidin-4-amine (GSK2606414), a Potent and Selective First-in-Class Inhibitor of Protein Kinase R (PKR)-like Endoplasmic Reticulum Kinase (PERK). *J. Med. Chem.* **55**, 7193-7207, doi:10.1021/jm300713s (2012).
107 Cullinan, S. B. *et al.* Nrf2 is a direct PERK substrate and effector of PERK-dependent cell survival. *Molecular and cellular biology* **23**, 7198-7209, doi:10.1128/mcb.23.20.7198-7209.2003 (2003).
108 Yoon, C. H., Miah, M. A., Kim, K. P. & Bae, Y. S. New Cdc2 Tyr 4 phosphorylation by dsRNA-activated protein kinase triggers Cdc2 polyubiquitination and G2 arrest under genotoxic stresses. *EMBO reports* **11**, 393-399, doi:10.1038/embor.2010.45 (2010).
109 Koromilas, A. E. Roles of the translation initiation factor eIF2alpha serine 51 phosphorylation in cancer formation and treatment. *Biochimica et biophysica acta* **1849**, 871-880, doi:10.1016/j.bbagrm.2014.12.007 (2015).
110 Boyce, M. *et al.* A selective inhibitor-of eIF2 alpha dephosphorylation protects cells from ER stress. *Science (New York, N.Y.)* **307**, 935-939, doi:10.1126/science.1101902 (2005).
111 Tsaytler, P., Harding, H. P., Ron, D. & Bertolotti, A. Selective Inhibition of a Regulatory Subunit of Protein Phosphatase 1 Restores Proteostasis. *Science (New York, N.Y.)* **332**, 91-94, doi:10.1126/science.1201396 (2011).
112 Chen, Y. A. *et al.* Sephin1, which prolongs the integrated stress response, is a promising therapeutic for multiple sclerosis. *Brain* **142**, 344-361, doi:10.1093/brain/awy322 (2019).
113 Krzyzosiak, A. *et al.* Target-Based Discovery of an Inhibitor of the Regulatory Phosphatase PPP1R15B. *Cell* **174**, 1216-+, doi:10.1016/j.cell.2018.06.030 (2018).

114 Ho, K. H. *et al.* Guanabenz Sensitizes Glioblastoma Cells to Sunitinib by Inhibiting GADD34-Mediated Autophagic Signaling. *Neurotherapeutics* **18**, 1371-1392, doi:10.1007/s13311-020-00961-z (2021).
115 Anand, A. A. & Walter, P. Structural insights into ISRIB, a memory-enhancing inhibitor of the integrated stress response. *The FEBS journal* **287**, 239-245, doi:10.1111/febs.15073 (2020).
116 Zyryanova, A. F. *et al.* ISRIB Blunts the Integrated Stress Response by Allosterically Antagonising the Inhibitory Effect of Phosphorylated eIF2 on eIF2B. *Mol. Cell* **81**, 88-+, doi:10.1016/j.molcel.2020.10.031 (2021).
117 Rabouw, H. H. *et al.* Small molecule ISRIB suppresses the integrated stress response within a defined window of activation. *Proc. Natl. Acad. Sci. U. S. A.* **116**, 2097-2102, doi:10.1073/pnas.1815767116 (2019).
118 Nguyen, H. G. *et al.* Development of a stress response therapy targeting aggressive prostate cancer. *Sci Transl Med* **10**, doi:10.1126/scitranslmed.aar2036 (2018).
119 Lee, D. M., Seo, M. J., Lee, H. J., Jin, H. J. & Choi, K. S. ISRIB plus bortezomib triggers paraptosis in breast cancer cells via enhanced translation and subsequent proteotoxic stress. *Biochemical and Biophysical Research Communications* **596**, 56-62, doi:10.1016/j.bbrc.2022.01.082 (2022).
120 Zanconato, F., Cordenonsi, M. & Piccolo, S. YAP/TAZ at the Roots of Cancer. *Cancer Cell* **29**, 783-803, doi:10.1016/j.ccell.2016.05.005 (2016).
121 Varelas, X. The Hippo pathway effectors TAZ and YAP in development, homeostasis and disease. *Development (Cambridge, England)* **141**, 1614-1626, doi:10.1242/dev.102376 (2014).
122 Piccolo, S., Dupont, S. & Cordenonsi, M. The Biology of YAP/TAZ: Hippo Signaling and Beyond. *Physiological Reviews* **94**, 1287-1312, doi:10.1152/physrev.00005.2014 (2014).
123 Hansen, C. G., Moroishi, T. & Guan, K. L. YAP and TAZ: a nexus for Hippo signaling and beyond. *Trends in cell biology* **25**, 499-513, doi:10.1016/j.tcb.2015.05.002 (2015).
124 Zanconato, F. *et al.* Genome-wide association between YAP/TAZ/TEAD and AP-1 at enhancers drives oncogenic growth. *Nat. Cell Biol.* **17**, 1218-1227, doi:10.1038/ncb3216 (2015).
125 Dey, A., Varelas, X. & Guan, K. L. Targeting the Hippo pathway in cancer, fibrosis, wound healing and regenerative medicine. *Nature reviews. Drug discovery* **19**, 480-494, doi:10.1038/s41573-020-0070-z (2020).
126 Calses, P. C., Crawford, J. J., Lill, J. R. & Dey, A. Hippo Pathway in Cancer: Aberrant Regulation and Therapeutic Opportunities. *Trends in Cancer* **5**, 297-307, doi:https://doi.org/10.1016/j.trecan.2019.04.001 (2019).
127 Janse van Rensburg, H. J. & Yang, X. The roles of the Hippo pathway in cancer metastasis. *Cellular Signalling* **28**, 1761-1772, doi:https://doi.org/10.1016/j.cellsig.2016.08.004 (2016).
128 Moroishi, T., Hansen, C. G. & Guan, K.-L. The emerging roles of YAP and TAZ in cancer. *Nat. Rev. Cancer* **15**, 73-79, doi:10.1038/nrc3876 (2015).
129 Kapoor, A. *et al.* Yap1 activation enables bypass of oncogenic Kras addiction in pancreatic cancer. *Cell* **158**, 185-197, doi:10.1016/j.cell.2014.06.003 (2014).
130 Zanconato, F. *et al.* Transcriptional addiction in cancer cells is mediated by YAP/TAZ through BRD4. *Nature medicine* **24**, 1599-1610, doi:10.1038/s41591-018-0158-8 (2018).
131 Lau, A. N. *et al.* Tumor-propagating cells and Yap/Taz activity contribute to lung tumor progression and metastasis. *The EMBO journal* **33**, 468-481, doi:10.1002/embj.201386082 (2014).
132 Zhang, W. *et al.* YAP promotes malignant progression of Lkb1-deficient lung adenocarcinoma through downstream regulation of survivin. *Cancer Res* **75**, 4450-4457, doi:10.1158/0008-5472.can-14-3396 (2015).
133 Mohseni, M. *et al.* A genetic screen identifies an LKB1-MARK signalling axis controlling the Hippo-YAP pathway. *Nat Cell Biol* **16**, 108-117, doi:10.1038/ncb2884 (2014).

134 Wang, G. *et al.* Targeting YAP-Dependent MDSC Infiltration Impairs Tumor Progression. *Cancer Discovery* **6**, 80-95, doi:10.1158/2159-8290.cd-15-0224 (2016).
135 Cheng, H. *et al.* Functional genomics screen identifies YAP1 as a key determinant to enhance treatment sensitivity in lung cancer cells. *Oncotarget* **7**, 28976-28988, doi:10.18632/oncotarget.6721 (2016).
136 Noguchi, S. *et al.* An integrative analysis of the tumorigenic role of TAZ in human non-small cell lung cancer. *Clinical cancer research : an official journal of the American Association for Cancer Research* **20**, 4660-4672, doi:10.1158/1078-0432.ccr-13-3328 (2014).
137 Bartucci, M. *et al.* TAZ is required for metastatic activity and chemoresistance of breast cancer stem cells. *Oncogene* **34**, 681-690, doi:10.1038/onc.2014.5 (2015).
138 Basu-Roy, U. *et al.* Sox2 antagonizes the Hippo pathway to maintain stemness in cancer cells. *Nat. Commun.* **6**, 6411, doi:10.1038/ncomms7411 (2015).
139 Cordenonsi, M. *et al.* The Hippo transducer TAZ confers cancer stem cell-related traits on breast cancer cells. *Cell* **147**, 759-772, doi:10.1016/j.cell.2011.09.048 (2011).
140 Castellan, M. *et al.* Single-cell analyses reveal YAP/TAZ as regulators of stemness and cell plasticity in Glioblastoma. *Nat Cancer* **2**, 174-188, doi:10.1038/s43018-020-00150-z (2021).
141 Lin, L. *et al.* The Hippo effector YAP promotes resistance to RAF- and MEK-targeted cancer therapies. *Nature genetics* **47**, 250-256, doi:10.1038/ng.3218 (2015).
142 Pobbati, A. V. & Hong, W. A combat with the YAP/TAZ-TEAD oncoproteins for cancer therapy. *Theranostics* **10**, 3622-3635, doi:10.7150/thno.40889 (2020).
143 Pearson, J. D. *et al.* Binary pan-cancer classes with distinct vulnerabilities defined by pro- or anti-cancer YAP/TEAD activity. *Cancer Cell* **39**, 1115-1134.e1112, doi:10.1016/j.ccell.2021.06.016 (2021).
144 Pearson, J. D. & Bremner, R. Simplifying cancer: binary pan-cancer superclasses stratified by opposite YAP/TEAD effects. *Molecular & cellular oncology* **8**, 1981111, doi:10.1080/23723556.2021.1981111 (2021).
145 Meng, Z., Moroishi, T. & Guan, K. L. Mechanisms of Hippo pathway regulation. *Genes & development* **30**, 1-17, doi:10.1101/gad.274027.115 (2016).
146 Aragona, M. *et al.* A mechanical checkpoint controls multicellular growth through YAP/TAZ regulation by actin-processing factors. *Cell* **154**, 1047-1059, doi:10.1016/j.cell.2013.07.042 (2013).
147 Azzolin, L. *et al.* Role of TAZ as mediator of Wnt signaling. *Cell* **151**, 1443-1456, doi:10.1016/j.cell.2012.11.027 (2012).
148 Das, A., Fischer, R. S., Pan, D. & Waterman, C. M. YAP Nuclear Localization in the Absence of Cell-Cell Contact Is Mediated by a Filamentous Actin-dependent, Myosin II- and Phospho-YAP-independent Pathway during Extracellular Matrix Mechanosensing. *The Journal of biological chemistry* **291**, 6096-6110, doi:10.1074/jbc.M115.708313 (2016).
149 Dupont, S. *et al.* Role of YAP/TAZ in mechanotransduction. *Nature* **474**, 179-183, doi:10.1038/nature10137 (2011).
150 Enzo, E. *et al.* Aerobic glycolysis tunes YAP/TAZ transcriptional activity. *The EMBO journal* **34**, 1349-1370, doi:10.15252/embj.201490379 (2015).
151 Feng, X. *et al.* Hippo-independent activation of YAP by the GNAQ uveal melanoma oncogene through a trio-regulated rho GTPase signaling circuitry. *Cancer Cell* **25**, 831-845, doi:10.1016/j.ccr.2014.04.016 (2014).
152 Li, P. *et al.* αE-catenin inhibits a Src-YAP1 oncogenic module that couples tyrosine kinases and the effector of Hippo signaling pathway. *Genes & development* **30**, 798-811, doi:10.1101/gad.274951.115 (2016).

153 Azzolin, L. *et al.* YAP/TAZ incorporation in the β-catenin destruction complex orchestrates the Wnt response. *Cell* **158**, 157-170, doi:10.1016/j.cell.2014.06.013 (2014).
154 Varelas, X. The Hippo pathway effectors TAZ and YAP in development, homeostasis and disease. *Development (Cambridge, England)* **141**, 1614-1626, doi:10.1242/dev.102376 (2014).
155 Liu-Chittenden, Y. *et al.* Genetic and pharmacological disruption of the TEAD-YAP complex suppresses the oncogenic activity of YAP. *Genes & development* **26**, 1300-1305, doi:10.1101/gad.192856.112 (2012).
156 Jiao, S. *et al.* A peptide mimicking VGLL4 function acts as a YAP antagonist therapy against gastric cancer. *Cancer Cell* **25**, 166-180, doi:10.1016/j.ccr.2014.01.010 (2014).
157 Wang, Z. *et al.* Interplay of mevalonate and Hippo pathways regulates RHAMM transcription via YAP to modulate breast cancer cell motility. *Proc Natl Acad Sci U S A* **111**, E89-98, doi:10.1073/pnas.1319190110 (2014).
158 Sorrentino, G. *et al.* Metabolic control of YAP and TAZ by the mevalonate pathway. *Nat Cell Biol* **16**, 357-366, doi:10.1038/ncb2936 (2014).
159 Gronich, N. & Rennert, G. Beyond aspirin-cancer prevention with statins, metformin and bisphosphonates. *Nature reviews. Clinical oncology* **10**, 625-642, doi:10.1038/nrclinonc.2013.169 (2013).
160 Johnson, G. L. & Lapadat, R. Mitogen-activated protein kinase pathways mediated by ERK, JNK, and p38 protein kinases. *Science (New York, N.Y.)* **298**, 1911-1912, doi:10.1126/science.1072682 (2002).
161 Sun, Y. *et al.* Signaling pathway of MAPK/ERK in cell proliferation, differentiation, migration, senescence and apoptosis. *Journal of Receptors and Signal Transduction* **35**, 600-604, doi:10.3109/10799893.2015.1030412 (2015).
162 Guo, Y. J. *et al.* ERK/MAPK signalling pathway and tumorigenesis. *Experimental and Therapeutic Medicine* **19**, 1997-2007, doi:10.3892/etm.2020.8454 (2020).
163 Burotto, M., Chiou, V. L., Lee, J. M. & Kohn, E. C. The MAPK Pathway Across Different Malignancies: A New Perspective. *Cancer* **120**, 3446-3456, doi:10.1002/cncr.28864 (2014).
164 Chang, L. & Karin, M. Mammalian MAP kinase signalling cascades. *Nature* **410**, 37-40, doi:10.1038/35065000 (2001).
165 Pearson, G. *et al.* Mitogen-activated protein (MAP) kinase pathways: regulation and physiological functions. *Endocrine reviews* **22**, 153-183, doi:10.1210/edrv.22.2.0428 (2001).
166 Dhillon, A. S., Hagan, S., Rath, O. & Kolch, W. MAP kinase signalling pathways in cancer. *Oncogene* **26**, 3279-3290, doi:10.1038/sj.onc.1210421 (2007).
167 Ahmad, M. K., Abdollah, N. A., Shafie, N. H., Yusof, N. M. & Razak, S. R. A. Dual-specificity phosphatase 6 (DUSP6): a review of its molecular characteristics and clinical relevance in cancer. *Cancer biology & medicine* **15**, 14-28, doi:10.20892/j.issn.2095-3941.2017.0107 (2018).
168 Caunt, C. J. & Keyse, S. M. Dual-specificity MAP kinase phosphatases (MKPs): Shaping the outcome of MAP kinase signalling. *Febs Journal* **280**, 489-504, doi:10.1111/j.1742-4658.2012.08716.x (2013).
169 Dhanasekaran, D. N. & Johnson, G. L. MAPKs: function, regulation, role in cancer and therapeutic targeting. *Oncogene* **26**, 3097-3099, doi:10.1038/sj.onc.1210395 (2007).
170 Unal, E. B., Uhlitz, F. & Bluthgen, N. A compendium of ERK targets. *Febs Letters* **591**, 2607-2615, doi:10.1002/1873-3468.12740 (2017).
171 Lavoie, H. & Therrien, M. Regulation of RAF protein kinases in ERK signalling. *Nature Reviews Molecular Cell Biology* **16**, 281-298, doi:10.1038/nrm3979 (2015).
172 Bhartiya, D. & Singh, J. FSH-FSHR3-stem cells in ovary surface epithelium: basis for adult ovarian biology, failure, aging, and cancer. *Reproduction (Cambridge, England)* **149**, R35-48, doi:10.1530/rep-14-0220 (2015).

173 Bang, Y. J., Kwon, J. H., Kang, S. H., Kim, J. W. & Yang, Y. C. Increased MAPK activity and MKP-1 overexpression in human gastric adenocarcinoma. *Biochem Biophys Res Commun* **250**, 43-47, doi:10.1006/bbrc.1998.9256 (1998).
174 Rao, A. & Herr, D. R. G protein-coupled receptor GPR19 regulates E-cadherin expression and invasion of breast cancer cells. *Biochimica et biophysica acta. Molecular cell research* **1864**, 1318-1327, doi:10.1016/j.bbamcr.2017.05.001 (2017).
175 Sulzmaier, F. J. & Ramos, J. W. RSK isoforms in cancer cell invasion and metastasis. *Cancer Res* **73**, 6099-6105, doi:10.1158/0008-5472.can-13-1087 (2013).
176 Gialeli, C., Theocharis, A. D. & Karamanos, N. K. Roles of matrix metalloproteinases in cancer progression and their pharmacological targeting. *The FEBS journal* **278**, 16-27, doi:10.1111/j.1742-4658.2010.07919.x (2011).
177 Maeda-Yamamoto, M. *et al.* Association of suppression of extracellular signal-regulated kinase phosphorylation by epigallocatechin gallate with the reduction of matrix metalloproteinase activities in human fibrosarcoma HT1080 cells. *J Agric Food Chem* **51**, 1858-1863, doi:10.1021/jf021039l (2003).
178 Simon, C. *et al.* PD 098059, an inhibitor of ERK1 activation, attenuates the in vivo invasiveness of head and neck squamous cell carcinoma. *British journal of cancer* **80**, 1412-1419, doi:10.1038/sj.bjc.6690537 (1999).
179 Chang, M. C. *et al.* Mesothelin enhances invasion of ovarian cancer by inducing MMP-7 through MAPK/ERK and JNK pathways. *The Biochemical journal* **442**, 293-302, doi:10.1042/bj20110282 (2012).
180 Hohmann, T. & Dehghani, F. The Cytoskeleton-A Complex Interacting Meshwork. *Cells* **8**, doi:10.3390/cells8040362 (2019).
181 Zhang, Y. H., Wei, W., Xu, H., Wang, Y. Y. & Wu, W. X. Inducing effects of hepatocyte growth factor on the expression of vascular endothelial growth factor in human colorectal carcinoma cells through MEK and PI3K signaling pathways. *Chinese medical journal* **120**, 743-748 (2007).
182 Bian, C. X. *et al.* P70S6K 1 regulation of angiogenesis through VEGF and HIF-1alpha expression. *Biochem Biophys Res Commun* **398**, 395-399, doi:10.1016/j.bbrc.2010.06.080 (2010).
183 Song, M. & Finley, S. D. Mechanistic insight into activation of MAPK signaling by pro-angiogenic factors. *BMC systems biology* **12**, 145, doi:10.1186/s12918-018-0668-5 (2018).
184 Soula-Rothhut, M. *et al.* The tumor suppressor PTEN inhibits EGF-induced TSP-1 and TIMP-1 expression in FTC-133 thyroid carcinoma cells. *Experimental cell research* **304**, 187-201, doi:10.1016/j.yexcr.2004.10.026 (2005).
185 Kidger, A. M. & Keyse, S. M. The regulation of oncogenic Ras/ERK signalling by dual-specificity mitogen activated protein kinase phosphatases (MKPs). *Seminars in cell & developmental biology* **50**, 125-132, doi:10.1016/j.semcdb.2016.01.009 (2016).
186 Arkell, R. S. *et al.* DUSP6/MKP-3 inactivates ERK1/2 but fails to bind and inactivate ERK5. *Cell Signal* **20**, 836-843, doi:10.1016/j.cellsig.2007.12.014 (2008).
187 Kondoh, K. & Nishida, E. Regulation of MAP kinases by MAP kinase phosphatases. *Biochimica et Biophysica Acta (BBA) - Molecular Cell Research* **1773**, 1227-1237, doi:https://doi.org/10.1016/j.bbamcr.2006.12.002 (2007).
188 Thai, A. A., Solomon, B. J., Sequist, L. V., Gainor, J. F. & Heist, R. S. Lung cancer. *Lancet* **398**, 535-554, doi:10.1016/s0140-6736(21)00312-3 (2021).
189 Bender, E. Epidemiology: The dominant malignancy. *Nature* **513**, S2-S3, doi:10.1038/513S2a (2014).
190 Lemjabbar-Alaoui, H., Hassan, O. U., Yang, Y. W. & Buchanan, P. Lung cancer: Biology and treatment options. *Biochimica Et Biophysica Acta-Reviews on Cancer* **1856**, 189-210, doi:10.1016/j.bbcan.2015.08.002 (2015).

191 Inamura, K. Lung Cancer: Understanding its Molecular Pathology and the 2015 WHO Classification. *Frontiers in Oncology* **7**, doi:10.3389/fonc.2017.00193 (2017).
192 Noguchi, M. *et al.* SMALL ADENOCARCINOMA OF THE LUNG - HISTOLOGIC CHARACTERISTICS AND PROGNOSIS. *Cancer* **75**, 2844-2852, doi:10.1002/1097-0142(19950615)75:12<2844::aid-cncr2820751209>3.0.co;2-# (1995).
193 Bade, B. C. & Dela Cruz, C. S. Lung Cancer 2020 Epidemiology, Etiology, and Prevention. *Clinics in Chest Medicine* **41**, 1-+, doi:10.1016/j.ccm.2019.10.001 (2020).
194 Collisson, E. A. *et al.* Comprehensive molecular profiling of lung adenocarcinoma. *Nature* **511**, 543-550, doi:10.1038/nature13385 (2014).
195 Herbst, R. S., Morgensztern, D. & Boshoff, C. The biology and management of non-small cell lung cancer. *Nature* **553**, 446-454, doi:10.1038/nature25183 (2018).
196 Drosten, M. & Barbacid, M. Targeting KRAS mutant lung cancer: light at the end of the tunnel. *Molecular Oncology* **16**, 1057-1071, doi:10.1002/1878-0261.13168 (2022).
197 Zeitouni, D., Pylayeva-Gupta, Y., Der, C. J. & Bryant, K. L. KRAS Mutant Pancreatic Cancer: No Lone Path to an Effective Treatment. *Cancers (Basel)* **8**, doi:10.3390/cancers8040045 (2016).
198 McCormick, F. Progress in targeting RAS with small molecule drugs. *The Biochemical journal* **476**, 365-374, doi:10.1042/bcj20170441 (2019).
199 Arbour, K. C. *et al.* Effects of Co-occurring Genomic Alterations on Outcomes in Patients with KRAS-Mutant Non-Small Cell Lung Cancer. *Clinical Cancer Research* **24**, 334-340, doi:10.1158/1078-0432.ccr-17-1841 (2018).
200 Devarakonda, S., Morgensztern, D. & Govindan, R. Genomic alterations in lung adenocarcinoma. *Lancet Oncol.* **16**, E342-E351, doi:10.1016/s1470-2045(15)00077-7 (2015).
201 Zeitouni, D., Pylayeva-Gupta, Y., Der, C. J. & Bryant, K. L. KRAS Mutant Pancreatic Cancer: No Lone Path to an Effective Treatment. *Cancers* **8**, 22, doi:10.3390/cancers8040045 (2016).
202 Jackson, E. L. *et al.* Analysis of lung tumor initiation and progression using conditional expression of oncogenic K-ras. *Genes & development* **15**, 3243-3248, doi:10.1101/gad.943001 (2001).
203 Guerra, C. *et al.* Tumor induction by an endogenous K-ras oncogene is highly dependent on cellular context. *Cancer Cell* **4**, 111-120, doi:10.1016/s1535-6108(03)00191-0 (2003).
204 Marjanovic, N. D. *et al.* Emergence of a High-Plasticity Cell State during Lung Cancer Evolution. *Cancer Cell* **38**, 229-+, doi:10.1016/j.ccell.2020.06.012 (2020).
205 Xia, Y. F. *et al.* Reduced cell proliferation by IKK2 depletion in a mouse lung-cancer model. *Nat. Cell Biol.* **14**, 257-+, doi:10.1038/ncb2428 (2012).
206 Chen, Z. *et al.* A murine lung cancer co-clinical trial identifies genetic modifiers of therapeutic response. *Nature* **483**, 613-617, doi:10.1038/nature10937 (2012).
207 Winslow, M. M. *et al.* Suppression of lung adenocarcinoma progression by Nkx2-1. *Nature* **473**, 101-U120, doi:10.1038/nature09881 (2011).
208 McFadden, D. G. *et al.* Mutational landscape of EGFR-, MYC-, and Kras-driven genetically engineered mouse models of lung adenocarcinoma. *Proceedings of the National Academy of Sciences* **113**, E6409-E6417, doi:doi:10.1073/pnas.1613601113 (2016).
209 Lavoie, H., Gagnon, J. & Therrien, M. ERK signalling: a master regulator of cell behaviour, life and fate. *Nature Reviews Molecular Cell Biology* **21**, 607-632, doi:10.1038/s41580-020-0255-7 (2020).
210 Hymowitz, S. G. & Malek, S. Targeting the MAPK Pathway in RAS Mutant Cancers. *Cold Spring Harbor Perspectives in Medicine* **8**, doi:10.1101/cshperspect.a031492 (2018).
211 Ambrogio, C. *et al.* KRAS Dimerization Impacts MEK Inhibitor Sensitivity and Oncogenic Activity of Mutant KRAS. *Cell* **172**, 857-+, doi:10.1016/j.cell.2017.12.020 (2018).
212 Drosten, M. & Barbacid, M. Targeting the MAPK Pathway in KRAS-Driven Tumors. *Cancer Cell* **37**, 543-550, doi:10.1016/j.ccell.2020.03.013 (2020).

213 Castel, P., Rauen, K. A. & McCormick, F. The duality of human oncoproteins: drivers of cancer and congenital disorders. *Nature reviews. Cancer* **20**, 383-397 (2020).
214 Fedele, C. *et al.* SHP2 inhibition diminishes KRASG12C cycling and promotes tumor microenvironment remodeling. *The Journal of experimental medicine* **218**, doi:10.1084/jem.20201414 (2021).
215 Wu, M. *et al.* Improvement of the anticancer efficacy of PD-1/PD-L1 blockade via combination therapy and PD-L1 regulation. *Journal of Hematology & Oncology* **15**, 24, doi:10.1186/s13045-022-01242-2 (2022).
216 Miura, Y. & Sunaga, N. Role of Immunotherapy for Oncogene-Driven Non-Small Cell Lung Cancer. *Cancers (Basel)* **10**, doi:10.3390/cancers10080245 (2018).
217 Mao, Y. P., Sun, S. G. & Irvine, K. D. Role and regulation of Yap in Kras(G12D)-induced lung cancer. *Oncotarget* **8**, 110877-110889, doi:10.18632/oncotarget.22865 (2017).
218 Johnson, R. & Halder, G. The two faces of Hippo: targeting the Hippo pathway for regenerative medicine and cancer treatment. *Nature reviews. Drug discovery* **13**, 63-79, doi:10.1038/nrd4161 (2014).
219 Hsu, P. C. *et al.* Inhibition of yes-associated protein suppresses brain metastasis of human lung adenocarcinoma in a murine model. *Journal of cellular and molecular medicine* **22**, 3073-3085, doi:10.1111/jcmm.13582 (2018).
220 Chen, H. Y. *et al.* R331W Missense Mutation of Oncogene YAP1 Is a Germline Risk Allele for Lung Adenocarcinoma With Medical Actionability. *Journal of clinical oncology : official journal of the American Society of Clinical Oncology* **33**, 2303-2310, doi:10.1200/jco.2014.59.3590 (2015).
221 Shao, D. D. *et al.* KRAS and YAP1 converge to regulate EMT and tumor survival. *Cell* **158**, 171-184, doi:10.1016/j.cell.2014.06.004 (2014).
222 Magnen, C. L., Shen, M. M. & Abate-Shen, C. Lineage Plasticity in Cancer Progression and Treatment. *Annual Review of Cancer Biology* **2**, 271-289, doi:10.1146/annurev-cancerbio-030617-050224 (2018).
223 Quintanal-Villalonga, Á. *et al.* Lineage plasticity in cancer: a shared pathway of therapeutic resistance. *Nature reviews. Clinical oncology* **17**, 360-371, doi:10.1038/s41571-020-0340-z (2020).
224 LaFave, L. M. *et al.* Epigenomic State Transitions Characterize Tumor Progression in Mouse Lung Adenocarcinoma. *Cancer Cell* **38**, 212-228.e213, doi:https://doi.org/10.1016/j.ccell.2020.06.006 (2020).
225 Yang, D. *et al.* Lineage tracing reveals the phylodynamics, plasticity, and paths of tumor evolution. *Cell* **185**, 1905-1923.e1925, doi:10.1016/j.cell.2022.04.015 (2022).
226 Bi, M. *et al.* ER stress-regulated translation increases tolerance to extreme hypoxia and promotes tumor growth. *The EMBO journal* **24**, 3470-3481, doi:10.1038/sj.emboj.7600777 (2005).
227 Back, S. H. *et al.* Translation attenuation through eIF2alpha phosphorylation prevents oxidative stress and maintains the differentiated state in beta cells. *Cell metabolism* **10**, 13-26, doi:10.1016/j.cmet.2009.06.002 (2009).
228 Chen, J., Lecuona, E., Briva, A., Welch, L. C. & Sznajder, J. I. Carbonic anhydrase II and alveolar fluid reabsorption during hypercapnia. *American journal of respiratory cell and molecular biology* **38**, 32-37, doi:10.1165/rcmb.2007-0121OC (2008).
229 Ghaddar, N. *et al.* The integrated stress response is tumorigenic and constitutes a therapeutic liability in KRAS-driven lung cancer. *Nat Commun* **12**, 4651, doi:10.1038/s41467-021-24661-0 (2021).
230 Igarashi, T. *et al.* Clock and ATF4 transcription system regulates drug resistance in human cancer cell lines. *Oncogene* **26**, 4749-4760, doi:10.1038/sj.onc.1210289 (2007).

231 Tanabe, M. *et al.* Activating Transcription Factor 4 Increases the Cisplatin Resistance of Human Cancer Cell Lines. *Cancer Res.* **63**, 8592-8595 (2003).
232 Rouschop, K. M. *et al.* PERK/eIF2α signaling protects therapy resistant hypoxic cells through induction of glutathione synthesis and protection against ROS. *Proc Natl Acad Sci U S A* **110**, 4622-4627, doi:10.1073/pnas.1210633110 (2013).
233 Rouschop, K. M. *et al.* The unfolded protein response protects human tumor cells during hypoxia through regulation of the autophagy genes MAP1LC3B and ATG5. *The Journal of clinical investigation* **120**, 127-141, doi:10.1172/jci40027 (2010).
234 Yang, H. *et al.* HSP90/AXL/eIF4E-regulated unfolded protein response as an acquired vulnerability in drug-resistant KRAS-mutant lung cancer. *Oncogenesis* **8**, 45, doi:10.1038/s41389-019-0158-7 (2019).
235 Albert, A. E. *et al.* Adaptive Protein Translation by the Integrated Stress Response Maintains the Proliferative and Migratory Capacity of Lung Adenocarcinoma Cells. *Molecular cancer research : MCR* **17**, 2343-2355, doi:10.1158/1541-7786.mcr-19-0245 (2019).
236 Gwinn, D. M. *et al.* Oncogenic KRAS Regulates Amino Acid Homeostasis and Asparagine Biosynthesis via ATF4 and Alters Sensitivity to L-Asparaginase. *Cancer Cell* **33**, 91-107.e106, doi:https://doi.org/10.1016/j.ccell.2017.12.003 (2018).
237 Wu, H. *et al.* Integration of Hippo signalling and the unfolded protein response to restrain liver overgrowth and tumorigenesis. *Nat Commun* **6**, 6239, doi:10.1038/ncomms7239 (2015).
238 Shreberk-Shaked, M. *et al.* A Division of Labor between YAP and TAZ in Non-Small Cell Lung Cancer. *Cancer Res* **80**, 4145-4157, doi:10.1158/0008-5472.can-20-0125 (2020).
239 Jewer, M. *et al.* Translational control of breast cancer plasticity. *Nat Commun* **11**, 2498, doi:10.1038/s41467-020-16352-z (2020).
240 Ghaddar, N. *et al.* Detection of Lung Tumor Progression in Mice by Ultrasound Imaging. *Journal of visualized experiments : JoVE*, doi:10.3791/60565 (2020).
241 Scheuner, D. *et al.* Translational control is required for the unfolded protein response and in vivo glucose homeostasis. *Mol Cell* **7**, 1165-1176, doi:10.1016/s1097-2765(01)00265-9 (2001).
242 Wang, S., Raven, J. F., Durbin, J. E. & Koromilas, A. E. Stat1 phosphorylation determines Ras oncogenicity by regulating p27 kip1. *PLoS One* **3**, e3476, doi:10.1371/journal.pone.0003476 (2008).
243 Garassino, M. C. *et al.* Different types of K-Ras mutations could affect drug sensitivity and tumour behaviour in non-small-cell lung cancer. *Annals of oncology : official journal of the European Society for Medical Oncology* **22**, 235-237, doi:10.1093/annonc/mdq680 (2011).
244 Caiola, E. *et al.* Base excision repair-mediated resistance to cisplatin in KRAS(G12C) mutant NSCLC cells. *Oncotarget* **6**, 30072-30087, doi:10.18632/oncotarget.5019 (2015).
245 Brunelli, L., Caiola, E., Marabese, M., Broggini, M. & Pastorelli, R. Comparative metabolomics profiling of isogenic KRAS wild type and mutant NSCLC cells in vitro and in vivo. *Scientific Reports* **6**, 28398, doi:10.1038/srep28398 (2016).
246 Agalioti, T. *et al.* Mutant KRAS promotes malignant pleural effusion formation. *Nat Commun* **8**, 15205, doi:10.1038/ncomms15205 (2017).
247 Bustin, S. A. *et al.* The MIQE guidelines: minimum information for publication of quantitative real-time PCR experiments. *Clinical chemistry* **55**, 611-622, doi:10.1373/clinchem.2008.112797 (2009).
248 Kim, D., Langmead, B. & Salzberg, S. L. HISAT: a fast spliced aligner with low memory requirements. *Nat Methods* **12**, 357-360, doi:10.1038/nmeth.3317 (2015).
249 Wright, G. W. & Simon, R. M. A random variance model for detection of differential gene expression in small microarray experiments. *Bioinformatics (Oxford, England)* **19**, 2448-2455, doi:10.1093/bioinformatics/btg345 (2003).

250 Oertlin, C. *et al.* Generally applicable transcriptome-wide analysis of translation using anota2seq. *Nucleic acids research* **47**, e70, doi:10.1093/nar/gkz223 (2019).
251 Subramanian, A. *et al.* Gene set enrichment analysis: a knowledge-based approach for interpreting genome-wide expression profiles. *Proc Natl Acad Sci U S A* **102**, 15545-15550, doi:10.1073/pnas.0506580102 (2005).
252 Mohanty, K., Blackwell, J., Egan, T. & Muller, M. Characterization of the Lung Parenchyma Using Ultrasound Multiple Scattering. *Ultrasound in medicine & biology* **43**, 993-1003, doi:10.1016/j.ultrasmedbio.2017.01.011 (2017).
253 Rajesh, K. *et al.* The eIF2α serine 51 phosphorylation-ATF4 arm promotes HIPPO signaling and cell death under oxidative stress. *Oncotarget* **7**, 51044-51058, doi:10.18632/oncotarget.10480 (2016).
254 Wu, H. *et al.* Integration of Hippo signalling and the unfolded protein response to restrain liver overgrowth and tumorigenesis. *Nat. Commun.* **6**, 6239, doi:10.1038/ncomms7239 (2015).
255 Marjanovic, N. D. *et al.* Emergence of a High-Plasticity Cell State during Lung Cancer Evolution. *Cancer Cell* **38**, 229-246.e213, doi:10.1016/j.ccell.2020.06.012 (2020).
256 Cha, Y. J. & Shim, H. S. Biology of invasive mucinous adenocarcinoma of the lung. *Translational Lung Cancer Research* **6**, 508-512 (2017).
257 Garrido, P. *et al.* Updated guidelines for predictive biomarker testing in advanced non-small-cell lung cancer: a National Consensus of the Spanish Society of Pathology and the Spanish Society of Medical Oncology. *Clinical & translational oncology : official publication of the Federation of Spanish Oncology Societies and of the National Cancer Institute of Mexico* **22**, 989-1003, doi:10.1007/s12094-019-02218-4 (2020).
258 Du, J., Liu, H., Mao, X., Qin, Y. & Fan, C. ATF4 promotes lung cancer cell proliferation and invasion partially through regulating Wnt/β-catenin signaling. *International journal of medical sciences* **18**, 1442-1448, doi:10.7150/ijms.43167 (2021).
259 Wang, R. *et al.* Overexpression of eukaryotic initiation factor 4E (eIF4E) and its clinical significance in lung adenocarcinoma. *Lung Cancer* **66**, 237-244, doi:10.1016/j.lungcan.2009.02.001 (2009).
260 Khoury, T. *et al.* Eukaryotic Initiation Factor-4E and Cyclin D1 Expression Associated with Patient Survival in Lung Cancer. *Clinical lung cancer* **10**, 58-66, doi:10.3816/CLC.2009.n.009 (2009).
261 Li, Y. K. *et al.* Elevated expression of eukaryotic translation initiation factor 4E is associated with proliferation, invasion and acquired resistance to erlotinib in lung cancer. *Cancer Biology & Therapy* **13**, 272-280, doi:10.4161/cbt.18923 (2012).
262 Gantenbein, N. *et al.* Influence of eukaryotic translation initiation factor 6 on non-small cell lung cancer development and progression. *European journal of cancer (Oxford, England : 1990)* **101**, 165-180, doi:10.1016/j.ejca.2018.07.001 (2018).
263 Díaz-García, C. V. *et al.* Prognostic value of dual-specificity phosphatase 6 expression in non-small cell lung cancer. *Tumor Biology* **36**, 1199-1206, doi:10.1007/s13277-014-2729-8 (2015).
264 Unni, A. M. *et al.* Hyperactivation of ERK by multiple mechanisms is toxic to RTK-RAS mutation-driven lung adenocarcinoma cells. *eLife* **7**, doi:10.7554/eLife.33718 (2018).
265 Ito, T. *et al.* Paralog knockout profiling identifies DUSP4 and DUSP6 as a digenic dependence in MAPK pathway-driven cancers. *Nature genetics* **53**, 1664-1672, doi:10.1038/s41588-021-00967-z (2021).
266 Masgras, I. *et al.* Absence of Neurofibromin Induces an Oncogenic Metabolic Switch via Mitochondrial ERK-Mediated Phosphorylation of the Chaperone TRAP1. *Cell reports* **18**, 659-672, doi:10.1016/j.celrep.2016.12.056 (2017).

267 Gao, R. *et al.* YAP/TAZ and ATF4 drive resistance to Sorafenib in hepatocellular carcinoma by preventing ferroptosis. *EMBO molecular medicine* **13**, e14351, doi:10.15252/emmm.202114351 (2021).
268 Zhang, W. *et al.* Downstream of mutant KRAS, the transcription regulator YAP is essential for neoplastic progression to pancreatic ductal adenocarcinoma. *Sci Signal* **7**, ra42, doi:10.1126/scisignal.2005049 (2014).
269 Noto, A. *et al.* Stearoyl-CoA-desaturase 1 regulates lung cancer stemness via stabilization and nuclear localization of YAP/TAZ. *Oncogene* **36**, 4573-4584, doi:10.1038/onc.2017.75 (2017).
270 Kim, H. M. & Koo, J. S. Immunohistochemical Analysis of Cancer Stem Cell Marker Expression in Papillary Thyroid Cancer. *Frontiers in endocrinology* **10**, 523, doi:10.3389/fendo.2019.00523 (2019).
271 Parsons, M. J., Tammela, T. & Dow, L. E. WNT as a Driver and Dependency in Cancer. *Cancer Discovery* **11**, 2413-2429, doi:10.1158/2159-8290.cd-21-0190 (2021).
272 Tammela, T. *et al.* A Wnt-producing niche drives proliferative potential and progression in lung adenocarcinoma. *Nature* **545**, 355-359, doi:10.1038/nature22334 (2017).
273 Zhou, B. *et al.* Claudin-18-mediated YAP activity regulates lung stem and progenitor cell homeostasis and tumorigenesis. *The Journal of clinical investigation* **128**, 970-984, doi:10.1172/jci90429 (2018).
274 Feng, Y.-X. *et al.* Cancer-specific PERK signaling drives invasion and metastasis through CREB3L1. *Nat. Commun.* **8**, 1079, doi:10.1038/s41467-017-01052-y (2017).
275 Zyryanova, A. F. *et al.* ISRIB Blunts the Integrated Stress Response by Allosterically Antagonising the Inhibitory Effect of Phosphorylated eIF2 on eIF2B. *Mol Cell* **81**, 88-103.e106, doi:10.1016/j.molcel.2020.10.031 (2021).
276 Küper, A. *et al.* Overcoming hypoxia-induced resistance of pancreatic and lung tumor cells by disrupting the PERK-NRF2-HIF-axis. *Cell Death Dis* **12**, 82, doi:10.1038/s41419-020-03319-7 (2021).
277 Bar-Sagi, D., Knelson, E. H. & Sequist, L. V. A bright future for KRAS inhibitors. *Nature Cancer* **1**, 25-27, doi:10.1038/s43018-019-0016-8 (2020).
278 Zismanov, V. *et al.* Phosphorylation of eIF2α Is a Translational Control Mechanism Regulating Muscle Stem Cell Quiescence and Self-Renewal. *Cell stem cell* **18**, 79-90, doi:10.1016/j.stem.2015.09.020 (2016).

Appendices